# Application of Additive Manufacturing for Improved Thermal Management of Hot Sheet Metal Forming Tools

by

Rumbidzai Muvunzi

*Dissertation presented for the degree of*
*Doctor of Philosophy in Industrial Engineering in the*
*Faculty of Engineering at*
*Stellenbosch University*

Supervisor: Prof Stephen Matope
Co-supervisor: Prof Thomas M. Harms

March 2020

# DECLARATION

By submitting this thesis electronically, I declare that the entirety of the work contained therein is my own, original work, that I am the sole author thereof (save to the extent explicitly otherwise stated), that reproduction and publication thereof by Stellenbosch University will not infringe any third party rights and that I have not previously in its entirety or in part submitted it for obtaining any qualification.

Date: March 2020

# ABSTRACT

In hot stamping, a blank or sheet of metal at high temperature (800-900 °C) is formed and cooled simultaneously by the tools. The rapid cooling of the blank causes transformation to a martensitic microstructure with high tensile strength (1 500 MPa) which enables the parts to acquire crash resistant properties. Accordingly, the process is used to produce vehicle components for improving safety of passengers. However, the hot stamping tools are exposed to high thermal load as they come into contact with the hot blanks. To aid in the cooling, the tools have a network of drilled channels in which a coolant circulates to extract heat. Due to machining restrictions, the straight drilled channels are unable to ensure consistent cooling of geometrically complex parts. If the tools are not evenly cooled, thermal stresses are induced and this compromises the tool service life and quality of parts (hardness properties). Moreover, the average cooling time in hot stamping occupies at least 30 % of the total cycle time. Thus, one of the major challenges in hot stamping research is to find ways of reducing the cycle time. The above mentioned challenges can be resolved through exploiting the design freedom offered by Additive Manufacturing technologies in the producing of tools with cooling channels which conform to the shape of tools. This has already been extensively investigated in the injection moulding and die casting tooling industry. However, there is limited information on the design and manufacturing parameters of hot stamping tools with conformal cooling channels.

The aim of this research was to apply Additive Manufacturing as a tool for improving thermal management of hot stamping tools. The first objective was to identify the parameters required for an effective thermal management system of hot stamping tools. A method for identifying the structural conformal cooling system parameters was developed based on the technical limitation of the Selective Laser Melting process, principles of mechanics and heat transfer. The developed method was validated using finite element analysis simulation on a typical benchmark component. The second objective of the study was to develop a model for predicting minimum cycle time in hot stamping under ideal conditions. The model was developed using heat transfer principles and study of the stages in hot stamping. The model is a useful benchmark tool which is applicable in cycle time prediction. The third and fourth objectives were to design and manufacture a hot stamping tool with conformal cooling channels for a benchmark part. The fifth objective was to investigate the impact of the tool with conformal cooling channels on cycle time. In view of that, experiments were conducted to compare the performance of the optimised tool and the conventional one under typical industry like conditions. According to the results, the conformable tool shows the potential of reducing cooling time by 29 %

# OPSOMMING

Gedurende warmstempeling word ’n ru-stuk of plaat metaal by ’n hoë temperatuur (800-900 °C) deur gereedskap gevorm en terselfdertyd afgekoel. Die vinnige afkoeling van die plaat veroorsaak omskakeling na ’n martensitiese struktuur met hoë treksterkte (1 500 MPa), wat die gestempelde onderdele plettervaste eienskappe gee. Daarom word hierdie proses gebruik vir die vervaardiging van voertuigonderdele om passasiersveiligheid te verbeter. Nietemin word die warmstempelingsgereedskap weens die hoë temperatuur van die metaalplaat aan ’n hoë termiese las blootgestel. Om afkoeling aan te help, beskik die gereedskap oor ’n netwerk boorkanale waarin ’n koelmiddel sirkuleer om hitte te onttrek. As gevolg van masjineringsbeperkinge kan die reguit boorkanale egter nie gelykmatige afkoeling van geometries komplekse onderdele verseker nie. Indien die gereedskap nie gelykmatig afkoel nie, veroorsaak dit termiese spanning, wat die gebruiksduur van die gereedskap verkort en die gehalte van onderdele (hardheidseienskappe) verlaag. Daarbenewens neem gemiddelde afkoelingstyd gedurende warmstempeling ten minste 30% van die algehele siklustyd in beslag. Een van die groot uitdagings van warmstempeling is dus om na maniere te soek om die siklustyd te verkort. Bogenoemde uitdagings kan die hoof gebied word deur gebruik te maak van die ontwerpvryheid wat additiewe vervaardigingstegnologieë bied vir die vervaardiging van gereedskap met pasgemaakte, konforme koelkanale. Dít is reeds uitvoerig ondersoek in die inspuitvorming- en matrysgietingsgereedskapbedryf, maar inligting oor die ontwerp- en vervaardigingsparameters van warmstempelingsgereedskap met konforme koelkanale is nog beperk.

Die doel van hierdie navorsing was om additiewe vervaardiging te gebruik as ’n metode om die termiese bestuur van warmstempelingsgereedskap te verbeter. Dít is bereik deur eers die vereiste parameters vir ’n doeltreffende termiese bestuurstelsel vir warmstempelingsgereedskap te bepaal. ’n Metode vir die vasstelling van die strukturele parameters vir ’n konforme afkoelingstelsel is derhalwe op grond van die tegniese beperking van die selektiewe lasersmeltproses, beginsels van meganika sowel as warmteoordrag ontwikkel. Die ontwikkelde model is gestaaf met ’n eindige-elementontledingsimulasie van ’n tipiese standaardonderdeel. Die tweede oogmerk van die studie was om ’n model te ontwikkel vir die voorspelling van minimum siklustyd vir warmstempeling in ideale omstandighede. Die model is met behulp van warmteoordragbeginsels en ’n studie van warmstempelingsfases ontwikkel, en is ’n nuttige standaardmetode vir siklustydvoorspelling. Die derde en vierde doelwitte was om ’n warmstempelingsinstrument met konforme koelkanale vir ’n standaardonderdeel te ontwerp en te vervaardig. Die eindproduk is ’n warmstempelingsinstrument met innoverende konforme koelkanale op grond van ’n werklike standaardonderdeel. Die vyfde doel was om die impak van die instrument met konforme koelkanale op afkoeltyd te ondersoek. Vir dié doel is eksperimente uitgevoer om die werkverrigting van die geoptimaliseerde instrument met dié

van die konvensionele een in soortgelyke omstandighede as in die bedryf te vergelyk. Die resultate toon dat die instrument met konforme koelkanale afkoeltyd moontlik met 29% kan verkort.

# ACKNOWLEDGEMENTS

To Prof Dimitrov, I acknowledge the valuable guidance, patience and thorough supervision shown during my study. You have been very supportive and considerate. Although you are no longer around physically, your memory and legacy remain. Many thanks go to Prof Matope who was always there when I needed him. He taught me to be a good researcher and I was greatly inspired by his intellectual suggestions. There were many times when I felt that I was stuck, and Prof Matope was always there to help me keep on track. I also want to thank Prof Harms for his valuable input which fashioned my research. I am greatly thankful for all the time and intellectual contribution that he gave to this study. My heartfelt gratitude goes to the Organization for Women in Science for the Developing World (OWSD), the Swedish Development Agency and the Schlumberger Foundation, for the generous financial support during this study and for helping me to realise my long-awaited dream.

I want to thank the staff at STC-LAM: Devon, Chad, Thembi, Ashley and Angelo. Thank you so much for all the kind assistance and work done in the manufacture of the tool inserts. I am deeply touched by your commitment and diligence. Thank you Xola for your valuable assistance and advice during the design and manufacture of the tool. Thank you Nicholas for assisting me with the simulation software. You were always available when I needed help. I want to thank the other colleagues in our research group: Philip, Martin, Emad, William and Lameck, for their valuable support and taking time to discuss my research with me. I want to thank Dr Andrias Sterzing and all the other colleagues (Julia, Stefan, Thomas, Soreen) at Fraunhofer Institute. Thank you Matthias and Cornelia for helping me with the experiments and measurements. It has been a wonderful experience to work with you. You showed a lot of support during my experimental work. To my best friends, Cathey and Zvie, thank you guys for the prayers, motivation and love.

To my late father, Enock. You always believed that this day would come and continuously encouraged me to pursue the Engineering field. I am forever grateful to you for leading me onto this exciting path. Thank you, mum, for your support, even in the darkest moments. To my husband Tinashe, you have been a shoulder to lean on and an anchor of support. I value your patience and support during my study. You did not mind all those nights when I was away from you. Instead you shared the burden with me until the end. To my son Jason, thank you for your patience and prayers during my absence. You have been my source of strength and motivation.

Above all, I thank my Lord and saviour Jesus Christ, for the abundant grace that has been with me throughout this journey.

# TABLE OF CONTENTS

# LIST OF FIGURES

# LIST OF TABLES

# LIST OF SYMBOLS

| Symbol | Description | Units |
|---|---|---|
| A | Surface area | $m^2$ |
| Bi | Biot number ($Bi=hL/k$) | |
| C | Specific heat capacity | J/kgK |
| CI | Measure of consistency | |
| D | Connector pipe diameter | mm |
| E | Latent heat energy | J/kg |
| F | Force | N |
| $f$ | shape factor | |
| $F_l$ | Force per unit length | N/m |
| Gr | Grashof number ($G=L^3\rho^2 g\Delta T\beta/\mu^2$) | |
| $h$ | Convection heat transfer coefficient | $W/m^2K$ |
| L | Length | m |
| $l_T$ | Total length of all cooling channels | m |
| M | Bending moment | Nm |
| Nu | Nusselt number ($Nu=hD/k$) | |
| P | Pressure | MPa |
| Pr | Prandtl Number ($P=\mu c/k$) | |
| Q | Heat | J |
| R | Interfacial heat transfer coefficient | $W/m^2K$ |
| Re | Reynold's number | |
| RI | Random index | |
| T | Temperature | K / °C |
| t | Time | s |
| U | Phase fraction | |
| V | Volume of blank | $m^3$ |
| $\dot{W}$ | Rate of work done | W |
| Y | Shortest distance between the center of consecutive cooling channels | mm |
| Z | Distance cooling channel center to die surface | |
| $d$ | Cooling channel diameter | mm |
| $f_r$ | Friction factor | |
| $k$ | Thermal conductivity | W/mK |
| $m$ | Mass | kg |

| | | |
|---|---|---|
| $n$ | Number of cooling channels | |
| $r$ | Radius of cooling channel | mm |
| $s$ | Blank thickness | mm |
| $v$ | velocity | m/s |
| $x$ | Distance | mm |
| $y$ | Shortest distance between the circumferences of consecutive cooling channels | mm |
| $z$ | Shortest from tool surface to cooling channel circumference | mm |

## Greek Symbols

| Symbol | Description | Units |
|---|---|---|
| $\sigma_m$ | Yield stress | $N/m^2$ |
| $\sigma_y$ | Maximum allowable stress | $N/m^2$ |
| α | Stress dependent transformation constant | |
| δ | Deflection | |
| μ | Viscosity | Kg/sm |
| τ | Delay time | s |
| $\varepsilon$ | Emissivity of blank | |
| $\eta$ | Viscosity | kg/ms |
| $\lambda$ | Fraction of plastic work converted into heat | $K^{-1}$ |
| $\rho$ | Density of blank | $kg/m^3$ |
| $\sigma$ | Stefan Boltzmann constant | $Wm^{-2}K^{-4}$ |
| $\epsilon$ | Strain rate | $s^{-1}$ |

## Subscripts

| Subscript | Description | |
|---|---|---|
| a | Ambient | |
| av | Average | |
| b | Blank | |
| bd | Surface area of blank exposed to die | |
| bot | Bottom | |
| bp | Surface area of blank exposed to punch | |
| c | Cooling channels | |
| con | Conduction | |

| | | |
|---|---|---|
| conv | Convection | |
| **Subscript** | **Description** | |
| cw | Cooling channel wall | |
| d | Tool | |
| fac | Floor and ceiling surfaces in the plant | |
| form | Forming phase | |
| g | Air gap conductance | |
| ms | Martensite | |
| o | Initial | |
| t | Value of a parameter at a given time | |
| w | Water | |

## Abbreviations

| Abbreviation | Description | |
|---|---|---|
| AM | Additive Manufacturing | |
| DMD | Direct Metal Deposition | |
| EBM | Electronic Beam Melting | |
| SLM | Selective Laser Melting | |
| STL | Standard Tessellation Language | |

# CHAPTER 1 : INTRODUCTION

## 1.1. Background

Hot-stamping is a thermo-mechanical process which produces parts with a high tensile strength and low weight. As a result, hot stamping is suitable for producing vehicle components because of the need to improve safety through high strength parts which are crash resistant. Fuel consumption is decreased by reducing the overall weight of vehicle components (Lv *et al.*, 2016). The process can either be direct or indirect. For direct hot stamping, the sheet metal or blank is heated to about 800-900 °C before it is formed and cooled rapidly in a closed tool (Karbasian and Tekkaya, 2010). In the indirect process, the blank is cold-formed before exposure to the furnace and cooling. This is shown in Figure 1-1.

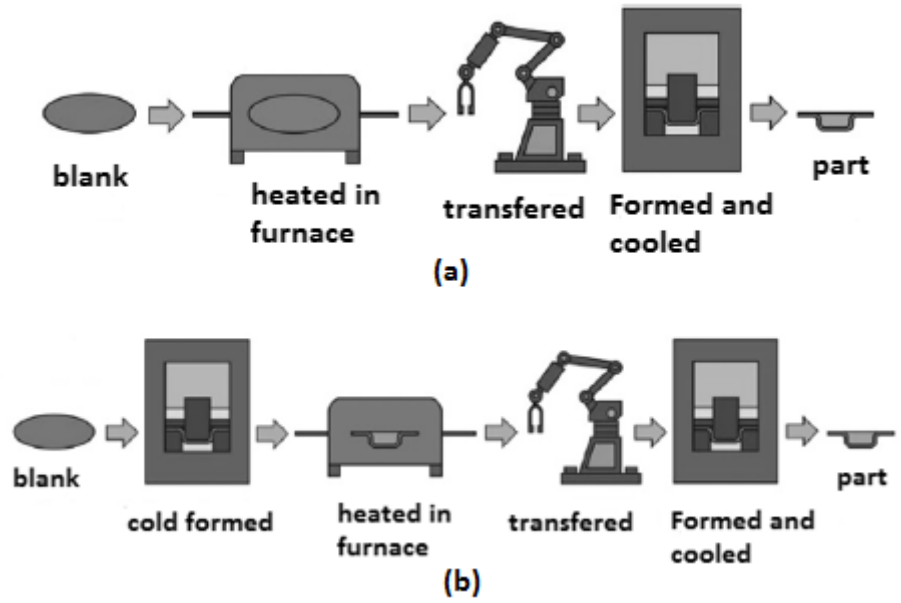


Figure 1-1: a) Direct and b) Indirect Hot Stamping process (Karbasian and Tekkaya, 2010).

The hot blanks must be rapidly cooled (above 27 °C/s) to facilitate the transformation of the microstructure from an austenite to a martensitic structure which is associated with high strength (1500 MPa) (Steinbeiss *et al.*, 2007). To allow rapid cooling of the hot blanks, the forming tools are produced with cooling channels. The channels allow the coolant to transfer heat from the tool system (Figure 1-2). The tools must be effectively cooled at a minimum cooling rate of 27 °C/s (Steinbeiss *et al*., 2007). If the cooling system is not designed properly, heat is accumulated in the tools, lowering their ability to cool the parts at the required rate. This does not only compromise the quality of the parts, but also leads to severe tool wear and high tool maintenance costs.

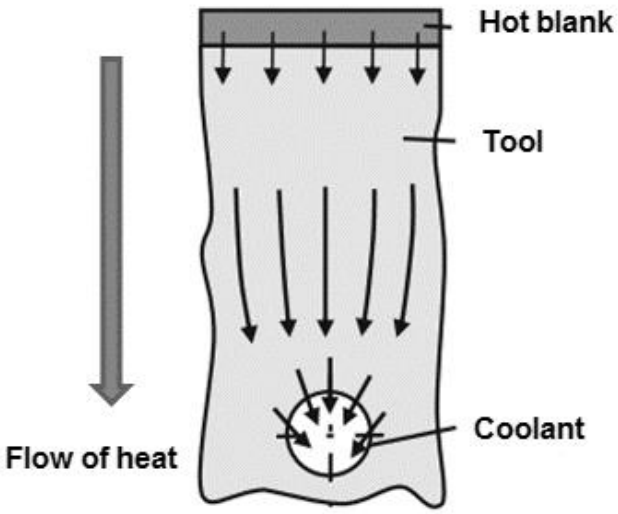


Figure 1-2: Heat flow from blank to coolant (Steinbeiss *et al.*, 2007)

High-temperature gradients cause the tool surface to be exposed to adhesive wear and failure (Wang *et al*., 2014). Tools with complex geometry require complicated deep drilling and segmentation when creating cooling channels. This makes the tool making process challenging. A significant amount of cutting tools and energy is required for performing machining operations (Mueller *et al.*, 2013). Thus, it is necessary to explore other methods of manufacturing the tools.

The most practised method of producing cooling channels is straight drilling. For parts with complex geometry, the straight drilled channels do not offer consistent cooling because of limitations in their structure. Inconsistent cooling causes distortion and non-uniform hardness, compromising the quality of parts. Also, non-uniform cooling causes generation of thermal stress which leads to tool degradation and failure. Hence it is important to reduce thermal stress as much as possible by ensuring uniform cooling of the tools. Much of previous research has focused on the optimisation of straight drilled channels. Steinbeiss *et al.* (2007), proposed an evolutionary algorithm for optimizing the position and arrangement of cooling channels. Ye *et al*.(2013) and Lim (2014), developed mathematical models for calculating cooling parameters for straight drilled channels to maximize cooling performance. However, machining restrictions remained a limiting factor in designing effective cooling channels.

At least 30 % of the total cycle time in hot stamping is spent on the cooling stage of the process (Mueller *et al*., 2013). A way to reduce the cooling time is by increasing the heat transfer rate through improved cooling systems design. For parts with complex geometry, it takes longer to cool off the sections with intricate features. Hence, to attain a faster cooling rate, the cooling system should be

oriented such that all the critical sections on the part are accessed timely. Thus, the aim of the study is to improve cooling performance of the hot stamping tools.

## 1.2. Problem Statement

The straight drilled cooling channels do not allow consistent cooling for parts with complex geometry. As a result, the cooling time is prolonged, and the products are prone to defects such as inconsistent hardness and distortion. Also, heat accumulates in the tools, causing them to wear quickly, thus shortening their service life. Moreover, it is challenging to manufacture the tools using conventional methods because of the complicated machining and tool segmentation when constructing the cooling channels. Hence it is necessary to devise ways of improving quality and reducing cycle time by enhancing the cooling capability of the tools.

These challenges can be resolved to a great extent, through the application of additive manufacturing (AM) to produce tools with optimized cooling systems. According to previous research, conformal cooling can reduce cycle time by 25 to 50 % (Au and Yu, 2013; Dimitrov *et al*., 2010; Mohamed *et al*., 2013). So far, research regarding parameters for conformal cooling design was mainly in the injection moulding industry. (Xu *et al*., 2001; Moammer 2011; Wang *et al*., 2011; Wang *et al*., 2011). It is of no doubt that AM processes are suitable for the production of hot stamping tools with optimised cooling systems. However; only a few authors in literature have investigated this (Mueller *et al.*, 2013; Gebauer *et al.*, 2016; Cortina *et al.*, 2018). These few studies did not generate enough information regarding the parameters used in the design and manufacture of the tools. Hence, the study seeks to investigate the parameters in which AM can be used to produce hot stamping tools with improved cooling capabilities.

## 1.3. Research Question

In which range of cooling system parameters is it viable to apply AM in the design and manufacture of hot sheet metal forming tools with conformal optimized cooling systems for improving thermal management?

## 1.4. Research Objectives

The aim of the study is to improve thermal management of hot sheet metal forming tools. The specific objectives are as follows:

- To identify parameters for an effective thermal management system of hot stamping tools
- To develop a model for predicting the minimum cycle time of the hot stamping process

- To design a hot stamping tool with a conformal cooling system that can be manufactured using AM
- To build the hot stamping tool using AM
- To investigate the impact of the additively built tool on the cycle time and quality of formed parts

## 1.5. Research Approach

- Identifying parameters for AM application in a hot stamping tool cooling system

The first stage of the research involves a structured literature review of the parameters used for designing cooling systems in hot stamping tools and of the use of AM in the creation of conformal cooling channels in tooling applications. Based on the literature, a detailed model for determining cooling system parameters for hot sheet metal forming tools for AM application, is developed. Basic mechanical and heat and transfer principles are also used in formulating the model. This maps the way forward in identifying the cooling system parameters for effective heat transfer in hot sheet metal forming tools. Finite Element simulation is used to investigate the influence of the identified parameters on the cycle time and quality of parts

- Developing a model for predicting minimum cycle time in hot stamping tools

The model relates the hot stamping process parameters to the cycle time. The model predicts the minimum cycle time for producing a hot formed part under ideal conditions. The model is used as a basis for designing the tool to ensure a reduction in cycle time without compromising the quality of parts. Thus, it provides a benchmark that can be used as a basis for increasing productivity. The model is formulated using heat transfer analysis.

- Designing a conformal cooling system for a rocker panel.

A hot stamping tool with conformal cooling channels for a typical benchmark part is designed. The part considered for the design is a rocker panel. The structural parameters are derived from the developed model. The layout is designed using the engineering design method. The design specifications are defined. The design is validated using finite element simulation.

- Manufacture of the tool with improved cooling features

After evaluating the performance of the tool using simulation, the tool is then physically manufactured. Hybrid manufacturing is used to reduce the cost of producing the tool and to obtain the required strength. This is achieved by firstly machining the base body and then building the portion with the complex channels on top.

- Investigate the impact of the additively built tool on the cycle time and quality

This involves experimental evaluation of the manufactured tool. The tool performance is evaluated based on the hardness distribution, temperature deviation and cooling time of the formed parts. Figure 1-3 gives a summary of the steps followed in the study.

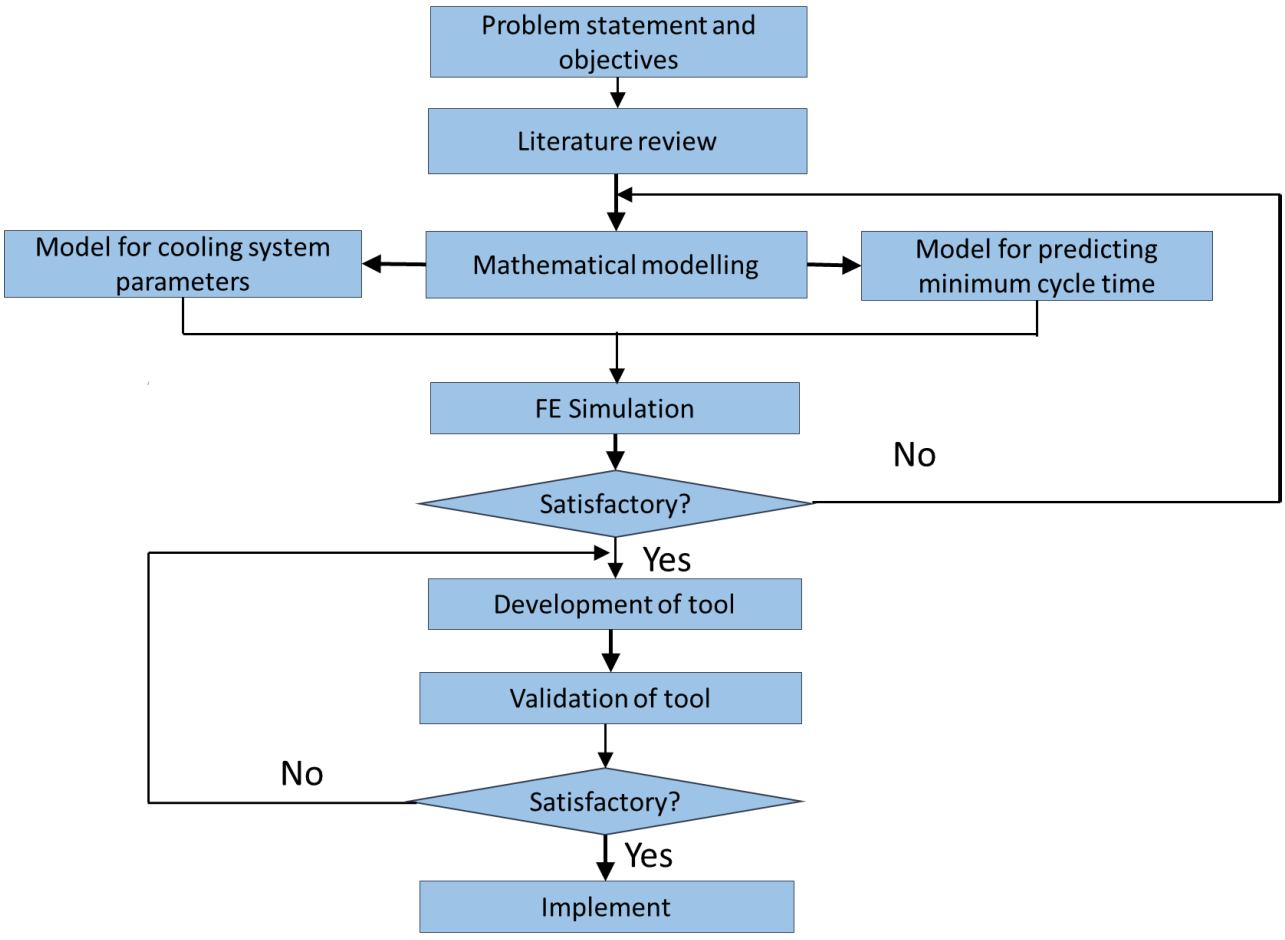


Figure 1-3: Methodology framework

Regarding Figure 1-3, the simulation results are regarded as satisfactory when the parameters from the model have a positive outcome. Also, if the results from the tool validation are in line with the simulation results they are considered satisfactory.

## 1.6. Significance of Research

One of the greatest areas of concern in hot stamping is the prolonged cooling time which occupies a significant part of the cycle time. A reduction in the cooling time would lead to significant cost savings. Another challenge in hot stamping is that the cooling efficiency of the blank affects the final hardness. Conformal cooling has significantly reduced cycle time and improved quality in other tooling applications. Therefore, it is necessary to further investigate its application in hot stamping. This will provide information on the viability and application parameters. Previous research has shown that AM processes can produce sheet metal forming tools with mechanical properties (density) comparable with those manufactured with conventional methods, although there have not been many studies regarding AM based cooling systems for hot stamping tools. The high tool loads experienced in hot stamping creates a challenge for AM processes. Thus, the study seeks to identify the range of parameters suited for the application of AM based cooling systems in hot stamping tools.

## 1.7. Dissertation Outline

The dissertation has eight chapters in total. The first chapter explains the background of the problem and highlights the aim, objectives and research question. The second chapter gives a thorough literature review of the cooling system parameters and of the design of AM based conformal cooling channels. This includes important aspects such as the design rules and manufacturing constraints. The theory behind the mechanics and heat transfer in hot stamping tools is also explained. This maps the way forward for the development of the models. In the third chapter, the models for determining cooling system structural parameters and predicting minimum cycle time are formulated and presented. The research design and methodology are explained in the fourth chapter. The fifth chapter focuses on the design of the tool with an improved cooling system and finite element simulation. The sixth chapter gives an account of the steps involved in the manufacture of the improved tool with conformal cooling channels and the experimental setup. The seventh chapter presents and discusses the experimental results and compares them with those obtained from the simulation. The last chapter gives a summary of the research, focusing on its contribution to the body of knowledge and areas that need further study. Figure 1-4 shows the outline of the dissertation.


Figure 1-4: Dissertation outline

## 1.8. Summary

The purpose of the chapter was to give the background to the problem and to highlight the aims and objectives of the study. An account of the challenges associated with conventional hot stamping tools was given. These include prolonged cooling time, reduced quality and tool service life. At present, there is limited literature on the application of AM based conformal cooling channels in hot stamping. There is a need for further investigation of the parameters and procedures to be used during design and manufacturing. Accordingly, this has prompted the researcher to investigate the structural parameters viable for the application of AM in the production of hot stamping tools with enhanced cooling capabilities. The following chapter gives an in-depth literature study of the subject in question.

# CHAPTER 2 : LITERATURE REVIEW

## 2.1. Introduction

The purpose of this chapter is to highlight the state of technology on the application of Additive Manufacturing (AM) to improve cooling system performance in hot stamping tools. Currently, literature on this subject is still limited. The chapter also gives an outline of previous research aimed at improving cooling system design in hot stamping tools and limitations in this subject area. In its structure, the chapter first gives an in-depth study of the hot stamping process and the thermal challenges involved. Secondly, the literature on the research efforts made to improve thermal management in hot stamping tools, is given. This is followed by an explanation of the applicable AM processes and the theoretical aspects behind the thermal management of the hot stamping process. Lastly, a summary and gap analysis are given to map the current research into the existing body of knowledge.

## 2.2. Hot Stamping Process

According to Karbasian and Tekkaya (2010), hot stamping can either be direct or indirect. For the direct process, the sheet metal (blank) is firstly heated in a furnace to between 900 and 950 °C for 5 to 10 minutes before it is plastically deformed in a forming press to take advantage of the formability at high temperature. When in contact with the tool, the sheet is cooled rapidly at a cooling rate of at least 27 K/s to achieve the required tensile strength (1500 MPa) (Lim *et al.*, 2014; Abdulhay *et al.*, 2011). During the indirect process, the blank is firstly formed before it is heated and cooled (Karbasian and Tekkaya, 2010). The cooling rate determines the resultant microstructural transformation which governs the resultant tensile strength and hardness (Liu *et al*., 2013). One major advantage of the hot stamping process is that the parts have a high strength to weight ratio. According to a study by Sheng *et al.* (2013), hot stamping can reduce the weight of rocket components by 20 %. Also, reports from the industry sector show that replacing hot stamping with cold stamping can reduce the weight of parts by 30 to 35% (Bohler-Uddeholm, 2016). According to reports from industry, the overall weight of a vehicle can be reduced by 25% after using hot stamped parts. (USLAB, 2016). On the other hand, hot stamping has challenges. These include low productivity because of the slow forming and cooling process. Moreover, the laser cutting of the blank after forming is costly because of the resultant high strength of the blank (Mori, 2015). Figure 2-1 shows the limitations of the hot stamping process.

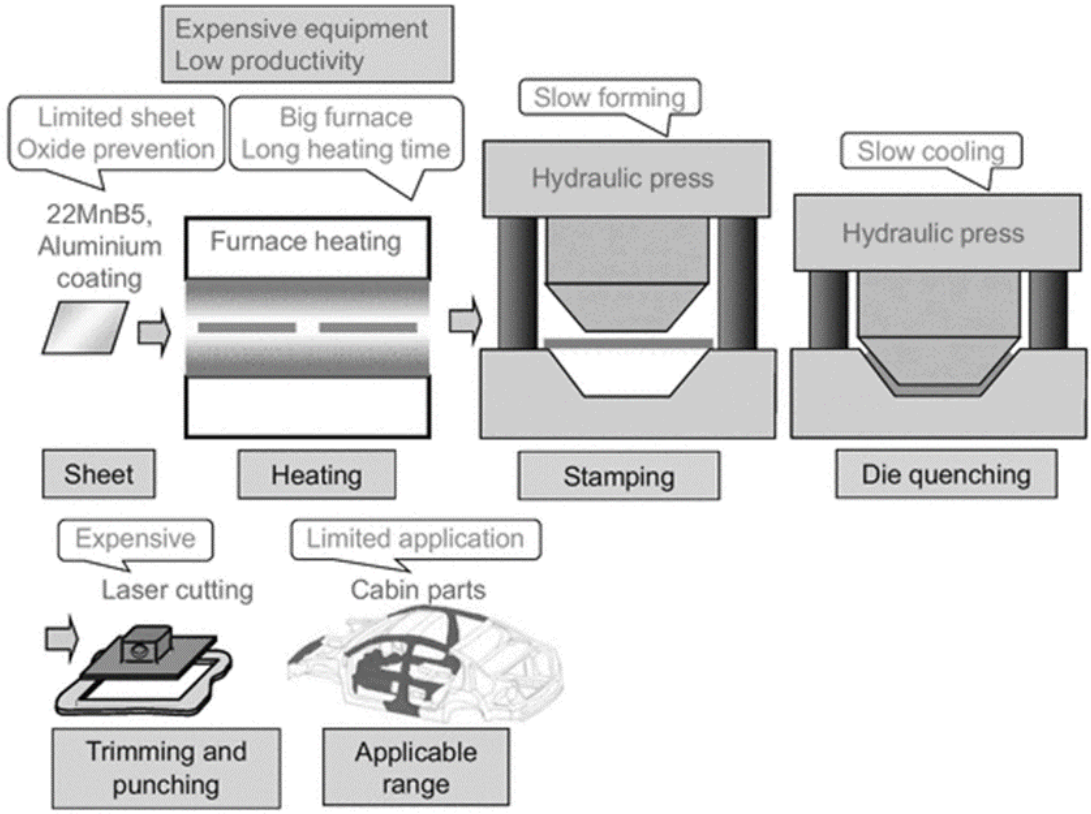


Figure 2-1: Hot stamping process and its limitations (Mori, 2015)

The blank steels used for the manufacture of hot stamping parts include 22MnB5, 27MnCrB5 and 37MnB4 (Choi *et al.*, 2014). The blank thickness varies from 1.0 to 2.6 mm (Nakagawa *et al.*, 2015). Recent research has focused on the use of thinner blanks to further reduce the weight of components produced by hot stamping. Nakagawa *et al.* (2015) and Lee *et al.* (2012) studied the formability of blanks with 0.6 mm thickness. Table 2.1 and Table 2.2 show the chemical composition and mechanical properties of the blanks The high strength is achieved by adding boron to carbon, manganese and chromium composition (Nikravesh *et al.*, 2015). Boron has a major impact on the hardening of the part through reducing softer microstructural changes. The Mn and Cr improve the hardenability of the part after quenching.

Table 2.1: Chemical composition (weight %) of hot stamping steel blanks (Naderi and Bleck, 2008)

| Steel | Al | B | C | Cr | Mn | N | Ni | Si |
|---|---|---|---|---|---|---|---|---|
| 20MnB5 | 0.04 | 0.001 | 0.16 | 0.23 | 1.05 | - | 0.01 | 0.40 |
| 22MnB5 | 0.03 | 0.002 | 0.23 | 0.16 | 1.18 | 0.005 | 0.12 | 0.22 |
| 8MnCrB3 | 0.05 | 0.002 | 0.07 | 0.37 | 0.75 | 0.006 | 0.01 | 0.21 |
| 37MnCrB5 | 0.03 | 0.002 | 0.25 | 0.34 | 1.24 | 0.004 | 0.01 | 0.21 |
| 37MnB4 | 0.03 | 0.001 | 0.33 | 0.19 | 0.81 | 0.006 | 0.02 | 0.31 |

Table 2.2: Properties of hot stamping steel blanks (Naderi and Bleck, 2008)

| Steel | Martensitic start temperature (°C) | Critical cooling rate (°C/s) | Yield stress before hot stamping (MPa) | Yield stress after hot stamping (MPa) | Tensile strength before hot stamping (MPa) | Tensile strength after hot stamping (MPa) |
|---|---|---|---|---|---|---|
| 20MnB5 | 450 | 30 | 505 | 967 | 637 | 1354 |
| 22MnB5 | 410 | 27 | 457 | 1010 | 608 | 1478 |
| 8MnCrB3 | - | - | 447 | 751 | 520 | 882 |
| 37MnCrB5 | 400 | 20 | 478 | 1097 | 638 | 1611 |
| 37MnB4 | 350 | 14 | 580 | 1378 | 810 | 2040 |

The most commonly used blank material is 22MnB5 because it is more ductile and attains the highest tensile strength after quenching (1478 MPa) (Hu *et al.*, 2013). The blank is coated with an aluminium silicon (AlSi) layer by a hot-dip galvanization process (Boher *et al.*, 2012). The AlSi bath consists of 10 % Si, 3 % Fe and 87 % Al (Karbasian and Tekkaya, 2010); it serves to protect the blank from scaling and surface decarburization during the hot stamping process (Boher *et al.*, 2012; Borsetto *et al.*, 2009). When heated, the AlSi coating melts and reacts with Fe which diffuses from the blank to form AlSiFe and $AlFe_3$. The AlSiFe which is produced has a higher melting point hence it forms a solid protective layer after the heating process (Grauer *et al.*, 2015). The thickness of the coating lies between 23 and 32 µm (Merklein and Lechler, 2006). The blank can be initially heated through using roller furnaces which move at controlled speeds. Resistance heating was proposed by Mori *et al.* (2005); it involves electrifying the blank with electrodes to allow current to flow. The resistance of the blank material generates heat. Induction heating can also be used. When induction heating is used,

the efficiency of the inductor determines the heating efficiency of the blank (Karbasian and Tekkaya, 2010).

The continuous cooling transformation (CCT) graph shows the change of the blank microstructure with cooling rate. A complete microstructural transformation from austenite to martensite is required to reach the required tensile strength. Figure 2-2 shows the CCT graph for 22MnB5. The graph in Figure 2-2 shows the presence of a minimum cooling rate for full martensitic transformation.

**Key**

A - Austenite

B - Bainite

F – Ferrite

M- Martensite

P- Pearlite

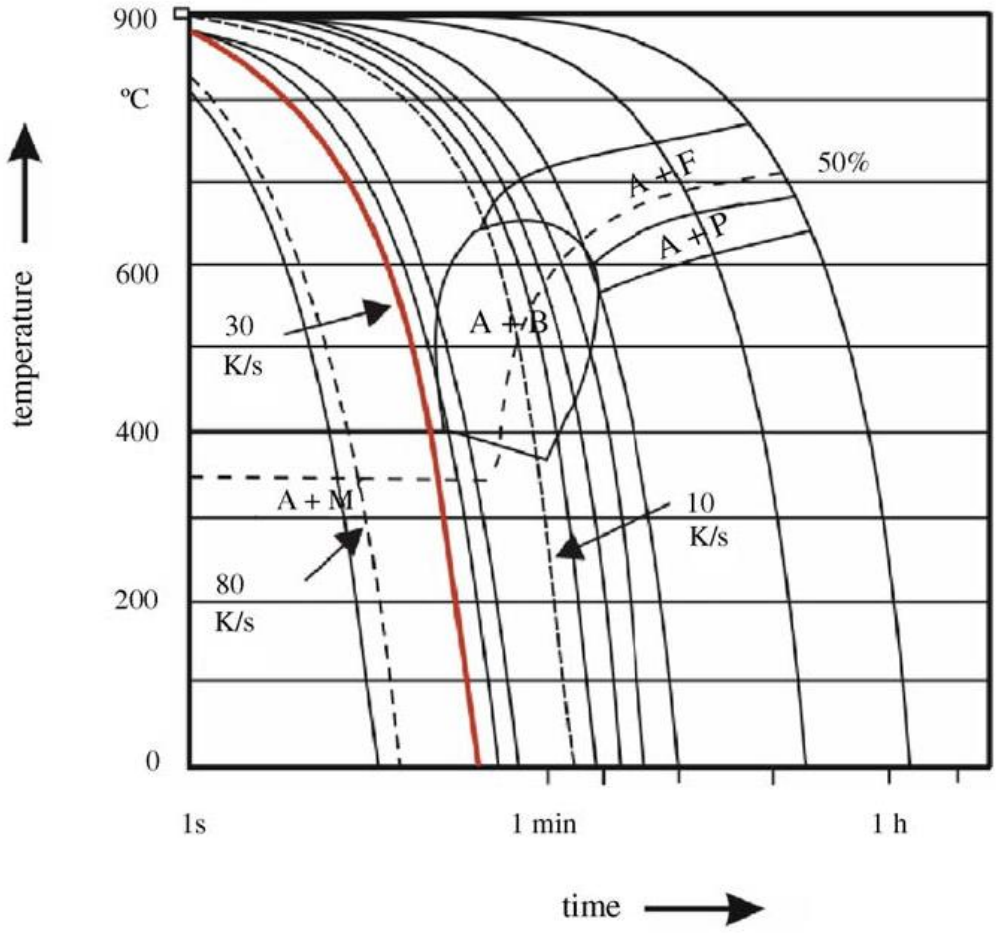


Figure 2-2: CCT graph for 22MnB5 steel (Merklein and Lechler, 2006)

## 2.3. Theoretical Considerations in the Hot Stamping Process

The internal heat lost by the blank during the hot stamping process is generally expressed by Equation.2-1 below:

$$Q(t) = mC_b \frac{dT_b}{dt} \quad 2\text{-}1$$

Equation.2-1 can be further expanded as shown below (Yunus, 2015):

$$Q(t) = \rho_b V C_b \frac{dT_b}{dt} \quad 2\text{-}2$$

During transportation to the press, heat is lost through convection and radiation (Abdulhay *et al.*, 2011). Equation 2-3 below can be used to explain the heat transfer (Merklein *et al.*, 2009):

$$Q = hA(T_b - T_a) \quad 2\text{-}3$$

The blank is considered as a plate which loses heat by convention. The upper and lower surfaces are shown in Figure 2-3 (Liu *et al.*, 2013; Shapiro, 2009):

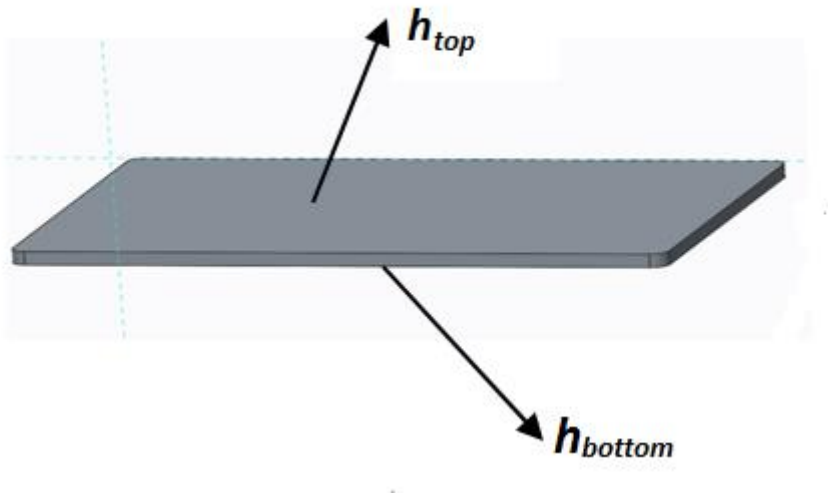


Figure 2-3: Heat transfer on the upper and lower surfaces (Muvunzi *et al.*, 2017)

The convective heat transfer coefficients at the top and bottom surfaces of the blank can be expressed using Equation 2-4 and 2-5. The parameters *Gr*, *Pr*, *k* and *L* represent the Grashof number, Prandtl number, thermal conductivity and length scale of the blank.

$$\dot{h}_{top} = [0.14(Gr \times Pr)^{0.33}]\frac{k}{L} \quad 2\text{-}4$$

$$\dot{h}_{bottom} = [0.27(Gr \times Pr)^{0.25}]\frac{k}{L} \quad 2\text{-}5$$

The heat lost by radiation can be expressed using the Stefan Boltzmann law shown in Equation 2-6:

$$Q_{rad} = AS_{rad}\sigma\varepsilon(T_1^4 - T_2^4) \qquad 2\text{-}6$$

The parameters A, $\varepsilon$, $S_{rad}$ and σ represent the blank surface area, emissivity, radiation shape factor and the Stefan Boltzmann constant. When the blank is positioned on the forming press, its top surface loses heat due to convection and radiation. Part of the bottom surface loses heat because of the contact with the die while other portions are cooled by air in the die cavity.

During the forming and cooling stage, the hot blank encounters the punch and die. It is then deformed as a result of the force applied by the punch. Soon after forming, the blank is cooled by the tools to the required microstructure (martensitic). At this stage, heat transfer depends on the thermal conductivity of tool material and the design of the cooling system (Steinbeiss *et al.*, 2007).

As stated before, the tool should effectively cool the hot blank at a minimum rate of 27 °C/s as shown in Equation 2-7:

$$\frac{dT_b}{dt} > 27\ °C/s \qquad 2\text{-}7$$

The heat absorbed by the tool as a result of the contact with the hot blank can be explained using Figure 2-4.

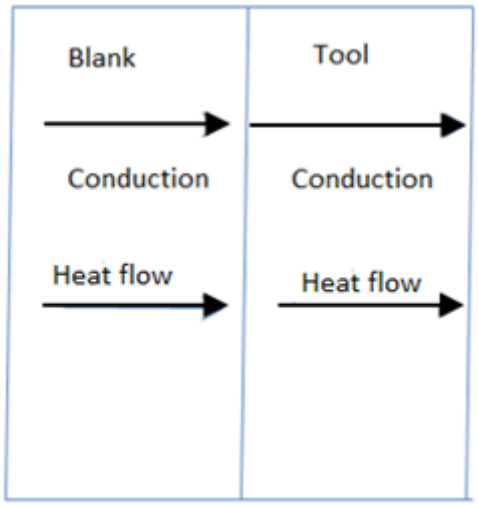


Figure 2-4: Heat transfer between blank and tool

Using Fourier's law of heat conducting, the heat transferred to the tool can be explained by Equation 2-8 (Li *et al.*, 2015; Shi *et al.*, 2013):

$$\frac{\partial}{\partial x}\left(\lambda_s \frac{\partial T}{\partial x}\right) + \frac{\partial}{\partial y}\left(\lambda_s \frac{\partial T}{\partial y}\right) + \frac{\partial}{\partial z}\left(\lambda_s \frac{\partial T}{\partial z}\right) + q_v = \rho C_b \frac{\partial T}{\partial t} \qquad 2\text{-}8$$

Equation 2-9 can be further simplified as shown:

$$\lambda_s\left(\frac{\partial^2 T_d}{\partial x^2}+\frac{\partial^2 T_d}{\partial y^2}+\frac{\partial^2 T_d}{\partial z^2}\right)+q_v=\rho C_b\frac{\partial T_b}{\partial t} \quad 2\text{-}9$$

The exchange of heat between blank and tool can be summarised using Equation 2-10 (Li *et al.*, 2015):

$$-\lambda_s\frac{\partial T}{\partial n}=R(T_b-T_d) \quad 2\text{-}10$$

The interfacial heat transfer can be regarded as equivalent to the change in internal energy according to the heat balance method as shown in Equation 2-11. The amount of heat that is transferred between the tool and blank depends on the interfacial heat transfer coefficient (*R*) at the blank die interface (Caron *et al.*, 2014):

$$AR(T_b-T_d)=\rho V C_b\frac{dT}{dt} \quad 2\text{-}11$$

The surface topography has an effect on the overall contact surface area thus the quantity of heat transfer is affected as shown in Figure 2-5 (Liu *et al.*, 2013; Zhao *et al.*, 2015; Kim *et al.*, 2015; Ji *et al.*, 2015):

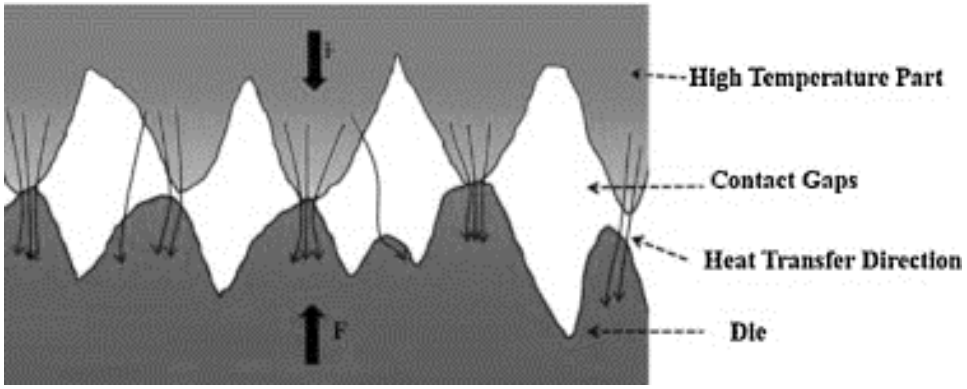


Figure 2-5: Surface topography at the blank and die interface (Chang *et al.*, 2016)

Other parameters affecting R include temperature, contact pressure and scaling factors (Chang *et al.*, 2016; Ikeuchi and Yanagimoto, 2011; Hu *et al.*, 2013; Altan and Tekkaya, 2012). The resultant microstructure of the blank is highly influenced by the value of *R.* which is a critical parameter for measuring the heat transfer efficiency of the tool. The heat transferred from the coolant to the blank can be expressed using Equation 2-12 (Ying and Zhong-De, 2014; Muvunzi *et al.*, 2017):

$$Q=h_w A_c(T_c-T_w) \quad 2\text{-}12$$

## 2.4. Challenges of Hot Stamping Tools

The hot stamping tool has two major functions; namely to form the blank to the required geometry and to extract heat from the blank (Altan and Tekkaya, 2012). Typical examples of tool steels currently in use include X38CrMoV5, X40CrMoV5 and X15CrMoV12 (Escher and Wilzer, 2015). The tool is composed of a punch, counterpunch, die and blank holder as shown in Figure 2-6

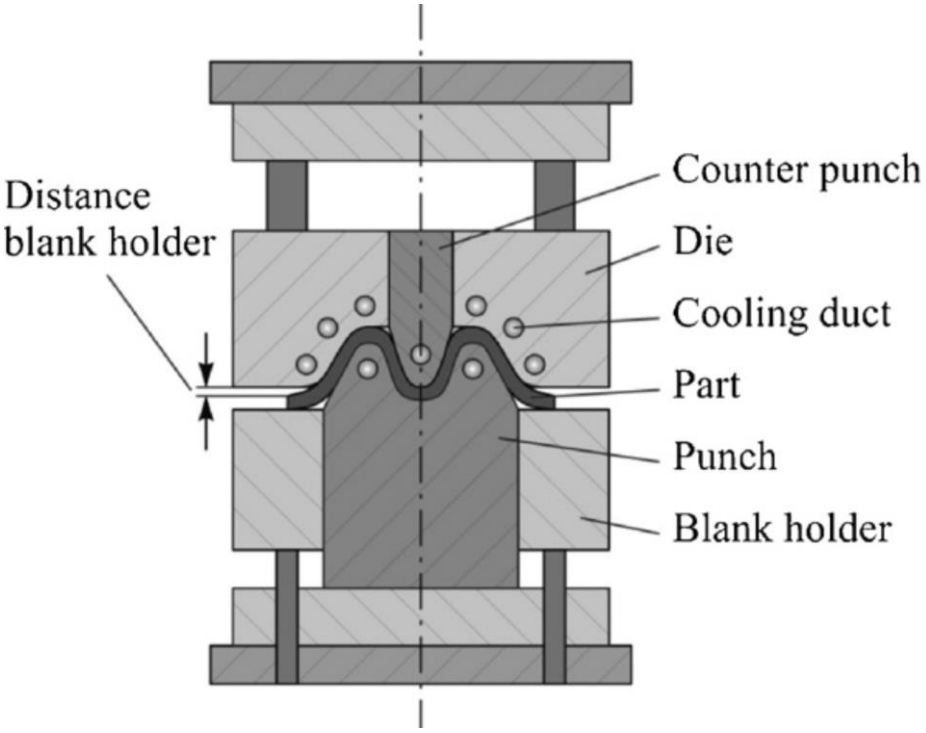


Figure 2-6: Hot stamping tool (Karbasian and Tekkaya, 2010)

The tools have a network of cooling channels to allow the coolant to circulate and extract heat. The heated blank should be uniformly cooled at a rate (27 °C/s for 22MnB5 blanks) that facilitates the transformation to the required martensitic structure (Steinbeiss *et al*., 2007). The rate of heat transfer from the blank determines the cooling time. According to Mueller (2013), at least 30 % of the cycle time is spent on the cooling stage. Hence it is necessary to devise ways of reducing cooling time through increasing the heat extraction of the coolant. During mass production, the tools are continuously exposed to the hot blanks and this causes them to rise in temperature. This leads to thermal softening of the tool surface, making it vulnerable to increased adhesive wear (Ye *et al.*, 2013). A rise in tool temperature also compromises the quality of the formed parts because it makes the tool unable to cool off the blanks at the required minimum cooling rate (27 °C/s) which in turn facilitates the required microstructural transformation (Lim *et al.*, 2014). According to Schieck *et al.* (2011), there are three methods of producing cooling systems; these include drilling channels, inserting tubes prior to casting and the use of shell structures. The most commonly used method in industry is drilling channels. Thus, the study focuses on this current practice. Due to machining

restrictions, it is difficult to drill channels which conform to the part geometry and at the same time maintain a constant distance from the tool surface to the cooling channels. Also, it is difficult to evenly distribute the channels throughout the tool and access all critical hotspots. This leads to inconsistent cooling which may cause thermal stresses, cracks, reduction of tool life and high tool maintenance costs (Boher *et al.*, 2012). Furthermore, if the blanks are not evenly cooled, defects associated with non-uniform cooling (distortions) tend to increase (Lim *et al.*, 2014). For the casting method, it is difficult to position the tubes in the moulds and there is the risk that the tubes may melt during pouring of the molten metal. Also, air bubbles can form during casting and this affects the heat transfer. Another challenge is that the channels could distort during the casting process and this will affect the flow of coolant in the tools (Altan and Tekkaya, 2012). The other method involves dividing the tool into the upper shell and core to improve flexibility. This method involves intensive machining and the tool may be prone to leakages (Escher and Wilzer, 2015).

The hot stamping tools should be able to withstand high thermal and mechanical stresses encountered during the forming and quenching process. Hence it is a requirement for the tools to have a high heat transfer capability which is necessary for reduction of cycle time, improved quality and reduction in tool maintenance and replacement costs. Thus, the study seeks to improve the cooling performance using AM. The next section sheds more light on the previous studies on the application of AM to improve the cooling capability of hot stamping tools.

## 2.5. Previous Studies on AM Based Conformal Cooling Channels in Hot Stamping Tools

Only a few authors in literature have investigated the application of AM in the construction of conformal cooling channels for hot stamping tools. For example, Cortina (2018), investigated the impact of AM based conformal cooling channels on a demonstrator tool insert as shown in Figure 2-7. In the study, a base body of CRV-L tool steel material was machined and AISI H13 tool steel powder was deposited using Direct Metal Deposition (DMD) to create the conformal cooling channel. The thermal performance of the built tool was then compared with the conventional tool using Finite Element simulation. The results of the simulation showed that the maximum temperature of the conformable tool was 43, 6 °C less and it had a more uniform distribution compared to the conventional tool (Cortina *et al.*, 2018). No physical hot stamping tests were conducted. Instead, a series of compression tests were done to test the strength of tools. There were no cracks or distortion in the deposited portion of the build tool, thus, showing that tools manufactured with DMD can have mechanical properties which are comparable with conventionally manufactured tools. However, the study was focused on a small tool insert with a single cooling channel. Thus, it could not provide

information on the parametric design of a standard hot stamping tool with many cooling channels. Also, the study was mainly focused on the tool, and information on the effect of the conformable tool on cycle time and blank quality, was not provided.

Figure 2-7: Punch with a conformal cooling channel (Cortina *et al.*, 2018)

Another study aimed at highlighting the impact of AM based conformal cooling channels on hot stamping tools, was done by Gebauer *et al.*, (2016). In the study, conformal cooling channels were produced for a hot forming gear pan tool shown in Figure 2-8. The gear pan's complex geometry did not allow for straight drilling of cooling channels. As a result, the tool was exposed to severe thermomechanical wear and some of the formed parts had undesirable non-uniform hardness distribution and distortions (Gebauer *et al.*, 2016). To create the optimized tool using hybrid manufacturing, a base body was firstly machined and the portion with the conformal cooling channels was printed on top using Selective Laser Melting (SLM). Materials used for the base and built sections were tool steel 1.2343 and 1.2709 respectively. According to the results, a 70 % reduction in cooling time was achieved (Gebauer *et al.*, 2016). Also, the formed components had the desired dimensional accuracy. Thus, it was proven that SLM is a suitable process for manufacturing hot forming tools with intricate geometry and allows a reduction in cycle time. In the study, a series of thermal and mechanical simulations were done to identify the most suitable cooling parameters for the part. However, the information on the structural parameters used, was not provided. Thus, there is a need for more research in this area.

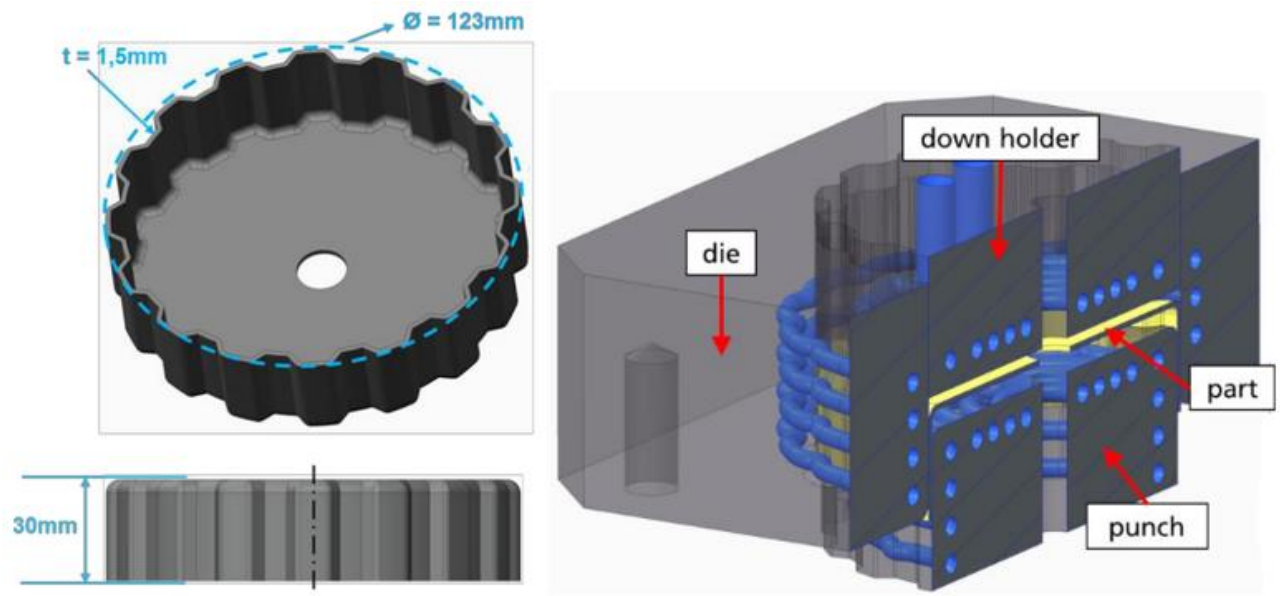


Figure 2-8: Gear pan tool with conformal cooling channels (Gebauer *et al.*, 2016)

Mueller *et al.* (2014) studied the effect of a hot stamping tool insert with an optimized cooling structure manufactured using SLM on the hot stamping process. A typical hot stamped part was used as a case study. To illustrate the impact of the optimized cooling system, the corresponding tool geometry was composed of curves and cavities which are difficult for straight cooling channels to access, thus revealing the limitations of the conventional cooling system design. The design of the optimized cooling structure was based on the results obtained from the Finite Element simulation runs. According to the simulation, a 45 % reduction in cooling time could be achieved. Hybrid tooling was used to construct the tool insert as a measure to reduce costs. This involved using the usual conventional (turning, milling and drilling) methods to construct the lower part of the tool and SLM to build the upper section with the optimised cooling channels This was followed by heat treatment in order to allow hardening and stress relief of the tool insert. A series of hot stamping runs were conducted using the tool insert under conditions similar to those in the actual production. The results of the study revealed a 50 % reduction in cooling time which translated to a reduction in the overall cycle time by 20 %. Figure 2-9 shows the layout for the conventional and optimised cooling system. However, information on the cooling system design was not provided.

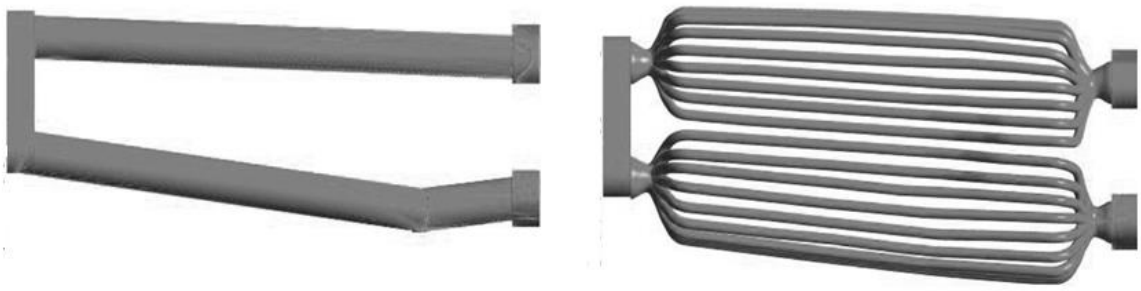

Figure 2-9: Conventional (left) and conformal optimised cooling layout of the case study part (Mueller *et al.*, 2014)

## 2.6. Previous Methods Used to Improve Cooling System Performance

Since the aim of the study is to improve cooling capability of hot stamping tools, it is important to investigate previous studies of this subject. These include models for cooling system design, use of optimisation algorithms and other manufacturing processes. The following section discusses each of these methods.

### 2.6.1. Mathematical models for improved cooling system design

In industry, the design of cooling systems is mainly done based on experience (Lv *et al.*, 2016). So far, some researchers have developed automatic computer aided design (CAD) software to aid in the design process (Xian and Wang, 2014; Kim *et al.*, 2018). However, there is no standard practice in literature for determining cooling system parameters. On the other hand, some researchers have proposed mathematical models for effective cooling system design to improve the heat transfer rate between the hot blank and the tools. The structural parameters are shown in Figure 2-10. The parameters *d*, *z* and *y* represent the diameter of the cooling channels, the minimum distance from tool surface to cooling channel circumference and the minimum distance between cooling channels respectively (Ying and Zhong-De, 2014).

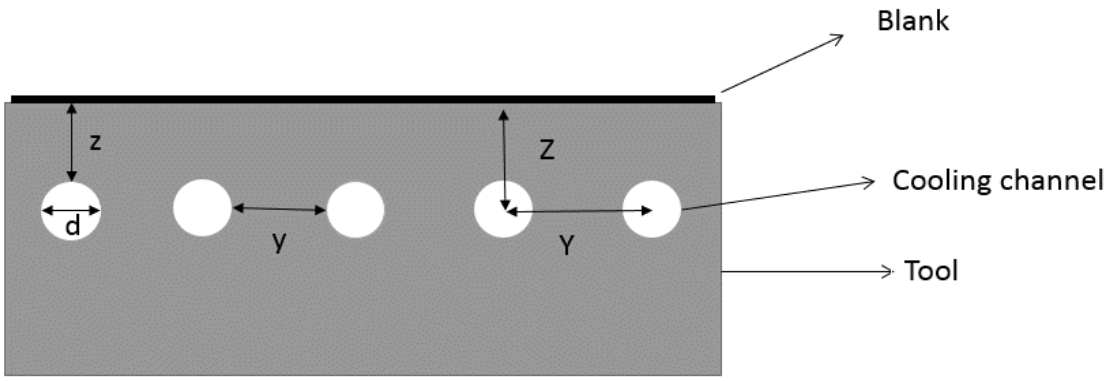


Figure 2-10: Cooling system parameters

As a general rule, the drilling of the cooling channels should depend on the allowable stress of the tool material (Lim *et al*., 2014). Furthermore, the cooling channels should be structured in such a way that the tool retains sufficient strength to conduct the stamping operation (Lei *et al.*, 2012). The lesser the distance between the cooling channels, the better the cooling effect (Lim *et al.*, 2014). Results from literature show that decreasing *d* and reducing *z* increases the cooling rate while reducing y increases the cooling uniformity (Zhong-de *et al.*, 2010; Jiang *et al.*, 2018).

Different assumptions were used in formulating the models and most of them are difficult to apply in real life. Although the models provide a guideline on the arrangement of the channels, machining restrictions remain a major challenge for tools with complex geometry since the cooling channels do not conform to the shape of the tool. On the other hand, the models can be useful in providing design guidelines for both straight and conformal cooling channels. Thus, the study sought to discover a way of designing cooling channels with parameters that facilitate effective cooling, at the same time allowing the channels to conform to the geometry of the part. In the following section, each of the models is reviewed.

Hung *et al.* (2019), used fractional factorial simulation experiments on a flat tool to develop empirical equations for the effect of different cooling system parameters on the cooling system performance. In the study, the empirical equations were obtained using regression analysis and validated using physical experiments (Hung *et al.*, 2019). The results of the study showed that the simulation results were very similar to those from physical experiments. Thus, the empirical equations were useful in obtaining optimum cooling system parameters for the tools. However, the limitation of the study is that the distance between consecutive cooling channel centres (*Y*) was not considered in the analysis. For the structural parameters, the parameters considered were the diameter, distance from tool surface to cooling channels and distance between cooling channels and outer edges. Also, the models were developed based on the technical limitations of the drilling method. However, in this study, the

cooling system design model was developed taking into consideration the design flexibility of the AM process.

Chen *et al.* (2019), developed a parameter window for designing cooling channels based on heat transfer theory and finite element simulation. In the study, the technical limitations of the drilling method were also used to establish the parameter window. For example, the minimum distance *z* used for the analysis is 10 mm and a *y/d* ratio between 1 and 2 to avoid deformation and cracking of the channels during drilling. The parameter window was aimed at fulfilling the quality requirements of attaining high cooling rate (55 °C/s) and low-temperature deviation (≤±5 °C) after cooling (Chen *et al.*, 2019). The experimental results showed that the parameter window was able to fulfil the quality requirements in terms of the cooling performance and is useful when determining effective parameters using the drilling method. However, for the AM based cooling channels, there is a need to consider the technical limitations of the AM technology.

Xie *et al.* (2018) used a multi-objective reliability optimization to determine the most effective cooling system design parameters for increasing cooling effectiveness and strength of the tool. It was assumed that the heat loss to the environment is negligible. Thus, the heat lost by the blank was regarded as equal to the heat absorbed by the coolant as shown in Equation 2-13 (Xie *et al.*, 2018):.

$$\mathrm{Q} = \mathrm{C}_w \rho_w v_w (\mathrm{n}\pi \mathrm{r}^2 t)\Delta T_w \qquad 2\text{-}13$$

Thus, the radius for the cooling channels was calculated using Equation 2-14 (Xie *et al.*, 2018).

$$r \geq \sqrt{\frac{Q}{n\pi \mathrm{C}_w \rho_w v_w t \Delta T_w}} \qquad 2\text{-}14$$

This was followed by a mechanical analysis to determine the distances *y* and *z* based on Equation 2-15 (Xie *et al.*, 2018).

$$y \geq \frac{2F}{\sigma_m A - F} r \qquad 2\text{-}15$$

$$z \geq \left( \frac{1}{\sigma_m A - F} \sqrt{\frac{3\sigma_m A F}{L} - 1} \right) r \qquad 2\text{-}16$$

A multi-objective particle optimization (MOPSO) algorithm was then used to obtain the optimum combination of parameters ($z$ = 9.92, $y$ = 8.58, d = 8). A series of microstructural and hardness tests

performed on the formed part proved that the part had the required hardness and martensitic microstructure.

According to the model developed by Ying and Zhong-de (2014), the amount of heat transferred from the tool surface to the cooling channels is determined using the shape factor analysis (Hagen, 1999). This is shown in Equation 2-17.

$$Q = k_d f_1 (T_d - T_{cw}) \quad 2\text{-}17$$

It was assumed that the surface of the tool die is flat. This assumption may not hold in cases where the tools have complex geometric features. The shape factor $f_1$ was defined using Equation 2-18 (Hagen, 1999).

$$f_1 = \frac{2\pi l}{ln\left[\left(\frac{2Y}{\pi d}\right) sin\left(\frac{2\pi Z}{Y}\right)\right]} \quad 2\text{-}18$$

Substituting equation 2-18 into 2-17 results in the following;

$$Q = \frac{2\pi l k_d (T_d - T_{cw})}{ln\left[\left(\frac{2Y}{\pi d}\right) sin\left(\frac{2\pi Z}{Y}\right)\right]} \quad 2\text{-}19$$

Making *Z* the subject of the equation results in (Ying and Zhong-De 2014);

$$Z = \frac{Y}{2\pi} sin^{-1}\left[\frac{\pi d}{2Y} * e^{\frac{2\pi l k_d (T_d - T_{cw})}{Q}}\right] \quad 2\text{-}20$$

The distance from the die surface to the cooling channel centre *(Z)* and the centre distance between channels (Y) are defined by Equation 2-21 and 2-22.

$$Z = z + \frac{d}{2} \quad 2\text{-}21$$

$$Y = y + d \quad 2\text{-}22$$

Substituting Equation 2-21 and 2-22 into 2-20 and making *z* the subject gives (Ying and Zhong-De 2014);

$$z = \frac{\frac{(y+d)}{d} sin^{-1}\left[\frac{\pi d}{2(y+d)} * e^{\frac{2\pi l k_d (T_d - T_{cw})}{Q}} - \pi\right]}{2\pi} \quad 2\text{-}23$$

To obtain the diameter, a quantity $d_{cw}$ was defined as the cross-sectional diameter of all cooling channels which can be calculated as shown in Equation 2-24 (Ying and Zhong-De 2014).

$$d_{cw} = \sqrt{\frac{4Q}{C_{pw}\rho_o \pi v (T_{out} - T_{in})}} \quad 2\text{-}24$$

The diameter of a single channel was obtained by using Equation 2-25 (Ying and Zhong-De, 2014).

$$d = \frac{d_{cw}}{\sqrt{n}} \quad 2\text{-}25$$

The model was used in determining the optimum cooling channel parameters required for a hot stamping die. Finite Element simulation of the forming process was then conducted using Pam-stamp software (Lim *et al.*, 2014). The blank material was 22MnB5 with a thickness of 3 mm and an initial temperature of 810 K. The cooling rate obtained using the tool with the improved cooling system was 30 °C/s and the final blank temperature was 210 °C. The limitation associated with the developed model is that it is biased towards thermal analysis. The authors did not consider the strength requirements of the tools after drilling the cooling channels. This might have negative implications for the tool life because drilling intensifies the stresses in the tool structure. The method is also difficult to apply in real life because of the intensive machining involved in order to maintain the geometrical requirements.

Another proposed model is based on the assumption that all the heat lost by the blank is transferred to the coolant in the channels (Lim *et al.*,2014). The cooling channel diameter is selected based on the thickness of the blank as shown in Table 2.3. The selection criteria were established by an experimental study done by Lin and Chou (2002).

Table 2.3: Blank thickness and cooling channel diameter range (Lin and Chou, 2002)

| **Blank thickness, s (mm)** | **Cooling channel diameter, d (mm)** |
|---|---|
| $s \leq 2$ | $8 \leq d \leq 10$ |
| $2 < s \leq 4$ | $10 \leq d \leq 12$ |
| $4 < s \leq 6$ | $12 \leq d \leq 14$ |

The selection method in Table 2.3 was developed based on experiments conducted with injection moulding tools. When it comes to hot sheet metal forming, the process requirements and materials are different, hence the method might need to be revised. According to the model, Z (distance from the die surface to cooling channel centre), is determined using Equation 2-26 and *y* depends on the maximum yield stress of the die material (Lim *et al.*, 2014).

$$Z = k_d \left[ \frac{A_{cw}(T_d - T_w)}{W.C_b(T_{b_o} - T_{b_i})} - \frac{1}{h_w} \right] \quad 2\text{-}26$$

Straight drilling was used to obtain the channels. In order to increase the number of channels, the tool was split into sections using the triangular method. The model was used to determine optimum cooling channel parameters on a die for making a roof sidecar component using 3 mm 22MnB5 steel. One of the tools had a minimum number of cooling channels to reduce costs; this resulted in a cooling rate of 52.8 °C/s. The other tool had the maximum number of cooling channels; it resulted in a cooling rate of 70 °C/s and a reduction in cooling time by 3s. The cooling rate achieved by both tools is above the minimum cooling rate of 27 °C/s. Hence, applying the model caused an improvement in the cooling system performance.

According to another model developed by Zhong-de *et al*. (2010), the cross-sectional radius ($r_c$) is obtained using equation 2-27 (Ying and Zhong-De, 2014).

$$r_c = \sqrt{\frac{Q_5}{C_w \rho_w \pi v (T_{out} - T_{in})}} \quad 2\text{-}27$$

The radius of a single channel is then calculated using Equation 2-28.

$$r = \frac{r_c}{\sqrt{n}} \quad 2\text{-}28$$

This is similar to equation 2-24. The model was developed to fulfil the deformation requirements of the tool material. According to Zhong-de *et al*. (2010), the cooling channels must be structured such that the resultant bending stress does not exceed the maximum yield stress of the tool material. The acceptable ranges for cooling channel parameters were determined using this principle. In the study, simulation trials were done to rank the cooling channel parameters in terms of their influence on the final blank temperature. The results showed that *z* is the most influencing parameter followed by *y* and *d* respectively. Hardness, tensile strength and elongation tests were conducted on samples from the formed part. The results of the study showed that average hardness, tensile strength, and elongation for the three samples were 1053 MPa, 1563 MPa, and 6 % respectively (Ying and Zhong-De, 2014).

Another model was developed by Lv *et al.*,(2016). According to the model, the diameter was selected based on heat transfer analysis. This was achieved by calculating the minimum mass of water required for a cooling cycle which was expressed using Equation 2-29. The quantities $T_{W_1}$ and $T_{W_2}$ represent the inlet and outlet water temperatures in the cooling system,

$$m_w = \frac{Q_w}{C_w(T_{W_2} - T_{W_1})} \quad 2\text{-}29$$

The mass of the coolant was also expressed using Equation 2-30:

$$m_w = \frac{\pi}{4} n d^2 v t_c \rho_w \quad 2\text{-}30$$

Substituting Equation 2-29 into 2-30 resulted in the following:

$$\frac{\pi}{4} n d^2 v t_c \rho_w = \frac{Q_w}{C_w(T_{W_2} - T_{W_1})} \quad 2\text{-}31$$

The area covered by the channels was derived using equation 2-32:

$$A_c = n\pi d l_w \quad 2\text{-}32$$

Thus, the diameter of the channels was expressed using equation 2-33:

$$d = \frac{4 Q_w l_w}{C_w v t_c \rho_w (T_{W_2} - T_{W_1}) A_c} \quad 2\text{-}33$$

In the study, the stress factor diagram proposed by Lim *et al.*,(2014) was used in calculating the minimum distance between cooling channels. The model was used to calculate the cooling system parameters for a hot stamping tool and a series of Finite Element analysis simulations were conducted on the tool. According to the simulation results, the cooling rate of the blank was above the required 27K/s and the structural strength of the tool was within the safe range. Thus, the designed cooling system fulfilled the cooling system requirements. The authors highlighted that the cooling system layout can be further improved by arranging the cooling channels based on the cooling degree of the different portions of the tool.

### 2.6.2. Critical Analysis of the mathematical models

The models developed by Hung *et al.* (2019) and Chen *et al.* (2019) can be very useful in the design and manufacture of hot stamping tools with drilled cooling channels. This is because they were both validated using simulation and physical experiments. Secondly, they both caused the tool to meet the required cooling efficiency and strength requirements. However, they were both developed considering the restrictions of the drilling method and might not necessarily be applicable for the AM based conformal cooling system design. The mechanical analysis method used by Xie *et al.* (2018) is useful in relating the stamping force to the safe range of cooling system parameters. Thus, it can be applied in the design of both straight drilled and conformal cooling channels to identify parameters which do not compromise tool structural strength.

The cooling channel parameters determined by using the model developed by Ying and Zhong-de (2014) were able to meet the cooling requirements of the hot stamping dies. This is evident from the cooling rates achieved using the cooling channel parameters which are above the 27 K/s for martensitic transformation (Karbasian and Tekkaya, 2010). Furthermore, a final tool temperature of 210 °C/s was attained. The model seems to be relatively easier to apply when compared to other models. However, the model does incorporate the strength requirements of the tool as the die must retain adequate strength after drilling of the channels. When the model was formulated, it was assumed that the contact resistance between the blank and die is zero. This may not be possible because the contact resistance is affected by the surface roughness of die and the contact pressure (Caron *et al.*, 2014)

When Lim *et al.* (2014) formulated their model, deformation requirements of the tool material were considered. Thus, longer service life of the tools is expected. Another advantage is that the validation of the model was done by measuring the quality of the formed part. To test uniformity, three samples taken from the formed part were tested for hardness, strength, elongation and microstructural transformation. The results indicated that the part had an average tensile strength above 1500 MPa, yield strength above 1000 MPa, elongation above 6 % and a full martensitic transformation. However, the effect of cycle time was not mentioned.

The cooling channel parameters obtained using the model developed by Lim *et al.* (2014) were validated in terms of cooling performance and quality of the formed parts. Two designs were validated; one of the designs had the minimum number of cooling channels to reduce the costs of making the tool. The other design had the maximum number of cooling channels to reduce cycle time. When both designs were tested on a hot stamping tool, the formed parts were above 1500 MPa. Another advantage of the model is that it caters for the strength requirements of the tool. The challenge of the model is in the procedure used to select the cooling channel diameter which was developed for injection moulding tools. It may be necessary to revisit the procedure when it comes to hot stamping since the process and material parameters are different.

Lv *et al.* (2016) developed a model which is almost similar to the one proposed by Lim *et al.* (2014). The differences between the two models are that Lv *et al.* (2016) introduced a parameter for the thermal efficiency of the tool, thus indicating that not all the heat lost by the blank is directly absorbed by the coolant. Another difference is that the diameter of the tool was derived from heat transfer principles. However, in both cases, they used stress factor analysis in order to meet the structural strength requirements. The major limitation of the model developed by Lv *et al.* (2016) is that it merely gives a range for the possible distances *z*, thus it is necessary to select the optimum parameters through simulation or further calculations. However, all the calculated ranges resulted in the

production of parts with the required quality characteristics and strength requirements. The authors recommended that the cooling channels should be arranged based on the cooling degree of the proportions of the tool. They also concluded that smaller cooling channels increase the cooling uniformity of the parts.

Table 2.4: Comparison of proposed mathematical models for straight drilled cooling system design in literature

| **Authors** | **Model formulation** | **Mechanical analysis of the tool allowable stress** | **Methods used to evaluate the model** | **Parameters used** | **Impact of model** |
|---|---|---|---|---|---|
| Hung *et al.* (2019) | Empirical equations for determining the effect of structural parameters on cooling system performance. Equations formulated using experiments and regression analysis | No mechanical analysis was done to fulfil tool deformation requirements | An evaluation was done using finite element analysis and experiments using a flat hot stamping tool | $d$ = 10 mm, Z=32 mm, Y= 28 mm | Cooling rates of up to 86 °C/s |
| Chen *et al.* (2019) | Parameter window developed based on heat transfer analysis and technical limitations of the drilling method | No mechanical analysis was done to fulfil tool deformation requirements | Finite element simulation | $d$ = 10-12 mm, Z=16-17 mm, $\frac{y}{d}$= 1-2 | Cooling rates above 55 °C/s and a final blank temperature deviation of 7 °C |
| Xie *et al.* (2018) | The energy balance principle and mechanical analysis were used to develop equations for determining possible parameter combinations. Optimum parameters obtained using multi- | Mechanical analysis was done by taking the cooling channels as a beam under applied load | Finite element analysis Simulation and experimentation | $d$ = 8 mm, Z=12.58 mm, Y= 15.92 mm | Average stress of tool reduced by 19.6 % and average blank temperature reduced by 6.4 % |

| | | | | | |
|---|---|---|---|---|---|
| | objective reliability-based optimization | | | | |
| Lv *et al.* (2016) | Used heat transfer analysis equations and a stress factor model proposed by Lim *et al.* (2014) to develop suitable parameter combinations | The mechanical analysis was done using stress factor analysis | Finite Element Simulation and Experimentation | *d* = 8 mm, Z=1.25d to 1d, Y not given | Increased cooling uniformity. Final blank strength and hardness of 1 502 MPa and 507. 7 HV |
| Lim *et al.* (2014) | Heat transfer analysis used to develop equations for designing the cooling system. A stress factor model developed for identifying parameters which preserve the tool structural strength | The mechanical analysis was done using stress factor analysis | Finite Element Simulation and Experimentation. | Y = 17mm, d = 10 mm and Z=13mm | Cooling rates of 58 °C/s and 70 °C/s |
| Zhong-de *et al.* (2010) | Use of the heat balance theory to formulate equations for cooling system design | No mechanical analysis was done on the tool | Finite Element Simulation | | Cooling rates above 30 °C/s and martensitic transformation above 93 % |

The first objective of the research is to determine the parameters for effective thermal management of hot stamping tools. The quantities *d*, *y*, and *z* are part of the crucial parameters affecting heat transfer in hot stamping tools. Hence it is necessary to use an appropriate method for determining the parameters. Table 2.4 gives a detailed comparison of the models.

According to the analysis, the models developed by Lim *et al.* (2014) and Lv *et al.* (2016) had the highest cooling performance. In both cases, the structural requirements of the tool were considered. On the other hand, both models have their limitations and there is room for improvement. Since the study is focused on AM application, there is a need to devise a cooling system design method suited for the application, taking into consideration the technical limitations of the AM processes.

### 2.6.3. Optimisation methods

Although the mathematical models mentioned previously can be utilized in identifying structural cooling channel parameters for effective cooling, the challenge lies in the drilling of the channels to ensure that the parameters are maintained. Mathematical models are cost-effective and relatively easier to use when compared to other optimization methods which involve a lot of finite element simulations and iterations. On the other hand, iterations can be useful when comparing different possible solutions. The following section focuses on the different optimisation methods for cooling system design.

Lee *et al.* (2018) developed a sliced die for improving cooling system design in hot stamping tools. The sliced tool was composed of divided tool pieces which were joined together. For each piece, half of a cooling channel conforming to the part geometry was machined on each side as seen in Figure 2-11. A constant distance between the tool surface and the cooling channels was maintained.

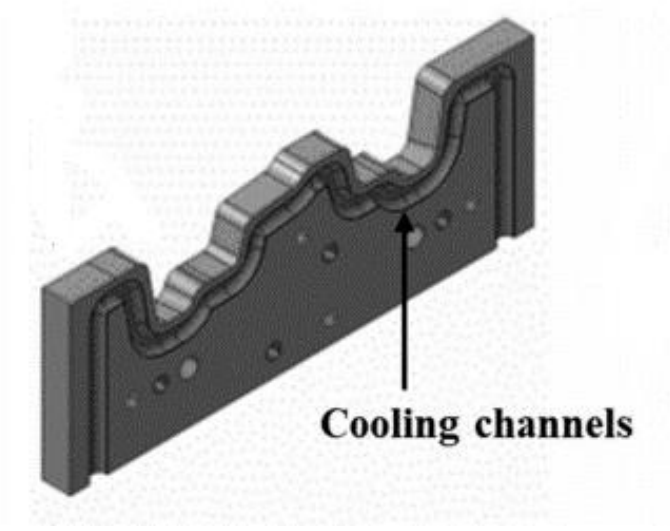


Figure 2-11: Slice with machined conformal cooling channels (Lee *et al.*, 2018)

The slices were joined to allow the coolant to enter the tool through two separate entrance and exit points at shorter travel distance for more effective cooling. This is different from the conventional tool which had only one inlet and outlet points (Lee *et al.*, 2018). According to the experimental results, the sliced die and conventional die had average cooling rates of 67 °C/s and 57 °C/s respectively. Also, the maximum temperature after the cooling phase of the blank was 150 °C for the conventional tool and 70 °C for the sliced die. Thus, the sliced tool had a higher cooling performance compared to the conventional tool. However, the time and costs involved in machining and design of the die slices could be of great concern.

Quan *et al.* (2016) used the Multi-Objective Particle Swarm Optimization (MOPSO) method to optimize the cooling system structural parameters. The optimized solution resulted in a cooling rate of up to 42 K/s. A series of hot stamping experiments confirmed the results from the FE simulation. Although a higher cooling rate was achieved, the procedure was intensive and time-consuming considering the number of test points used in the experiments.

Another optimization method was proposed by He *et al.* (2016). The difference between the evaluation of the method and others mentioned in literature is that it involved the application of longitudinal conformal cooling channels. Straight channels were used for evaluating other optimization methods. According to the study, the cooling system structural parameters were optimized based on the response surface and the multi-objective optimization methods. The Optimum Latin Hypercube method was used to devise a design matrix with 17 factors and 50 levels. Evaluation of the different cooling system designs was done based on the average temperature and the difference between the maximum and minimum temperature of the tool surface using FE simulation. The challenge with this method is that it is computationally intensive because of the large number of simulation trials involved. After the simulation trials, the tool was built using the method shown in Figure 2-12

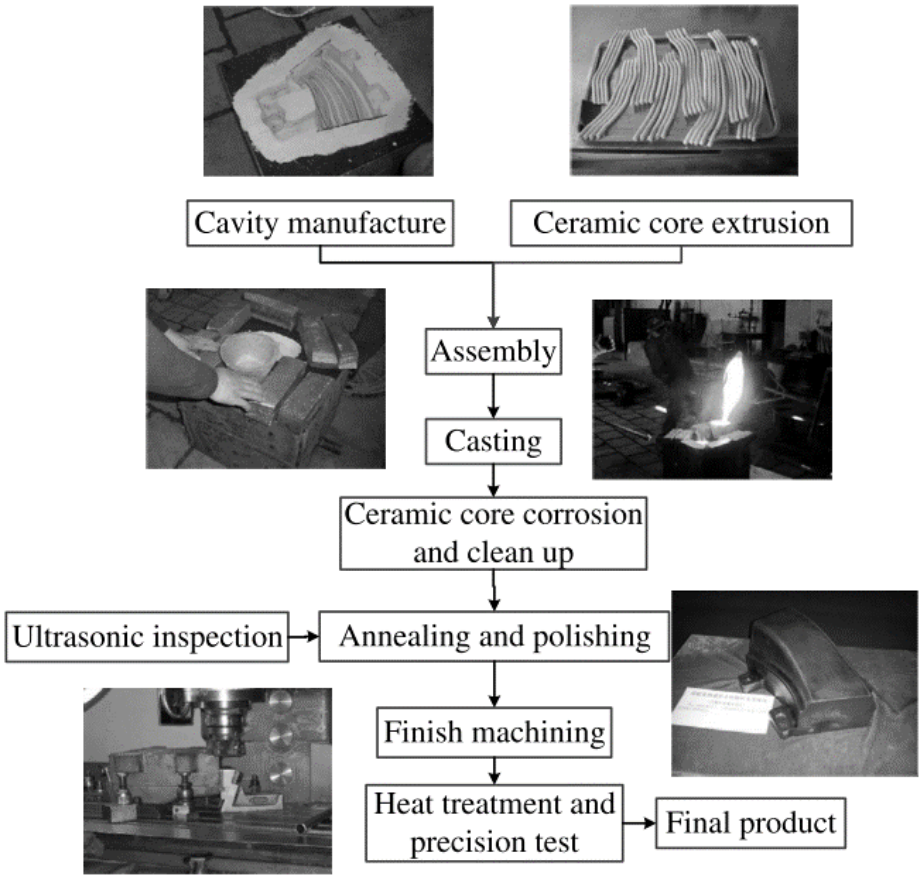


Figure 2-12: Process chain for the tool insert ( He *et al.*, 2016)

The tool inserts, together with the optimized cooling system, led to a reduction in the average tool temperature by 11.7 % and a reduction in the temperature deviation on the tool surface by 28.2 %.

Zamari and Yussof (2015) used Heuristic and Taguchi optimization methods to determine optimum cooling system parameters. They replicated laboratory experiments for analysing the cooling performance of the tools by using Finite Element simulation.

On the other hand, the limitation of the study is that a restricted range of parameters was considered for optimization. Different results might have been obtained if the parameter range had been increased. Another challenge with the study is that no comparison with the previous cooling system design was indicated.

Hot stamping experiments were conducted on both tools and their performance was evaluated. According to the results, the tool for the square box part led to a cooling rate of 40 °C/s which is above the minimum cooling rate (27 °C/s). On the other hand, the temperature of the B-pillar tool was not recorded during the experiments because it was difficult to insert sensors inside the tool. To prove the cooling effectiveness of the optimised cooling structure, tensile strength measurements were conducted. The formed B-pillar had a tensile strength of 1387 and 1587 MPa using coolant flow

rates of 1 and 3 m/s respectively. Thus, the high cooling performance was achieved. A major conclusion that can be derived from this study is that straight cooling channels have the same major effect as conformal cooling channels for the same layout. Liu *et al.*,(2013) used an evolutionary algorithm proposed by Steinbeiss (2007) to optimize the cooling system structural parameters for two sets of tools. One of the tools was for producing a square box part of a car body structure. As a result of the simplicity of the tool geometry for the square box part, straight drilled channels were used for the cooling system. The other tool was used to produce a B-pillar; thus, it had a complex geometry. The authors made use of the so-called pre-embedding method to create cooling channels which conformed to the shape of the part. This involved inserting curved pipes in a sand mould prior to casting as shown in Figure 2-13. Although the pre-embedding method led to higher cooling performance, there are challenges involved. Placement and positioning of the pipes in the sand mould are very difficult tasks. Also, there is a high chance that the pipes could melt during pouring of the metal (Escher and Wilzer, 2015). Furthermore, there is the risk that the cooling channels could collapse, thereby distorting the cooling channels.

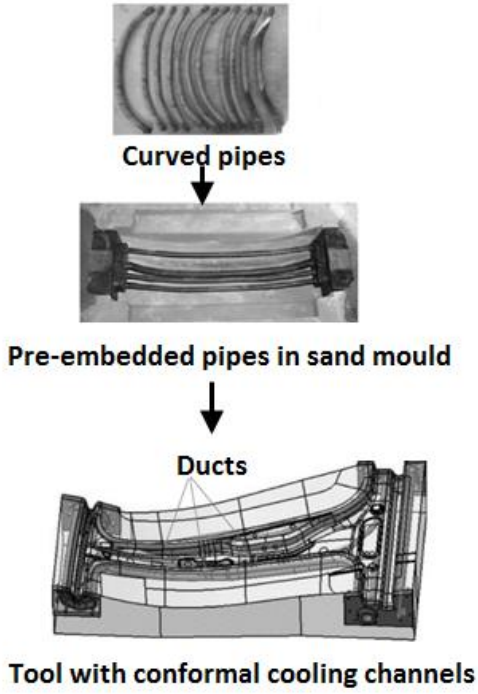


Figure 2-13: Pre-embedding method (Liu *et al.*, 2013)

Steinbeiss *et al*. (2007) proposed an evolutionary algorithm which generates possible cooling channel parameters, depending on the geometry of the component to be formed (Steinbeiss *et al*., 2007). The optimum parameters are selected based on their cooling ability. Figure 2-14 explains the algorithm.

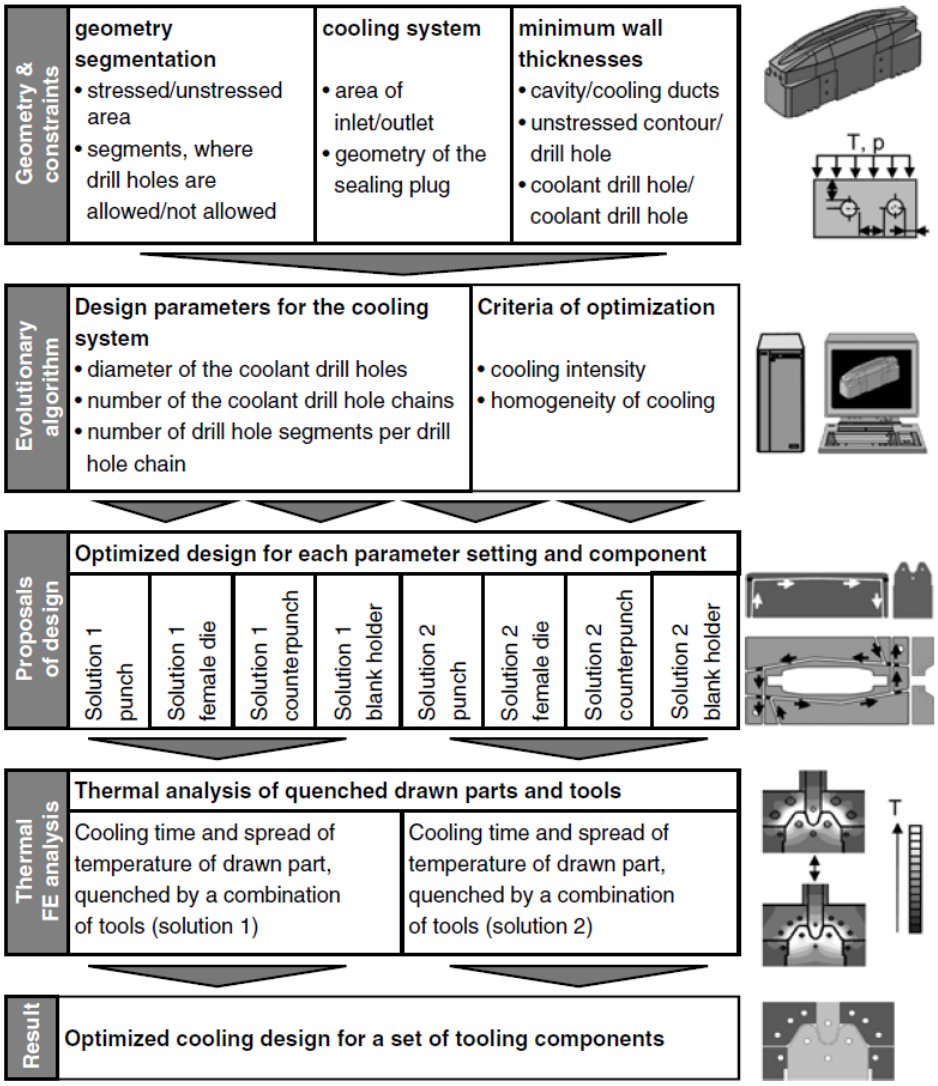


Figure 2-14: Procedure for the evolutionary algorithm (Lam *et al.*, 2004)

The algorithm was used in designing the cooling system for a hot stamping tool made with 1.2379 tool steel. The tool is used for forming 22MnB5 blanks using Finite Element Simulation (Steinbeiss *et al.*, 2007). Cooling channel diameters of 8 to 16 mm were used to form the 1.75 mm thick blanks. When a diameter of 8 mm was used, a cooling time of 19.2 s was attained. Diameters of 10-16 mm resulted in a cooling time of 20.1 s. The challenge with the algorithm is that it involves a lot of iterations and this can be very costly and time-consuming (Steinbeiss *et al.*, 2007). Also, it is more focused on thermal analysis, while mechanical analysis has not been mentioned.

### 2.6.4. Critical Analysis of the optimization methods

The optimization methods explained above were useful in identifying the most effective cooling system parameters using a given range. In most cases, the Design of Experiments (DOE) approach was used to come up with a different combination of parameters, depending on the possible range (Zamri and Yusoff, 2015, 2018; He *et al.*, 2016; Quan *et al.*, 2016; Chen *et al.*, 2017; Li *et al.*, 2018).

This is followed by an evaluation of the different geometric parameters using Finite Element Simulation software. The limitation of these methods is that the evaluation is confined to the given range of the possible combination of parameters derived from the DOE approach. Thus, a different outcome may be obtained when the range of possible parameters is increased. On the other hand, cases involving a wider range of possible parameter combinations require many iterations and simulation runs. This makes the process computationally intensive and time-consuming. For example, the study which was conducted by He *et al.* (2016) involved the use of the Optimum Latin Hypercube method to devise a design matrix with 17 factors and 50 levels. Also, the results are biased towards the type of DOE approach used in creating the parameter combination. Table 2.5 shows an analysis of the optimization methods found in literature to date.

The two optimisation methods (Taguchi and Heuristic), which were used by Zamari and Yussof (2015), pointed out different optimum parameters for the same tool parameters. Thus, it is necessary to select a proper DOE method for selecting the most applicable parameter combinations. It is important to consider all the critical process requirements (cooling rate, uniformity, stress on the tool) in order to identify the most effective structural parameters for the cooling system. In other cases, the strength requirements of the tool were not considered and there was a bias on the cooling performance only. The Evolutionary algorithm, which was developed by Steinbeiss *et al.* (2007), was mainly focused on identifying parameters with the best cooling performance, however, the strength requirements of the tool were not mentioned. Thus, a different set of results might have been obtained if all the critical requirements had been encompassed. Liu *et al.* (2013) also used the evolutionary algorithm and included all the critical process requirements.

Table 2.5: Optimisation methods for cooling system parameters

| **Authors** | **Optimisation methods used** | **Optimum parameters** | **Validation methods used** | **Results obtained/ Quality improvement** |
|---|---|---|---|---|
| Lee *et al.* (2018) | Optimized the geometry of the cooling channels by using a sliced die with conformal cooling channels | Cooling channel profile made parallel to the tool surface | Finite Element analysis using computational fluid dynamics (CFD) and experimentation (ANSYS, 2019) | Optimized tool caused an increase in cooling rate by 10 K/s and a decrease in tool temperature by 80 K. |
| Li *et al.* (2018) | Topology optimization method used to determine optimum combination of parameters | Specific optimised parameters not given | Finite Element Simulation with CFD (Hexagon, 2019). | A cooling rate of 42 ℃/s. |
| Zamri and Yusoff (2018) | Heuristic optimization method used to determine optimum combination of parameters | $d$=8, $Y$=16, $Z$=12 mm | Finite Element Simulation with ANSYS and physical experiments (ANSYS, 2019) | Increased final tensile strength and hardness of formed parts |

| | | | | |
|---|---|---|---|---|
| Chun *et al*. (2015) | Used finite element simulation to evaluate different combinations of parameters | *d*=6 and 8 mm<br>*y*=5 and 10 mm | Finite Element Simulation with FLUENT (ANSYS, 2019) | A decrease in the final temperature of hot formed parts |
| Chen *et al.* (2017) | Parametric modelling with Box-Behnken experiments and response surface analysis. | *d*=12, *Y*=18, *Z*=18 mm | Finite Element Simulation Analysis with ABAQUS. A segmented tool was used in the analysis to minimize computation time | Maximum blank temperature is 158.7 °C/s |
| (Quan *et al.*, 2017) | Multi-Objective Swarm Optimisation<br>Box-Behnken design of experiments | *d* (8.3729 and 10 mm), *Z* (10 and 18 mm) and *Y* (20-24 mm) | Finite Element Simulation with Marc Software and experiments | |
| He *et al.* (2016) | Latin Hypercube method<br>Multi-objective optimization method<br>Response surface method | Conformal cooling channels, *d* = 4-6 mm, *Z* = 13-17 mm, *Y* not given | Finite Element simulation with ABAQUS (SIMULEON, 2019) | Average blank temperature after exit from furnace reduced by 11.7%<br>Temperature deviation on the blank surface reduced by 28.2 %. |

| | | | | |
|---|---|---|---|---|
| Zamri and Yusoff, (2015) | Taguchi and Heuristics optimisation methods | $d$ = 8 mm, $y$ = 10 mm, $z$ = 8mm | Finite Element simulation with COSMO software (Cosmo Tech, 2019) | A cooling rate of 22.242 kJ/s. Low Von Mises stress < 35 MPa |
| Liu *et al.* (2013) | Evolutionary algorithm<br>Generation of possible solutions using the algorithm | $d$ = 8mm, $z$ = 8 mm, $y$ = 8mm | Finite Element simulation with ABAQUS (SIMULEON, 2019) | A cooling rate of 40 ℃/s<br>Tensile strength of 1387 and 1587 MPa |
| Steinbeiss *et al.* (2007) | Evolutionary algorithm<br>Generation of possible solutions using the algorithm | $d$ = 8 and 12 mm for punch, $d$ = 8 and 10mm for blank holder. $Z$ = 10 – 15 mm and $Y$ not given | Finite Element simulation | Increased cooling uniformity<br>Reduction in cooling time by 1.1 seconds using an optimized system |

## 2.7. Comparison of Different Cooling Channel Configurations in Hot Stamping Tools

According to Lee *et al.* (2018), conformal cooling channels which are parallel to the tool surface have a higher cooling performance compared to longitudinal channels. This was validated experimentally by comparing the performance of a sliced die with drilled conformal cooling channels and straight drilled channels. This is, however, different from the simulation study, conducted by Hu *et al.* (2016), which involved comparing the cooling performance of various designs. In the study, the longitudinal, serpentine, transverse and parallel layouts were compared at different Reynolds number and outlet pressures. (Hu *et al.*, 2016). CFD was used as a tool for evaluating the layouts based on the maximum temperature, average temperature, cooling uniformity, and coolant pressure drop. To measure the cooling performance, a parameter known as the Figure of Merit was defined based on the blank temperature and coolant pressure. The results of the study indicated that the longitudinal conformal cooling channels had the highest Figure of Merit, thus showing the best cooling performance as compared to the other configurations. However, if the insert had a bigger length, a different result might have been obtained since longer cooling channels tend to gain more heat as the coolant travel distance increases.

The limitation of the study is that the authors could not identify a cost-effective method of manufacturing the tool insert with a conformal cooling channel in order to validate the results from the simulation. Thus, they performed experiments to validate the accuracy of the CFD analysis with a single straight cooling channel. However, the most important conclusion drawn from the study is that conformal cooling channels have a higher cooling performance as compared to the traditional straight cooling channels used in hot stamping. This is because the conformal cooling channels allows for a reduced distance between the cooling medium and tool surface. Another limitation of the study is that there was no optimization of the cooling system structural parameters (*d, y* and *z*) mentioned. A different outcome might have been obtained if the structural parameters had been kept constant in all cases to make a fair comparison of the different layouts.

Thus, the most appropriate channel network configuration depends on the specific geometry of the part. Also, it is necessary to present alternative solutions and evaluate them. Decision making tools such as the Analytic Hierarchy Process (AHP), Quality Function Deployment

(QFD) and other decision matrix techniques, can be useful in selecting the most suitable design (Renzi *et al*., 2017).

As mentioned before, the study investigated the application of AM in trying to improve thermal management of hot stamping tools. Based on the analysis from the literature, AM based cooling channels have a higher cooling performance for parts with complex geometry as compared to traditional straight-line channels. The next section reviews the AM processes that can be applied to produce conformal cooling layouts and presents their advantages and limitations.

## 2.8. Overview of AM Processes Applicable in Hot Stamping Tooling

Metal-based AM processes, which can be used for producing tooling applications, include Selective Laser Melting (SLM), Direct Metal Deposition (DMD) and Electronic Beam Melting (EBM). The first stage for all AM processes involves creating a three dimensional model of the component using CAD software and converting it into an STL file (Wong and Hernandez, 2012). The STL file is then imported into management software for pre-processing operations such as selecting the optimum orientation and providing support structures (Negi *et al.*, 2012). The information is then transferred to the machine process control which actuates servo mirrors to direct the movement of the laser beam based on CAD geometry (Wong and Hernandez, 2012; Campanelli *et al*., 2010). The following sections give a brief overview of each of the applicable AM processes.

### 2.8.1. Selective laser melting (SLM)

In SLM, a layer of metal powder is firstly spread on a build table using a roller or scraper mechanism. The powder is initially preheated to a temperature below the melting point. The preheating is important because it aids in sintering of the powder and also helps to reduce thermal gradient between the powder and the part, thus reducing residual stresses that cause warpage of the part (Rodriguez *et al.*, 2012). The laser then selectively scans the powder layer guided by the CAD model, providing the energy required for melting of the powder particles. The worktable then moves upwards by a distance which is equivalent to the thickness of each layer (van Belle *et al.*, 2013). The process is repeated layer by layer until the part is completed (Dadbakhsh *et al.*, 2012). This is shown in Figure 2-15.

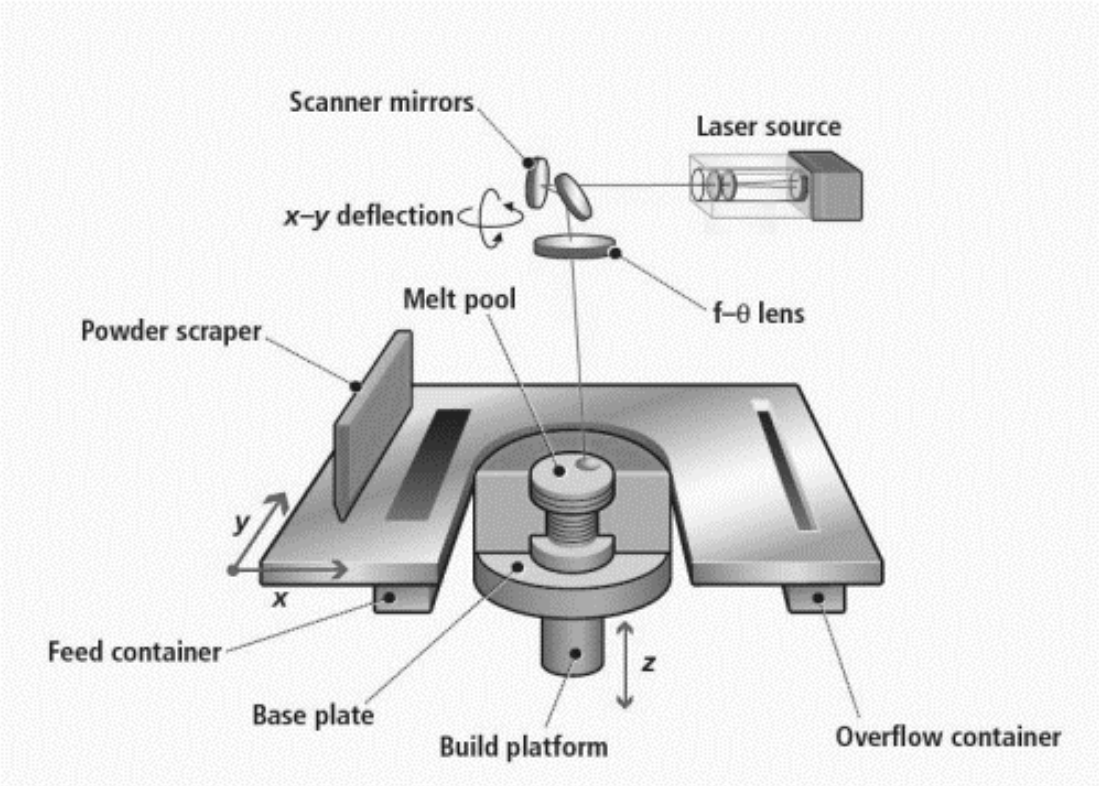


Figure 2-15: Selective Laser Melting process (Yasa *et al.*, 2011)

The thickness and density of each layer are key factors used in determining the amount of powder to be melted in a single scan. Parts produced have the challenge of having a poor surface finish because of the layer-wise addition strategy. The quality of the surface finish can be improved by reducing the layer thickness (Yadroitsev *et al.*, 2012). The process is conducted in a neutral gas environment (nitrogen or argon) to prevent oxidation of the molten material (Foroozmehr *et al.*, 2016). SLM is an attractive process because of its ability to produce parts that have a nearly full density structure with mechanical properties that can compete with conventionally manufactured parts (Gu *et al.*, 2012). SLM is compatible with materials such as tool steels, titanium and its alloys (Kruth *et al.*, 2010).

The major challenge of the SLM process is the steep thermal gradients exposed to the part which induce thermal stresses and may lead to distortion of the part (Dadbakhsh *et al.*, 2012). The steep thermal gradients make the layers expand and contract at different rates and this causes the formation of residual stresses (Vora *et al.* 2015; Gu *et al.* 2012; Song *et al.*, 2014). The stresses negatively affect the resultant dimensional accuracy of the parts produced. Research efforts have been inclined towards the management of the residual stresses using post heat treatment. Other shortcomings of the SLM process include porosity of build parts and the limited materials in use (Thijs *et al.*, 2010).

The SLM process is very complex as it involves various parameters (powder feed rate, scan speed, scanning pattern, laser power) which affect the resultant geometric accuracy and mechanical properties of the formed part. Challenges are faced when selecting optimum process parameters for producing parts with acceptable geometrical accuracy and mechanical properties (Bariani *et al*., 2008; Foroozmehr *et al*., 2016).

The SLM process is accompanied by high costs due to the machine, material and energy costs. One possible method of reducing the costs is through the production of hybrid parts or parts with lattice structures in order to save material, time and energy consumption (Yan *et al.*, 2014).

### 2.8.2. Electron beam melting

The EBM process is similar to SLM except that it utilizes an electron beam with a high voltage (30-60 KV) as the source of heat, unlike the SLM processes which utilize a laser as the heat source *(*Murr *et al.*, 2012). To avoid oxidation, the process is conducted in a high vacuum closed chamber (Wong and Hernandez, 2012). This is different from the SLM process which occurs in the presence of neutral gas. Electromagnetic lenses focus the beam and the deflection coils control its movement on the build table as shown in Figure 2-16.

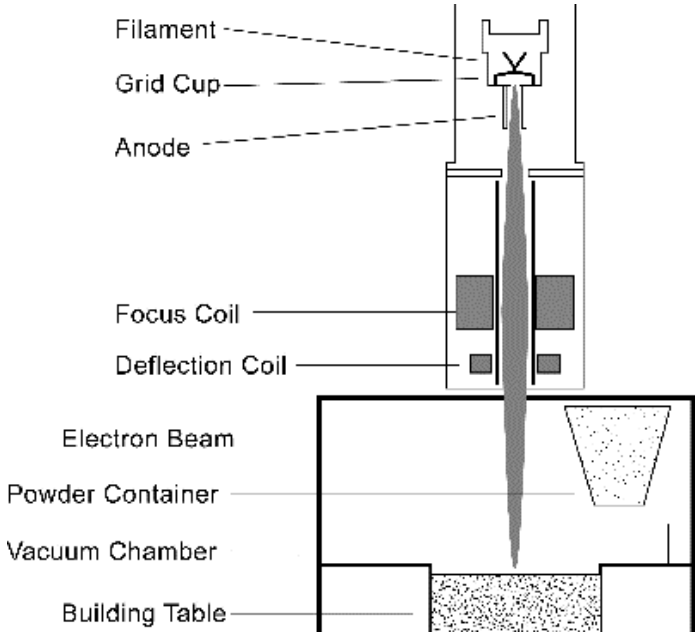


Figure 2-16: Electron beam melting (Biamino *et al.*, 2011)

A layer of powder with a thickness of about 100 µm is spread on the build table. The electron beam then preheats the powder using a high current (30 mA) to a temperature of about 0.8T (where T is the melting point of powder in degrees Celsius) (Sing *et al.*, 2015; Murr *et al.*, 2012). The powder is melted layer by layer based on the geometry from the CAD model until

the part is completed (Sing *et al.*, 2015; Wong and Hernandez, 2012). EBM has the advantage of having high build rates as a result of high scanning speeds and deep penetration rates (Gong *et al.*, 2014). According to previous studies, parts produced with EBM have the challenge of poor surface finish and dimensional inaccuracy. For example, Koike *et al.* (2011) investigated the capability of EBM in manufacturing Ti-6Al-4V ELI parts for dental applications. The parts produced had a poor surface finish which was characterized by a rippled surface appearance and the presence of unsolidified powder. On the other hand, efforts were made to identify the effect of process parameters on the quality of parts. Karlsson *et al.* (2013) studied the effect of layer thickness and powder size on the quality of parts. The parts produced with the smallest powder particles (25 to 45 µm) were observed to have unsolidified powder on the surfaces.

### 2.8.3. Direct metal deposition

In Direct Metal Deposition (DMD), a high-powered laser (Nd:YAG, fibre or diode laser) is used to create a melt pool on the metal surface. This is followed by the deposition of metal powder or wire on the melt pool to form a bond with the substrate as shown in Figure 2-17 (Bhattacharya *et al.*, 2011; Dutta *et al.*, 2009). The laser beam is moved to another location based on the CAD geometry, moving layer by layer. The powder is fed by an inert gas stream (helium or argon) and then melted by laser radiation. Layer thickness varies from 0.1 to 3 mm in a single-phase, depending on the process parameters (velocity, powder feed rate, and laser power) (Ocylok *et al.*, 2014). The difference between DMD and other AM processes such as SLS and SLM lies in the supply of the powder material. In DMD, the powder is supplied by a nozzle while in Selective Laser Sintering (SLS) and SLM, the part is created in a powder bed (Guo and Leu, 2013). DMD can produce parts with mechanical properties that are comparable with those manufactured conventionally. A study was done to investigate the mechanical properties of two high strength alloy steel parts (316 stainless steel and H13 stainless steel) produced by DMD (Riza *et al.*, 2014). Cylindrical specimens were produced and tested for tensile strength and ductility. The tests were conducted under high strain rate and quasi-static dynamic conditions.

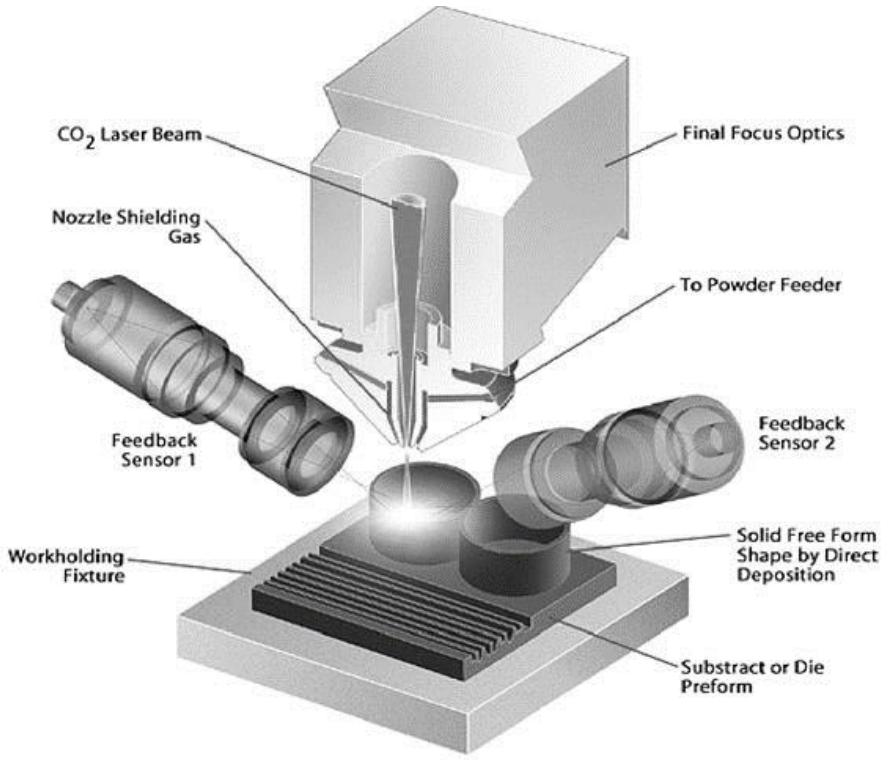


Figure 2-17: Direct Metal Deposition process (Dutta *et al.*, 2009)

The results showed that parts produced could withstand high impact and axial loads with properties similar to conventionally manufactured parts. DMD can be used to repair damaged coatings and to produce wear resistant coatings (Dutta *et al*., 2009). DMD offers many advantages which include its compatibility with a broad range of materials such as ceramics, polymers, pure metals, high melting point alloys such as Ti-based alloys tool steels, Ni-based alloys and Fe based stainless steels ( Dinda *et al.*, 2009; Gharbi *et al.*, 2014; Wu *et al.*, 2004; Imran *et al.* 2012; Zhang e*t al.* 2014). Other advantages include the ability to manufacture complex geometric parts, improved thermal control and the reduction of tool replacements costs through repair *(*Kaierle *et al.*, 2012).

The efficiency of the DMD process is influenced by parameters such as the scan speed, laser diameter, and powder flow rate. These parameters have an influence on the thermal history of the part, hence affecting its thermal cycle (Gharbi *et al.*, 2014). The quality characteristics of the process such as the dimensional accuracy and surface finish are influenced by the laser energy input, powder particle size, and gas flow rate. Common defects which occur during the DMD process include declining of side surfaces, uneven surface finish and non-uniform thickness of layers (Zhu *et al.*, 2012). There is a need for reliable modelling of the DMD process for process planning and design purposes. Research efforts have been conducted to develop

models for predicting the behaviour and outcomes of the process (Pinkerton, 2015). An increase in the laser scanning speed and powder feed rate caused a reduction in the width of the layer (Sun and Hao, 2012). During the DMD process, the newly deposited layer reheats the previously deposited layers and this causes complex thermal distribution in the part. This affects the microstructure of the formed part and its mechanical performance, resulting in distortion and cracking. This is also true for SLM and EBM.

## 2.9. Factors Affecting AM Application for Thermal Management in Hot Stamping Tools

Factors affecting the application of AM in the construction of conformal cooling channels include the geometry of part, cycle time and quality characteristics of formed parts, production volume, hardness, tool maintenance costs and frequency.

### 2.9.1. Geometry of the part

Due to the high costs associated with AM, conformal cooling channels are more cost-effective for cases in which it is difficult or impossible to construct drilled channels. Examples of typical geometries have been presented by various authors (Lei and Xing, 2013; Stoll *et al.*, 2016; Cortina *et al.*, 2018). In all cases, there were positive results in terms of cycle time reduction and quality improvement. If the part has a simple geometry in which straight channels can be easily drilled, the conformal cooling will not make a greater impact unless other factors are considered. This is mainly because `the performance of the AM based cooling channels is more or less similar to the straight channels for the same geometry (Cortina *et al.*, 2018). Liu *et al.* (2013) designed cooling system layouts for a square box part and a B-Pillar. A conformal cooling layout arrangement was used for the B-pillar because of its complex geometric structure and straight channels were adopted for the square box part. The results for the performance of tools were almost similar. The competitive advantage of AM lies in its unlimited geometric freedom which allows for the construction of adaptive cooling channels for parts with complex geometry. Figure 2-18 shows three typical hot stamping parts.

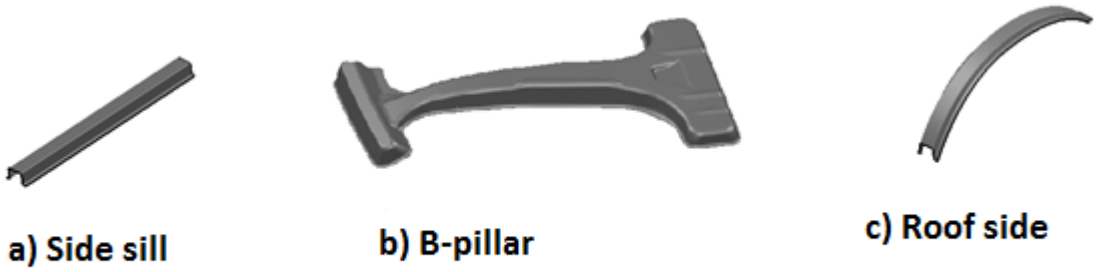


Figure 2-18: Hot stamped parts with: a) simple geometry; b), c) complex geometry

Of the three parts, the side sill has a simple geometry which can accommodate straight drilled channels. The B-pillar has a relatively complex geometry in which straight channels cannot access other curved portions due to machining restrictions. The roof side has a complex geometry which is difficult or not possible for straight channels due to its curvature. Thus, it will be more economically beneficial to apply conformal cooling to the B-pillar and roof side component as compared to the side sill.

### 2.9.2. Cycle time and quality characteristics

The quality of the formed parts (strength and uniformity of the formed part) depends on the cooling rate of the part in the closed tools. A cooling rate above 27 °C/s will enable the blank to exhibit the required tensile strength properties (Lim *et al.*, 2014). If the portions on the part cool at different rates, a non-uniform microstructure is obtained, causing the part to have non-uniform hardness properties. Also, the formed parts could have dimensional deviations as a result of non-uniform cooling (Liu, Lei, and Xing, 2013; Ye *et al.*, 2013; Lim *et al.*, 2014b; Lv *et al.*, 2016b). According to previous studies, the temperature of the tool must be maintained below 200 $^{o}$C (Lei *et al.*, 2013). Hence, it is important to lower the tool temperature as much as possible, using cooling channels which are closer to the tool surface. Based on previous literature and experience of the hot stamping process, defects arising from a poor cooling system include dimensional distortions, low or non-uniform hardness and tensile strength. Depending on the intensity and cost implications associated with the above-mentioned defects, it may be necessary to replace the conventional method with an AM based cooling system.

### 2.9.3. Tool maintenance and replacement costs

As mentioned earlier, an improperly designed cooling system leads to high internal thermal gradients within the tool system, thus leading to the generation of thermal stresses (Lim *et al.*, 2014b). This eventually leads to cracking, deformation, and failure of the tools (Escher and

Wilzer, 2015). On the other hand, a proper cooling system layout reduces thermal gradients on the tool surface. Thus, a prolonged tool service life is guaranteed. Another challenge with a poorly designed cooling system is the gradual rise in temperature during mass production (Zhong-de *et al.*, 2010). This causes thermal softening on the tool surface and eventually leads to deformation of the tool, resulting in distorted parts. Also, the tool will not be able to cool off the blanks at the desired cooling rate to enable martensitic transformation. Depending on the cost implications of the reworks and tool replacements, it may be beneficial to replace the conventional cooling system with a conformal cooling layout. The next section discusses other tooling applications which were investigated for AM based conformal cooling channels.

## 2.10. Use of AM for Thermal Management in Other Tooling Applications

The following section discusses previous studies on the use of AM in other tooling applications.

### 2.10.1. Moulding tools

In the injection moulding industry, a lot of research was done pertaining to the manufacture of AM based cooling channels to improve quality and reduce cycle time (Dimitrov and Bester, 2005; Saifullah and Masood, 2007; Dimitrov, 2010; Qian *et al.*, 2012; Au and Yu, 2013; Khan *et al.*, 2014; Mazur *et al.*, 2017; Wu *et al.*, 2017). This is mainly because of the cooling time in injection moulding which can constitute over 50 % of the total cycle time using conventional straight-drilled moulds (Lin and Chou, 2002). Just like in hot stamping, the cooling process also plays an important role in the resultant quality. Non-uniform cooling results in defects such as distortions, hot spots and sink marks (Li *et al.*, 2018). According to previous studies, a significant reduction in cycle time (20-50 %) and quality improvement was achieved after using moulds with AM based cooling systems (Saifullah and Masood, 2007; Rännar *et al.*, 2007; Dimitrov, 2010; Au and Yu, 2013; Li *et al.*, 2018; Park *et al.*, 2019). In a local study at Stellenbosch University, a mould with AM based cooling channels for a cutlery drainer case-study was designed and manufactured (Moammer, 2011). The manufactured mould shown in

Figure 2-19 caused a reduction in cycle time by 30.78 % which translated to an annual cost saving of R 1,181,950 (Moammer, 2011).

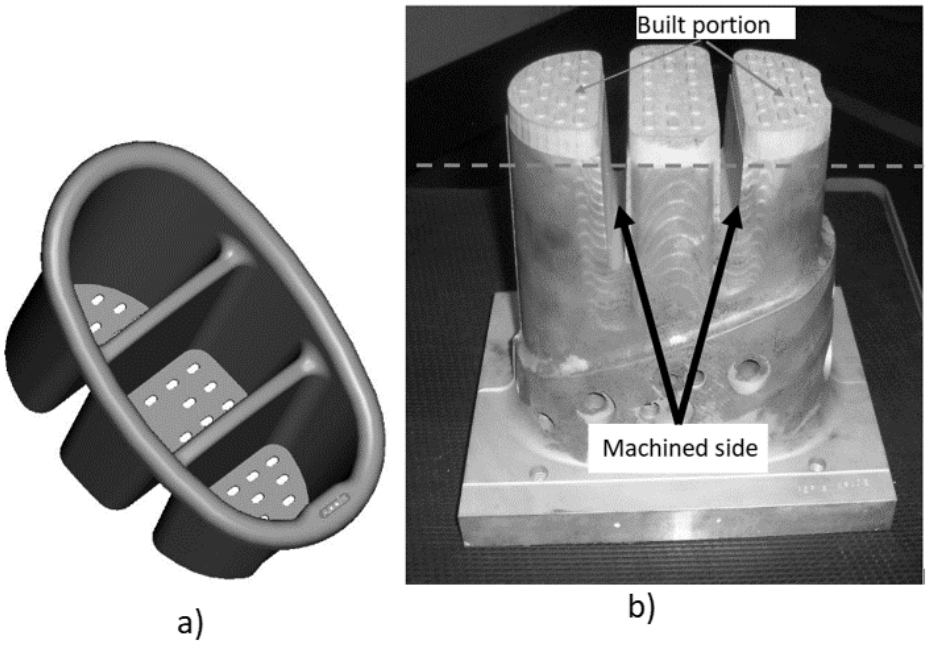


Figure 2-19: a) Cutlery drainer b) Mould for cutlery drainer

As part of the study, an evaluation model for identifying the most suitable cooling system design for any injection moulding part, was developed (Moammer, 2011).

Clearly, it is seen from the literature that the application of AM based conformal cooling channels in injection moulding has been thoroughly explored. As a result, the South African injection moulding industry has embraced this technology (Oyesola *et al.*, 2018). Models for governing parameter selection in the designing and manufacture of AM based cooling channels for injection moulding tools, are already in existence (Mayer, 2009; Moammer, 2011). Regarding hot stamping tools, there is still a need for further study regarding the parameters and procedures involved. The high forming loads and temperature in hot stamping present a challenge in the cooling system design. The next section presents other hot forming applications in which the potential of using AM based cooling systems was investigated.

### 2.10.2. Other forming applications

The application of AM in sheet metal forming tools is still under investigation. Previous studies were focused on the application of AM in the production of prototype tools and those for short production runs (Levy *et al*., 2003). This was done to reduce the time for product development. Cheah *et al.* (2002) conducted a study on the application of Selective Laser Sintering (SLS),

Stereolithography (SLA), high-speed CNC milling and conventional tooling, to make prototype tools for sheet metal forming. The conventional tool had the highest production cost of $3000, while SLA, high-speed CNC and SLS had costs of $151.20, $150, and $136.80 respectively. This shows that the prototype tools manufactured using AM processes were cost-effective when compared to conventional tooling. Another study was conducted on the production of forming tools for stretch formed jewellery (Gulati, 2011). The designed rapid tools successfully formed the structural units of the jewellery in the correct dimensions. However, the rapid growth of AM technology and its success in the thermal management of plastic moulds, has compelled researchers to investigate how it can be applied in hot forming tools with thermal challenges.

Hölker *et al*. (2013) evaluated the performance of extrusion die inserts with conformal cooling channels. This was done to eradicate the problem of overheating which is associated with extrusion tools. In the experiments, the conformal cooling channels of the die insert were constructed using selective laser melting. When an extrusion speed of 6 m/min was used on dies with conformal cooling, there was a reduction in the temperature of the insert by 41 °C and the formed part by 20 °C. There was no overheating and no surface defects were observed. A higher speed (24 m/min), caused the part to have a 4 °C reduction in temperature while the tool temperature did not change. However, surface defects were observed. Another study was done using a conformable hot aluminium extrusion die as shown in Figure 2-20 (Hölker and Tekkaya, 2016). Using hybrid manufacturing, the critical portion insert was constructed using SLM. Investigations were done to test the performance of powdered tools steels 1.2344 and 1.2709 for the build. The tests revealed that portions built using tool steel 1.2344 did not have adequate strength as compared to 1.2709. A novel coolant supply system was constructed in the die insert to target the hot spots. This led to an exit temperature reduction of part by 11 % using a coolant and 6 % not using a coolant. The portions of the die insert constructed using SLM were able to resist the high mechanical and thermal loads.

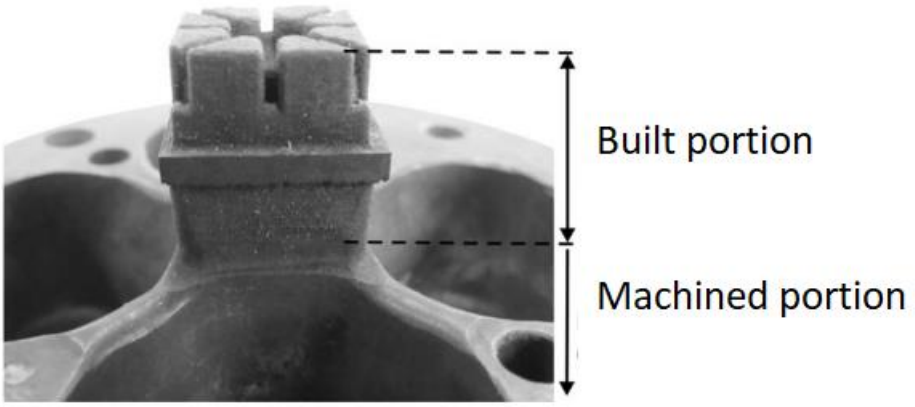


Figure 2-20: Top of extrusion die (Hölker and Tekkaya, 2016)

Huskic (2012) carried out a study on the manufacture of forging dies with conformal cooling channels. In the study, one of the tools was fully additive and the other tool was produced using hybrid manufacturing as shown in Figure 2-21. The base material was tool steel 1.2344 and the additive part was produced using tool steel 1.2709. Tests on the tools showed that they could withstand 500 forming trials. The tools were able to withstand high mechanical loads and there were no damages observed (Huskic *et al.*, 2013).

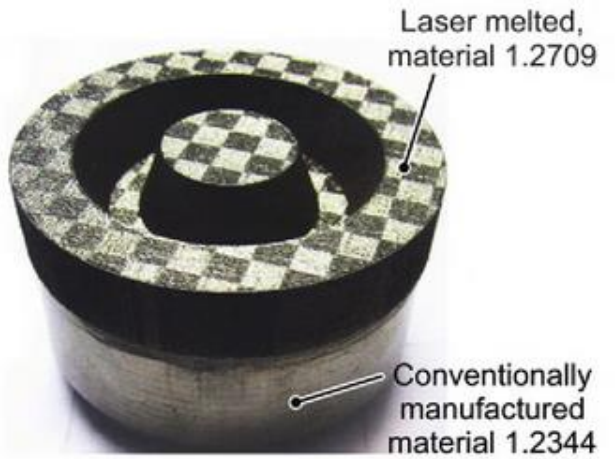


Figure 2-21: Hot forging die with conformal cooling channels

## 2.11. Design Rules for Conformal Cooling With AM Processes in Hot Stamping Tools

Conformal cooling channels, as the name suggests, refers to channels which follow the geometry of a part. This is necessary to overcome the machining restrictions associated with straight drilled channels as shown in Figure 2-22. According to EOS, the recommended

material used for tooling is tool steel 1.2709 (EOS, 2019). Due to the orientation of the tools, it is more cost-effective and easier to implement the conformal cooling system on the punch insert\s as compared to the die. This is because part of the flange can be considered as the built section.

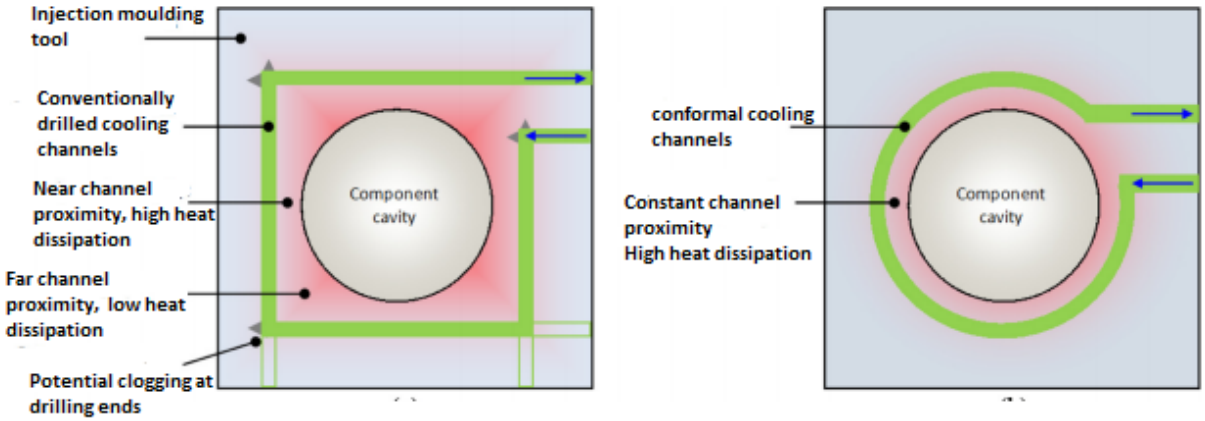


Figure 2-22: Conventional drilled channels (left) and conformal cooling channels (right) (Mazur *et al.*, 2016)

### 2.11.1. Design for sufficient cooling

The cooling rate of the blanks should exceed 27 °C/s to ensure the martensitic transformation of the blanks. According to previous studies, the resultant temperature of the tool should be less than or equal to 200 °C to ensure that a cooling rate of 27 °C/s is achieved (Lim *et al.*, 2014). In order to ensure an increased cooling rate, the distance between the tool surface and the cooling channels must be reduced. Thus, the above-mentioned is considered in the formulation of the model. It is important to keep the cooling channels as short as possible. This will allow water to enter and leave the insert quickly, allowing a faster heat removal process. The tool contact surface should be smooth and not exhibit any scales or gaps in order to increase the surface area in contact with the blank for effective heat transfer.

### 2.11.2. Design for uniform cooling

The cooling channels must be distributed in such a way that there is uniform cooling of the hot blank. Non-uniform cooling of the blanks results in reduced tool life and defects such as warpages. Furthermore, if the tools are not uniformly cooled, thermal stresses develop which leads to a reduction in the tool life (Liu *et al.*, 2013). Hence the goal is to maximize the number

of channels and use the smallest possible diameter. The distance from the tool surface to the cooling channels should be kept constant to allow for uniform cooling on the tool surface.

### 2.11.3. Design for the strength of the tool

The punch and die must retain adequate strength to perform the stamping operations. Increasing the number of cooling channels and reducing the distance from tool surface to cooling channel diameter results in increased cooling performance. However, this must be done in such a way that the strength of the die is not compromised. For fatigue design, the allowable stress limits are reduced. To preserve the structural strength of the tool, the maximum bending stress of the tools after inserting the cooling channels should not exceed the maximum allowable stress of the tool material.

### 2.11.4. Design for coolant pressure

The inlet and outlet pressure of the coolant must allow for rapid flow of coolant. Turbulent flow is associated with high velocity and ensures a faster heat removal rate as it occurs at Reynolds numbers above 4 000. According to experiments done by Lim *et al* (2014), if Reynolds number is above 10 000, the conventional heat transfer coefficient decreases. To achieve optimal heat transfer, adequate coolant pressure differential must be maintained to achieve the above mentioned Reynolds number range in terms of coolant mass flow rate and passage diameter.Thus, in the experiments, a suitable Reynolds number lying between 4000 and 10 000 was chosen to ensure a rapid flow of fluid. To ensure adequate coolant pressure, the coolant mass flow rate and diameter should permit the above-mentioned range. The cross-sectional area of the cooling channels should be maintained as constant to allow a constant water flow volume rate through. Other factors affecting the frictional pressure losses in the cooling channels include the length of cooling channels, diameter, coolant flow rate, and surface roughness. Equation 2-34 accounts for pressure loss (Valiantzas, 2008), where $f$ is the friction factor.

$$P_{loss} = f\frac{\rho_c v L}{2d} \qquad 2\text{-}34$$

### 2.11.5. Design for tool assembly

Hot stamping tools are composed of several inserts with cooling channels which are joined using connector plugs to prevent leakage of the coolant. Thus, a tool insert with conformal

cooling channels should be designed in a way that it can be easily integrated into the available cooling system pattern. In that way, the cooling channels can be made longitudinal to the tool surface and joined at the end to allow connection with the channels in the corresponding insert. Another way is for the insert to have its own coolant inlet and outlet points. This will allow easier assembly of the tool inserts.

### 2.11.6. Building round holes with SLM

According to previous experimental studies, the smallest diameter which can be built parallel to the substrate plate is 0.7 mm (Thomas, 2010). There is no need for support structures if the holes are built in a vertical position as shown in Figure 2-23.

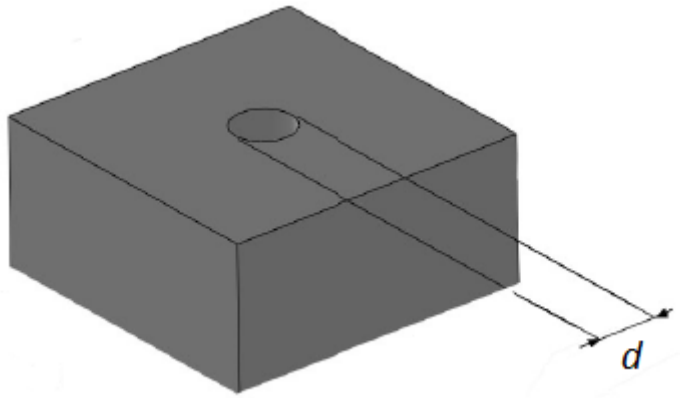


Figure 2-23: Hole in a vertical position

Holes that are built in a horizontal position are not self-supporting. Based on previous studies, the maximum diameter which can be built without the use of support structures is 7 mm (Thomas, 2010). Figure 2-24 shows holes in the horizontal orientation.

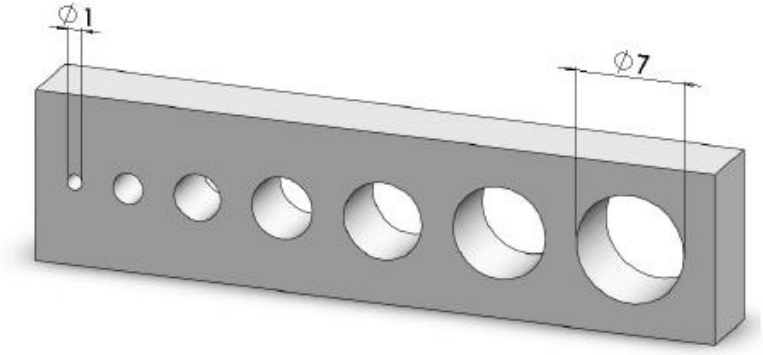


Figure 2-24: Holes in a horizontal position.

The challenge with building small holes in a horizontal orientation is the sagging effect that may occur on the top layers of the holes. This tends to reduce the accuracy and surface finish. On the other hand, the roughness of the cooling channels helps to generate more surface area for molecular interaction, thus increasing heat transfer. Holes larger than 7 mm will require support structures to prevent distortion. The support structures must be carefully designed so that they are easily accessible during post-processing. Another way to minimize the sagging effect is to build the cooling channel with an apex on the circular profile as shown in Figure 2-25. The apex helps to increase the self-supporting effect of the cooling channel.

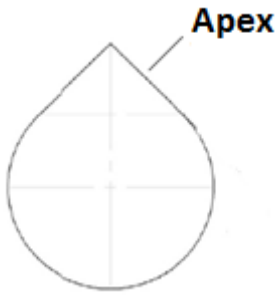


Figure 2-25: Cooling channel with apex for self-support

In general, the tolerance for building round holes using SLM is ± 0.5 mm. The next section of the chapter explains the mechanical and heat transfer theory behind the process of hot stamping. This creates a foundation for the formulation of a model for determining suitable cooling system parameters.

## 2.12. Challenges in the Application of AM in Hot Stamping Tools

A major challenge in the manufacture of AM based conformal cooling channels is to determine the correct structural parameters, considering the technical limitations of AM technology. The few authors that have looked at this subject area have not mentioned the exact parameters that were used (Mueller *et al.*, 2013; Gebauer *et al.*, 2016). They have relied on the use of FE analysis simulation and iterations to define optimised parameters. The challenge with these methods is the computational intensity and resources required. Thus, it is important to present methods for identifying suitable parameters for AM based conformal cooling channels, which are easier to apply.

Another challenge is the limited size of the AM machines. At present, most SLM machines are often limited to sizes of between 200 and 300 mm (Levy *et al.*,2003). Previous studies have only focused on the manufacture of tools within the building envelope of AM machines

(Mueller *et al.*, 2013; Gebauer *et al.*, 2016; Cortina *et al.*, 2018). For hot stamping tools, some of the inserts have sizes exceeding 300 mm, depending on the specific part. Therefore, it may be necessary to devise a way to apply AM in the manufacture of larger tool inserts with conformal cooling channels. On the other hand, the rapid growth of AM technology is expected to bring about machines with larger build volumes to cater for larger parts.

An issue of concern is the limited material envelope. The most common tool steel powders used are ALSI H13 and tool steel 1.2709 (Mueller *et al.*, 2013; Cortina *et al.*, 2018). There is a need to explore the production of other tool steels. On the other hand, the growth of AM technology is expected to pave the way forward for the development of new materials that will offer added functionality (thermal conductivity, corrosion and wear resistance) to the tools.

It is difficult for the AM process to produce a part with high dimensional accuracy. This is mainly because of the shrinkage and stir-stepping process associated with AM processes (Kruth *et al.*, 2010). There is a need to further improve the accuracy and surface roughness of AM processes through optimization of process parameters and machine design. Thus, post-processes such as machining and polishing are done to ensure that the tools achieve the required dimensions. On the other hand, surface roughness of cooling channel increase friction on the walls thereby, accelerating heat transfer (Xu, 1999). Another challenge is that rapid temperature changes that occur during melting and solidification of powder lead to the generation of residual stresses (Mercelis and Kruth, 2006). In order to remove the stresses, the tools should be tempered (Cortina *et al.*, 2018).

The equipment and powder costs associated with the AM process is of major concern. Thus, when evaluating the potential of AM as opposed to conventional methods, it is important to weigh the benefits against the investment costs. In hot stamping, the benefits are realized through cycle time reduction, prolonged tool life, and quality improvement. This depends on several factors which are discussed in the following section.

Despite the advantages brought about by using conformal cooling, there are still challenges. Tools with features such as deep grooves may not be affected by the cooling capabilities of the channels (Beal *et al.*, 2007). Secondly, conformal cooling is not cost-effective for tools with basic geometry because of the associated costs. In order to reduce costs, hybrid manufacturing can be used as an option whereby part of the mould is made using AM processes and the other part using conventional methods such as machining (Homar *et al.*, 2012).

## 2.13. Summary and Gap Analysis

The chapter has reviewed the different methods used to improve cooling efficiency in hot stamping and their merits and demerits. An intensive literature study of the hot stamping process and the basic AM processes used in the manufacture of tools, were presented. Based on the available literature, it is quite clear that there is a growing need to improve the cooling capacity of hot stamping tools. The focus is on reducing cycle time, improving the quality of hot-formed parts and prolonging the working life of the tools. This is proven by the several models and optimization methods which were proposed for designing cooling systems for conventional straight drilled channels. The challenge is that almost all the models were developed under the restrictions of the straight drilling method. For example, a larger distance from tool surface to cooling channels ($z > 5$ mm) was often used to reduce the magnitude of stresses after drilling the channels. However, for the AM based conformal cooling channels, these restrictions do not hold since the cooling channels are constructed through additive processes. Contrary to hot stamping, a lot of research was done on injection moulding. This involved the development of various methods for determining the cooling system parameters based on the principles of plastic crystallization. For hot stamping, the process requirements and materials are different. There are high mechanical loads and operating temperatures in hot stamping, and this distinguishes it from other processes. Thus, there is a gap in the identification of parameters for conformal cooling in hot stamping tools. Hence the researcher seeks to fill the gap through developing a method for determining parameters for conformal cooling system design in hot stamping tools. In order to achieve this, the researcher makes use of mechanical and heat transfer principles using the proposed methods in literature as a starting point. This will be combined with the technical limitations and basic design rules associated with AM.

In the quest to improve the cooling system design, most authors have used Finite Element simulation runs on different cooling system parameter combinations, and comparing their cooling efficiency. However, most of the studies were on parts with simple basic geometry and only a few authors applied the models to tools with complex geometry. As mentioned earlier, other challenges with the use of these optimization methods lie in the intensive computational time and other resources required to enable the analysis. Also, most of the optimization methods were geared towards increasing cooling efficiency and there has not been much focus on the structural strength of the tools. Moreover, it is difficult to maintain the parameters in real life when using conventional drilling because of machining restrictions. While it is clear

from various research findings that conformal cooling has a higher cooling efficiency when compared to straight drilled channels, there is limited research dedicated to hot stamping tools. Only a few authors have investigated the performance of hot stamping tools with conformal cooling channels. These authors have not provided information on the design parameters and procedures that were used to develop the conformable tool inserts. Thus, there is a need for more investigation in this area. This has prompted the researcher to study the design and manufacture of hot stamping tools with conformal cooling channels.

For the few authors who investigated the application of AM based cooling channels in hot stamping, the sizes of the tool inserts studied were relatively small. Generally, all the tool inserts studied were within the building envelope of most SLM machines (length, width, and height of 250-300 mm). To date, there is no available literature on the manufacture of large-sized tool inserts with AM based conformal cooling channels. This is a challenge because hot stamping tool inserts are generally larger in size. Thus, there is a gap in the development of cost effective methods for designing hot stamping large-sized tools with AM based cooling systems.

Another challenge is that only a few authors in literature have evaluated the performance of a conformably designed tool using both finite element analysis and physical experiments. In most cases, only finite element simulations were done. The reason could be the high costs associated with manufacturing the tool.

The surface roughness in the cooling channels caused by the SLM process has a positive impact on heat transfer as it increases the friction of the channel walls. Previous studies in literature have shown that surface roughness enhances convection heat transfer (Ventola *et al.*, 2014; Guo and Gong, 2015). This is as a result of the increased surface area of the channel walls which will be in contact with the coolant in the channels. A possible explanation can be explained using the Gnielinski Correlation in Equation 2-35.

$$Nu_D = \frac{(f/8)\,(Re_D - 1000)Pr}{1 + 12.7(f/8)^{1/2}(Pr^{2/3} - 1)} \qquad 2\text{-}35$$

The equation explains turbulent flow in a circular tube with a rough surface. Regarding the equation, the quantity *f*, represents the friction factor which has a direct proportion with the

Nusselt number. As the Nusselt number increases, the heat transfer coefficient also increases according to the Equation 2-36 below

$$Nu_D = \frac{h_{cw} L}{k} \qquad 2\text{-}36$$

However, there is need for further studies to identify the trade-off between the enhanced cooling and increased flow resistivity.

# CHAPTER 3 : BASIC LAYOUT CONSIDERATIONS

## 3.1. Introduction

The purpose of this chapter is to present the heat transfer equations for the cooling system and to propose a mathematical method for determining the cooling system parameters for a hot stamping tool with conformal cooling channels. The model is derived from previous literature, mechanical and heat transfer principles and considers the manufacturing constraints of the SLM process. In the chapter, the model for predicting minimum cycle time is also developed so that it can be used for benchmark purposes to justify the need for an improved cooling system design

## 3.2. Heat Transfer during Forming and Cooling

Figure 3-1 shows the heat transferred from blank to the cooling system during the forming and cooling stage.

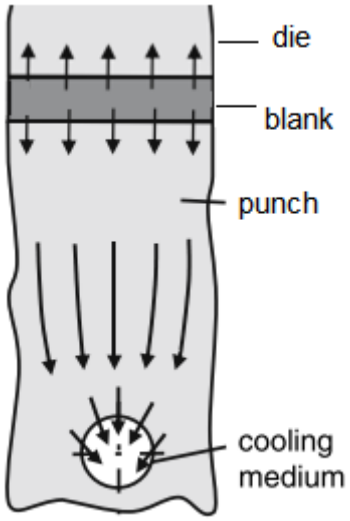


Figure 3-1: Flow of heat during forming and cooling (Steinbeiss et al., 2007)

The following heat transfer scenarios and work rates are considered for the forming and cooling stages (Muvunzi *et al.*, 2017)

- Heat absorbed by the die from the blank surface ($\dot{Q}_1$)
- Heat absorbed by the die from the alternate blank surface ($\dot{Q}_2$)
- Heat transferred from the punch surface to the internal die cooling channel walls ($\dot{Q}_3$)
- Heat transfer from the internal die cooling channel walls to the coolant ($\dot{Q}_4$)
- Heat carried by the coolant in the die cooling channels ($\dot{Q}_5$)
- Rate of work done on the blank as a results of frictional forces ($\dot{W}_1$)
- Rate of work done on the blank due to plastic deformation ($\dot{W}_2$)

- Heat released in the blank due to metallurgical transformations (assuming exothermic) ($\dot{Q}_6$)

During forming, the blank gains heat from the work done due to frictional forces ($\dot{W}_1$) and plastic deformation ($\dot{W}_2$). It loses heat as it comes into contact with the punch ($\dot{Q}_2$) and the die ( $\dot{Q}_1$). Heat is also gained from metallurgical transformations ($\dot{Q}_6$). It is assumed that the heat lost to the environment by the tool is negligible. Accordingly, it follows that the sum of heat lost by the blank during forming and cooling can be expressed as shown in Equation 3-1 (Muvunzi *et al.*, 2017)

$$\dot{Q}_{form} = (\dot{Q}_1 + \dot{Q}_2) - (\dot{W}_1 + \dot{W}_2 + \dot{Q}_6) \qquad 3\text{-}1$$

Heat gained by the tool (punch/die) as a result of contact with the blank depends on the surface area of part, tool design and part geometry. It is assumed that the heat which is transferred from the die surface to the cooling channel walls $\dot{Q}_3$ is equal to the heat transferred from the cooling channel walls to the coolant $\dot{Q}_4$ and the heat carried by the moving coolant $\dot{Q}_5$ (Zhong-de *et al.*, 2010; Ying and Zhong-De, 2014). This is shown in Equation 3-2.

$$\dot{Q}_3 = \dot{Q}_4 = \dot{Q}_5 \qquad 3\text{-}2$$

The transient thermal differences between both water cooled punch and die are ignored for simplicity, Transients within the die are accounted for through the heat transfer coefficient ($h_c$). It is assumed that the heat from the blank is evenly distributed between the punch and die. Thus the heat transferred from the blank to the punch surface is expressed using Equation 3-3 (Ji *et al.*, 2015)

$$\dot{Q}_1 = h_c A(T_b - T_d) \qquad 3\text{-}3$$

The heat transfer coefficient mainly depends on the contact pressure and surface roughness of the tools (Bai *et al.*, 2012; Caron *et al.*, 2014; Li *et al.*, 2015; Zhao *et al.*, 2015).

The heat transferred from the tool surface to the cooling channel walls can be estimated using the conduction shape factor analysis as shown below (Hagen, 1999).

$$\dot{Q}_3 = k_d f_s (T_d - T_{cw}) \qquad 3\text{-}4$$

The shape factor can be expressed as shown below.

$$f_s = \frac{2\pi l}{ln\left[\left(\frac{2w}{\pi d}\right)\sinh_w\left(\frac{2\pi Zb}{w}\right)\right]} \quad 3\text{-}5$$

Thus, for a given amount of cooling channels ($n$), the total heat transferred from the tool surface to the cooling channels is expressed as shown below (Muvunzi *et al.*, 2017).

$$\dot{Q}_3 = nk_d \frac{2\pi l}{ln\left[\left(\frac{2w}{\pi d}\right) sinh_w\left(\frac{2\pi Zb}{w}\right)\right]}(T_d - T_{cw}) \quad 3\text{-}6$$

It can be concluded from Equation 3-6 that thermal conductivity and the number of cooling channels have an effect on the heat transfer from the tool surface to cooling channels.

The heat transferred from the cooling channels walls to the coolant can be expressed using the Equation 3-7. The parameters $h_{cw}$, $A_c$, $T_c$ and $T_w$ represent the heat transfer coefficient at the cooling channel wall, total surface area of cooling channels, temperature at the cooling channel wall and temperature of the cooling water respectively (Ying and Zhong-De, 2014):The parameter, $h_{cw}$ is dependent on the diameter, flow rate, surface roughness of cooling channels, thermal conductivity and specific heat capacity of the coolant (ESI, 2017).

$$\dot{Q}_4 = h_{cw}A_{cw}(T_{cw} - T_w) \quad 3\text{-}7$$

The heat carried by the coolant in the channels depends on the inlet and outlet temperature of the cooling system as shown in the equation below (Arpaci *et al.*,2000).

$$\dot{Q}_5 = \dot{m}c_w(T_{out} - T_{in}) \quad 3\text{-}8$$

The rate of work done due to friction depends on the contact force ($F$) and the sliding speed ($v_s$) as shown in Equation 3-9 (Haide, 2002).

$$\dot{W}_1 = f_r F v_s \quad 3\text{-}9$$

Equation 3-10 describes the rate of work done during plastic deformation (Kapoor and Nemat-Nasser, 1998; Hosford and Caddell., 2011)

$$\dot{W}_2 = \lambda V \int_0^{\epsilon} \sigma \, d\epsilon \quad 3\text{-}10$$

The martensitic transformation of the blank results in release of latent heat which can be expressed using (Gu *et al.*, 2015).

$$\dot{Q}_6 = mEU_{ms}/t \qquad 3\text{-}11$$

The fraction for martensitic transformation $U_{ms}$ is given by the Koistinen-Marbuger law as shown in Equation 3-12 (Gu *et al.*, 2015). The parameter $\alpha$, represents the stress dependent transformation constant and $T_{ms}$ is the martensitic start temperature

$$U_{ms} = 1 - e^{-\alpha(T_{ms}-T_b)} \qquad 3\text{-}12$$

Substituting Equation 3-12 into 3-11 results in the equation below.

$$\dot{Q}_6 = mE\left(1 - e^{-\alpha(T_{ms}-T_b)}\right)/t \qquad 3\text{-}13$$

## 3.3. Model for Determining Effective Cooling System Parameters

The cooling system structural parameters considered include the distance from the tool contact surface to the cooling channels, the minimum distance between cooling channels and the diameter of the channels as shown in Figure 3-2 (Shan *et al.*, 2013; Lim *et al.*, 2014; Ying and Zhong-De, 2014; Lv *et al.*, 2016a). Other parameters include the coolant mass flow rate ($v$) and the configuration (shape of the channels). The minimum distance between the channels was used as a constraint in the arrangement of the channels. According to Figure 3-2 (which is identical to Figure 2-7 repeated here for convenience), the parameters *Z* and *Y* can be calculated as shown in Equations 3-14 and 3-15.

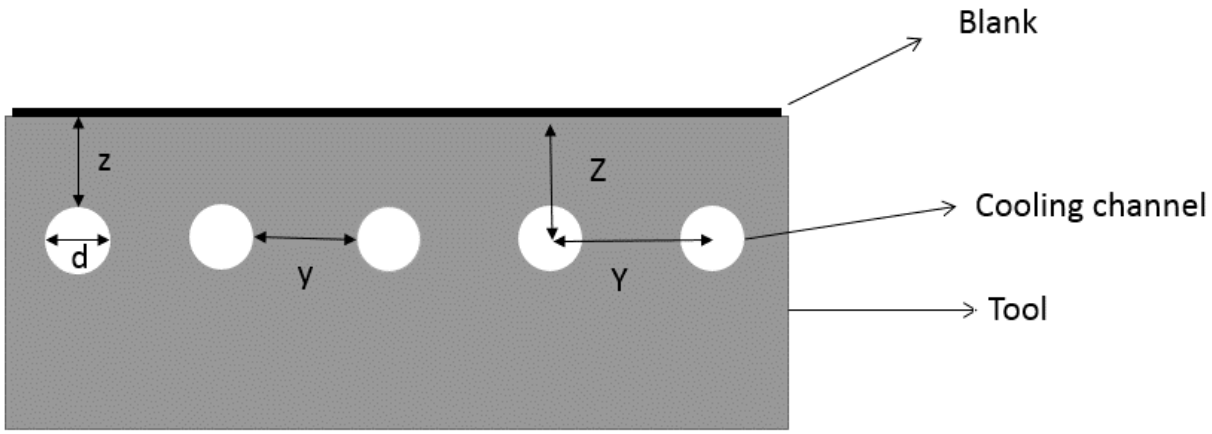


Figure 3-2: Cooling system structure

$$Z = z + {}^{d}/_{2} \qquad 3\text{-}14$$

$$Y = y + d \tag{3-15}$$

The diameter of the cooling channels should allow maximum heat transfer from the tool to the coolant, allow adequate coolant pressure and must be easier to build using SLM. The equation for heat transferred to the cooling channels can be used for obtaining the diameter for the cooling channels.

### 3.3.1. Diameter of cooling channels

As mentioned before, the heat transferred from the tools to the cooling channel walls can be expressed using Equation 3-7. The total surface area covered by the cooling channels is shown in Equation 3-16 where $l_T$ is the cumulative length of all cooling channels (Lim *et al.*, 2014):

$$A_c = n\pi d l_T \tag{3-16}$$

Substituting Equation 3-16 into Equation 3-7 results in the following equation.

$$Q = h_{cw} n\pi d l_T (T_c - T_w) \tag{3-17}$$

The heat released by the blank during the cooling process for a cooling time ($t$) is expressed using Equation 3-18:

$$Q = mC_b\left(T_{bo} - T_{b(t)}\right) \tag{3-18}$$

As mentioned before, it is assumed that the heat lost by the blank is equal to the heat absorbed by the coolant in the channels as expressed in the equation below.

$$mC_b\left(T_{bo} - T_{b(t)}\right) = h_w n\pi d l_T (T_c - T_w) \tag{3-19}$$

Thus, the equation for the diameter of the cooling channel can be expressed as follows:

$$d = \frac{mC_b\left(T_{bo} - T_{b(t)}\right)}{h_w n\pi l_T (T_c - T_w)} \tag{3-20}$$

Making $d$ the subject of the equation:

$$d \leq \frac{mC_b\left(T_{bo} - T_{b(t)}\right)}{h_w n\pi l_T (T_c - T_w)} \tag{3-21}$$

As mentioned before, effective heat transfer mainly occurs at Reynolds numbers ($Re$) between 4 000 and 10 000 as shown below (Lim *et al.*, 2014; Lv *et al.*, 2016):

$$4\,000 \leq Re \leq 10\,000 \tag{3-22}$$

The Reynolds number can be expressed using equation 3-23 (Arpaci *et al.*, 2000). The quantities $\eta_w$ and $\rho_w$ represent the viscosity and density of the cooling water, respectively:

$$Re = \frac{d\rho_w v}{\eta_w} \quad 3\text{-}23$$

Thus, substituting Equation 3-22 into 3-23 results in the following equation (Lim *et al.*, 2014):

$$\frac{4000\eta_w}{\rho_w v} \leq d \leq \frac{10\,000\eta_w}{\rho_w v} \quad 3\text{-}24$$

The diameter of built cooling channels should allow easier removal of the support structures (Xu *et al.*, 2001). The longer and complex the channels are, the more difficult it becomes to remove the support structures and unsolidified powder. In this case, the channels are built in a horizontal position parallel to the tool surface to increase the surface area for heat transfer. Hence, the design rules developed by Thomas (2010) regarding building holes not exceeding 7 mm in a horizontal position are applied as shown in Equation 3-25.

$$d \leq 7 \text{ mm} \quad 3\text{-}25$$

Much smaller diameters are possible ($d$ = 2 mm), however, clogging of the channel walls becomes an issue. In such cases it will be necessary to treat the cooling medium to prevent clogging. Other important factors for selection of suitable diameter include part geometry and pressure variation.

### 3.3.2. Distance from cooling channel diameter to tool surface

Equation 3-26 which describes the heat transfer from a blank contact surface to the cooling channels:

$$\mathrm{Q}_2 = k_d f(T_d - T_w) \quad 3\text{-}26$$

According to previous experimental results, reducing the distance $Z$ shown in Figure 3-2 causes an increase in heat transfer effectiveness (Ye *et al.*, 2013; Lv *et al.*, 2016).The parameters $T_d$ and $T_w$ represent the temperature of the tool and coolant respectively. The shape factor ($f$) describes the quantity of heat transferred to the channels and can be expressed in terms of the cooling channel parameters as shown in Equation 3-27 (Bergman *et al.*, 2011):

$$f = \frac{2\pi l}{ln\left[\left(\frac{2Y}{\pi d}\right) sinh_w \left(\frac{2\pi Z}{Y}\right)\right]} \quad 3\text{-}27$$

It can be seen from equation 3-27 that $f$ is inversely proportional to $Z$. Thus, a reduction in $Z$ results in increased heat transfer. On the other hand, the distance $Z$ should not compromise the structural strength of the tool. Calculations from various optimisation methods showed that a minimum 1:1 ratio of $d$ and $z$ caused the tool to have the required structural strength while improving cooling efficiency (Liu *et al.*, 2013; Lin *et al.*, 2014; Zamri and Yusoff, 2015, 2018). Thus, z should be greater than or equal to $d$ as shown below:

$$z \geq d \tag{3-28}$$

Substituting Equation 3-14 into 3-28 results in the following:

$$Z \geq 1.5d \tag{3-29}$$

According to Shan *et al.*(2013) and Xie *et al.*(2018), the maximum force per unit area acting on the tool ($\frac{F}{A}$) should not exceed the yield stress in order to avoid deformation and failure. This can be expressed using Equation 3-30:

$$\sigma_m \geq \frac{F}{A} \tag{3-30}$$

The press force acting per unit area is the stamping pressure. Hence, the equation can be written as follows, where $P_m$ is the maximum pressure:

$$\sigma_m \geq P_m \tag{3-31}$$

Rao and Schumacher (2004) alluded that the tensile stress acting on a tool with cooling channels is expressed by Equation 3-32 below.

$$\sigma = \frac{0.5Pd^2}{z^2} \tag{3-32}$$

Thus, it follows that the maximum allowable stress ($\sigma_y$) can be expressed as shown in Equation 3-33, given that $P_m$ is the maximum pressure acting on the tool:

$$\sigma_y = \frac{0.5P_m d^2}{z^2} \tag{3-33}$$

Substituting equation 3-31 into 3-33 will result in the following equation:

$$\sigma_y = \frac{0.5\sigma_m d^2}{z^2} \tag{3-34}$$

Hence the distance $z$ can be obtained using the equation below:

$$z_{min} = \sqrt{\frac{0.5\sigma_m d^2}{\sigma_y}} \tag{3-35}$$

Substituting Equation 3-35 into 3-14 results in the following equation below:

$$Z_{min} = \sqrt{\frac{0.5\sigma_m d^2}{\sigma_y}} + {}^{d}/_{2} \tag{3-36}$$

### 3.3.3. Distance between the consecutive cooling channels

Regarding Equation 3-35, the quantity $\frac{\sigma_m}{\sigma_y}$ represents the safety factor (Stephens, 2013). The minimum distance between cooling channels will be used as a constraint in the arrangement of the channels. It is assumed that the cooling channels are circular in shape and that the load acting on the part is uniform. A fatigue design would be suitable for high production runs. However, in this case the tool was designed for strength to allow the stamping operations. Thus, the effect of fatigue is beyond the scope of the study. Accordingly, the hot stamping tool can be considered a rectangular beam with uniform load as seen in Figure 3-3. Thus, the maximum allowable stress can be expressed using Equation 3-37 (Stephens, 2013).

$$\sigma_y = \frac{M_{max}}{W} \qquad 3\text{-}37$$

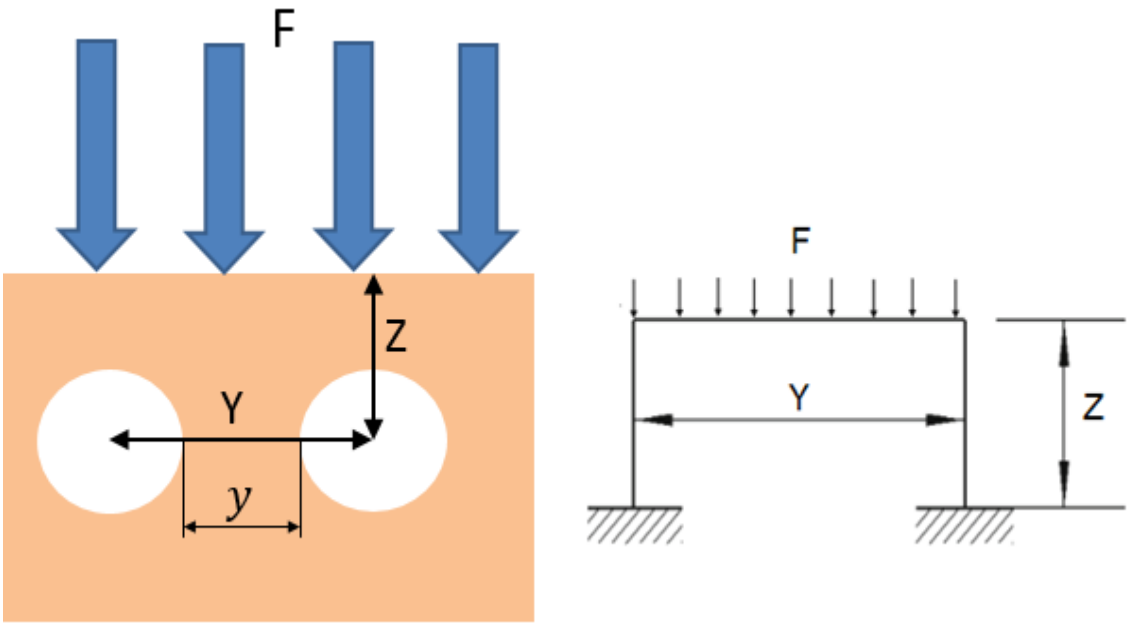


Figure 3-3 Cooling channels model

Using the model in Figure 3-3, the maximum bending moment of a rectangular beam can be expressed as shown in Equation 3-38 (Bansal, 2010):

$$M_{max} = \frac{F_l Y^2}{8} \geq \sigma_y \qquad 3\text{-}38$$

The section modulus, W, can be expressed using Equation 3-39 (Stephens, 2013) where L is the length of the part.

$$W = \frac{LZ^2}{6} \qquad 3\text{-}39$$

Thus, substituting Equations 3-38 and 3-39 into 3-37 results in the following expression:

$$\sigma_y = \frac{\frac{F_l Y^2}{8}}{\frac{LZ^2}{6}} \quad 3\text{-}40$$

Further simplification will result in Equation 3-41 (Xie *et al.*, 2018):

$$Y = \sqrt{\frac{4L\sigma_Y Z^2}{3F_l}} \quad 3\text{-}41$$

Thus Equation 3-41 is used to determine the minimum distance $Y_{min}$ between the channel centres according to Figure 3-3. Establishing the steps of the cooling channel parameters can be summarized using a flowchart as shown in Figure 3-4. The first stage on the flowchart is to determine the diameter of the cooling channel which should be less than 7 mm as indicated in Equation 3-25 (Thomas, 2010). This would depend on the geometry of part, length and ability to remove support material. The next stage is to establish $Z$ using Equations 3-36. After that the minimum distance between channels is calculated using Equation 3-41. This will be followed by the sizing of the supply pipes and design of the configuration of the cooling channels. Using the flowchart, calculations are made to identify cooling channel parameters.

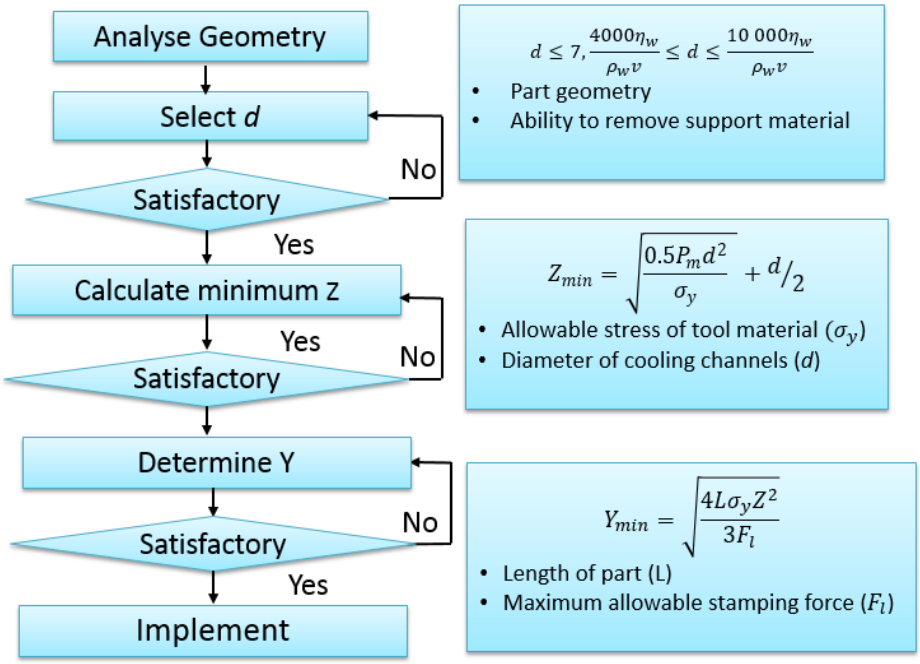


Figure 3-4: Flowchart for determining cooling system parameters

## 3.4. Sizing Of Inlet and Outlet Pipes

Figure 3-5 shows the parameters used to calculate the size of the inlet and outlet connector pipes.

Based on Figure 3-5, the length $l_c$ can be calculated using Equation 3-42.

$$l_c = L - 2Y \tag{3-42}$$

The number of cooling channels are then obtained from Equation 3-43.

$$n = \frac{l}{Y} \tag{3-43}$$

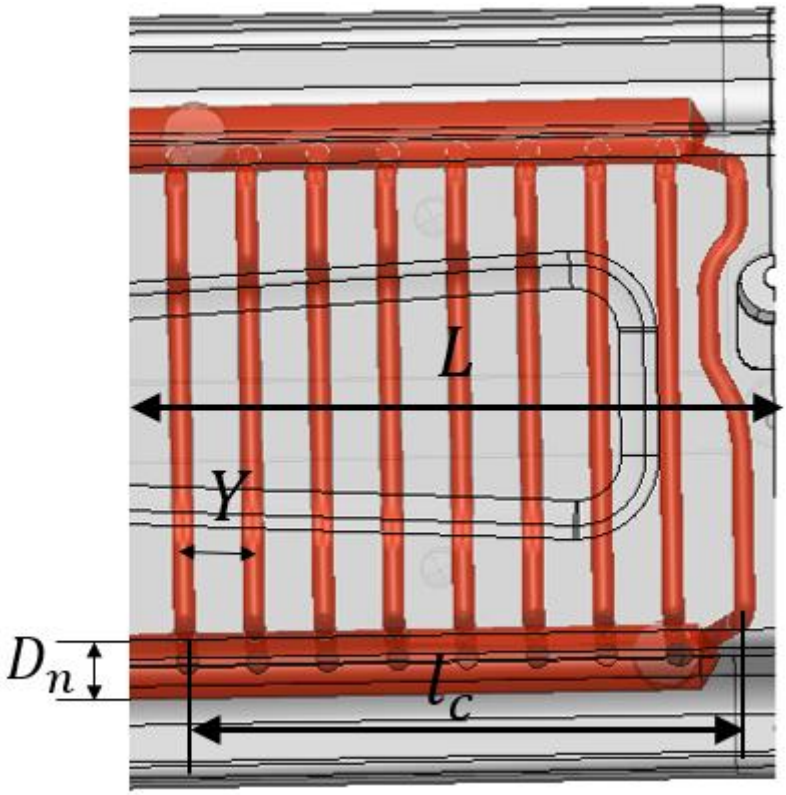


Figure 3-5: Conformal cooling parameters

For effective heat flow, the total cross-sectional area of the channels ($A_n$) can be calculated as shown below given that $A_d$ is the cross-sectional area of one cooling channel.

$$A_n = A_d \times n \tag{3-44}$$

Thus, for a constant flow cross-section, the connector pipe diameter $D_n$ is calculated using Equation 3-45

$$D_n = \sqrt{\frac{4A_n}{\pi}} \tag{3-45}$$

However different pressure drop and tool strength requirements could lead to different diameters The next section explains the development of a model for predicting the minimum cycle time..

## 3.5. Development of Model for Predicting Minimum Cycle Time

A mathematical model for predicting minimum cycle time was developed as a basis for the improved tool design to ensure a reduction in cycle time without compromising the quality of parts. A small Biot number ($Bi \leq 0.1$) is assumed because of the small thickness (0.6-3 mm) of the blank (Nakagawa *et al.*, 2015). The cycle time was considered as the time phase during the transfer, forming and cooling of the blank in closed tools. The equations for the stages were derived based on basic heat transfer and mechanical principles. The following assumptions were made in deriving the model;

- The blank is transferred in a horizontal position in order to maintain a constant height for easier positioning on the forming press. This is because the blank is formed in a horizontal position.
- Heat loss on the edges of the blank is considered negligible because of the small thickness (0.6-3 mm) associated with the blank (Abdulhay *et al.*, 2011).

The lumped heat capacitance method was used since it is applicable in situations when the Biot number is small ($Bi \leq 0.1$) and when the temperature gradient across a solid is considered negligible (Bergman *et al.*, 2011). In the event of a larger Biot number ($Bi > 0.1$), the temperature distribution within the solid becomes a function of position and time (Arpaci *et al.*, 2000). In such cases, the finite difference method becomes applicable since it allows determination of temperature at specific points and time phases on a solid body (Arpaci *et al.*, 2000). The use of graphical analysis (e.g. Heisler charts) is another option. Using the lumped heat capacitance method, differential equations for modelling the process phases are formulated. The differential equations are then solved using the time and temperature limits to formulate an equation governing the cycle time. The following section gives the mathematical models for each of the phases.

The transfer time ($t_{transfer}$) depends on the speed of the mechanical devices which are used to move the blank from the furnace to the stamping press. These can either be conveyor belts or robots. On the other hand, if a specific temperature change is required, the model for predicting cycle time can be derived using heat transfer analysis. Since the blank is transferred at a higher speed to prevent microstructural changes before reaching the press, the effect of natural convection is neglected. According to the analysis done by Shapiro (2009), the radiation heat transferred (107 $W/m^2$) was ten times more than the convection heat loss (8.3 $W/m^2$). Thus, the effect of convection was neglected in their model (Shapiro, 2009). The blank assumes a horizontal position as shown in Figure 3-6 so that it can be easily positioned on the stamping press.

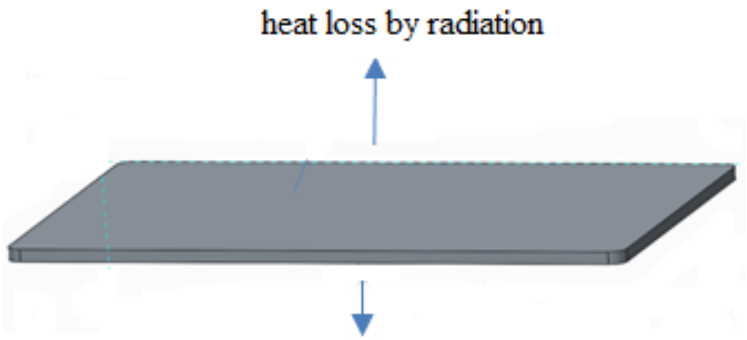


Figure 3-6: Blank position during transfer (Muvunzi *et al*., 2017)

Thus the radiative heat loss on both sides of the blank can be expressed using Equation 3-46 as shown below (Shapiro, 2009). The parameters $\sigma, \varepsilon, A_{b,} T_{fac}$ and $T_b$ represent the Stefan Boltzman constant, emissivity, surface area of blank, temperature of surrounding facilities and temperature of blank respectively.

$$Q = -2\sigma\varepsilon A_b(T_b^4 - T_{fac}^4) \tag{3-46}$$

The change in the internal energy of the blank at any given time is shown below

$$Q = C_b \frac{dT_b}{dt} \tag{3-47}$$

Substituting Equation 3-47 into 3-46 results in the following (Shapiro, 2009):

$$C_b \frac{dT_b}{dt} = -2\sigma\varepsilon A_b(T_b^4 - T_{fac}^4) \tag{3-48}$$

The equation can be simplified as shown below.

$$\frac{2\sigma\varepsilon A_b}{C_b}\int_0^t dt = \int_{T_{b_i}}^{T_b} \frac{dT}{(T_{fac}^4 - T_b^4)} \tag{3-49}$$

Thus, integrating and making $t_{\ transfer}$ the subject, will result in;

$$t_{transfer} = \frac{C_b}{8\sigma\varepsilon A_b {T_b}^3}\left\{ln\frac{(T_{fac}+T_b)/(T_{fac}-T_b)}{(T_{fac}+T_{b_i})/(T_{fac}-T_{b_i})} + 2\left[\tan\left(\frac{T_b}{T_{fac}}\right) - tan^{-1}\left(\frac{T_{b_i}}{T_{fac}}\right)\right]\right\} \tag{3-50}$$

Thus the transfer time can be predicted using Equation 3-50 (Shapiro, 2009).

During the forming stage, the punch moves to deform the blank. The heat exchanges during forming have been explained earlier in section 3.2. The time taken to perform the forming operation depends on the punch speed ($v_f$) and its displacement ($x_f$ ). Equation 3-51 gives the forming time $t_{forming}$.

$$t_{forming} = \frac{x_f}{v_f} \quad 3\text{-}51$$

During the cooling stage, heat is transferred because of contact between the blank and cold tool. The radiation effect is therefore considered negligible (Abdulhay *et al*., 2011). Equation 3-52 describes the heat lost by conduction (Abdulhay *et al*., 2011).

$$Q = -h_c A_b (T_b - T_d) \quad 3\text{-}52$$

Thus, the differential equation below is derived:

$$\rho V C_b \frac{dT}{dt} = -h_c A_b (T_b - T_d) \quad 3\text{-}53$$

The equation is solved as shown below:

$$\frac{dT}{(T_b - T_d)} = -\frac{A_b h_c dt}{\rho V C_b} \quad 3\text{-}54$$

$$\int \frac{dT}{(T_b - T_d)} = -\frac{A_b h_c}{\rho V C_b} \int dt \quad 3\text{-}55$$

$$ln(T_b - T_d) = -\frac{A_b h_c t}{\rho V C_b} + C \quad 3\text{-}56$$

$$e^{ln\left(T_{b_{(t)}} - T_d\right)} = e^{-\frac{A_b h_c t}{\rho V C_b} + C} \quad 3\text{-}57$$

$$T_{b_{(t)}} - T_d = e^{-\frac{A_b h_c t}{\rho V C_b}} * e^C \quad 3\text{-}58$$

$$T_{b_{(t)}} - T_d = Ce^{-\frac{A_b h_c t}{\rho V C_b}} \quad 3\text{-}59$$

Performing substitution at initial conditions to obtain the value of C when *t* is zero:

$$T_{b_{(0)}} - T_d = Ce^0$$

$$T_{b_{(0)}} - T_d = C$$

Substituting C into Equation 3-59 will result in Equation 3-60.

$$T_{b_{(t)}} = \left(T_{b_{(0)}} - T_d\right) e^{-\frac{A_b h_c t}{\rho V c_v}} + T_d \quad 3\text{-}60$$

Making *t* the subject of the equation results in;

$$t_{cooling} = \frac{\rho A_b l C_b}{A_b h_c} \ln \frac{\left(T_{b_{(0)}} - T_d\right)}{\left(T_{b_{(t)}} - T_{d(t)}\right)} \quad 3\text{-}61$$

$$t_{cooling} = \frac{\rho l C_b}{h_c} \ln \frac{\left(T_{b_{(0)}} - T_d\right)}{\left(T_{b_{(t)}} - T_{d(t)}\right)} \quad 3\text{-}62$$

Thus, the cooling time of the blank can be estimated using Equation 3-62. The total cycle time ($t_c$) is therefore given by Equation 3-63 (Muvunzi *et al.*, 2018).

$$t_c = t_{transfer} + t_{forming} + t_{cooling} \quad 3\text{-}63$$

Substituting Equations 3-50, 3-51 and 3-62 into 3-63 becomes Equation 3.52 (Muvunzi *et al.*, 2018):

$$t_c = t_{transfer} + \frac{x_f}{v_f} + \frac{\rho l C_b}{h_c} \ln \frac{\left(T_{b_{(0)}} - T_d\right)}{\left(T_{b_{(t)}} - T_{d(t)}\right)} \quad 3\text{-}64$$

Equation 3-64 above describes the cycle time for a hot sheet metal forming operation. On the other hand, if the transfer time is expressed as a function of temperature, then the cycle time can be expressed using Equation

3-65 (Muvunzi *et al.*, 2018).

$$t_c = \frac{C_b}{8\sigma\varepsilon A_b {T_b}^3}\left\{ln\frac{(T_{fac}+T_b)/(T_{fac}-T_b)}{(T_{fac}+T_{b_i})/(T_{fac}-T_{b_i})} + 2\left[\tan\left(\frac{T_b}{T_{fac}}\right) - tan^{-1}\left(\frac{T_{b_i}}{T_{fac}}\right)\right]\right\} + \frac{x_f}{v_f} + \frac{\rho l C_b}{h_c} \ln \frac{\left(T_{b_{(0)}} - T_d\right)}{\left(T_{b_{(t)}} - T_{d(t)}\right)} \quad 3\text{-}65$$

## 3.6. Development of Alternative Conformal Cooling Layouts

The techniques to be used for arranging the cooling channels were suggested by Park and Pham (2009). These include parallel, series and zigzag as shown in Figure 3-7. The techniques can be combined, depending on the geometry of the part. Spiral cooling is often used for parts with intricate

curves or circular features (Park and Pham, 2009). The parallel cooling method allows all the regions of the tool to be cooled simultaneously while the zigzag pattern causes different regions on the tool to be cooled at separate intervals, depending on the geometry of part (Hall and Krystofik, 2015).

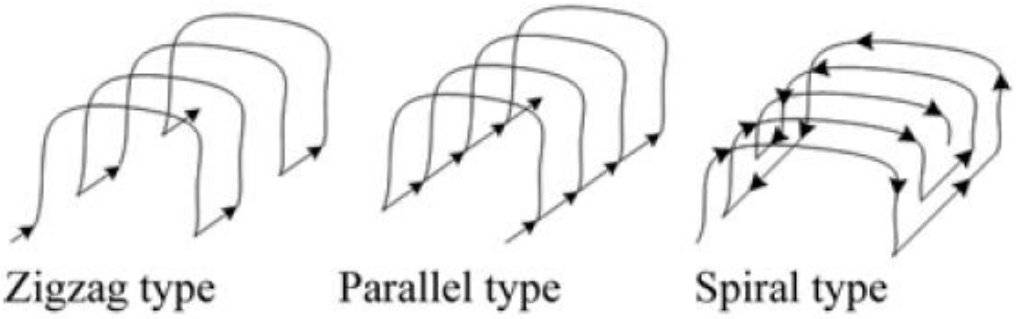


Figure 3-7: Arrangement of conformal cooling channels (Park and Pham, 2009)

### 3.6.1. Evaluating the possible layouts

After devising alternative layouts, a selection criterion is developed to evaluate possible layouts. The criteria are obtained from literature analysis and consultation with experts. The weights for the criteria, in terms of degree of importance, are determined using the Analytic Hierarchy Process (AHP) (Velasquez and Hester, 2013). This method is used because it is a credible systematic decision making tool applicable for assigning weights when dealing with more than one criteria (Ishizaka and Nemery, 2013). Also, the method has been extensively used in decision making for manufacturing applications (Vaidya and Kumar, 2006). Moreover, it has an inbuilt self-evaluation tool for checking the logical consistency of the assigned weights (Velasquez and Hester, 2013). The AHP process involves the steps listed below (Ishizaka and Nemery, 2013):

- Defining alternative solutions
- Defining the criteria
- Using the pairwise comparison to calculate weights of the criteria
- Checking consistency of the weights
- Assigning the weights

After defining the alternative layouts and selection criteria, the next step involves conducting the pairwise comparison of all criteria. Given that $i$ and $j$ represent two criteria, the decision maker provides a paired comparison of two on a scale from 1 to 9 as shown in Table 3.1 (Ishizaka and Nemery, 2013). The corresponding criterion becomes the reciprocal of the other. Thus $a_{ji} \rightarrow {}^{1}/_{a_{ij}}$

Table 3.1: Fundamental scale (Ishizaka and Nemery, 2013)

| **Degree of Importance** | **Definition** |
|---|---|
| **1** | **Equal Importance** |
| 2 | Weak |
| **3** | **Moderate Importance** |
| 4 | Moderate plus |
| **5** | **Strong Importance** |
| 6 | Strong plus |
| **7** | **Very strong** |
| 8 | Very very strong |
| **9** | **Extreme importance** |

A comparison matrix *A*, for $m$ criteria, is then completed as shown in Equation 3-66 (Brunelli, 2015).

$$A = \begin{bmatrix} a_{11} & a_{12} & \dots & a_{1m} \\ a_{21} & a_{22} & \dots & a_{2m} \\ \vdots & \vdots & \ddots & \vdots \\ a_{m1} & a_{m2} & \dots & a_{mm} \end{bmatrix} \quad 3\text{-}66$$

In Equation 3-67 the matrix is then normalised by dividing each value in the matrix by the column sum as shown (Chuang, 2001):

$$A_w = \begin{bmatrix} \frac{a_{11}}{\sum_{i=1}^{m} a_{i1}} & \frac{a_{12}}{\sum_{i=1}^{m} a_{i2}} & \dots & \frac{a_{1m}}{\sum_{i=1}^{m} a_{im}} \\ a_{21} & a_{22} & \dots & a_{11} \\ \vdots & \vdots & \ddots & \vdots \\ \frac{a_{m1}}{\sum_{i=1}^{m} a_{i1}} & \frac{a_{m2}}{\sum_{i=1}^{m} a_{i2}} & \dots & \frac{a_{mn}}{\sum_{i=1}^{m} a_{im}} \end{bmatrix} \quad 3\text{-}67$$

The next step is to calculate the weight *c* using the matrix in Equation 3-68 (Chuang, 2001):

$$C = \begin{bmatrix} C_1 \\ \vdots \\ \vdots \\ C_m \end{bmatrix} = \begin{bmatrix} \frac{\frac{a_{11}}{\sum_{i=1}^{m} a_{i1}} + \frac{a_{12}}{\sum_{i=1}^{m} a_{i2}} + \cdots \frac{a_{1m}}{\sum_{i=1}^{m} a_{im}}}{m} \\ \vdots \\ \frac{\frac{a_{m1}}{\sum_{i=1}^{m} a_{i1}} + \frac{a_{m2}}{\sum_{i=1}^{m} a_{i2}} + \cdots \frac{a_{mm}}{\sum_{i=1}^{m} a_{im}}}{m} \end{bmatrix} \quad 3\text{-}68$$

The consistency of the calculated weights are then calculated by firstly obtaining the product of *P* and *C* and computing the principle eigenvalue as shown in Equation 3-69 (Chuang, 2001):

$$A.C = \begin{bmatrix} a_{11} & a_{12} & \dots & a_{1m} \\ a_{21} & a_{22} & \dots & a_{2m} \\ \vdots & \vdots & \ddots & \vdots \\ a_{m1} & a_{m2} & \dots & a_{mm} \end{bmatrix} \begin{bmatrix} C_1 \\ \vdots \\ \vdots \\ C_m \end{bmatrix} = \begin{bmatrix} x_1 \\ x_2 \\ \vdots \\ x_m \end{bmatrix} \quad 3\text{-}69$$

In Equation 3-70, the measure of consistency *C1* is then calculated (Ishizaka and Nemery, 2013):

$$CI = \frac{\delta_a - m}{m - 1} \quad 3\text{-}70$$

The obtained *CI* is then divided by the random index value (*RI*) to check the consistency. The standard random index values for criteria 1 to 10 are shown in Table 3.2 (Ishizaka and Nemery, 2013).

Table 3.2: Random Indices (Ishizaka and Nemery, 2013)

| n | 1 | 2 | 3 | 4 | 5 | 6 | 7 | 8 | 9 | 10 |
|---|---|---|---|---|---|---|---|---|---|---|
| RI | 0 | 0 | 0.58 | 0.9 | 1.12 | 1.24 | 1.32 | 1.41 | 1.45 | 1.49 |

If the ratio *CI/RI* is less than or equal to 0.1, the consistency is satisfactory (Brunelli, 2015). However, if it is greater than 0.1, then the weights are inconsistent; the process will need to be started again and the weights re-assigned (Brunelli, 2015).

## 3.7. Summary

The purpose of this chapter was to present the heat transfer scenarios during hot stamping and to develop a model for determining conformal cooling system structural parameters for a hot stamping tool. The model is formulated using previous literature on the design of cooling channels in hot stamping tools. Additionally, principles of heat transfer and mechanics are used in order to design parameters that allow effective heat transfer without compromising the structural strength of the tool. Furthermore, AHP for evaluating alternative conformal cooling layouts, is presented. The tool is used to decide the most suitable design by assigning weights to different criteria and comparing the total scores of each design.

# CHAPTER 4 : METHODOLOGY

## 4.1. Research Design

The purpose of this chapter is to explain the methods used in order to answer the research question and fulfil the objectives of the study. As mentioned in Chapter 1, the research question is centred on identifying the parameters viable for the application of AM so as to improve thermal management of hot sheet metal forming tools. To answer the question, a quantitative research design was used because the parameters investigated in the study are measurable. Also, the study seeks to identify the viability and effect of a conformably cooled hot sheet metal forming tool on the cycle time and quality. A quantitative research design would therefore allow an investigation of the relationship between the variables involved. The research methods used include modelling, engineering design and experimentation. The next section explains how and why these methods were used in this study.

### 4.1.1. Modelling

Modelling is a method of representing a physical system or object in a conceptual, mathematical, schematic or logical manner for explanatory, descriptive or prediction purposes (Dym, 2004). Modelling is a cost effective, less time consuming and safer method that allows an in-depth study of a system or object (Samarskii and Mikhailov, 2014). However, sometimes models do not include all the details to avoid complexity and are mostly based on approximations which can compromise accuracy. Hence, it is necessary to conduct physical experiments for validation purposes. In this study, mathematical models were used to predict the cooling system parameters which allow effective thermal management of hot stamping tools and to predict minimum cycle time of a hot sheet metal forming process. Thus, the method achieved the first two objectives of the research. The model for determining effective cooling parameters was developed and validated through the benchmark part using simulation and experimentation.

According to Carson and Cobelli (2013), mathematical models can either be developed by using experimental data or fundamental knowledge of a system. In this case, the models were developed by building on previous experimental results from literature and basic principles of heat transfer and mechanics. The model framework used in the study is shown in Figure 4-1. Based on the framework, existing knowledge on the subject is used together with certain assumptions to develop the model.

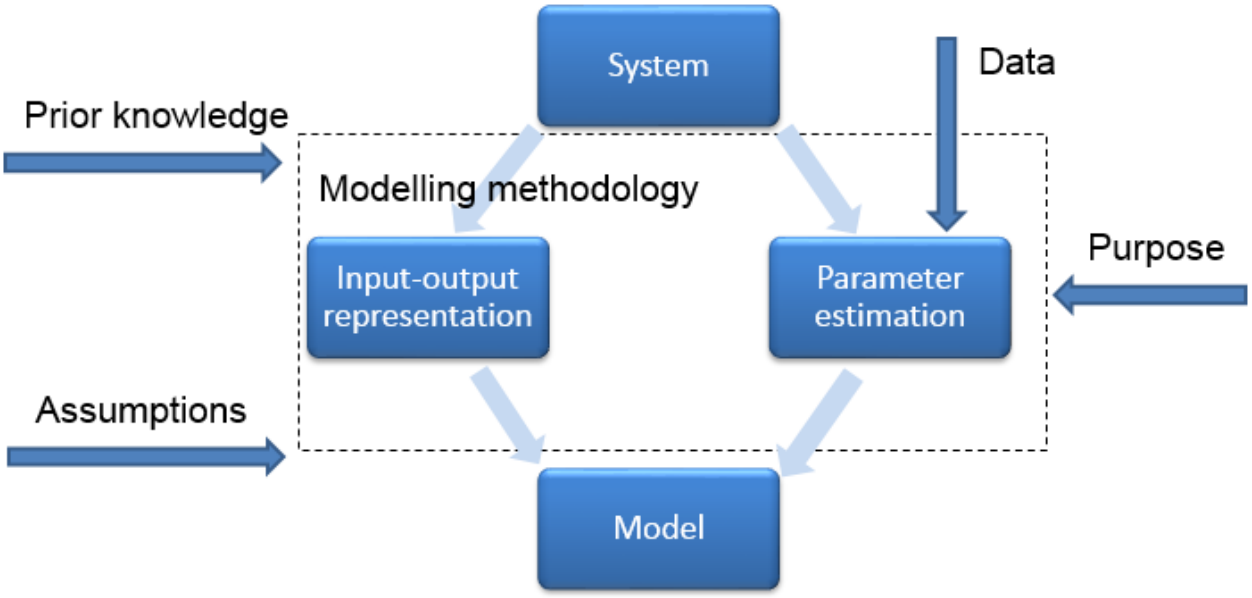


Figure 4-1: Model framework (Carson and Cobelli, 2013)

To solve a mathematical model and study its behaviour, simulation is often used (Dym, 2004). In other words, it is the same as performing experiments on the computer. It is a useful tool to test the validity of the mathematical model. It is mainly advantageous when it is dangerous, time consuming, expensive or impossible to conduct physical experiments (Samarskii and P., 2014).

### 4.1.2. Engineering design method

The engineering design method is a systematic and iterative process of establishing and defining engineering solutions for problems (Vorus, 2017). In the study, this method was used to achieve the third and fourth objectives which are focused on the design and manufacture of an AM based effective conformal cooling system for the benchmark part. An important advantage of using the engineering design method lies in the iterative approach which provides the opportunity to further improve a design (Dieter, 2000). On the other hand, it can be time consuming as each engineering problem is unique and might require certain steps to resolve (Pahl *et al.*, 2007). This is mainly because there is no universally agreed sequence of stages that leads to an engineering design, although the main components are similar (Dieter, 2000). Different authors have proposed their own design processes varying from five to more than twenty steps. In this case, a simplified approach of the engineering design process as shown in Figure 4-2, was used. Since the problem was defined in the first chapter and the necessary information was gathered in the second chapter, the next stage involved coming up with possible designs. The possible solutions were then analysed against evaluation criteria. After evaluating each solution, the most suitable design was selected and evaluated using simulation. Further improvements were made to the design and the simulation was repeated until the final design

was developed. The fifth chapter gives in-depth details of how the method was used to develop the improved cooling system.

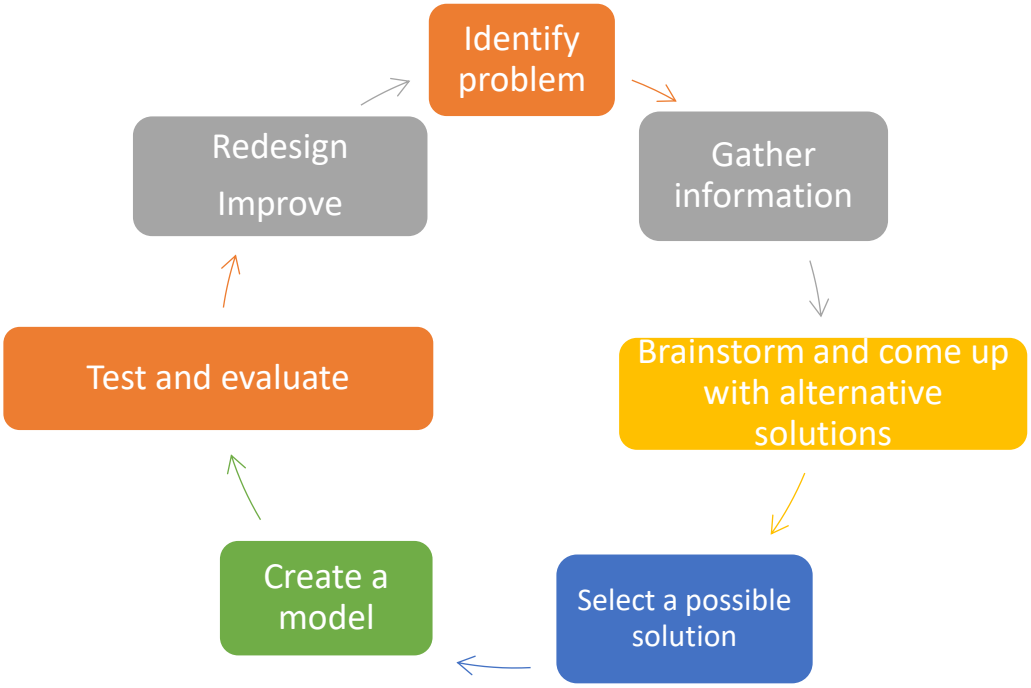


Figure 4-2: Engineering design process (Jack, 2013)

### 4.1.3. Experimental method

In manufacturing, the experimental method is mainly used to investigate the relationship between process parameters and their effect on quality characteristics (Antony, 2014). The method is used to achieve the last objective of the study. The main reason is that the last objective is centred on investigating the impact of the improved cooling system on quality and cycle time. Proper application of the experimental method in manufacturing can result in quality improvement, reduced manufacturing costs and improved process yields (Montgomery, 2012). However, if not properly conducted, experiments can produce artificial results and be subjected to bias (Antony, 2014). In the present study, replication and randomisation are used to minimise the presence of bias. Replication increases the sample size thereby increasing the viability of the results (Montgomery, 2012). A replicate is a complete repetition of the same experimental conditions. Also, the forming parameters such as stamping force and displacement are adopted from the actual mass production process in order to reduce the probability of obtaining artificial results.

The experimental method involves formulating a hypothesis and determining whether the hypothesis is true (Coutelieris and Kanavouras, 2018). In the study, the hypothesis is that a conformal cooling system used in place of a conventional cooling system results in a reduction in cycle time and improvement in quality. Experiments were thus conducted using the conformal cooling tool and its

performance was compared to the conventional tool. Chapter 5 gives in-depth information on the experiments. The performance of the tools was measured based on the temperature and quality of the formed parts (hardness distribution). The controllable factors for the experiments include the configuration of the cooling channels, cooling time and temperature of coolant.

The traditional method of designing experiments allows the variation of one parameter while other parameters are kept constant. The challenge with this approach is that it involves several experimental runs thus consuming time and resources. Secondly, it does not give information on the optimum balance of all parameters involved. Thirdly, it does not provide information on the interaction between factors (Rodrigues and Iemma, 2014).

Measures were taken to avoid levels which are too close or too far apart in order to obtain the correct information (Rodrigues and Iemma, 2014). Full factorial designs can be costly and time consuming. For this situation, a central composite design was considered because of the need to identify the best combination of parameters for minimising the cooling time and maximising quality (minimum hardness deviation) at a minimum cost.

## 4.2. Overall Research Approach

The overall approach which was adopted to achieve the goal of the research is highlighted in the flowchart in Figure 4-3. It shows how the research methods were interrelated. Based on the information in the flowchart, the first method which was used is modelling; this was followed by the engineering design method. Lastly, experimentation was conducted to validate the model. The next section gives an in-depth step by step technical explanation of how modelling was used to achieve the first two objectives of the study.

## 4.3. Mathematical Modelling

The goal of the cooling system design model is to reduce cooling time through increasing heat transfer, to allow uniform cooling and to ensure that the structural strength of the tool is preserved. The model for predicting cycle time is a useful benchmark tool that can be used as a basis for increasing productivity without compromising quality. It serves to show the minimum possible cycle time that can be achieved for a given part. The cooling system structural parameters considered include the distance from the tool contact surface to the cooling channels, the minimum distance between cooling channels and the diameter of the channels as shown in Figure 3-2.

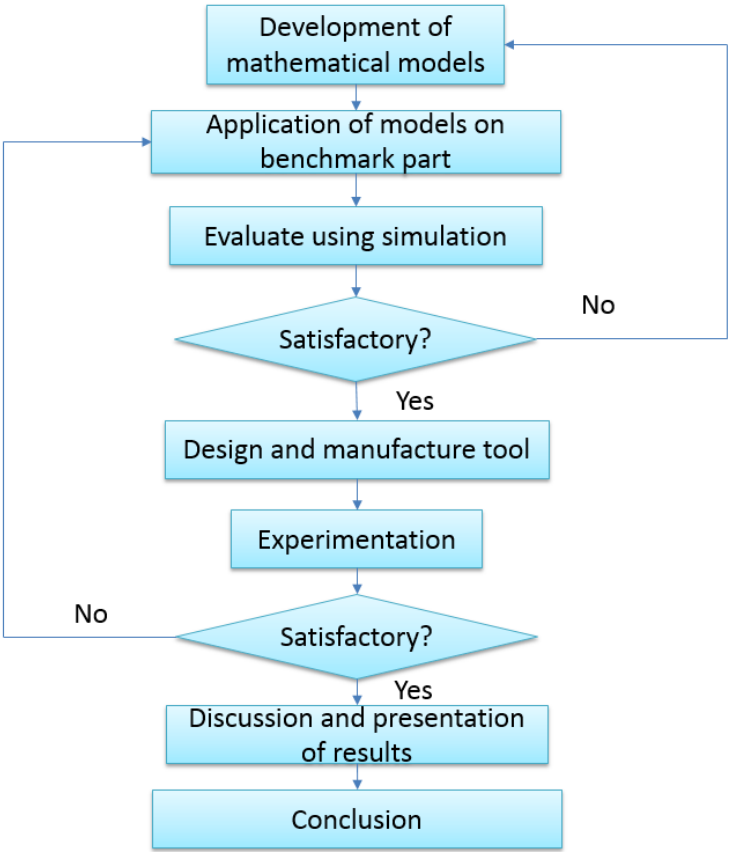


Figure 4-3: Approach used in the study

## 4.4. Application of Model to a Typical Benchmark Part

To investigate the viability of using AM in the manufacture of hot stamping tools with parameters obtained from the model, a real-life benchmark part is used. The selection criteria for qualifying the part include the geometric complexity of part, cooling capability of tools, production volume of parts and hardness requirements as shown in Table 4.1. When the conditions 2 and 3 in the shaded region of the table are met, then there is an opportunity to further improve the current cooling system. Thus, a part will qualify as a benchmark. Regarding the geometric complexity, if the straight cooling channels do not conform to the shape of the part then it qualifies as a benchmark part. This also applies to cases in which it is difficult to drill cooling channels because of the complexity of the tool geometry. Thermal challenges associated with uneven cooling include non-uniform hardness, fractures and warpages. It is economically viable to target a part which is produced in medium to high volumes such that the costs associated with constructing the improved tool design is outweighed by the reduction in cycle time, defects and increased press capacity. Uniform hardness of a part can be attained if it is cooled evenly. Thus conformal cooling channels can be used where there is a strong need to improve hardness uniformity. Due to their unlimited freedom of design, conformal cooling channels can also be applied when there is need for different hardness requirements on a part.

Table 4.1: Factors considered when selecting benchmark part

| Factor | Classification of 3 cooling conditions | | |
|---|---|---|---|
| | **Condition 1** | **Condition 2** | **Condition 3** |
| Geometric complexity | Straight cooling channels conforming to part (simple geometry) | Straight channels not conforming to curved features of part | Straight drilled channels not possible due to complexity of geometry |
| Cooling capability of tools | Sufficient cooling of parts | Need for reducing cooling time | Presence of thermal challenges associated with insufficient cooling such as warpage (dimensional distortion), |
| Production volume of formed parts | Low volume production (<10 000) | Medium volume production (10 000-100 000) | High volume production (>100 000) parts per year |
| Hardness requirements | No strict requirement on hardness uniformity | Need for uniform hardness | Need for tailored hardness properties (regions with different hardness requirements on one part) |

### 4.4.1. Finite Element simulation

The purpose of the FE simulation is to evaluate the effect of the tool with structural parameters obtained from the model on the cooling time and quality characteristics of the formed part. The FE simulation process is shown in Figure 4-4


Figure 4-4: FE Model building

The purpose of the simulation is to compare the cooling system performance of the conformal and straight cooling layout. The results for the simulation are analysed based on the following:

i) Measuring the cooling performance by comparing the blank maximum temperature at the end of the cooling process with the initial temperature (Zamri and Yusoff, 2015; Hu and Ying, 2016)
ii) Evaluating the cooling uniformity by using the difference between the maximum and minimum temperature at the end of the cooling process (He *et al.*, 2016)
iii) Evaluating the quality of parts by measuring the hardness deviation of parts.

### 4.4.2. Expected results

A significant decrease in the cooling time is expected for parts formed using the tool with the modified cooling system. This is because the profile and geometry of the cooling channels is meant to increase the heat absorption by the water circulating in the tool. It is assumed that the tool life would be extended through reduction of thermal stresses. Also, the modified tool is expected to have a lesser temperature deviation due to the conformal arrangement of the channels. Thus, the quality of the parts was anticipated to improve through increased hardness uniformity.

## 4.5. Summary

The purpose of the chapter is to present the research methodology. The research methods used in the study are modelling, engineering design and experimentation respectively. An explanation of how and why those research methods were applied, is given. This included an overall research approach explaining the sequence of the methods. The first stage of the study involves mathematical modelling using literature study and basic principles of heat transfer and stress analysis. This maps the way forward in the development of a method for determining cooling system structural parameters and a model for predicting minimum cycle time. The chapter also gives a skeletal explanation of how the simulation is conducted and the expected results. The next chapter explains how the models were applied to the benchmark part. It also gives an in-depth step by step explanation of the simulation and design of the improved cooling system.

# CHAPTER 5 : DESIGN AND FE SIMULATION OF CASE STUDY TOOL

## 5.1. Introduction

This chapter explains how the proposed models were applied to a real-life benchmark part. The conformal cooling system design for the benchmark part is also explained. This is followed by a simulation process to evaluate the performance of the new design and compare it with the conventional straight cooling layout.

## 5.2. Real Life Benchmark Component

The part used as a benchmark is shown in Figure 5-1; it was provided by the research partner (Fraunhofer Institute for Machine Tools and Forming Technology). The dimensions of the part are shown in Figure 5-2. The component is a demonstrator part which resembles a rocker panel of an automobile vehicle. Using the criteria in Table 4.1, the part qualifies as a benchmark. This is because it has a relatively complex geometry with curved features beyond the reach of straight channels. Secondly, there was a need by the research partner to find ways of reducing cycle time and enhancing the quality of the part through achieving uniform hardness. Furthermore, the resembled part is a critical component for safety in an automobile vehicle with higher production volumes (>100 000 parts per year). Due to the above mentioned reasons, the component met the selection criteria in Table 4.1, accordingly, it was considered as the benchmark part. The CAD model for the part and tool assembly were then examined. The inability of the straight channels to conform to the shape of the part shows the shortcomings of the conventional cooling method.

Figure 5-1: Benchmark part

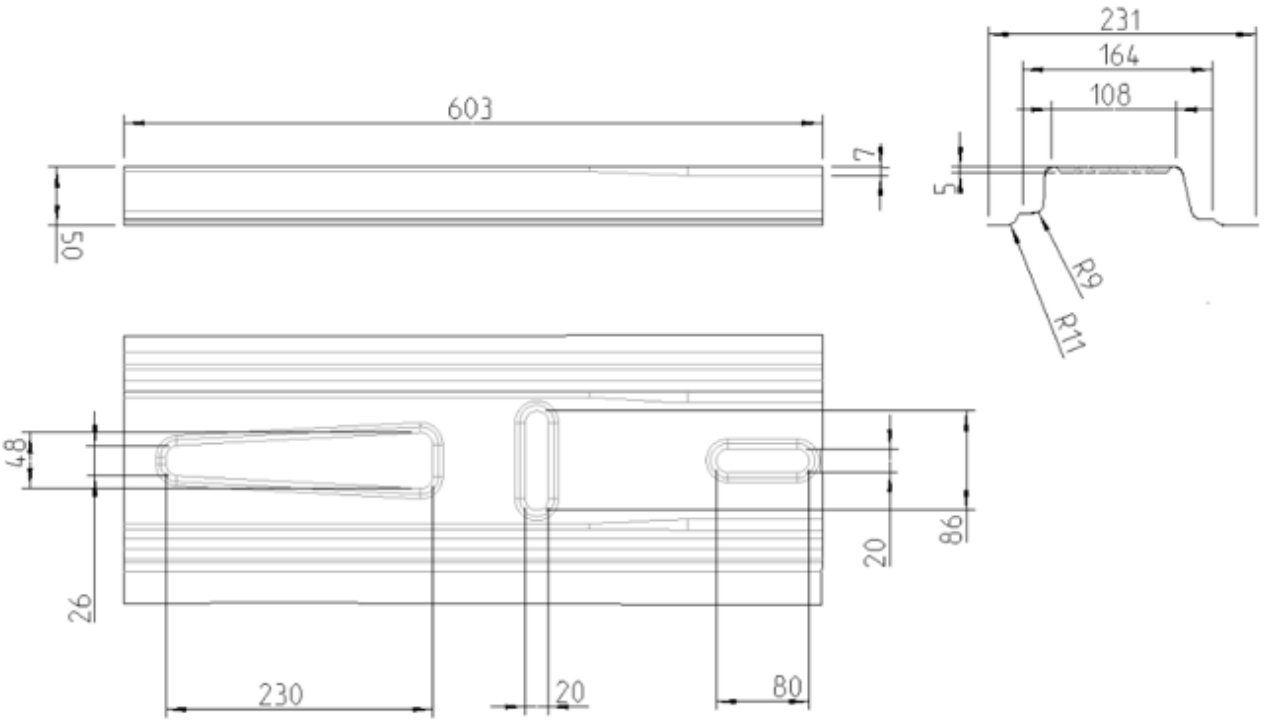


Figure 5-2: Benchmark part dimensions

The cooling system of the tool (punch and die) is shown in Figure 5-3. The improved cooling system is aimed at increasing cooling effectiveness by exploiting the design freedom of AM. This is achieved by the creation of conformal optimized cooling channels. In this case, SLM, an AM process for manufacturing functional parts, was used. This particular process was used because of the ability of the SLM process to produce fully dense metallic parts with mechanical properties, comparable to conventionally manufactured parts (Schmidt *et al.*, 2017). Also, the SLM machine is locally available at the STC-LAM (Stellenbosch Technology Centre Laboratory for Advanced Manufacturing). As mentioned earlier in the literature review, alternative processes that can be used include EBM and DMD. Only the punch was designed to reduce the costs associated with manufacturing the tool. Another reason is that the geometry of the punch makes it easier to manufacture additively using SLM as compared to the die. The cooling system parameters were then determined using the developed model.

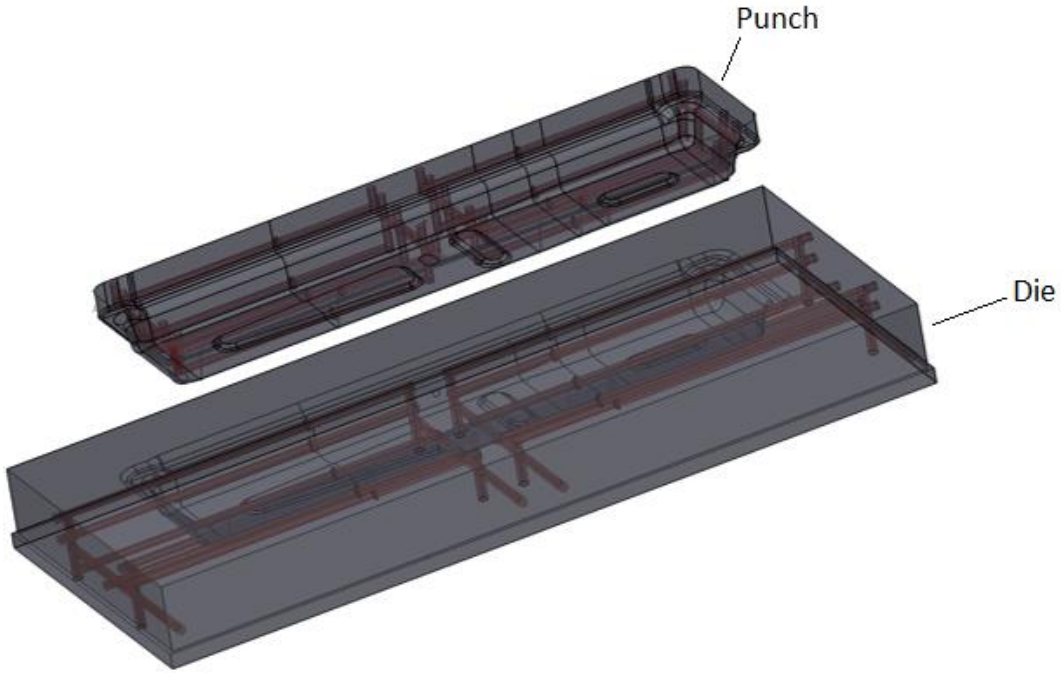


Figure 5-3: Cooling system of tool (punch and die)

The conventional hot stamping punch is a combination of three connected tool inserts (segments) as shown in Figure 5-4. Inserts number 1, 2 and 3 have lengths of 225, 300 and 220 mm, respectively. The tool is segmented into those lengths depending on the maximum drilling depth achievable, part complexity and length. Deeper drilling depths require more resources in terms of the tooling costs and CAM programs (Mueller *et al.*, 2014). The current cooling system layout with straight channels is shown in Figure 5-5. The cooling channels are 10 mm in diameter and the coolant flows in the direction as shown in Figure 5-4

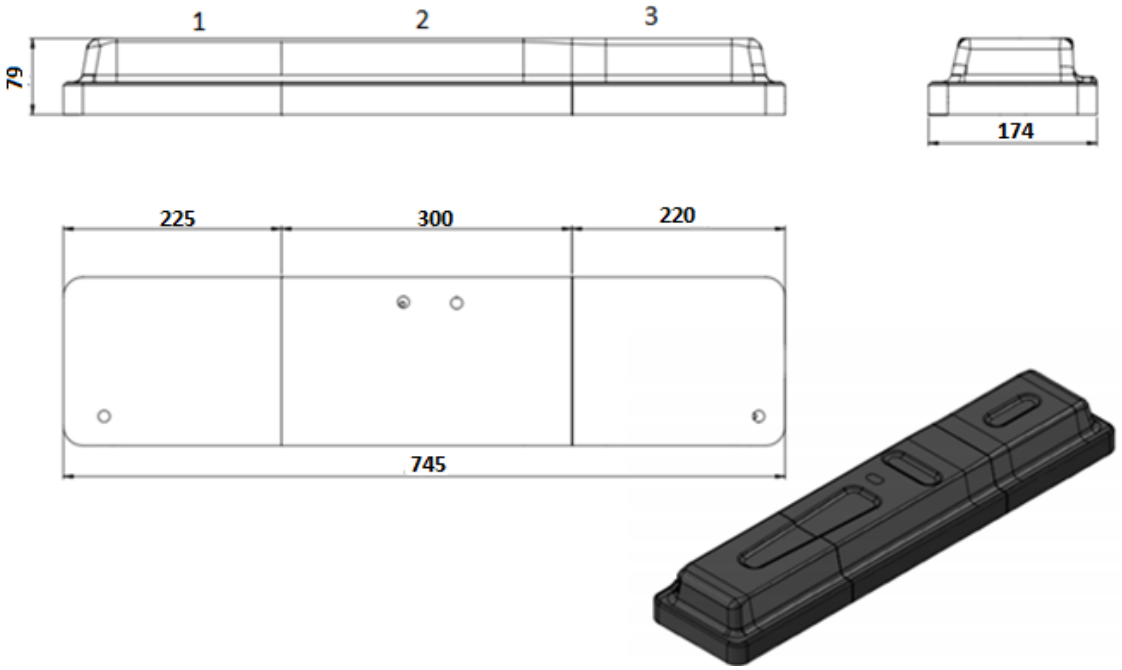


Figure 5-4: Dimensions of punch

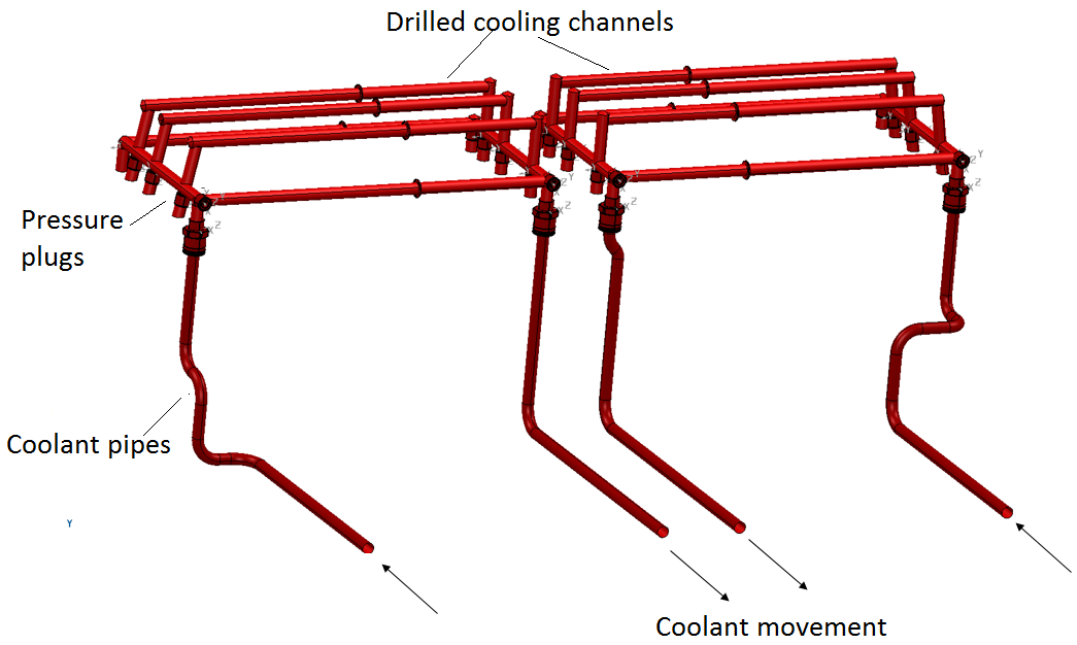


Figure 5-5: Flow of coolant in the conventional channels

In the next section, the minimum cooling time for the benchmark part is calculated. This is used as a basis for designing the tool to ensure a reduction in cycle time without compromising the quality.

## 5.3. Calculating Minimum Cycle Time as a Basis

To show that there is an opportunity to further reduce the cooling time by using an improved cooling system design, calculations for the minimum possible cooling time of the blank are made. The calculations are done based on the proposed model in Equation 3.61 which was derived in Chapter 3. Based on the experimental study which was done by Bosetti *et al.* (2010), the maximum heat transfer coefficient is approximately 3300 W/m$^{2^\circ}$C when considering the typical contact pressure ranges in industry. Other parameters used for the calculations are shown in Table 5-1.

$$t_{cooling} = \frac{\rho l C_b}{h_c} \ln \frac{(T_b - T_d)}{(T_{b_{(t)}} - T_{d(t)})} \qquad 5\text{-}1$$

$$t_{cooling} = \frac{7\,830 \times 0.0015 \times 650}{3300} \ln \frac{(800 - 25)}{(200 - 25)}$$

$$= 3.244\ s$$

Table 5-1: Process parameters

| Symbol | Parameter | Description |
|---|---|---|
| $C_b$ | Specific heat capacity of blank ($C_b$) | 650 J/kg˚C |
| $h_c$ | Heat transfer coefficient | 3300 W/m$^{2}$˚C |
| $l$ | Thickness of blank | 0.0015 m |
| $T_b$ | Initial temperature of blank | 800˚C |
| $T_{b(t)}$ | Targeted blank final temperature | 200 ˚C |
| $T_d$ | Initial temperature of tool (punch and die) | 25˚C |
| $\rho$ | Density of blank | 7 830 kg/m$^3$ |

According to the calculations made in Equation 3.61, the minimum cooling time is 3.24 s. This is below the conventional tool cooling time of 7 s. Thus, there is an opportunity to further reduce the cooling time through redesigning the cooling system. The following section explains the design of the conformal cooling channels.

## 5.4. Design Methodology for the Cooling System Configuration

As mentioned in Chapter 4, the engineering design method is used to develop the most suitable configuration for the conformal cooling system. Initially, Chapter 1 defines the problem which is the insufficient cooling of straight drilled channels. The necessary information was gathered in Chapter 2. Thus, the next step is to devise alternative conformal cooling layouts and evaluate them. The following section explains some of the design rules used in developing alternative layouts.

### 5.4.1. Design for manufacturability

Design for manufacturability is the practice of designing products in such a way that they are cost effective and easier to manufacture (Anderson, 2014). To simplify the manufacturing process and reduce costs, the conformal cooling system layout is split into a complex and less complex portion. This is done so that the complex portion is manufactured additively while the remaining section is machined. To reduce the costs associated with manufacturing the tool, emphasis should be on reducing the portion manufactured using Selective Laser Melting as much as possible. This is because

of the associated powder and energy costs involved. Increasing the built portion would also increase the time taken in producing the tool inserts. Hence, the geometry of cooling channels should be simplified as much as possible for the portions to be machined. Only the sections to be built should have complex geometry, which is unachievable using machining.

When designing the cooling system for the complex part of the hot stamping tool (which is produced using additive manufacturing), the following principles are applied.

- The distance from cooling channels to the tool surface is kept constant throughout.
- The minimum distance between the cooling channels ($y$), is used as a constraint in the arrangement of cooling channels.
- The cooling channels should conform to the part geometry.

### 5.4.2. Design for assembly

This refers to a practice of designing products to optimize the assembly process while ensuring proper functionality (Eastman, 2012). Hence, the cooling system is designed to allow easier assembly of the tool inserts. This is achieved by making the cooling channels parallel, longitudinal or spiral to the tool surface and joining them to a collector pipe which can be connected with another channel in the corresponding insert. The other strategy used is to place an inlet and outlet point on each insert. In that way, connector plugs are not required, making the tool assembly much easier and interchangeable. The tool assembly process should also be cost effective. The costs to be considered for the tool assembly include the labour cost, and the cost of connectors and sealing plugs. Also, the time taken to conduct the assembly operations, should be considered.

### 5.4.3. Design for cooling efficiency

In hot stamping, the cooling efficiency can be described by the cooling rate and cooling consistency (Karbasian and Tekkaya, 2010). As mentioned before, the cooling rate is increased through reducing the distance $z$ in Figure 3.2 and increasing the surface area occupied by the cooling channels (Jiang *et al.*, 2012; Lim *et al.*, 2014a; He, X.-D. Li, *et al.*, 2016; Hu, He and Ying, 2016; Lv *et al.*, 2016a). It is also important to keep the cooling channels as short as possible to allow the coolant to enter and leave the inserts quickly so as to permit a faster heat removal process. Cooling consistency is affected by the arrangement and distance between the channels (Lim *et al.*, 2014a; Lv *et al.*, 2016a). Thus, the cooling system is designed with the aim of improving both the cooling rate and cooling consistency. In this case, the distance from the tool surface to the centre of cooling channels (Z) from Figure 3.1 is obtained from the proposed model. Hence, the cooling effectiveness was measured based on geometry of the cooling channel network, surface area occupied by the cooling channels and how

they provide full coverage to the part during the cooling phase. The design of the cooling system has a great influence on the strength distribution of the produced part (Lin *et al.*, 2014). For the selected benchmark part, uniform hardness is required, thus the cooling channels should be uniformly distributed throughout to ensure even cooling of the blank. This is important in regions where the blank is in contact with the tool. On the other hand, some parts are required to have tailored properties. In such cases, the parts will have multi strength requirements to improve ductility and energy absorption properties. Thus, the cooling system design can be tailored to allow different cooling rates in the part regions.

### 5.4.4. Design of cooling channel networks

The design of the cooling system is done using Autodesk PowerSHAPE 2019 (Autodesk, 2019). Using the design software, the cooling lines are developed by offsetting from the tool surface as shown in Figure 5-6.

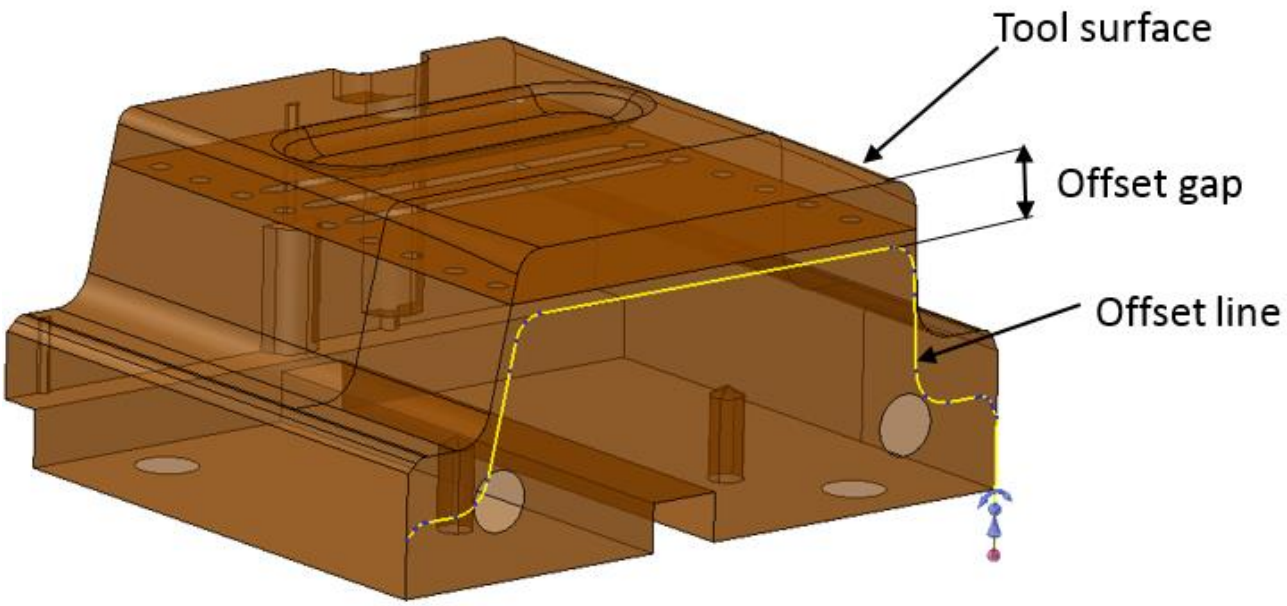


Figure 5-6: Offset from tool surface

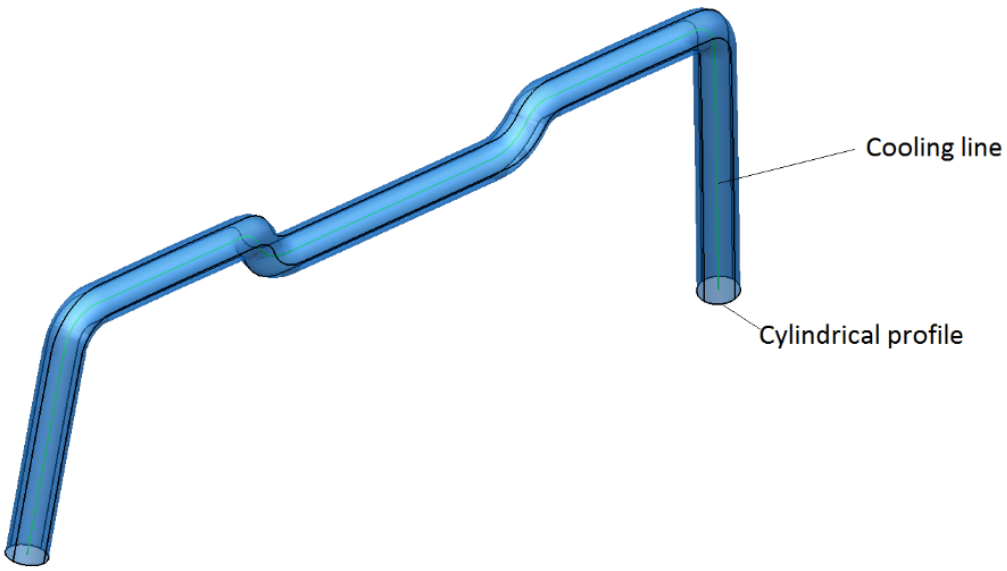


Figure 5-7: Cooling line and cylindrical profile

As a requirement to allow for uniform cooling, the cooling lines were uniformly distributed across the punch. The next stage was to develop the cylindrical profile around the cooling lines as shown in Figure 5-7. The cooling pipes are then joined and connected to the inlet and outlet points.

### 5.4.5. Development of alternative layouts

The possible conformal cooling channel designs in Figure 5-8 were developed based on the standard basic layouts proposed by Park and Pham (2009). In their study, they stated that the basic conformal cooling configurations are zig-zag, parallel and spiral (Park and Pham, 2009). Hu *et al.* (2016) used the same basic layouts and included the longitudinal cooling layout to develop possible conformal cooling designs. The next section explains how the evaluation criteria were used to select the most suitable layout, which was later improved.

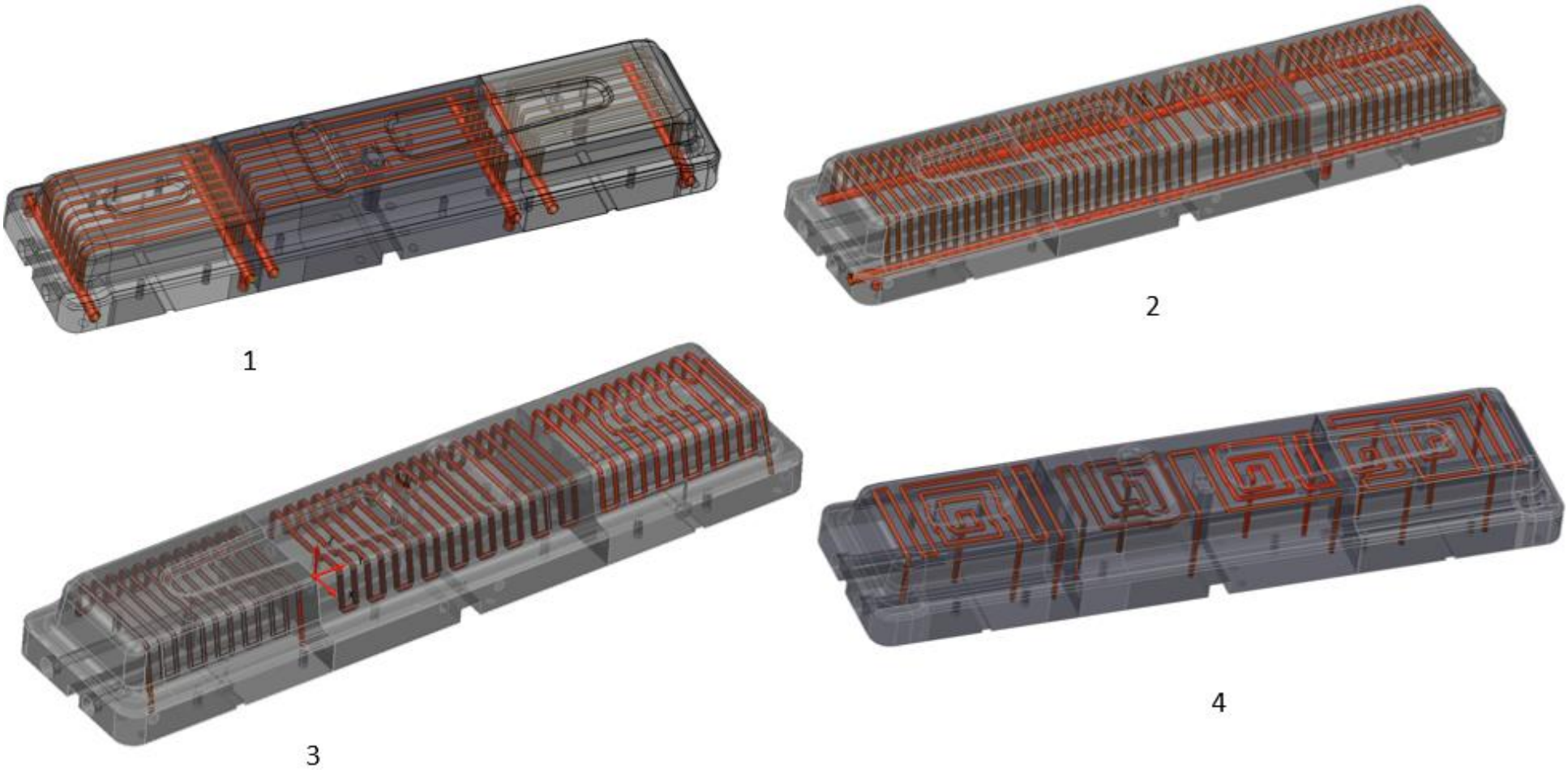


Figure 5-8: Different possible cooling system layouts (1-longitudinal, 2-parallel, 3-zig-zag, 4-spiral)

## 5.5. Analysis of the Alternative Layouts

A decision matrix for evaluating the possible cooling layouts was formulated. The matrix is a useful selection strategy for identifying the most suitable cooling system layout for a hot stamping tool from a quality and manufacturability perspective. The first and most important goal for improving quality is to design a layout which increases the cooling effectiveness as much as possible (Steinbeiss *et al.*, 2007; Lin *et al.*, 2014; He *et al.*, 2016).

Secondly, the arrangement of the cooling channels should allow the part to have the required hardness distribution at the end of the cooling process. In the event that uniform hardness is required, the cooling channels should be arranged uniformly to allow for even cooling and uniform microstructure (Liu, Lei and Xing, 2013; Lim *et al.*, 2014; Ying and Zhong-De, 2014). From a manufacturability perspective, the layout must be easier and more cost effective. (Steinbeiss *et al.*, 2007; Eastman, 2012). As mentioned earlier, hybrid manufacturing was considered to reduce the general costs. This is a combination of machining and Additive Manufacturing (Karunakaran *et al.*, 2012). Also, the cooling layout design should allow easier assembly of the tool inserts. In summary, six criteria were obtained from a different perspective.

- Quality perspective
    - Cooling effectiveness
    - Hardness distribution requirements
- Manufacturability
    - Ease of manufacture
    - Manufacturing cost
- Ease of tool assembly

### 5.5.1. Assigning weights to criteria

As mentioned in Chapter 3, the weights in the matrix are determined using the Analytic Hierarchy Process (AHP). The first step in the process is to formulate the pairwise comparison matrix using Equation 3.66 as shown in Table 5-2.

Table 5-2: Pairwise comparison Matrix

| | Cooling effectiveness | Hardness distribution requirements | Ease of manufacture | Manufacturing cost | Ease of tool Assembly |
|---|---|---|---|---|---|
| **Cooling effectiveness** | 1 | 1 | 4 | 3 | 7 |
| **Hardness distribution requirements** | 1 | 1 | 3 | 3 | 5 |
| **Ease of manufacture** | 1/4 | 1/3 | 1 | 1 | 3 |
| **manufacturing cost** | 1/3 | 1/3 | 1 | 1 | 4 |
| **Ease of tool assembly** | 1/7 | 1/5 | 1/3 | 1/4 | 1 |

The pairwise matrix in Table 5-2 is normalised using Equation 3.67 to develop another matrix shown in Table 5-3.

Table 5-3: Normalised matrix

| | Cooling effectiveness | Hardness distribution requirements | Ease of manufacture | Manufacturing cost | Ease of tool Assembly |
|---|---|---|---|---|---|
| **Cooling effectiveness** | 0.3668 | 0.3488 | 0.4286 | 0.3636 | 0.3500 |
| **Hardness distribution requirements** | 0.3668 | 0.3488 | 0.3214 | 0.3636 | 0.2500 |
| **Ease of manufacture** | 0.0917 | 0.1163 | 0.1071 | 0.1212 | 0.1500 |
| **manufacturing cost** | 0.1223 | 0.1163 | 0.1071 | 0.1212 | 0.2000 |
| **Ease of tool assembly** | 0.0524 | 0.0698 | 0.0357 | 0.0303 | 0.0500 |

The weights, in terms of degree of importance, are then obtained from the matrix using Equation 3.68. The consistency values are also calculated using Equation 3.69. Table 5-4 shows the calculated weights in descending order.

Table 5-4: Weighted matrix

| Criterion | Importance weighting | Consistency measure | Rank |
|---|---|---|---|
| **Cooling effectiveness** | 0.37 | 5.13 | 1 |
| **Hardness distribution requirements** | 0.33 | 5.13 | 2 |
| **Manufacturing cost** | 0.13 | 5.09 | 3 |
| **Ease of manufacture** | 0.12 | 5.06 | 4 |
| **Ease of tool assembly** | 0.05 | 5.02 | 5 |

Based on Equation 3.70, the consistency index is calculated as shown below.

$$CI = \frac{5.084 - 5}{4} \qquad 5\text{-}2$$

$$CI = 0.021$$

For $m = 5$, the corresponding value for *RI* for five criteria is 1.12 according to Table 3.2. Thus the consistency ratio is calculated as shown below.

$$CR = \frac{0.021}{1.12} = \mathbf{0.019} \qquad 5\text{-}3$$

Since the calculated consistency ratio is below the standard threshold of 0.1, the calculated weights are considered acceptable, thus they are used in the decision matrix.

### 5.5.2. Evaluation of the possible layouts

A close analysis of Table 5-5 shows that a considerable amount of machining is required for layout 2 and 3 because of the geometry of the channels. On the other hand, the channels occupy a larger surface area and provide full coverage for the part when compared to layout 1 and 4.

Thus a higher cooling uniformity is expected. Table 5-5 gives a detailed evaluation of the cooling efficiency of all the possible cooling layouts based on the geometry.

Table 5-5: Evaluating the efficiency of possible cooling channel layouts

| **Layout** | **Evaluation of cooling efficiency** |
|---|---|
| 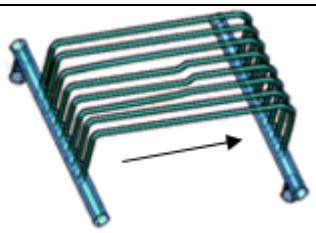 Longitudinal | • Cooling uniformity is less compared to the parallel type because of the larger flow distance along the lengths of the part. The coolant will increase in temperature as it moves along the length.<br>• A faster cooling rate is expected as compared to the zig-zag and parallel layouts because the cooling channels are oriented in a close to straight line to ensure a higher coolant travel speed. |
| 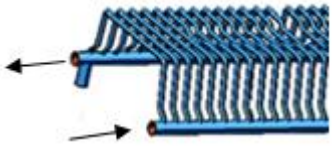 Parallel | • Individual cooling channels are supplied with coolant from the main supply channel. Uniform cooling will be guaranteed since the supply channel will have coolant with the same temperature.<br>• A faster cooling rate is expected when compared to all other layouts because the individual cooling channels have less travel distance. Hence, the coolant enters and leaves the channel quickly to ensure a faster heat removal process. |
| 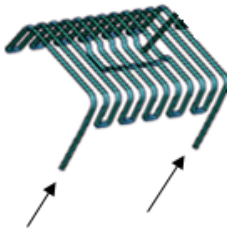 Zig-zag | • Different sections on the part receive coolant at different times according to the position from the supply pipe. Accordingly, the coolant will gain heat as the flow distance from the supply pipe increases. Hence, uniform cooling is not guaranteed |

| | |
|---|---|
| | • Since the parts have large sizes, this orientation reduces the cooling rate when compared to the longitudinal and parallel layouts as the coolant will take longer to travel in a zig-zag manner. |
| 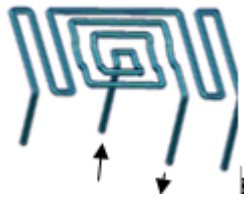 <br>Spiral | • The temperature of the coolant increases as it moves through the spiral. This causes the coolant temperature to vary with distance from supply pipe, thus uniform cooling is not guaranteed.<br>• The cooling rate will be reduced by the spiral nature of the flow channels which causes the coolant to travel a greater distance. |

The evaluation in Table 5-5 shows that the parallel cooling layout has the highest cooling efficiency. For the zig-zag layout, the curved portion of the cooling channels occupies a significant height of the inserts, thus it will be costly to manufacture. This is because the increased built height will result in more time, energy and powder. Also, the strength and quality of the tool inserts will be reduced since an increase in the built height leads to increased residual stresses, causing the inserts to have more distortions (Campanelli *et al.*, 2010).

For the spiral layout, the complex portion of the cooling channels only occupies a lesser height of the tool. However, the cooling channels do not provide enough coverage to ensure uniform cooling throughout the part. Table 5-6 shows the overall evaluation matrix. Based on the evaluation which was made in Table 5-6, layout 2 was chosen since it permits easier and cost-effective application of hybrid tooling. Also, layout 2 has a greater surface area occupied by the cooling channels

Table 5-6: Evaluation of possible cooling system layouts

| **Evaluation Criteria** | **Weight** | **Longitudinal** | | **Parallel** | | **Zig-zag** | | **Spiral** | |
|---|---|---|---|---|---|---|---|---|---|
| | | **Score** | **Total** | **Score** | **Total** | **Score** | **Total** | **Score** | **Total** |
| Cooling Effectiveness | 0.37 | 1.00 | 0.37 | 5.00 | 1.86 | 4.00 | 1.49 | 2.00 | 0.74 |
| Hardness distribution requirements | 0.33 | 3.00 | 0.99 | 4.00 | 1.32 | 4.00 | 1.32 | 3.00 | 0.99 |
| Ease of manufacture | 0.13 | 4.00 | 0.53 | 3.00 | 0.40 | 2.00 | 0.27 | 4.00 | 0.53 |
| Manufacturing costs | 0.12 | 3.00 | 0.35 | 3.00 | 0.35 | 1.00 | 0.12 | 4.00 | 0.47 |
| Ease of tool assembly | 0.05 | 4.00 | 0.19 | 3.00 | 0.14 | 2.00 | 0.10 | 3.00 | 0.14 |
| **Total weight (Highest figure would be favourable)** | | | **2.44** | | **4.07** | | **3.29** | | **2.88** |

## 5.6. Application of Proposed Model to Determine Cooling System Parameters

As mentioned in equation 3.13, the feasible diameter range for conformal cooling channel should be less than 7 mm using Selective Laser Melting (Thomas, 2010). According to Figure 3.6, the factors used in selecting the cooling channel diameter include the part geometry, length of cooling channels and ability to remove the unsolidified powder. Also, after analysing the specific tool geometry and consulting other experts, it was concluded that a lesser diameter ($d \leq 4$) would make it difficult to extract the unsolidified powder. At the same time, a larger diameter ($d > 5$) would require the use of support structures which are difficult to remove. Based on these factors, a diameter of 5 mm is selected to allow smooth flow of coolant, easier removal of unsolidified powder after building and eliminate the need for support structures.

The other parameters ($y$, $z$) are obtained using the proposed mathematical equations. Using mathematical modelling, the minimum distance from the tool surface to the cooling channel wall ($z$) is calculated as shown in Equation 3.23.

$$z = \sqrt{\frac{0.5\sigma_m d^2}{\sigma_y}} \quad 5\text{-}4$$

The quantity $\frac{\sigma_m}{\sigma_y}$ is the factor of safety which is assumed to be 1.5 (Harvey. 2007). Based on the calculations, the minimum $z$ is 4.33 mm which may be rounded up to 5 mm so as to improve the strength of the tool. This causes the value of $Z$ to be 7.5 mm according to Equation 3.1 derived in Chapter 3.

$$Z = z + {}^{d}/_{2} \quad 5\text{-}5$$

The minimum distance between the cooling channels is calculated as shown in Equation 3.29.

$$Y = \sqrt{\frac{4L\sigma_Y Z^2}{3F_l}} \quad 5\text{-}6$$

The parameters for surface area and length of the part are 0.184 $m^2$ and 0.603 m, respectively. The yield strength of 1.2709 is 1 000 MPa (EOS, 2019). The maximum force applied per unit length on the part is considered to be the product of surface area and maximum allowable stress according to Equation 3-30.

$$Y = \sqrt{\frac{4 \times 0.603m \times \frac{(1000 \times 10^6 Pa)}{1.5} \times (0.0075m)^2}{\frac{(3 \times 667 \times 10^6 Pa \times 0.184m^2)}{1m}}} \quad 5\text{-}7$$

$$= 15.67 \times 10^{-3} m$$

Since the cooling channel parameters ($d$, $Y$ and $Z$) in Figure 3.4 were obtained from the mathematical modelling, the next stage is to conduct the simulation analysis.

## 5.7. Sizing of Supply Pipes and Plugs

The final design in Figure 5-25 was composed of 4 inserts with each having a separate inlet and outlet pipe. The diameters of the inlet and outlet pipes were then determined using equations 3.30 to 3.32 derived in Chapter 3. Considering insert 1 and 4 in Figure 5-25, the number of cooling channels are calculated from 3.43 as shown.

$$L = l_C - (2Z) \quad 5\text{-}8$$

$$L = 200 - (2 \times 7.5)$$

$$= 185\ mm$$

Thus, the number of channels can be calculated as shown from Equation 3-43

$$n = \frac{l_C}{Y} \qquad 5\text{-}9$$

$$= \frac{185}{15.67}$$

$$= 12 \text{ channels}$$

The total cross-sectional area of the channels can be calculated as shown from Equation 3-44.

$$A_n = A_d \times n \qquad 5\text{-}10$$

$$= 19.635 \times 12 = 235.62\ mm^2$$

$$D_n = \sqrt{\frac{4An}{\pi}}$$

Hence, the cross-sectional diameter is calculated as shown from Equation 3-45

$$D_n = \sqrt{\frac{4 \times 235.62}{\pi}} \qquad 5\text{-}11$$

$$= 17.3\ mm$$

For insert 2 and 3,

$$l_c = 300 - (2 \times 7.5)$$

$$= 285\ mm$$

Therefore, the number of channels can be calculated as shown in from Equation 3-43

$$= \frac{285}{15.67}$$

$$= 19 \text{ channels}$$

The total cross-sectional area of the channels can be calculated as shown below

$$= 19.635 \times 19 = 373.065\ mm^2$$

Thus, the cross-sectional diameter for the supply of inserts 2 and 3 is calculated as shown from Equation 3-45.

$$D_n = \sqrt{\frac{4 \times 373.065}{\pi}} \qquad 5\text{-}12$$

$$= 21.79 \text{ mm}$$

As seen in the calculations, the required diameters, $D_n$ for the connector channels are 17.3 mm and 21.8 mm for the outward and mid tool inserts. However, it was not possible to use the calculated diameters due to limited space. Thus, the inlet and outlet diameters used for the inserts are 15 mm. Also, a diameter of 15 mm was necessary in order to preserve the structural strength of the tool. However, this causes a slight reduction in the surface area for the flow of the coolant. In order to counter this effect, a higher coolant inflow speed is used so that the required mass flow rate is achieved.

## 5.8. Finite Element Analysis to Evaluate Cooling System Layout

In this case, PAM-STAMP 2019 was used for the simulation calculations because it allows evaluation of the cooling system design, assessment of quality through hardness measurement and prediction of cycle time (ESI, 2019). The steps taken to perform the finite element simulation can be summarised using Figure 5-9. The purpose of the cyclic simulation is to evaluate the cooling system design of the tools. The tool movements and process specifications were imputed in the code using the tool editor function. Process definition was conducted using the available macro-commands on PAM-STAMP. In this case the macro-command used is Cyclic_Cooling_Mpa. A kinematics check was done using the analysis tool to ensure that the tool and process parameters were correctly set up. This was followed by the actual computation which was set to produce results from the blank hardness and temperature of the blank after every 2 seconds until the stamping and cooling cycles were completed. The procedure was repeated five times in both cases to ensure a fair comparison in both cases. The process was divided into stamping and cooling stages of the blank. The results obtained from the simulation include temperature and hardness maps which were then used to plot graphs in section section 5.9.

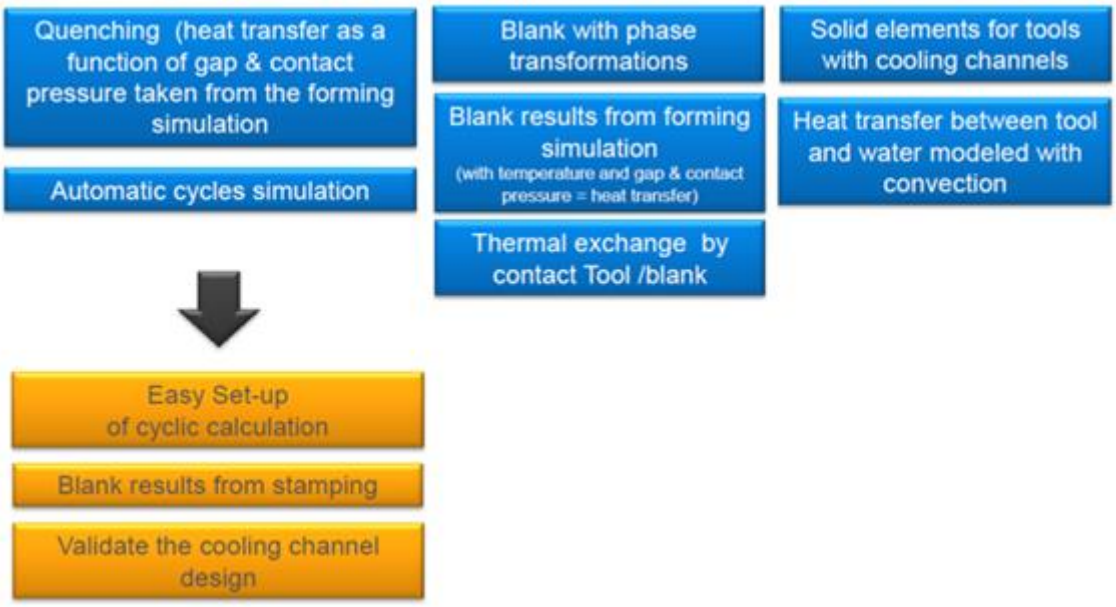


Figure 5-9: Cooling system design evaluation (ESI, 2019)

### 5.8.1. Properties of the blank

The blank material for the simulation is 22MnB5. The properties for the blank are given in Table 5-7 below.

Table 5-7: Blank properties

| **Property** | **Quantity** |
|---|---|
| Poisson's ratio | 0.3 |
| Emissivity | 0.7 |
| Density | 7 800 kg/m$^3$ |
| Coefficient for thermal expansion | $1.3\times10^{-5}$ °C$^{-1}$ |
| Mesh size | 0.003 m |
| Thickness | 1.5 mm |

The heat capacity and thermal conductivity of the blank which are expressed as a function of phase and temperature are indicated in Figure 5-10 and Figure 5-11 respectively.

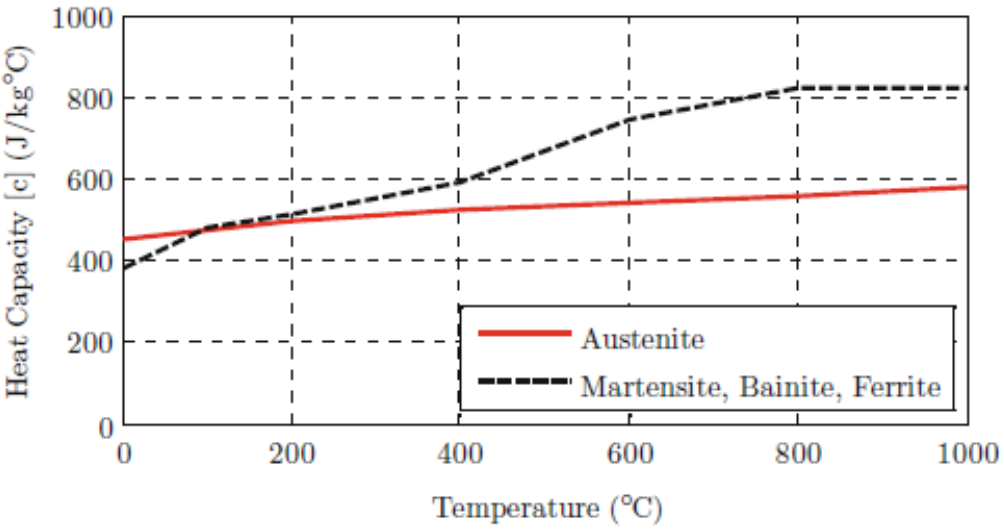


Figure 5-10: Heat capacity as a function of phase and temperature (ESI, 2015)

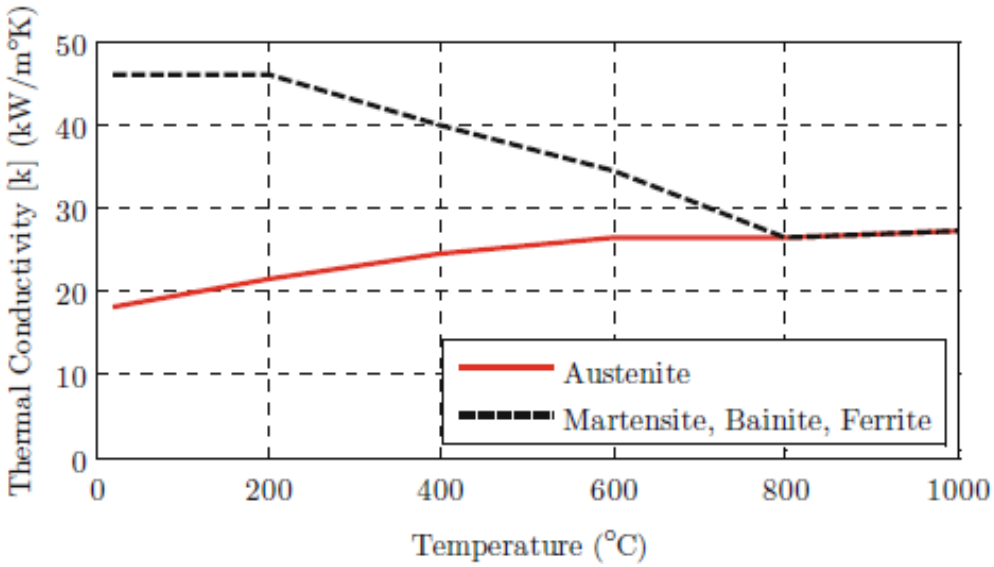


Figure 5-11: Thermal conductivity as a function of temperature and phase (ESI, 2015)

The calculations in the graphs include the effect of latent heat. The elastic modulus of the blank is showed in Figure 5-12. Addendum F gives the flow stress of the blank as a function of strain rate based on results from literature (ESI, 2015). The values used in the calculations for 22MnB5 are in the material database for PAM-STAMP.

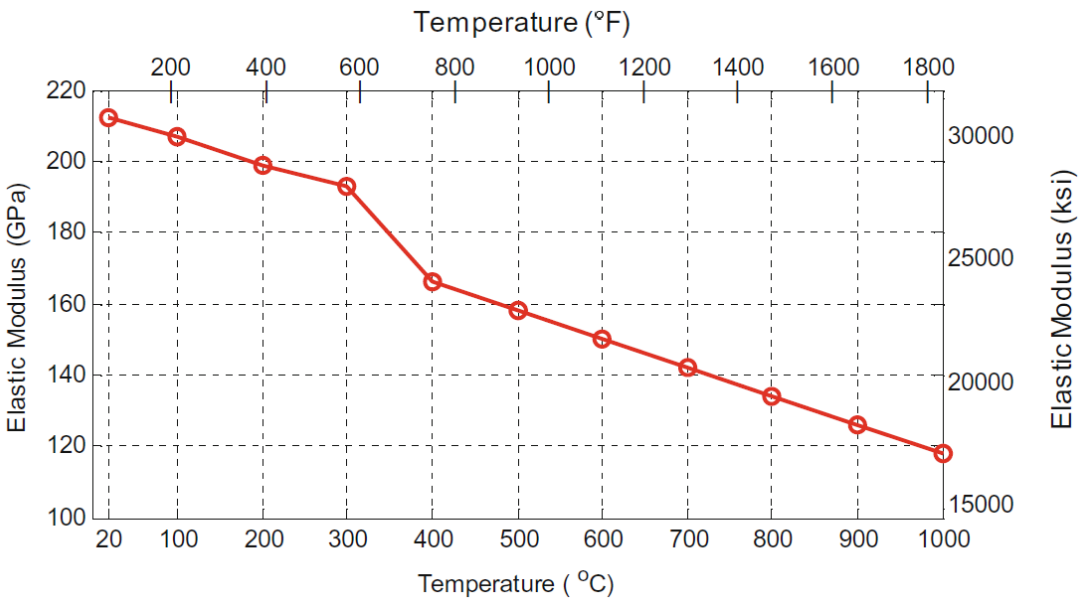


Figure 5-12: Elastic modulus as a function of temperature (ESI, 2015)

### 5.8.2. Properties of the tool

The tool material considered for the tool is H13 tool steel because of its high thermal fatigue resistance properties and wide application in the hot stamping industry (Escher and Wilzer, 2015). The material properties for the H13 tool steel are given in Table 5-8 (ESI, 2015). The specific heat capacity and thermal conductivity are entered as constants.

Table 5-8: Properties of H13 tool steel

| **Property** | **Quantity** |
|---|---|
| Thermal conductivity | 28 W/m$^2$°C |
| Specific heat capacity | 650 J/kg°C |
| Density | 7 800 kg/m$^3$ |

### 5.8.3. Stamping stage

The focus of the model was to evaluate the cooling system layout. The punch and die were in the form of shell elements during the stamping stage. The shell elements were created by exporting the top surfaces of the punch and die. During stamping, the die moved at a speed of 200 mm/s to deform the blank to the desired geometry. The temperature changes for the blank at this stage were considered negligible (ESI, 2018). This is based on results from literature

(Billur, 2013). The stamping simulation was conducted with assistance from ESI using the parameters below.

Table 5-9: Stamping parameters used

| **Property** | **Quantity** |
|---|---|
| Forming speed | 200 mm/s |
| Shell type | Quadrilateral shell elements |
| Forming distance | 40 mm |
| Press type | Single action |
| Tool material | H13 tool steel |
| Gap between die and punch | 2 mm (0.5 mm + thickness) |
| Mesh size | 0.003 m |
| Macro used | CyclicCooling_SingleAction.ksa. |
| Press force | 1 000 kN |
| Friction coefficient during forming | 0.4 |

A default friction coefficient value of 0.4 was provided in the code (ESI, 2018). This was based on previous results from literature (Geiger *et al*., 2008)

### 5.8.4. Cyclic cooling stage

During the cooling stage, the blank is held between the punch and die under the press force (1000 kN). Heat is transferred by conduction from the tool surface to the cooling channel walls and by convection to the coolant. This stage is considered by PAM-STAMP as thermal only and there are no mechanical calculations involved (ESI, 2018). Table 5-9 shows the parameters used for the cyclic cooling stage. Solid tools with cooling channels were used for the cyclic cooling stage as shown in Figure 5-13. The tools are required to have solid elements to enable the calculations for heat loss from the blank to the cooling channels. Visual Mesh is used to create the solid elements as explained in section 5.11.4. The initial temperature at the surface of the tools was 25 °C. To simplify the model, the initial blank temperature is assumed to be 800 °C. This assumption is close to reality since the blank would have lost some of the heat by radiation during transfer from the furnace.

Table 5-10: Cyclic cooling parameters

| **Property** | **Quantity** |
|---|---|
| Shell type | Tetrahedral solid elements |
| Element size | 0.003 |
| Ambient temperature | 25 °C |
| Cooling time | 2-10 s |
| Initial temperature of tools | 25 °C |
| Coolant temperature | 20 °C |

Other literature authors have made similar assumptions based on experience of the hot stamping process and previous experimental results (Shapiro, 2009; Lim *et al.*, 2014b; Ying and Zhong-De, 2014). The coolant is also assumed to be initially at 20 °C at the start of the process based on hot stamping experience. The pressure distribution is assumed to be constant and is picked from the previous stamping stage. The heat transfer to the environment is considered negligible (ESI, 2018).

### 5.11.1. Phase transformations and hardness calculations

Considering that the blank is formed when it has a full austenite microstructure, the decomposition of the austenite to other phases during the cooling stage is calculated in PAM-STAMP using the Johnson-Mehl-Avrami equation. Typically, the equation can be expressed as shown below, where *n* is the nucleation exponent and τ is the delay time.(ESI, 2018):

$$U(t) = U_{eq}(t) \times (1 - e^{-\left(\frac{t}{\tau}\right)^n}) \qquad 5\text{-}13$$

The hardness of the blank is estimated using the equation below (ESI, 2018):

$$HV = 188.5\left(U_f + U_p\right) + 283.8U_b + 514.4U_m \qquad 5\text{-}14$$

Where $U$ is the phase fraction; subscript $f$, $b$ and $m$ stand for ferrite, pearlite and martensite respectively.

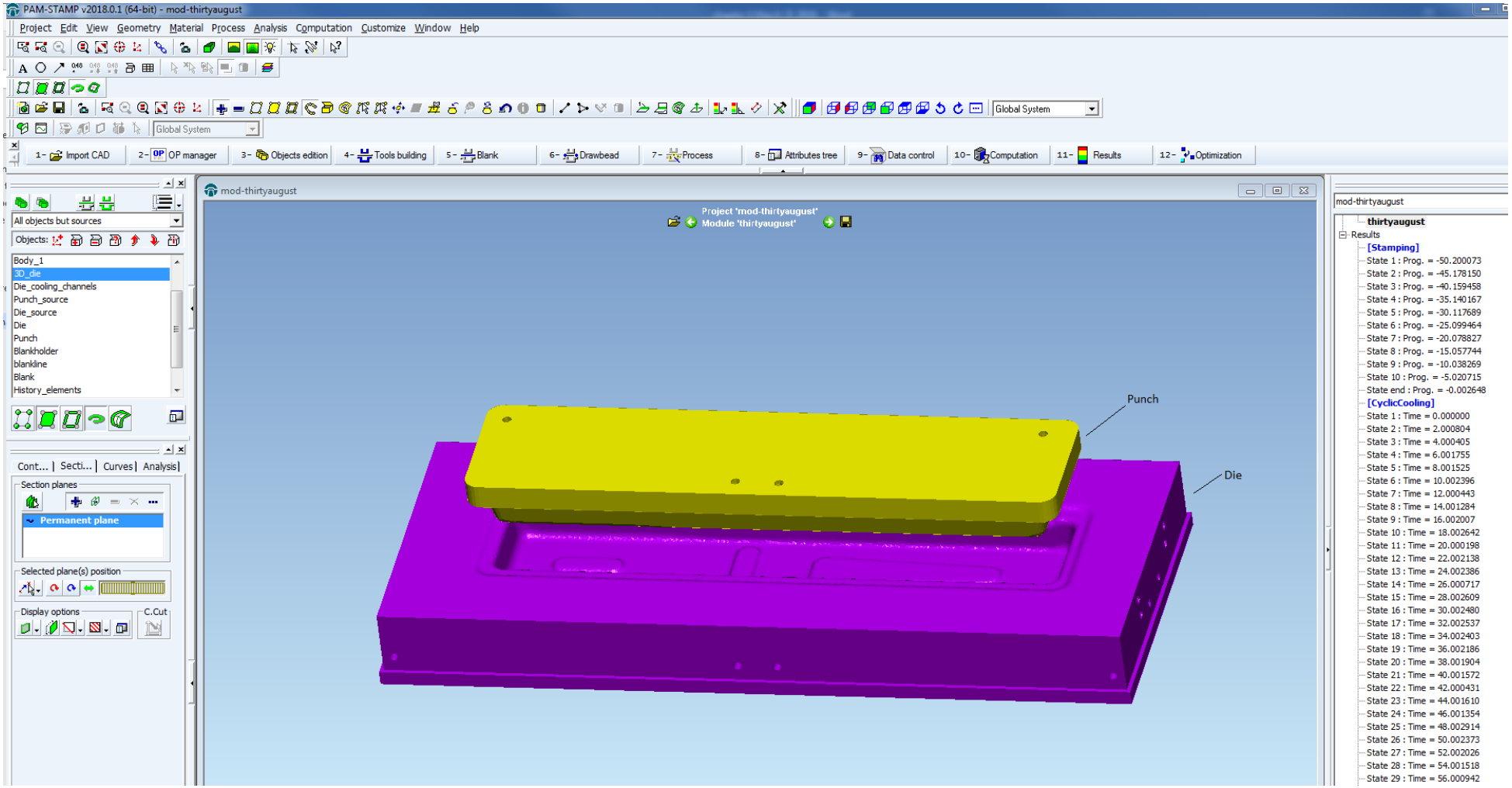


Figure 5-13: Simulation platform

### 5.8.5. Heat transfer scenarios during cooling of blank

According to Steinbeiss *et al.*(2007), the temperature of the blank is affected by the heat transfer to the tools, thermal conductivity of tool and heat transfer to the coolant as indicated in Figure 5-14. The next section explains each of these factors and how they were incorporated in the model.

| factors | technical potential for optimization |
|---|---|
| heat transfer pressing - tool | • preventing the formation of scale<br>• preventing/minimizing gaps in the contact zone |
| heat conductivity within the tool | • heat conductivity of the tool material<br>• cooling surface<br>• distance between tool surface and cooling surface |
| heat transfer tool - cooling system | • turbulent flow of the cooling medium<br>• temperature of the cooling medium |

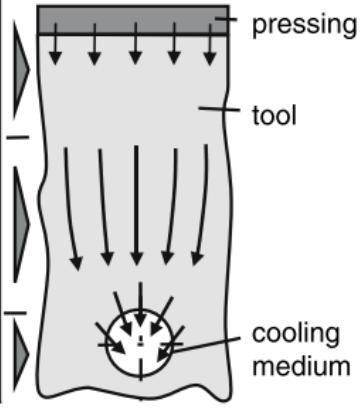


Figure 5-14: Factors affecting blank temperature

### 5.8.6. Heat transfer between blank and tool

The heat transfer between the blank and punch is expressed from Equation 3-3 as shown below.

$$\dot{Q}_1 = h_c A(T_b - T_d) \qquad 5\text{-}15$$

The heat transfer coefficient ($h_c$) at the interface between blank and punch was considered as a function of pressure and gap according to the graph in Figure 5-13. (ESI, 2015). The graph was obtained from experimental studies in literature (Merklein et al., 2009; Karbasian and Tekkaya, 2010) (ESI, 2015). The values are embedded in the PAM-STAMP simulation software and are provided in Figure 5-15.

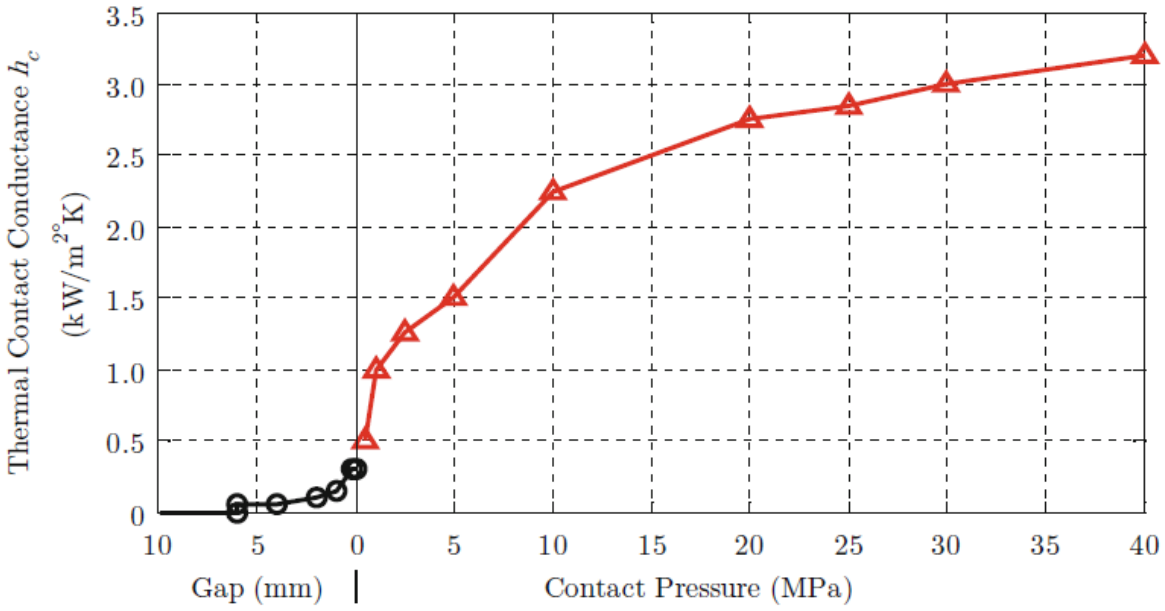


Figure 5-15: Heat transfer coefficient as a function of pressure and gap (Merklein *et al.*, 2009; ESI Group, 2017)

### 5.8.7. Heat transfer within the tool

The heat transfer within the tool is modelled automatically in PAM-STAMP using the thermal conductivity for H13 tool steel (28 W/m$^2$°C) as indicated in Table 5-8. Typically, the heat transfer from the tool surface to the cooling channel walls can be explained from Equation 3-4 as shown. (Ying and Zhong-De, 2014; Muvunzi *et al.*,2017)

$$\dot{Q}_3 = k_d f_s (T_d - T_{cw}) \qquad 5\text{-}16$$

### 5.8.8. Heat transfer between cooling channel walls and coolant

Heat transfer between the punch and coolant can be expressed from Equation 3-7 as shown below.

$$\dot{Q}_4 = h_{cw} A_{cw} (T_{cw} - T_w) \qquad 5\text{-}17$$

The heat transfer coefficient can be described as shown below.

$$h_{cw} = f(d, C_P, k, \rho, v_c, \mu) \qquad 5\text{-}18$$

Regarding Equation 5.18, $d$ is diameter of the tube, $Cp$ is the heat capacitance of the coolant, $k$ is conductivity of the coolant, $\rho$ is the density of the coolant, $v_c$ is the mean velocity of the coolant, $\mu$ is the viscosity of the coolant. The heat transfer coefficient in the cooling channels

was modelled in the simulation by assuming steady-state turbulent flow in a circular pipe using Equation 5-19 (ESI, 2018).

$$h_{cw} = 0.023\left(\frac{\mu C_p}{k}\right)^{0.8}\left(\frac{v_c}{\mu}\right)^{0.33}\frac{k}{d} \qquad 5\text{-}19$$

The effect of surface roughness was not considered in the PAM-STAMP code. Thus, a smooth surface was assumed since the main goal was to evaluate the cooling system layouts. However, a more accurate result would have been obtained if the effect surface roughness was considered. As a result of the assumption of smooth cooling channels, the results are conservative regarding heat transfer and would underestimate the pumping power. Nevertheless, some authors have alluded that surface roughness increases the heat transfer because of increased surface area and turbulence (Ventola *et al.*, 2014; Guo, Xu and Gong, 2015). Taking guidance from literature, an increased heat transfer is expected for the AM based conformal cooling channels.The parameters for the coolant (water) at an average of 20 °C are listed in Table 5-11.

Table 5-11: Properties of water ( Çengel and Ghajar, 2011)

| **Property** | **Quantity** |
|---|---|
| Density | 1000 kg/m$^3$ |
| Specific heat capacity ($C_p$) | 4 174 J/kgm$^3$ |
| Thermal conductivity ($k$) | 0.605 W/m°C |
| Viscosity ($\mu$) | 9.77×10$^{-4}$ |

As discussed before (Section 3.2.1) and taking guidance from literature, a coolant passage flow with a Reynolds number of 4000 to 10000 was targeted for a higher smooth pipe convection heat transfer (Lim *et al.*, 2014; Lv *et al.*, 2016). Thus, the coolant velocity is obtained from a maximum Reynolds number to achieve a higher cooling effect for the conformal (d=5 mm) and conventional tool (d=5 mm) using the equation below.

$$Re = 10\,000 \qquad 5\text{-}20$$

$$\frac{d\rho_w v}{\eta_w} = 10\,000$$

$$\frac{0.005 \times 1000v}{0.001} = 10\,000$$

$$= 2\ m/s \text{ for the conformal cooling tool}$$

For the conventional tool, the coolant velocity is calculated as shown below.

$$\frac{0.005 \times 1000v}{0.001} = 10\ 000$$

$$= 1\ m/s \text{ for the conventional tool}$$

Accordingly, the parameters for the tool are summarised in Table 5-12.

Table 5-12: Tool parameters

| **Parameter** | **Quantity** |
|---|---|
| Diameter for conformal cooling channels ($d$) | 0.005 m |
| Diameter for conventional cooling channels ($d$) | 0.01 m |
| Coolant velocity for conventional cooling channels ($v_c$) | 1 m/s |
| Coolant velocity for conformal cooling channels ($v_c$) | 2 m/s |

### 5.8.9. Generation of solid elements

The CAD models of the tools (conventional and conformal) were converted to IGES files, exported to Visual-Mesh software and transformed to PC files (ESI, 2019). Using the software platform, the models were cleaned, repaired and meshed. The meshing was done to a minimum size of 0.003 m using an automatic tool. This was the smallest possible size which could be used to increase the accuracy of the simulation process. Any smaller size caused the file to have an abnormally large size which was difficult to transfer to other simulation software. Tetrahedral elements were constructed because of their compatibility with the hot stamping simulation software.

## 5.9. Simulation Results

The results from the simulation were analysed in terms of the effect of the cooling layouts on the cooling time, temperature deviation and hardness distribution of the formed blank. The following section gives a detailed explanation.

### 5.9.1. Effect on cooling time

The graph in Figure 5-16 shows the change in maximum temperature of the blank for the conformal cooling and conventional tool.

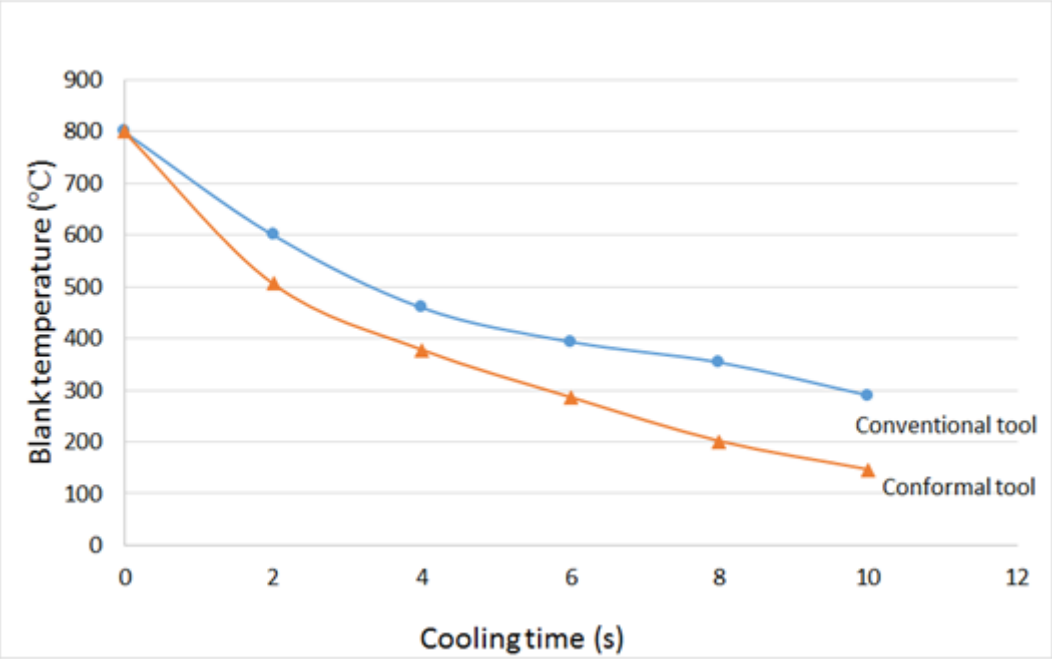


Figure 5-16: Change in the maximum temperature of blank with time

Looking at both temperature profiles, the conformal cooling tool results in a significantly reduced cooling time as compared to the conventional tool. The cooling trends in both cases are almost similar, showing an exponential decay in the way that the maximum temperature changes with time. The same trends were also reported from previous experimental results in literature (Lin *et al.*, 2014; Cortina *et al.*, 2018). Based on experience, the average cooling time in hot stamping is 8 s, although it can vary depending on the geometric complexity of parts. Therefore, this is considered as the standard cooling time. According to Addendum A2 a cooling time of eight seconds causes the blank to reach a maximum temperature of 201 °C for the conformal cooling tool and 353 °C for the conventional tool. This translates to an increase in the maximum cooling rate by 43 %. This is not far from previous results obtained from literature which ranged from 50 to 70 % (Mueller *et al.*, 2013; Gebauer *et al.*, 2016).

### 5.9.2. Temperature deviation on blank

The temperature deviation on the blank surface in both cases can be explained using Figure 5-17. The temperature curves in Figure 5-17 show that the way the temperature deviation changes with time for both tools is in a similar manner. From the graph, it can be seen that the conformal cooling tool caused less temperature deviation as compared to the conformal tool. This suggests that the conformal cooling channels increased the cooling uniformity of the blank.

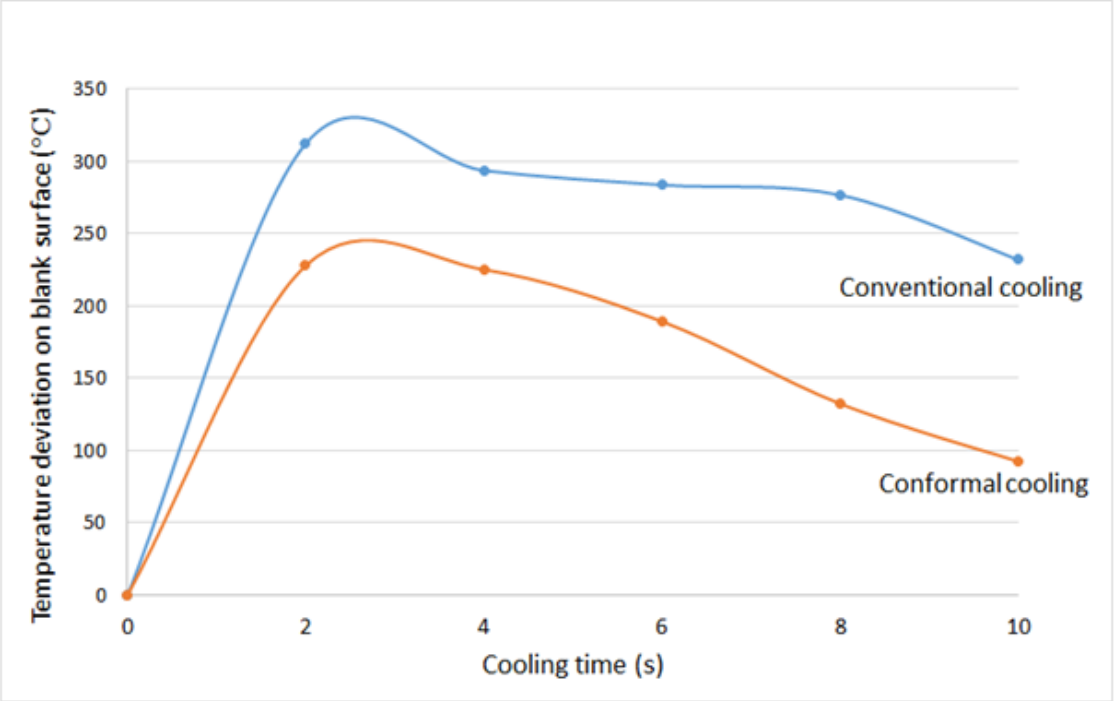


Figure 5-17: Temperature difference on blank ($T_{max}$ - $T_{min}$)

Figure 5-18 and Figure 5-19 shows the variation between the maximum and minimum temperature for both tools by providing more in-depth information.

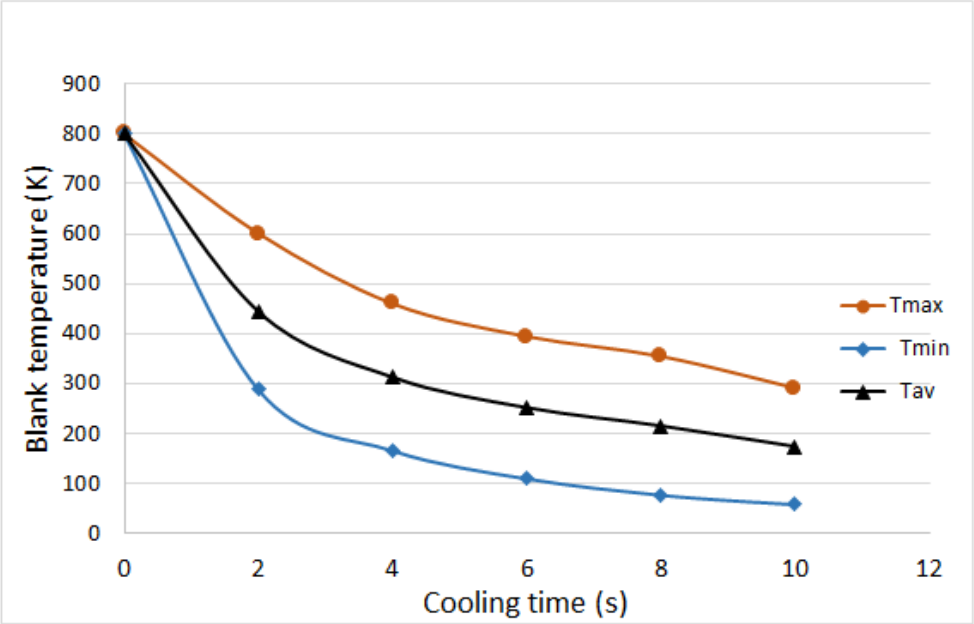


Figure 5-18: Maximum and minimum blank temperature for conventional tool

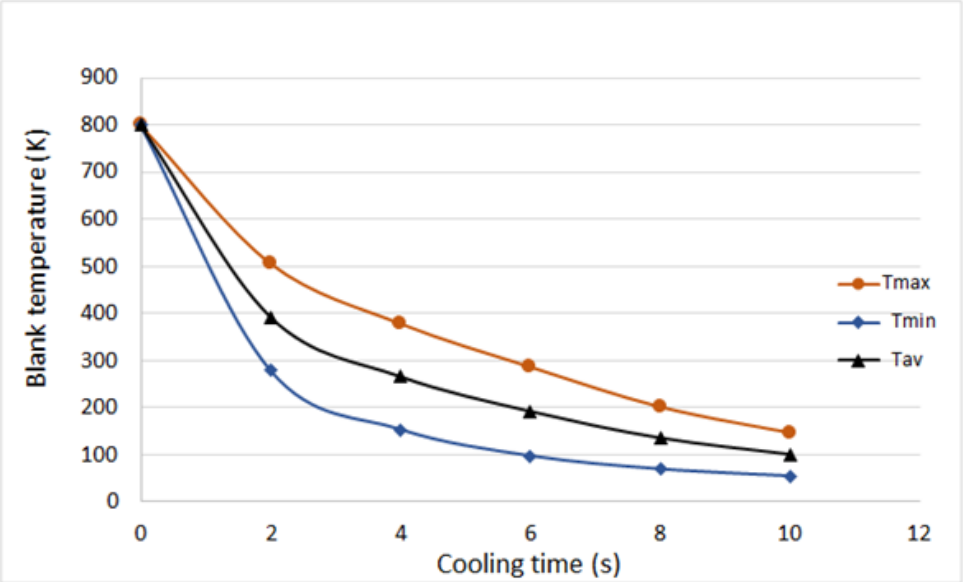


Figure 5-19: Maximum and minimum blank temperature for conformal cooling tool

Comparing the graphs, the conventional tool caused a greater difference between the maximum and minimum temperature of the formed parts. For the conformal cooling tool, there is a lesser gap between the maximum and minimum temperature. Thus, the conformal cooling tool caused an increase in temperature uniformity. Addendum A.2 shows that the first eight seconds caused a temperature deviation of 132 °C for conformal cooling and 277 °C for straight channels. Hence there was an increase in the temperature uniformity by 52 %.

### 5.9.3. Hardness distribution

This represented the hardness deviation of the formed part. In this case, the formed part was required to have uniform hardness, thus the aim was to minimize the hardness deviation as much as possible at the end of the cooling process. Figure 5-20 and Figure 5-21 shows how the maximum and minimum hardness changed with time.

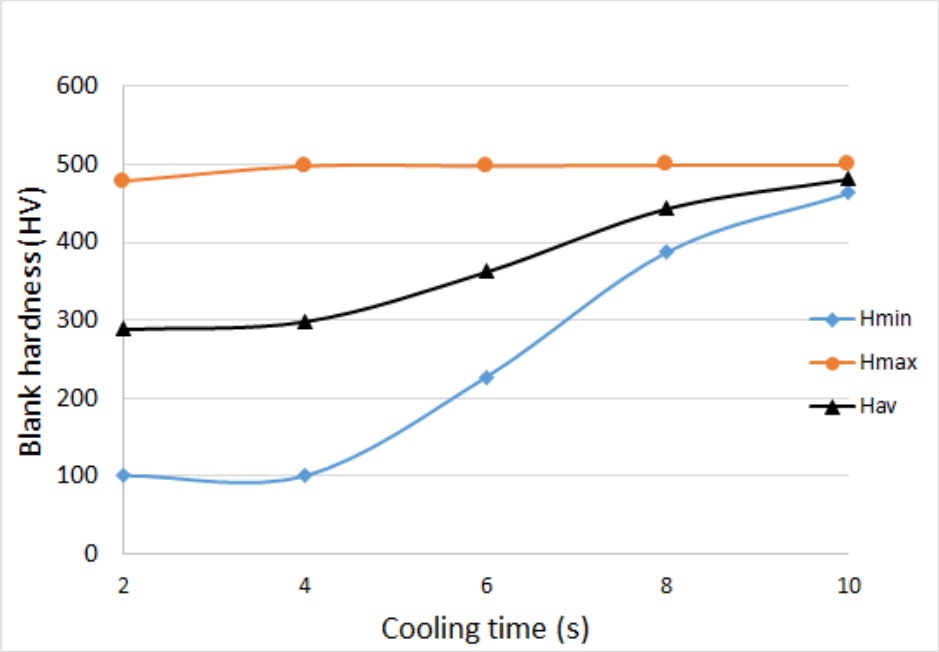


Figure 5-20: Hardness curves on blank formed using conventional tool

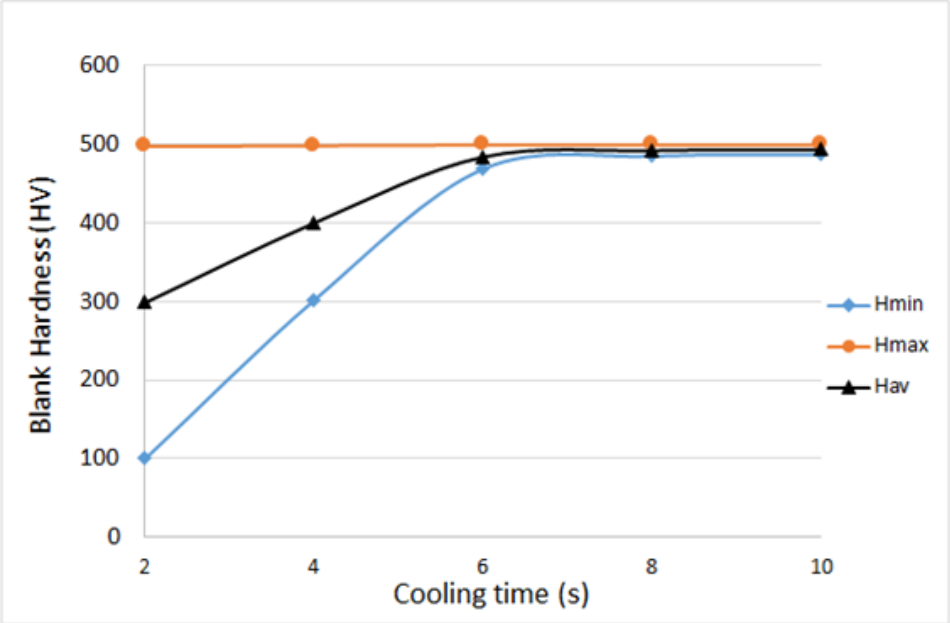


Figure 5-21 Hardness curves on blank formed using conformal cooling tool

As seen from Figure 5-21, the difference between the maximum and minimum hardness is more pronounced for the conventional tool. On the contrary, the conformal cooling tool caused less hardness deviation. Thus, it can be concluded that the conformal cooling tool increased the hardness uniformity.

### 5.9.4. Temperature deviation on punch

Figure 5-22 shows the temperature map of the punch after 10 seconds. As seen in the temperature profile, the region at the centre of the punch takes longer to cool off as compared to other sections. This is because there was not enough space for cooling channels at the mid-section because of the depression in the design.

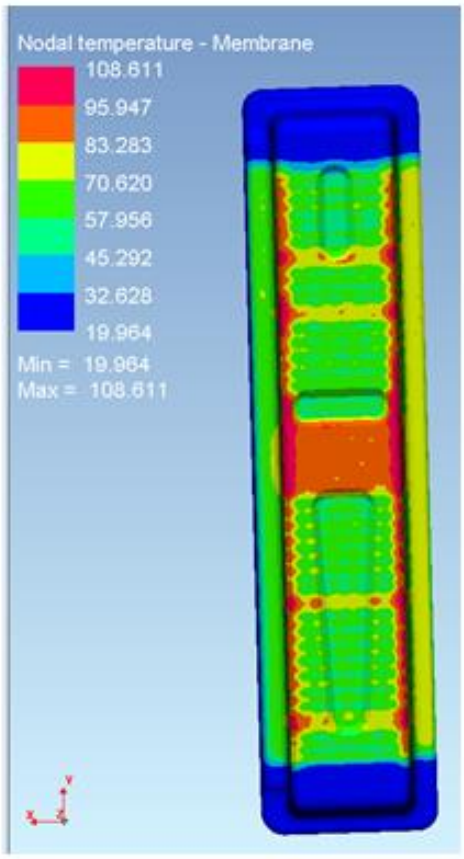


Figure 5-22: Temperature map of punch after 10 s

Also, it can be seen that the edges of the punch experienced slower cooling as compared to the rest of the part. This is because the distance from tool surface to the coolant wall is more at the edges (7 mm) than the rest of the part (5 mm). This can be explained using the wire cut cross section below.

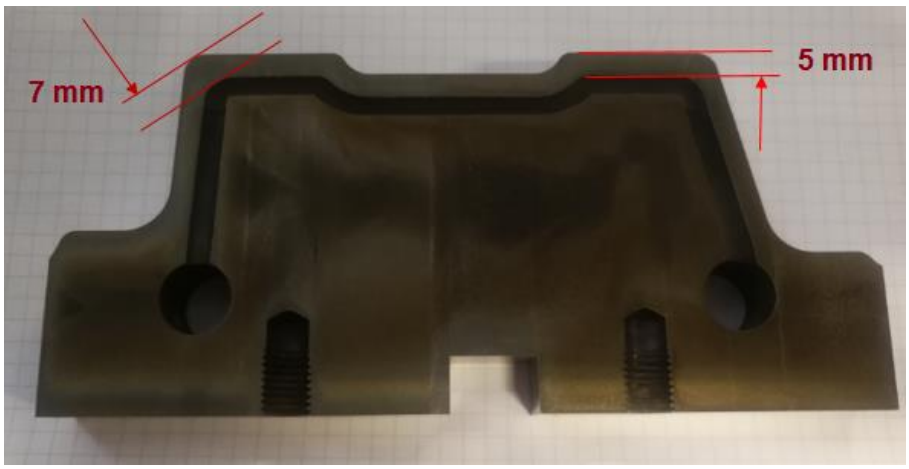


Figure 23: Wire cut cross section showing a conformal cooling channel

The conformal cooling design was further improved to incorporate one more cooling on each of inserts on the mid-section thus, increasing the number of channels from 9 to 10. Also, the design was further improved to eliminate the use of connecters by increasing the inlet and outlet points as shown in Figure 5-24. The final cooling system layout design is shown in Figure 5-25.

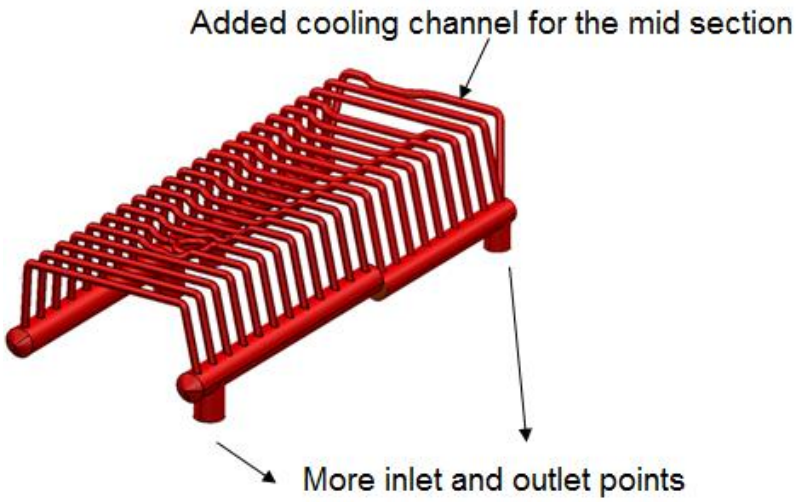


Figure 5-24: Improved design of the selected layout

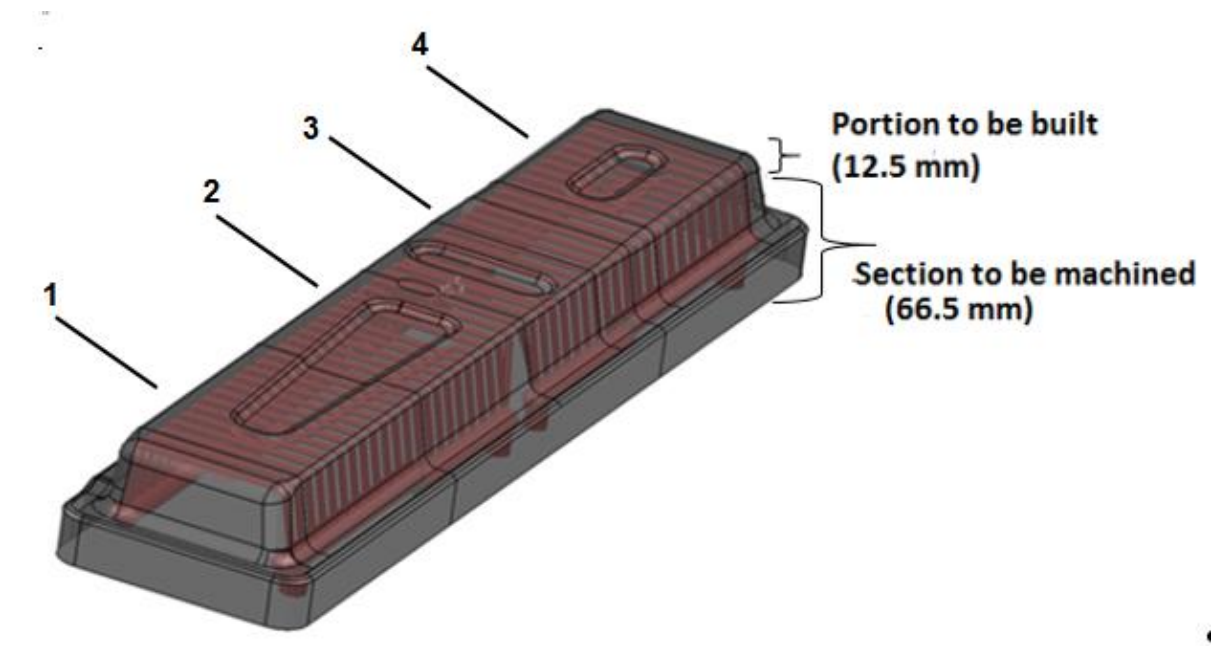


Figure 5-25: Improved design of the selected layout

### 5.9.5. Temperature results for improved design

The improved design was simulated to evaluate its cooling performance. Figure 5-27 shows the temperature profile graphs.

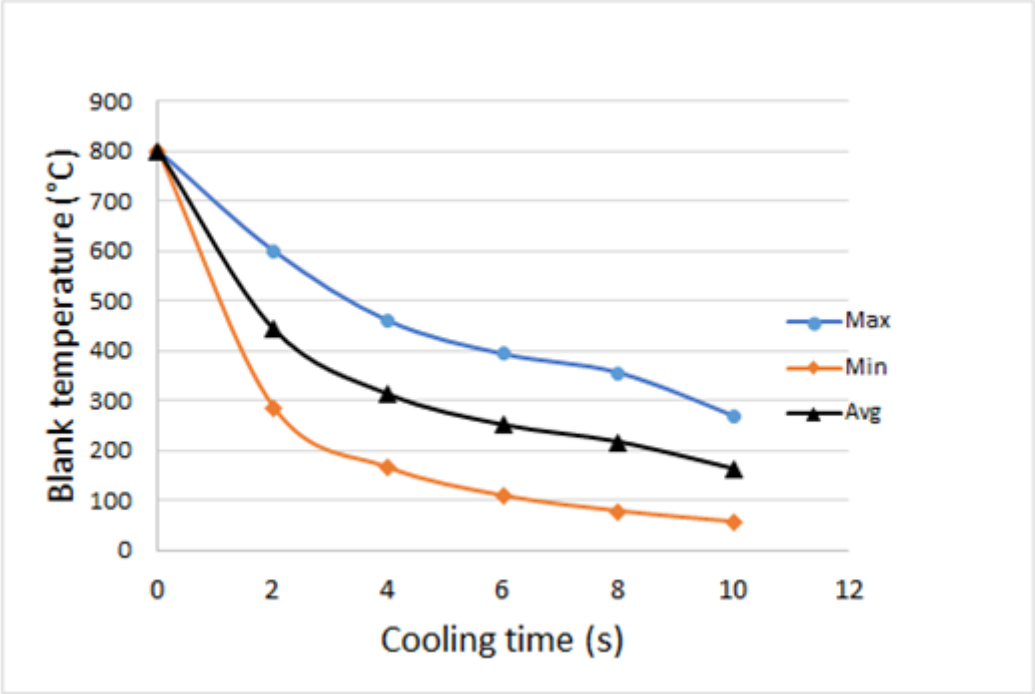


Figure 5-26: Temperature curves for conventional tool

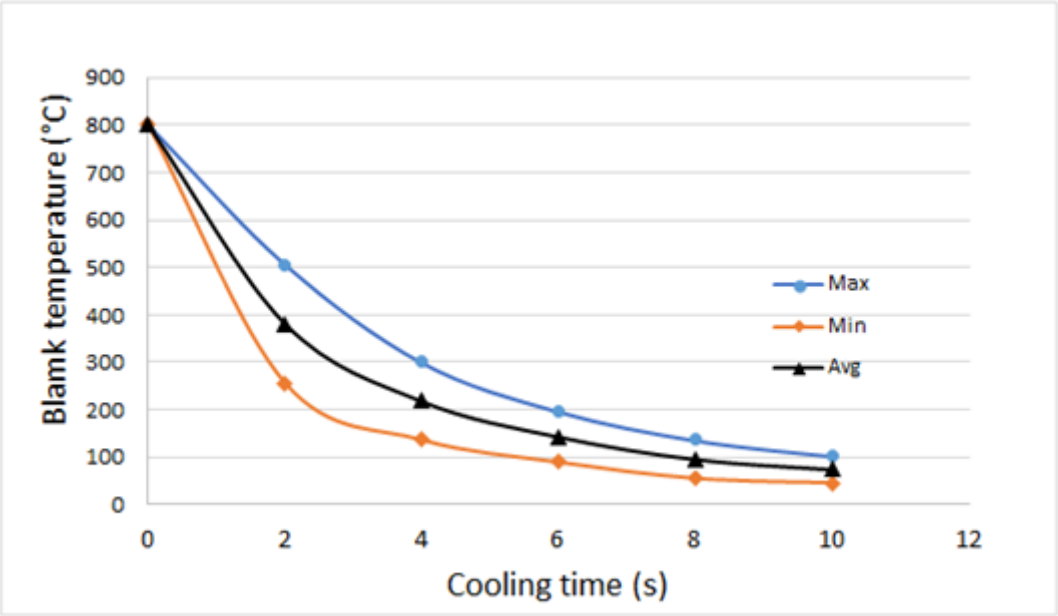


Figure 5-27: Temperature curves for conformal cooling tool

According to the graphs in Figure 5-27, there is a reduction in temperature deviation for the blank produced with the conformal cooling tool. The blank produced with the conformal cooling tool reached a temperature below 200 ºC after six seconds which is below the current standard cooling time of eight seconds. Accordingly, a cooling time reduction of 25 % is achievable. The temperature map of the punch after 10 s in the first cycle is shown in Figure 5-28 .

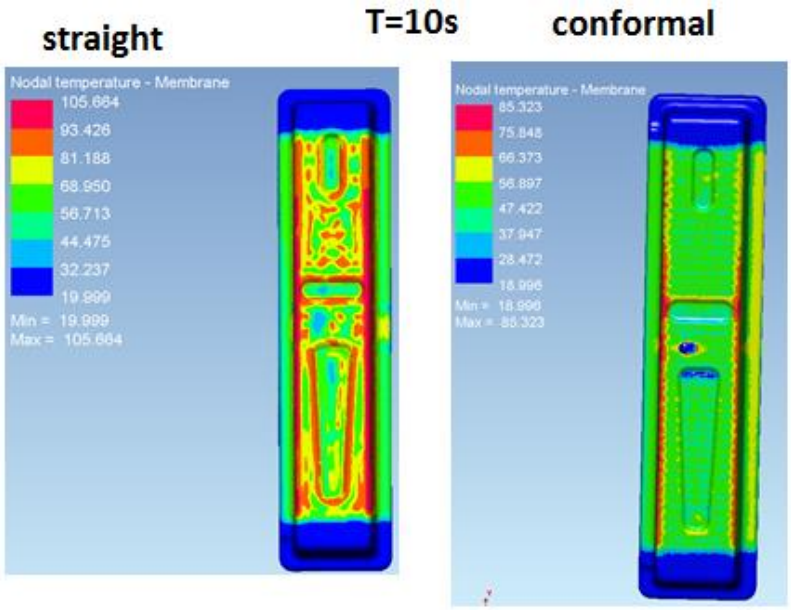


Figure 5-28: Temperature map of punch for the conventional (left) and conformal (right) tools after 10 s

The temperature map in Figure 5-28 shows a more uniform distribution as compared to the one in Figure 5-22. This is because of the uniform arrangement of the cooling channels at a constant distance from the tool surface. Hence, the conformal cooling tool is expected to experience less thermal stresses when compared to the conventional tool.

### 5.9.6. Hardness results for improved design

The hardness profile results are shown in Figure 5-29 and Figure 5-30.

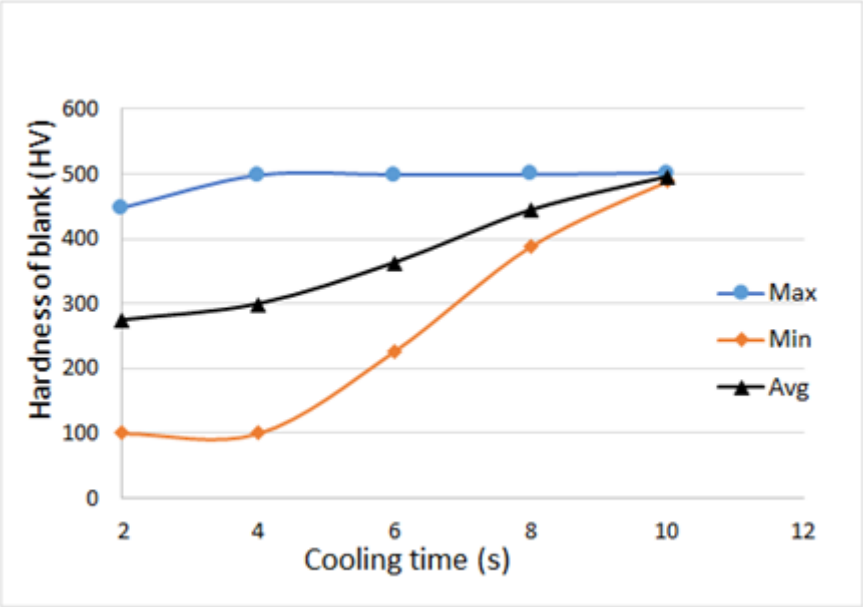


Figure 5-29: Hardness profile for conventional tool

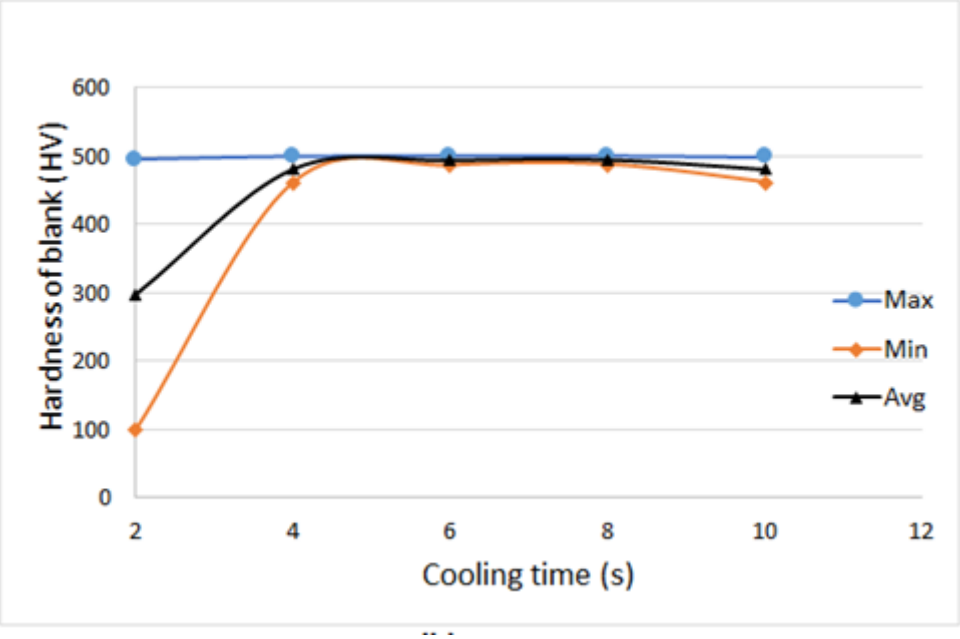


Figure 5-30: Hardness profile for improved conformal tool

As seen from the curves in Figure 5-30, the blank formed with the conformal cooling tool had a nearly uniform hardness structure earlier (5 s) than the conventional tool (10 s).

## 5.10. Summary

The purpose of the chapter was to present the application of the proposed model to the real-life case study part. The first point of call was to present the real-life benchmark component and evaluate it using the selection criteria. The aim was to reduce the cycle time for manufacturing the benchmark part and enhance its quality through uniform hardness. The calculated minimum cooling time was significantly below the actual time, thus justifying the need for an improved cooling system design. The proposed model for determining effective cooling system parameters was applied. Also, the design methodology for the conformal cooling system was presented. In this study, all four basic layouts (zig-zag, parallel, spiral and longitudinal) were adopted to suit the benchmark part geometry as shown in Figure 5-8. Accordingly, the spiral layout was made rectangular and the zig-zag layout was made to follow the part curvatures. Using the parameters obtained from the proposed method, the conformal cooling system was developed for the benchmark part. This was followed by simulation using PAM-STAMP to compare the performance of the conformal cooling tool against the conventional tool with straight channels. From the simulation results, it was noted that the conformal cooling tool can reduce the cooling time by 25 % and cause uniform hardness at a cooling time of 5 s. The next chapter (Chapter 5) describes the tool manufacturing process and the physical experiments.

# CHAPTER 6 : TOOL DEVELOPMENT AND EXPERIMENTATION

## 6.1 Introduction

In the previous chapter, the tool design for the benchmark was presented. As part of the design process, the proposed model was used to establish the cooling system structural parameters for the conformable tool. In this chapter, a detailed systematic description of the tool manufacturing process is given. This includes the challenges encountered during the manufacturing process. The experimental design and set up is also included.

## 6.2 Machined and Built Sections of Tool Inserts

As explained in the previous chapter, the most cost effective way of manufacturing the tool inserts was to use hybrid manufacturing (Karunakaran *et al.*, 2012). This is a combination of AM with conventional machining methods. This allowed the complex portions of the cooling channels to be manufactured additively while the rest of the tool components were machined. Thus, the CAD model of the tool was divided into two sections, namely the base body section to be machined and the top section to be built using SLM as shown in Figure 6-1 The red coloured tool sections in Figure 6-1 show the portions of the tool which were built additively. Considering the geometry of the inserts, it was necessary for the base part to be machined before building the upper portion with complex channels additively.

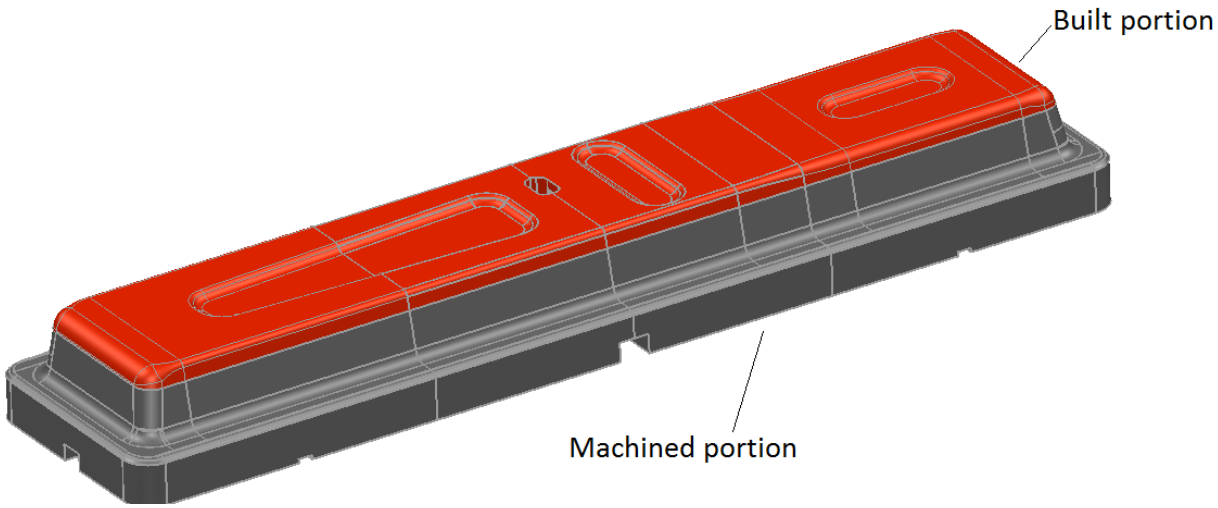


Figure 6-1: Built (red) and machined (grey) portions of tool

The CAD model of the tool inserts shows that the lowest point for the complex portion of the conformal cooling channels occupies a height of 15 mm from the tool surface as shown in Figure 6-2. However, a section from the lowest part of the complex channels to a height of 2.5 mm could be easily machined. Accordingly, subtracting this machinable section from the 15mm height meant that

only a height of 12.5 mm was to be built additively as earlier indicated in Figure 5-16. This reduction of the built height was beneficial in reducing the powder and energy costs of manufacturing the tool. Also, decreasing the built height was crucial for the reduction of residual stresses and distortions associated with increased heights (Campanelli *et al.*, 2010).

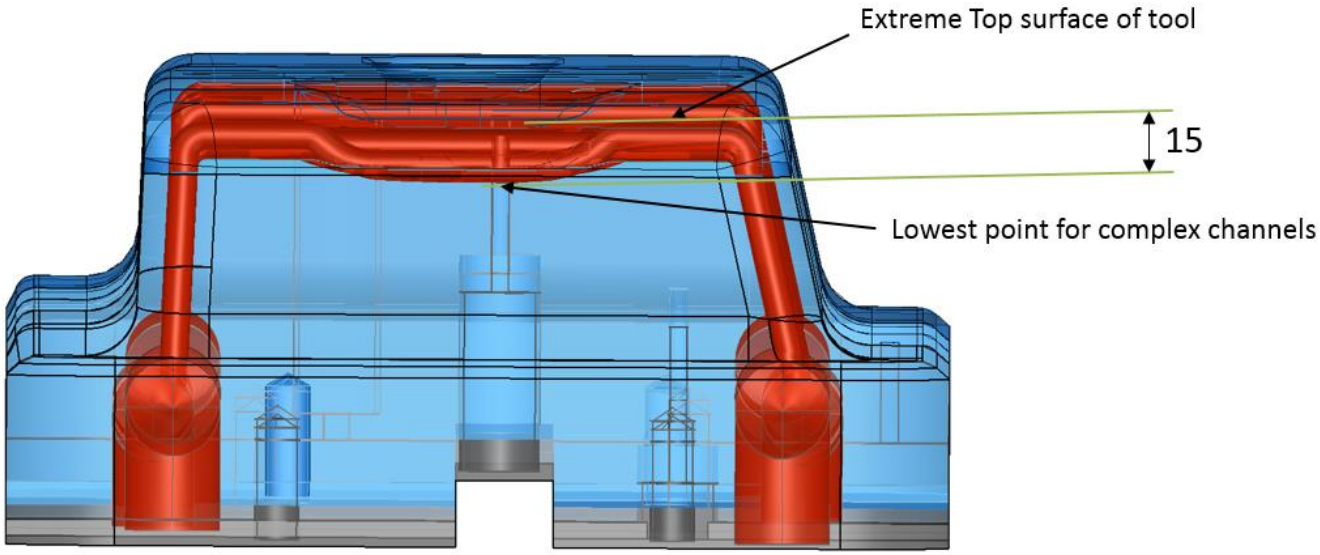


Figure 6-2: Height of complex conformal cooling channels

### 6.2.1. Machining of base parts

The CAD model portion representing the section to be machined was used to develop the CAM programs for machining. This involved exporting the CAD file to POWERMILL 2019 software which is used for generating the machining program instructions (Autodesk, 2019). POWERMILL was used because of its compatibility with CAD software (PowerSHAPE 2019). As mentioned earlier, the material used in manufacturing the base body is Hot Work Tool Steel 1.2344 because of its high strength, thermal crack resistance, wear resistance properties and wide application in the hot stamping industry (Escher and Wilzer, 2015). Tool steel 1.2709 was not used for the base body because it is costly and not easily available. However, an optimum situation would require the same materials for the base and top section. The machining programming codes and machining parameters used for the base parts are shown in Addendum B. The first stage of the machining process involved roughing of the tool steel blocks to obtain a near shape as shown in Figure 6-4 below. This was done on a 3-axis Deckel-Maho milling machine using a 6mm solid tungsten carbide MS4JC tool. The tungsten carbide material offers toughness and thermal resistant properties to the tool (Mistubishi Materials, 2019). The 3-axis Deckel-Maho milling machine in Figure 6-3 was used because of the simplified geometry of the unit blocks which could be milled using three axis movements. The inserts were machined with an overhang of 1 mm all around and the height was up to the parting line. This was done to give allowance for final machining around the inserts after the built process.


Figure 6-3: 3-axis Deckel-Maho milling machine

To machine the channels, drill bits with diameters (10 and 15 mm) equal to the holes to be machined, were each separately mounted on the 3-axis Deckel-Maho milling machine and directed to move in a vertical direction according to the machining program. The drill bit material was titanium nitride (TiN) coated carbide because of its high hardness (77-81 HRC), thermal and abrasive resistance properties (Mistubishi Materials, 2019). The second stage involved finishing of the insert blocks as shown in Figure 6-5.


Figure 6-4: Roughing of steel blocks

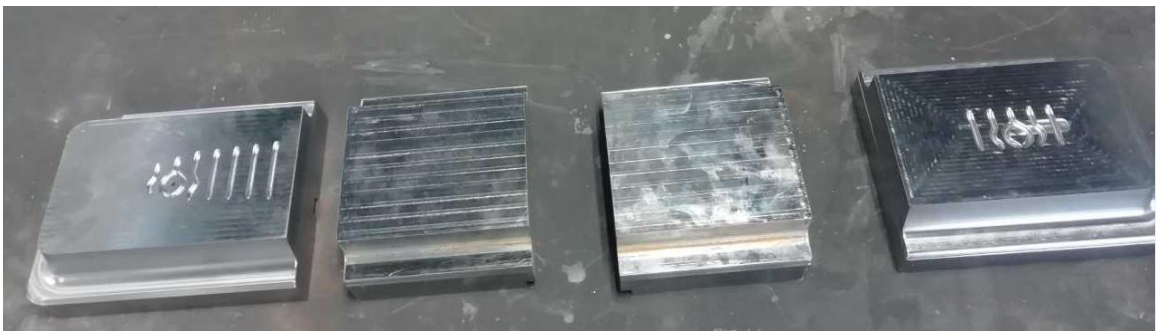

Figure 6-5: Machined base parts before drilling channels

The next step was to drill the 5 mm cooling channel holes on the steel blocks. A 5mm TiN coated carbide drill bit was used. One of the sides of the inserts had angled holes (77° to the horizontal plane) to conform to the part geometry as seen in Figure 6-6.

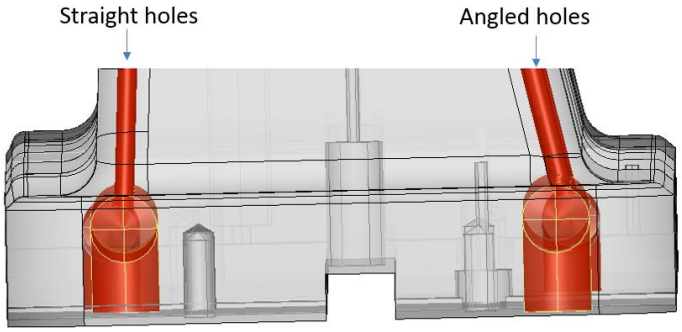


Figure 6-6: Holes drilled for the conformal cooling system

The 5-axis Hermle HSC milling machine shown in Figure 6-7 was used to drill the angled holes. This is because the angled holes required five axis movements of the drill bit to machine, unlike the straight holes which could be drilled on a 3-axis machine.

Figure 6-7: 5-axis Hermle HSC milling machine

The drilled base bodies of the inserts are shown in Figure 6-8 below


Figure 6-8: Insert blocks after drilling

## 6.3 Manufacture of the Built Portion

The M2 LaserCUSING machine at STC-LAM, shown in Figure 6-9, was used to produce the additively built portion. As mentioned earlier, this machine was used because of its ability to manufacture fully dense parts with mechanical properties comparable to conventionally produced parts (Schmidt *et al.*, 2017). The machine has a 200 W fibre laser and built envelop of 250×250×280 mm. To enable the built process, the CAD model for the built portion was firstly translated into an STL file. This allowed creation of small triangles which described the outline of the built portions, also known as triangulation. The STL file was then transferred to MAGICS® 2018 software to allow for pre-processing and simulation of the built section (Materialise, 2018). Pre-processing includes setting up the portion for building, and slicing of the model to avoid collapse of overhanging structures. The building time and material requirements were estimated at that stage. In this case, the built time was estimated to be 48 h per insert. Table 6.1 shows the machine set up parameters. To prepare for building, the inserts were individually sand blasted on the surfaces to be built. This was done to increase fusion between particles and base body during the building process. A base plate was prepared and drilled so that the inserts could be firmly bolted prior to building as shown in Figure 6-10. The insert blocks were separately placed in the M2 LaserCUSING machine to manufacture the top sections with the curved channels as shown in Figure 6-12.


Figure 6-9: M2 LaserCUSING

Table 6.1: Parameters used for the M2 LaserCUSING

| **Parameter** | **Measurement** |
|---|---|
| Laser power | 200 W |
| Layer thickness | 30 µm |
| Hatch spacing | 200 µm |
| Scanning speed | 600 mm/s |
| Focus diameter | 0.15 mm |

A layer thickness of 30 µm was used to improve accuracy of the build portion (Casalino *et al.*, 2015). The plane of each of the base body inserts was placed in line with the powder delivery system of the M2 LaserCUSING machine as shown in Figure 6-10. Since the top face of the base bodies were mostly flat surfaces, the powder scraper was used to align the top surfaces to the powder delivery platform together with some measurements. After flushing the chamber with an inert gas (nitrogen), the building of the conformal cooling channels was executed to a height of 13.5 mm, allowing an extra 1 mm for final machining. The material used for the build is maraging steel 1.2709 because it has excellent strength and toughness properties (Shellabear and Weilhammer, 2007). Also, it can be easily machined after building and post hardened to more than 50 HRC (EOS, 2011). After each build, the remaining powder was blown away using compressed air.

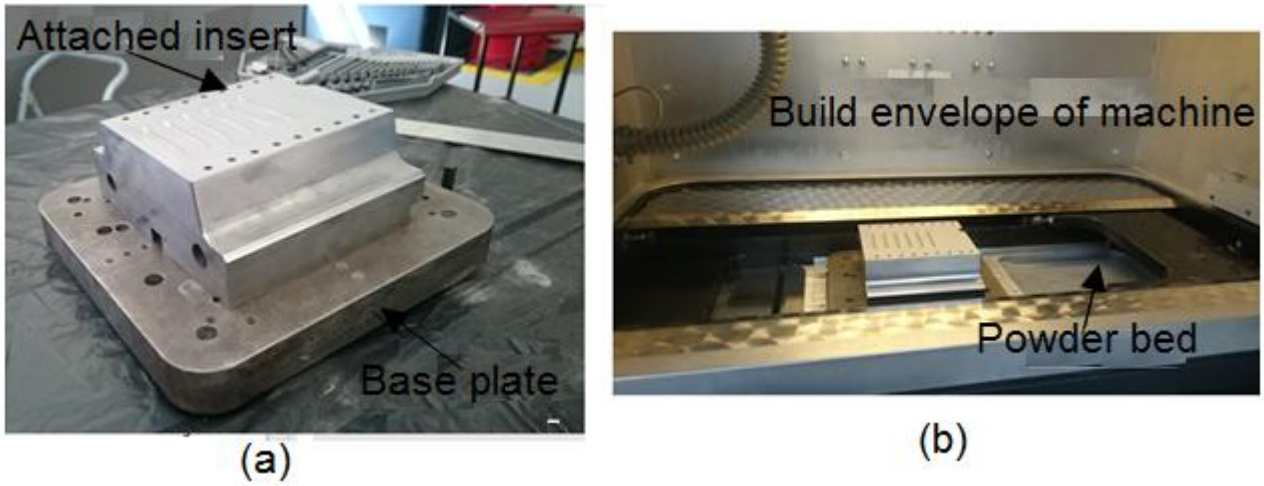


Figure 6-10: a) Insert attached on base plate b) insert placed on built chamber.

### 6.3.1. Heat treatment and final machining

The 1.2709 tool steel powder used has a martensitic crystal structure which is strengthened at 500 K (EOS, 2011). Thus, the precipitation heat treatment procedure was used for the inserts. Moreover, this heat treatment is recommended for hybrid parts using tool steel 1.2709 (EOS, 2011). It also allows the hardness to be increased to 54HRC which falls under the recommended standards for hot stamping tools (Escher and Wilzer, 2015). Besides, other researchers in literature who worked on additive manufacturing of forming tools, used this precipitation heat treatment procedure (Hölker-Jäger and Tekkaya, 2017). The procedure involved heating up the inserts to 540 °C at an increased temperature intensity of 100 °C/hr (EOS, 2011). The temperature (540 °C) was then held constant for 6-10 hrs. This was followed by cooling down the inserts at a uniform rate of 100 °C/hr which resulted in attaining a hardness of 54HRC. Rockwell hardness tests were then conducted to verify the resultant hardness. The graph in Figure 6-11 gives the guideline for the heat treatment procedure. A local heat treatment industrial partner conducted the heat treatment process.

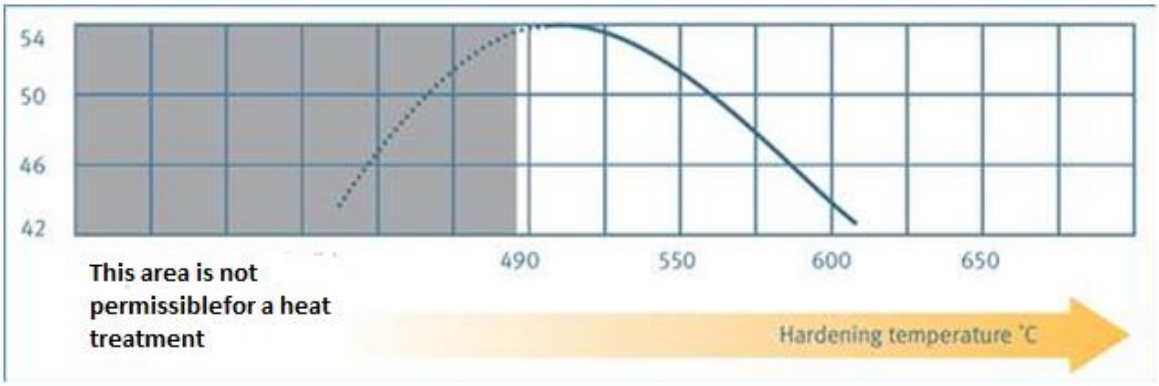


Figure 6-11: Hardening chart of standard 1.2709 (GmbH, 2018)

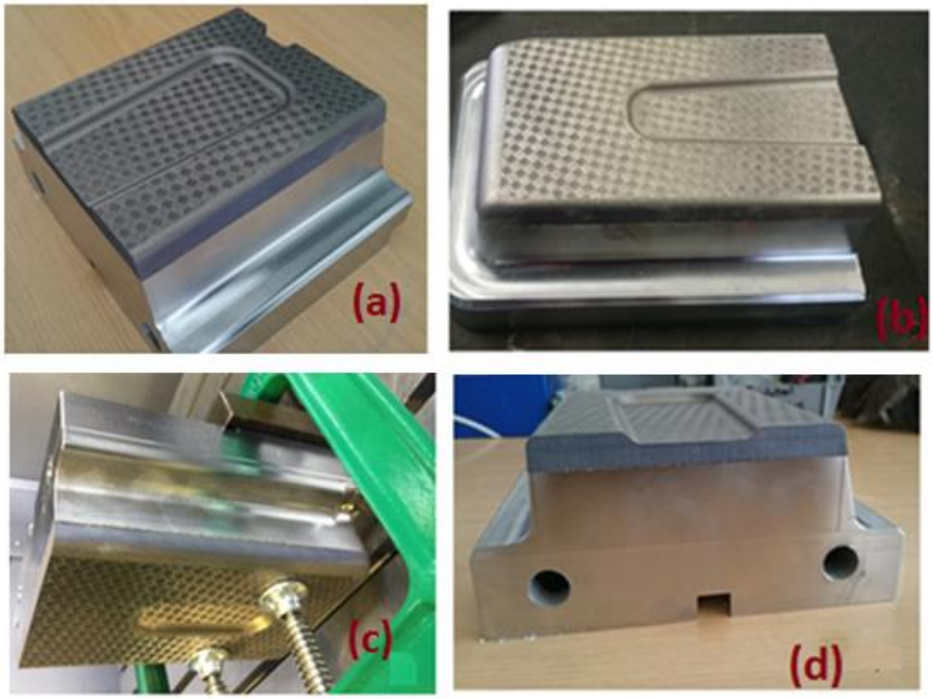


Figure 6-12: Tool inserts (a)-(d) with built section on top

The next stage involved a post machining process to obtain the required surface finish and tolerance. This helped to get rid of the high surface roughness associated with the SLM machine which lowers heat transfer on the tool surface during hot stamping (Caron *et al*, 2014). During the final machining, the excess 1 mm was removed.

## 6.4 Challenges Faced During the Manufacturing Process

After setting up the tool for the final machining, there was an error made in the orientation of the part. This caused damage on one side of the edge fillets by an offset of about 4 mm as shown in Figure 6-13. To resolve the challenge, the tool inserts were repaired by direct metal deposition (DMD) at the

Council for Scientific and Industrial Research (CSIR). A major difference between the two processes lies in the powder delivery system as previously explained in Chapter 2. The powder material (tool steel 1.2709) and other parameters used for the DMD are similar to the SLM process except for the particle size, laser power and spot size. For the DMD, a spot size of 2.5-3 mm, laser power of 200 W and particle size of 50-200 µm, were used. On the other hand, the corresponding parameters for the SLM were 0.15 mm, 200 W and 16-45 µm respectively.

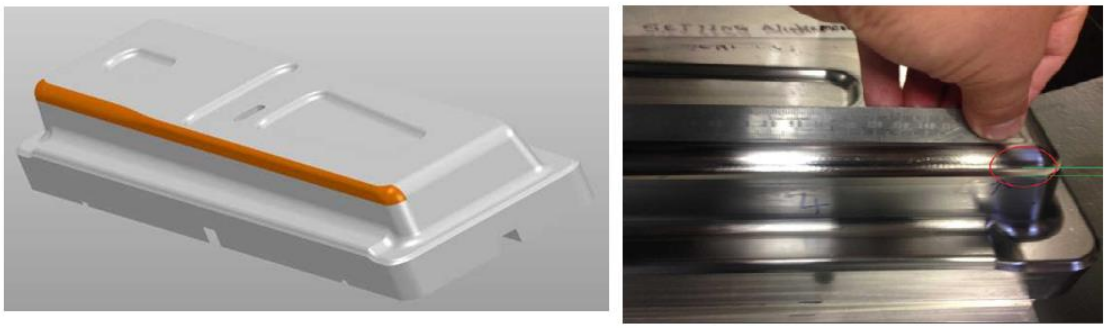

(a) (b)

Figure 6-13: a) CAD model showing the portion affected by the orientation error b) Picture showing the offset

The repaired tool inserts are shown in Figure 6-14 below. The inserts were repaired with an overhang of 2 mm as an allowance for final machining. The DMD method was used because it has been successfully applied in the hardening of additively manufactured parts causing improvement hardness and wear resistance (Černašėjus *et al.*, 2019).

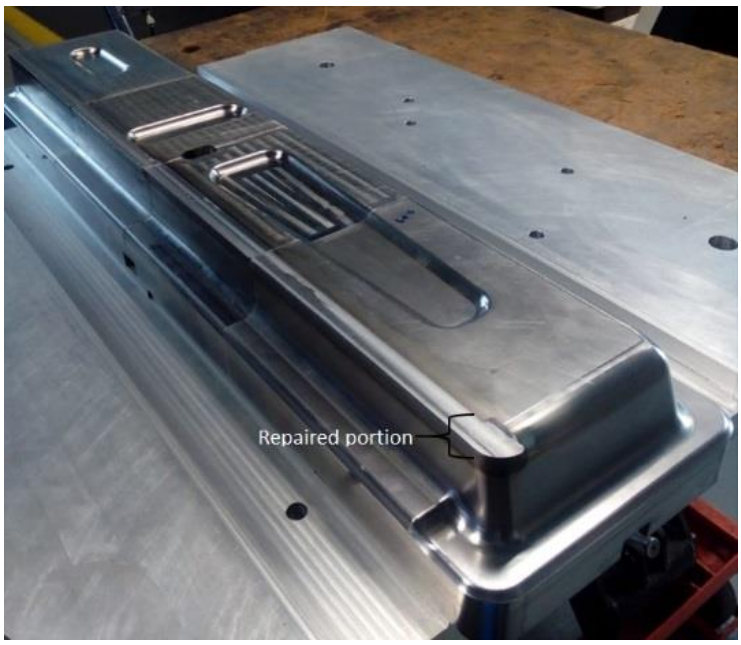


Figure 6-14: Repaired tool inserts

The inserts were then machined to the required geometry since the laser hardening process does not cause any geometric deviations (Davis, 2002). Thus, the final machining was done on the 5-axis Hermle HSC milling machine as shown in Figure 6-15.

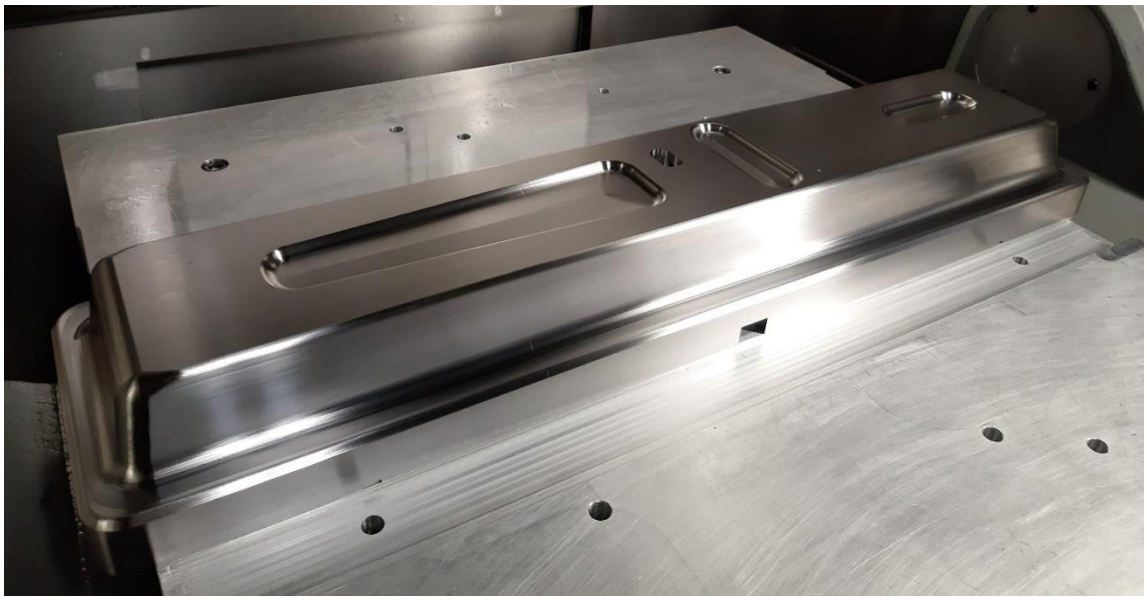

Figure 6-15: Tool after final machining

The next section explains the experimental design methods used to evaluate the performance of the manufactured conformal cooling tool and to compare it with the conventional tool.

## 6.5 Experiments

The goal of the experiments was to evaluate the effect of the conformal cooling system on the cycle time and quality of parts. Data on previous experiments on the conventional tool was already available. Accordingly, experiments with the conformal cooling tool were carried out to compare the results. As mentioned in Chapter 3, the full factorial method of designing experiments was used to allow a thorough investigation of the effect of the parameters. Also, there were only a few controllable factors (cooling time and flow rate) and not too many experimental runs involved. In total, there were three levels for the cycle time and three levels for the cooling flow rate. Two replicates were done for each experiment due to budgetary constraints. Therefore, a total of 18 experiments were conducted (3×3) ×2. The range for the coolant flow rate was calculated for the conformal cooling tool according to the condition that the Reynolds number should lie between 4 000 and 10 000 (Lim *et al.*, 2014). Based on the layout in Figure 6-16, the mass flow rates corresponding to the required range of Reynolds numbers are calculated separately using Equation 6-2.

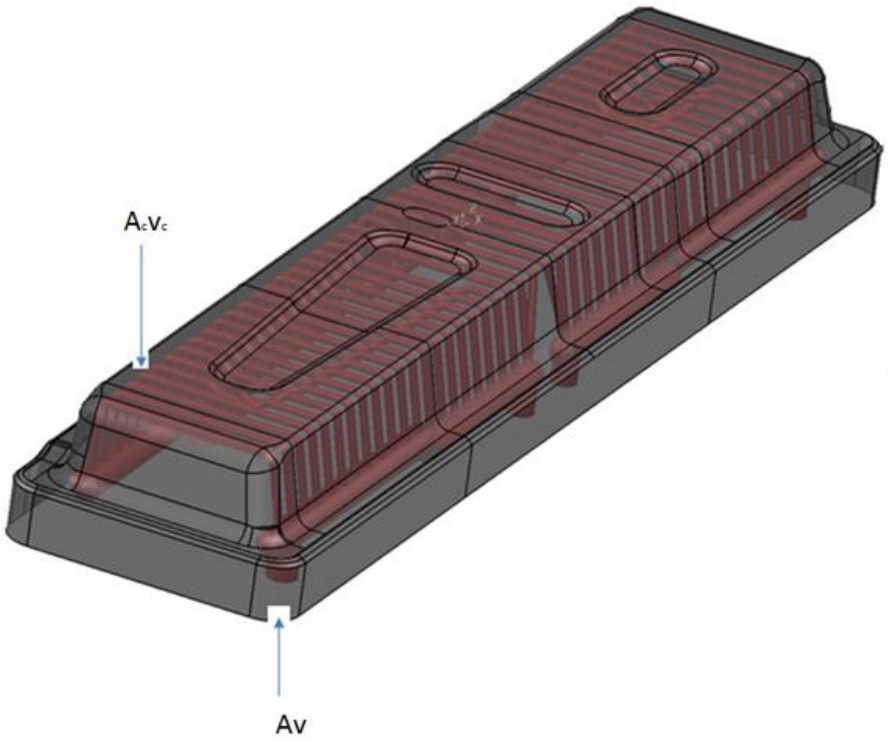


$$Av = nA_c v_c$$

Figure 6-16: Coolant flow for the conformal cooling tool

The mass flow rate for the conformal tool is calculated using Equation 6-1 and 6-2 according to the layout in Figure 6-16. Regarding equation 6-2, $\eta_w$ is the viscocity of water which is approximately 0.001 kg /ms at room temperature ( Çengel and Ghajar, 2011). The quantity $n$ is the average number of cooling channels in all the inserts. According to Equation 3.31, the mid-section had a total of 19 channels. However, it was split into two segments with nine channels each. On the other hand, the cooling channels on the extreme left and right had 12 channels each. Thus the average number of cooling channels was 11 per insert.

$$4\,000 \leq Re \leq 10\,000 \qquad 6\text{-}1$$

$$4\,000 \leq \frac{d\rho_w v}{\eta_w} \leq 10\,000$$

$$4\,000 \leq \frac{0.005 \times 1000v}{0.001} \leq 10\,000$$

$$0.8 \leq v \leq 2\ m/s$$

$$Av = nA_c v_c \qquad 6\text{-}2$$

$$Av = 11 \times \frac{\pi \times 0.005^2}{4} m^2 \times 0.8\, m/s$$

$$Av = 1.728 \times 10^{-4} m^3/s$$

$$\boldsymbol{Av = 10.38\ l/min}$$

$$Av = 11 \times \frac{\pi \times 0.005^2}{4} m^2 \times 2\, m/s$$

$$Av = 4.32 \times 10^{-4} m^3/s$$

$$Av = 25.91\ l/min$$

Accordingly, the range for the coolant flow rate considered is between 11 and 26 *l*/min. However, the SFAW Festo flowmeter which was available had a maximum flow measurement of 19 *l*/min. Thus, the values for the levels for the coolant flow rate were 11, 15 and 19 *l*/min indicating the lowest, medium and maximum value, respectively. The T25610-D Chiller unit could only maintain the temperature of the coolant at 20 °C, which is the lowest temperature used in hot stamping. The design of experiments matrix used for the conformal cooling system is explained in Table 6.2 below.

Table 6.2: DOE Matrix for the conformal cooling system

| **Factor** | **Cooling time (s)** | **Coolant flow rate (*l*/min)** |
|---|---|---|
| Level 1 | 2 | 11 |
| Level 2 | 5 | 15 |
| Level 3 | 8 | 19 |

### 6.5.1. Requirements for the experiment

The apparatus used to perform the experiments are shown in Table 6.3.

Table 6.3: Apparatus used in the experiments

| **Description** | **Apparatus used** |
|---|---|
| Forming | Hydraulic press Raster Zeulenroda PYZ |
| Cooling | Single T25610-D Chiller unit, SFAW Festo flowmeter |
| Temperature measurement | 4 K type thermocouples |
| Hardness measurement | Micro-Vickers hardness tester EMCOTEST MTC 010-0R |
| Blank cutting | Discotom-100/-10 |

### 6.5.2. Measurements

The cooling time of the blank in the closed tool was varied using the machine control unit. In this context, the cooling time was considered as the phase in which the blank is held in the forming tool before being extracted. The initial temperature of the blank was recorded using a thermocouple. A Festo flowmeter connected to the coolant supply was used to measure the coolant flow rate. In addition, the coolant supply had an in-built regulatory system which was useful in maintaining the coolant temperature at 20 °C. Three K-type thermocouples were positioned in the punch at 5 mm to the surface at the points shown in Figure 6-17. These locations were selected to gain an overview of the temperature changes on the whole punch. Also the locations are similar to those used in the experiments with the conventional tool.

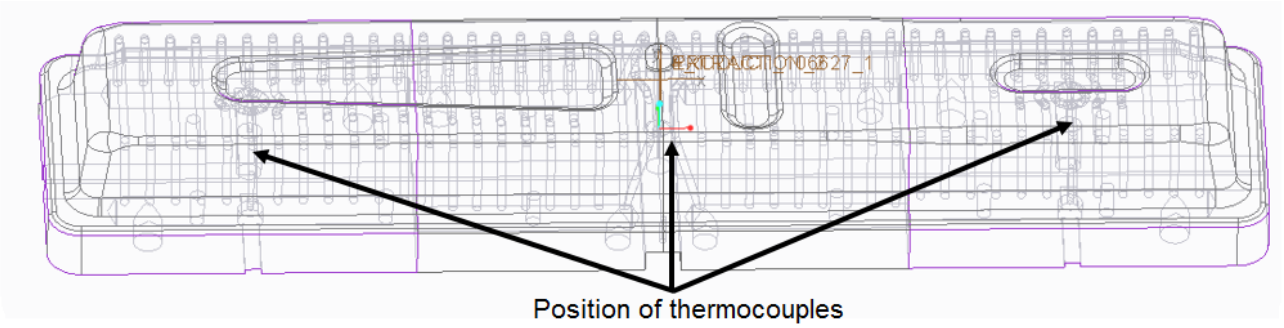


Figure 6-17: Position of thermocouples in the punch

The coolant used is water because it is economical, it has a high specific heat capacity of 4.2 KJ/kg°C which is good for absorbing heat and its viscosity allows it to flow freely in the channels. It is also the commonly used coolant in hot sheet metal forming applications. The range for the cooling time used in the experiments was 2-8 s which is comparable to the data on the conventional tool. Also, it was important to investigate the effect of reduced cooling time on the improved cooling system design. Figure 6-18 shows the experimental set up used for testing the manufactured tool. The experiments were conducted at the Fraunhofer Institute for machine tools and forming technology workshop.

The thermocouples, inserted in the punch at the left, right and centre to record the temperature changes, are shown in Figure 6 18. Other parameters used in the experiments are shown in Table 6.4 in accordance with previous experiments on the conventional tool.

Table 6.4: Experimental parameters

| **Parameter** | **Quantity** |
|---|---|
| Blank temperature when exiting oven | 950 °C |
| Transfer time of blank from oven | 10 s |
| Forming speed | 200 mm/s |
| Stamping pressure | 1000 kN |
| Cooling time | 2-8 s |
| Blank thickness | 1.5 mm |
| Press type | Hydraulic |

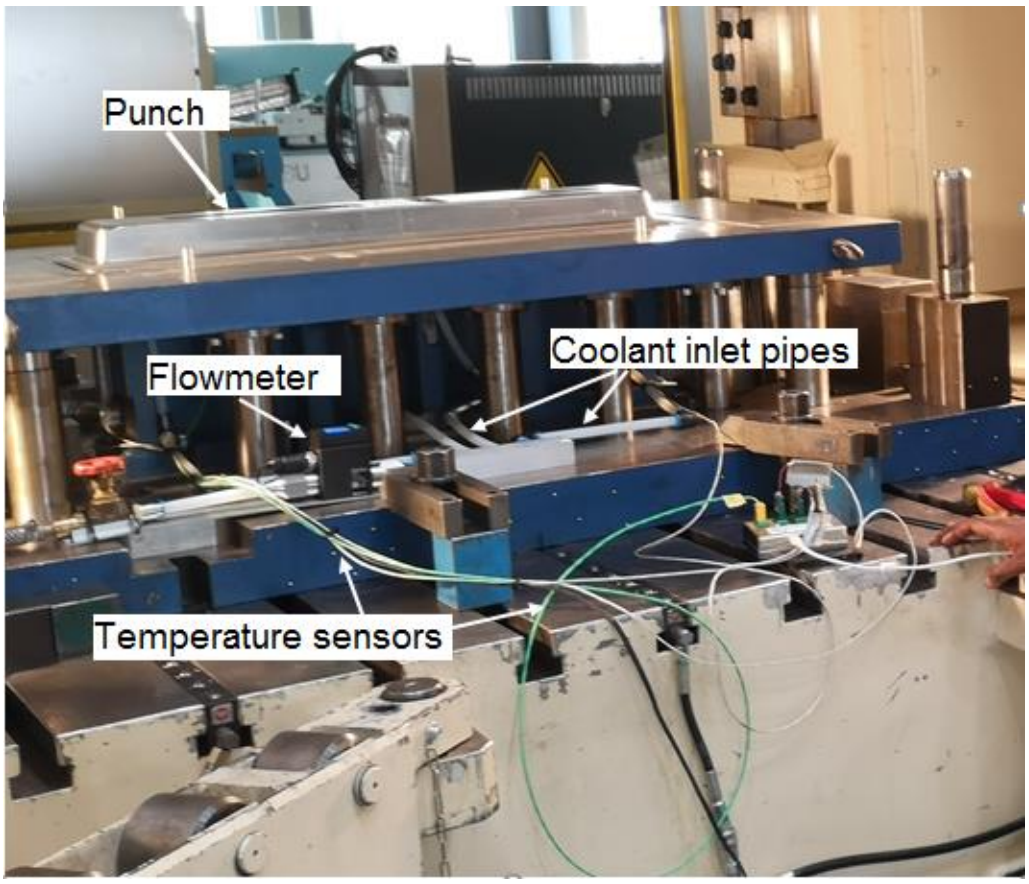


Figure 6-18: Experimental set up (Fraunhofer Institute for machine tools and forming technology workshop)

### 6.5.3. Expected results

To effectively measure the effect of the modified cooling system, comparisons were made between the experimental results obtained for both cooling systems. At this stage, it was expected that the conformal cooling tool would result in reduced cooling time and improved quality as depicted in the simulation results. Just like the simulation, the quality is evaluated by measuring the hardness deviation of the blank.

## 6.6 Conclusion

The aim of this chapter was to present the steps involved in the manufacture of the tool and the challenges involved. A detailed description of the stages involved in producing the tool is given. This includes machining of the base part, additive manufacture of the top part, hardening, stress relieving and final machining. In addition, the challenges encountered during the tool manufacture were explained. The manufacturing process addresses the fourth objective of the study and creates a foundation for the experimentation. A detailed explanation of the design of experiments was given. The experiments were designed to allow for comparison of the results with the available data for the

conventional tool. The parameters used in the experiments were explained in the chapter. This includes calculations for determining the mass flow rates which allow for effective cooling. Also included in the chapter, is the information on the equipment used in the experiments and why it was used. The expectations of the experiments are also pointed out. The next chapter presents the experimental results and addresses the last objective of the study.

# CHAPTER 7 : RESULTS AND VALIDATION OF TOOL

## 7.1 Introduction

In the previous chapter, the tool manufacture and experimental set-up was presented. In the present chapter, results from experiments are presented and discussed. Firstly, a description of the hot stamping process with the conformal cooling tool is given. Secondly, the results on the influence of temperature and cooling time on the cooling system layout are explained and discussed. This is followed by an analysis on the maximum hardness and deviation which are used as indicators for cooling intensity and quality respectively. Secondly, the effect of the coolant flow rate on the hardness is explained. Thus an overall effect of the improved tool design on the cycle time and quality is derived. Lastly, the results from the experiments are compared with those obtained from the finite element analysis for validation purposes.

## 7.2 Hot Stamping Process with Developed Tool

The blank was heated in the furnace for 10 minutes at 1000 °C to allow for the microstructural transformation. After heating, it was manually transferred to the furnace for 10 seconds and formed as shown in Figure 7-1.

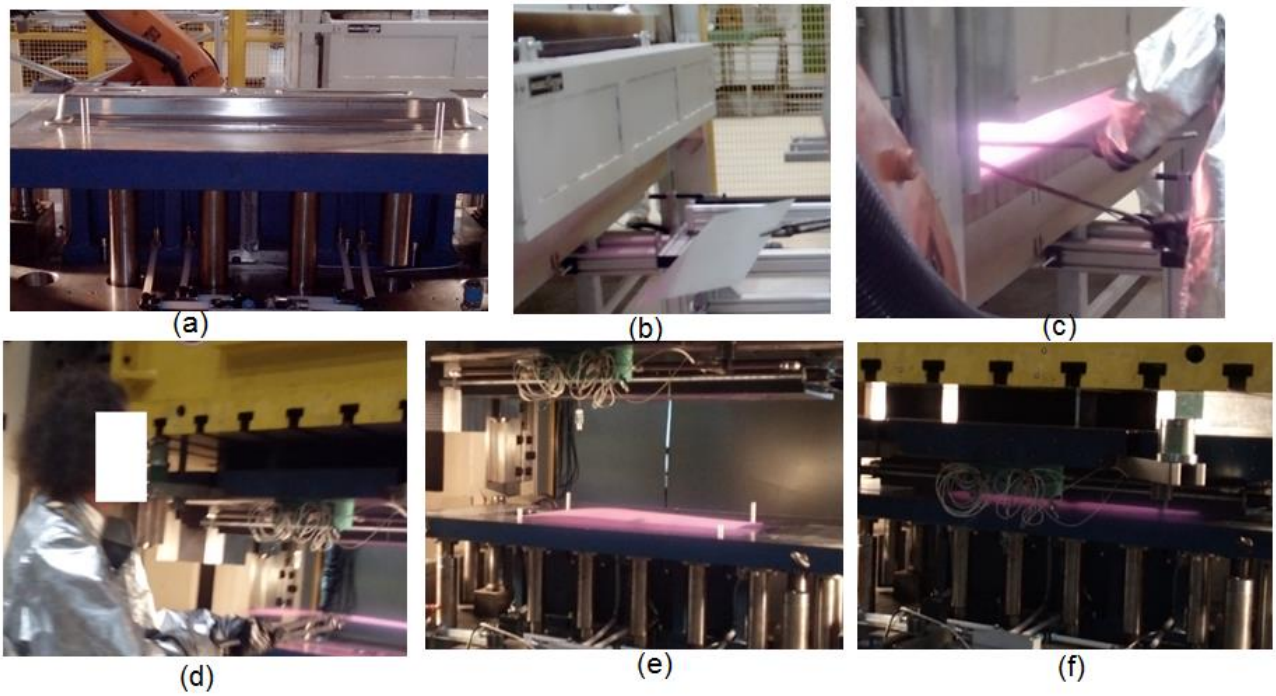


Figure 7-1: a) Developed tool b) blank placed in furnace c) blank retrieval d) blank placed on press e) blank on forming position f) blank formed

To establish the blank temperature prior to forming, a thermocouple was fixed on the blank as shown in Figure 7-2 below.

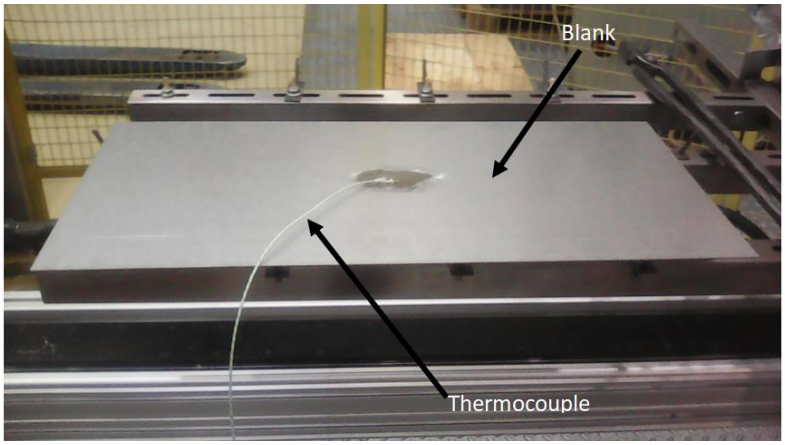


Figure 7-2: Blank with thermocouple

The thermocouple was broken when the die encountered the blank right before the forming operation. Figure 7-3 below shows blank with a depression showing the position at which the code was broken.

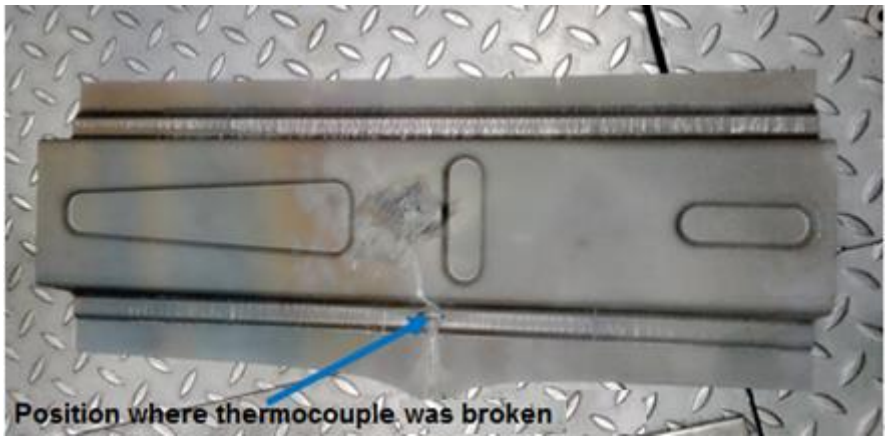


Figure 7-3: Blank showing position where thermocouple code was broken

The graph of the temperature profile shown in Figure 7-4 confirms the breaking point of the thermocouple at 900 °C after a transfer time of 10 s.

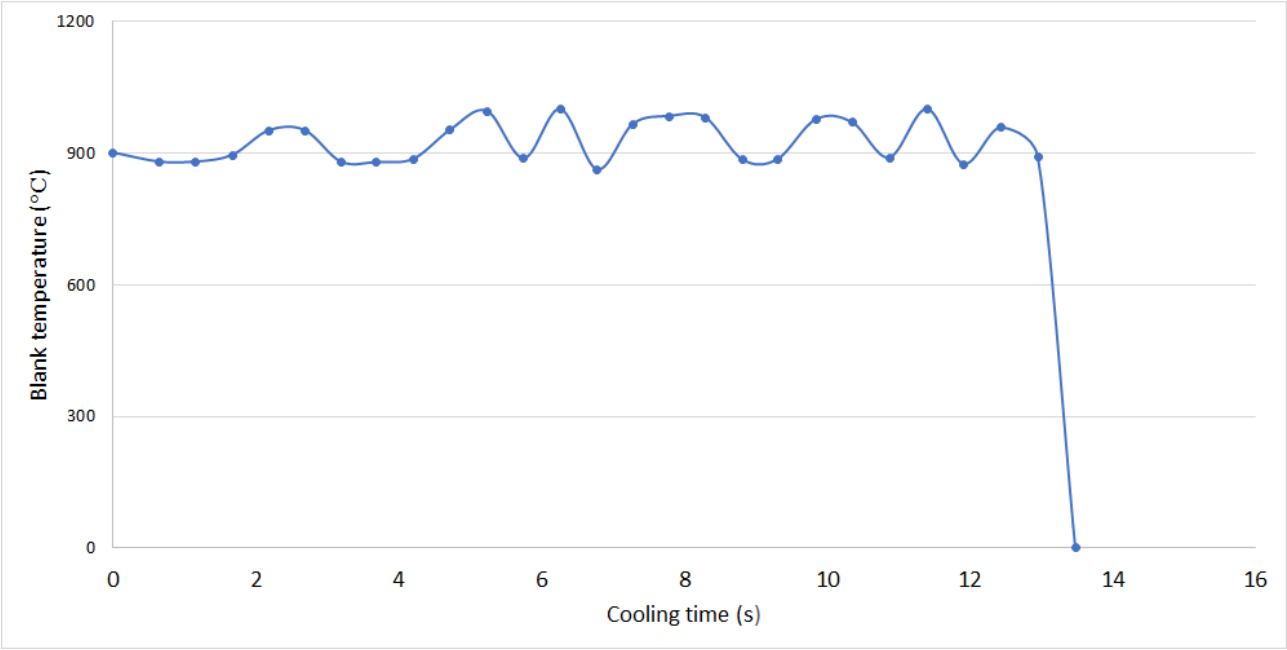


Figure 7-4: Blank temperature at the forming stage

Accordingly, the interpretation is that the blank was formed at 900 °C before the cooling stage which took place in the closed tool. Conversely, it was not possible to measure the initial blank temperature at the start of the cooling stage in the closed tool. Since the blank loses temperature as it contacts the die and punch during forming, it is clear that the cooling began when the punch came into contact with the blank at the start of the forming process.

## 7.3 Influence of Cooling System Design on Temperature

The following sections presents the effect of the cooling system layout design on the blank and tool temperature. As stated in the previous chapter, the temperature of the blank after cooling was measured using an infra-red temperature gun and the punch temperature was measured using 3 thermocouples inserted in the punch.

### 7.3.1 Blank temperature

The temperature of the blank after different cooling times is compared for both cooling system layouts as shown in Figure 7-5. The initial temperature of the blank before forming is 900 °C based on the measurements in section 7.2. The temperature after the forming stage was assumed to be 800 °C since it was difficult to measure in the closed tool. This assumption was made based on previous experimental results in literature (Shapiro, 2009; Lim *et al.*, 2014b; Ying and Zhong-De, 2014).

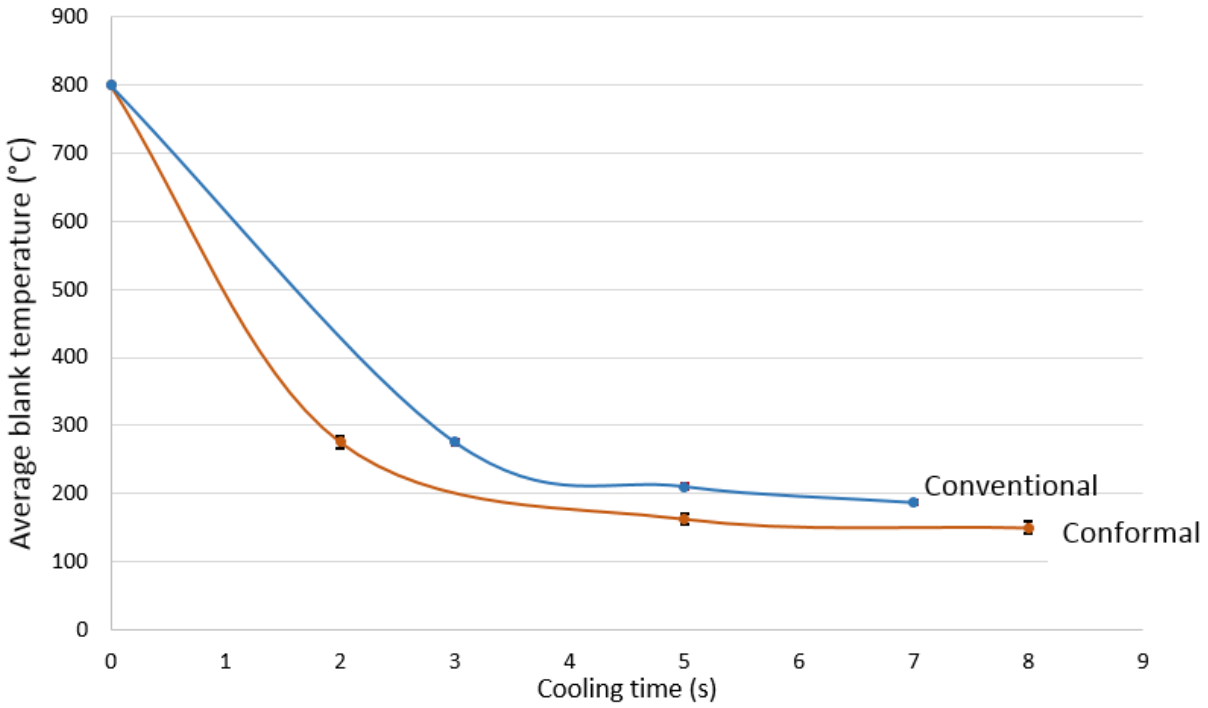


Figure 7-5: Mean blank temperature after cooling

As shown in Figure 7-5, the temperature profile of the blanks on the conformal cooling tool indicates a higher cooling rate as compared to the profile for the conventional tool. The higher cooling rate of the conformal cooling tool can be explained by the shorter distance (7.5 mm) between the cooling channels centre and tool surface. Theoretically, the blank temperature must be 200 °C or less to guarantee the required microstructural changes (Lim *et al.*, 2014; Ying and Zhong-De, 2014). After a cooling time of 5 s, the conformal cooling tool caused the blank to have an average temperature of 163 °C which is below 200 °C. Accordingly, a cooling time of 5 s is justifiable for the conformal cooling tool. On the other hand, the conventional tool caused the blank to reach an average temperature of 211 °C after 5 s. Thus, there was an increase in the blank cooling rate by 9.6 °C/s in the first 5 s.

### 7.3.2 Punch temperature

Figure 7-6 shows the position of sensors inside the punch. The cooling time was controlled using the machine control unit. Thus, it was difficult to stop and start the sensors in the punch during the cooling period. Hence, the sensor readings were taken for the whole cycle. A sharp rise of the temperature on the graph indicated the period in which the punch was in contact with the blank. All the recordings on the temperature profile of the sensors in the punch showed that the temperature did not go above 45 °C after 20 runs and it subsided soon after the cooling stage. Addendum E shows the rest of the temperature curves.

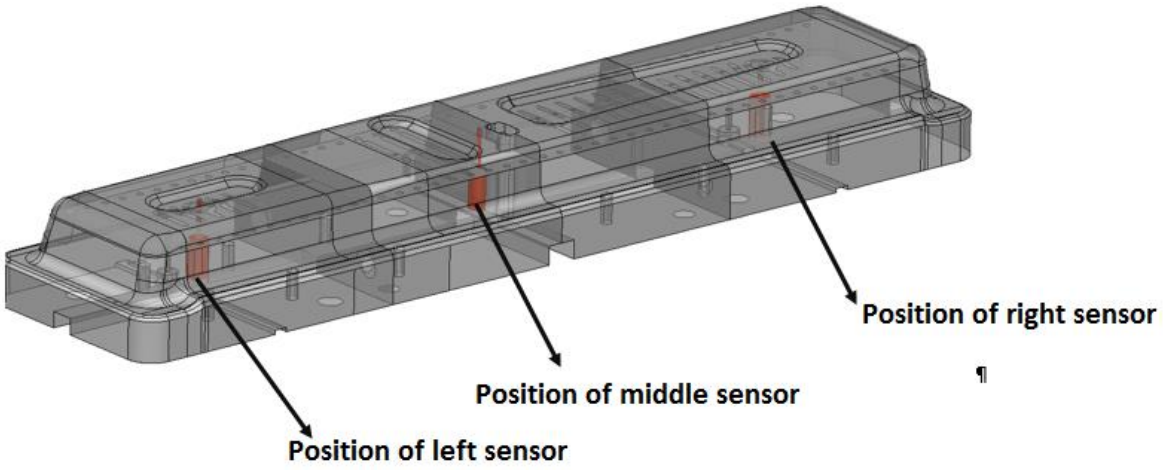


Figure 7-6: Position of sensors at 5 mm from surface in punch

Figure 7-7 shows the temperature profile of the sensors within a cooling time of 2 s.

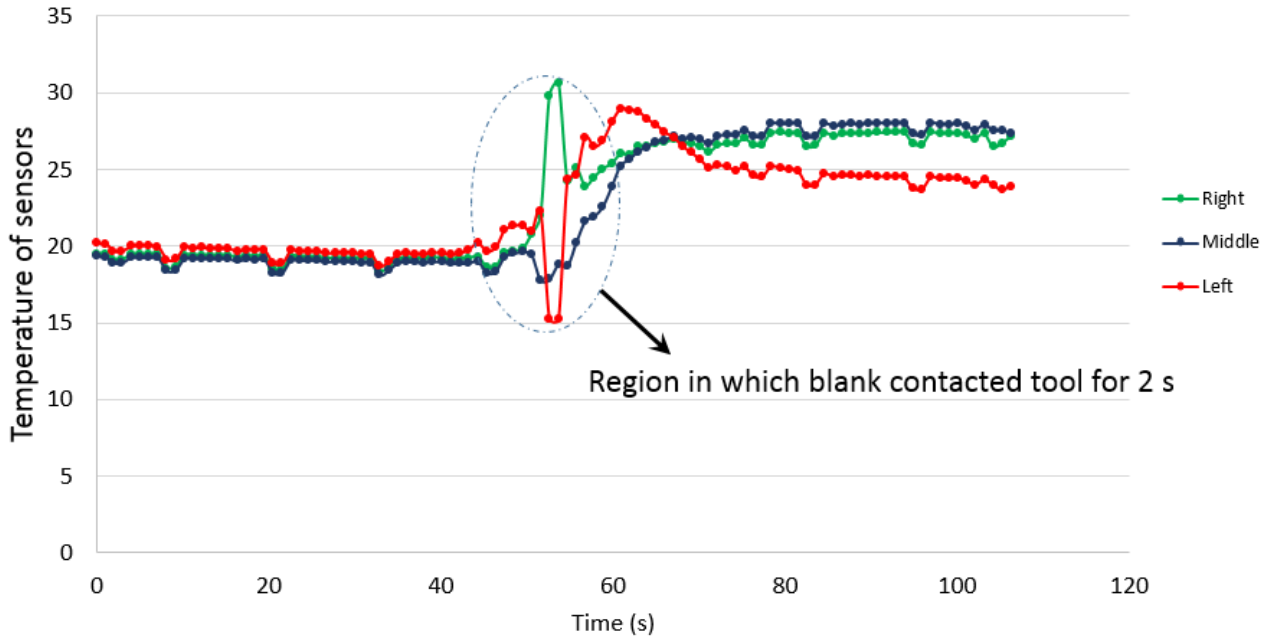


Figure 7-7: Temperature profile for sensors inserted in the punch at 2 s blank cooling time

The region in the dotted circle in Figure 7-7 shows the period in which the hot blank came in contact with the punch. The punch temperature rose sharply during contact but later subsided. The parallel design of the conformal cooling tool allows the coolant to absorb heat and release it from the tool system much faster when compared to the conventional tool.

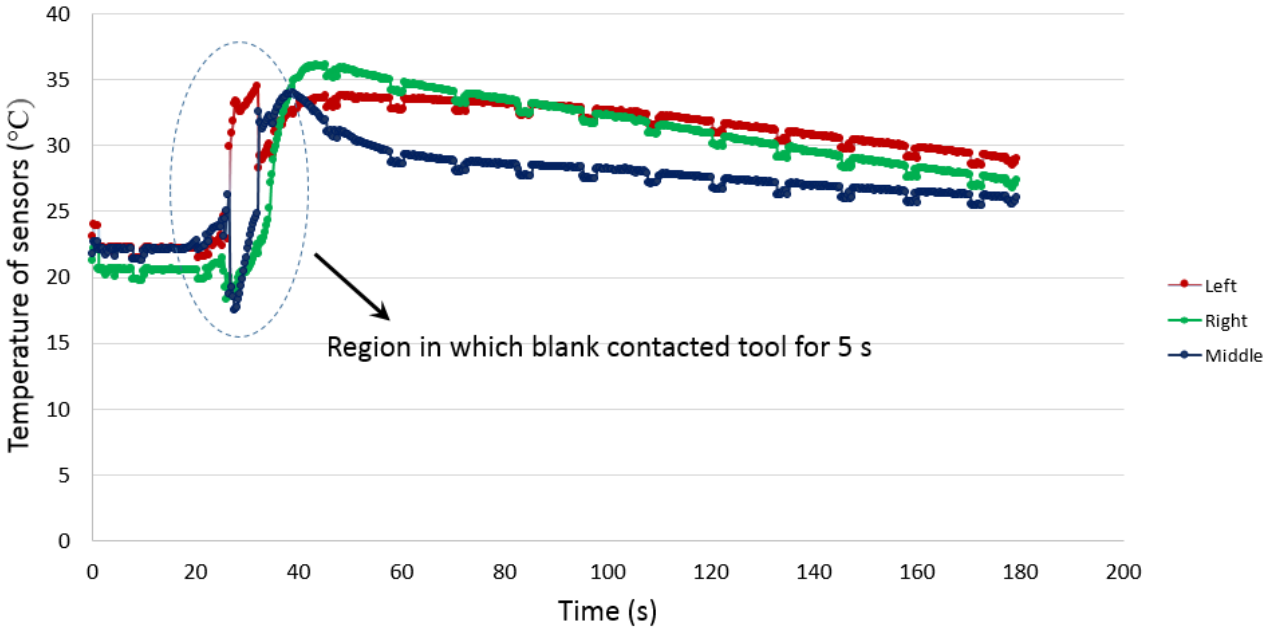


Figure 7-8: Temperature profile for sensors at 5 s blank cooling time

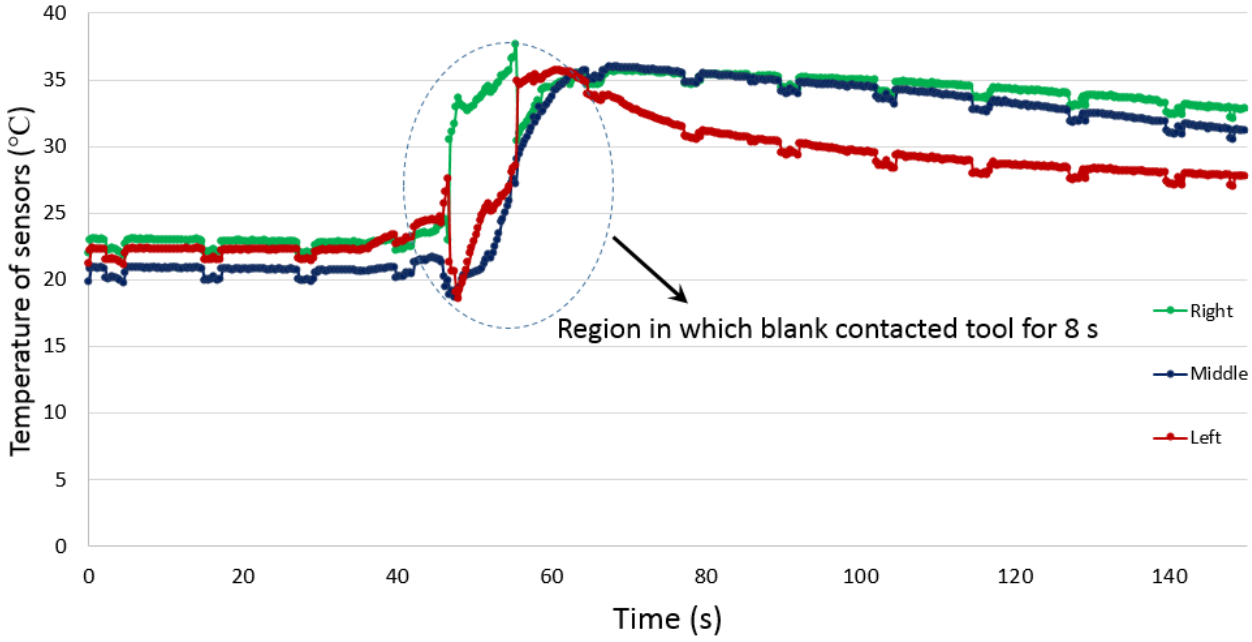


Figure 7-9: Temperature profile for sensors at 8 s blank cooling time

The temperature curves of the sensors in the conventional tool was not available: However; the available experimental data showed that the maximum temperature of the sensors incorporated in the conventional punch after producing 20 blanks is 70 °C during the press hardening tests (Pierschel *et al.*, 2015). For the conformal cooling tool, the maximum temperature after 20 blanks is 45 °C. Thus, the conformal cooling system caused the punch maximum temperature to decrease by 36 %.

### 7.3.3 Preliminary conclusions on the temperature

The following preliminary conclusions can be drawn on the effect of cooling system layout on temperature

- The conformal cooling tool caused the hot blanks to cool faster than the conventional tool. This is confirmed by the temperature curves in Figure 7-5. According to the calculations, the conformal cooling tool increased the cooling rate by 9.6 °C/s.
- According to the results the maximum temperature recorded on the conformal cooling sensors did not exceed 45 °C after hot forming 20 blanks. Thus; there was a reduction in the maximum temperature of punch by 36 % as compared to the conventional tool.
- The ability of the conformal cooling tool to cool faster can be explained by the parallel design of cooling channels which causes a faster and even heat distribution.

## 7.4 Influence of Cooling System Design and Flow Rate on Hardness

As mentioned before, the hardness of the blanks formed with the conventional tool was measured at cooling times of 3, 5 and 7 s. Data on the micro-Vickers hardness tests done on blanks formed with the conventional tool on the points PI; P2 and P3 shown in Figure 7-10 was available (Pierschel *et al.*, 2015).

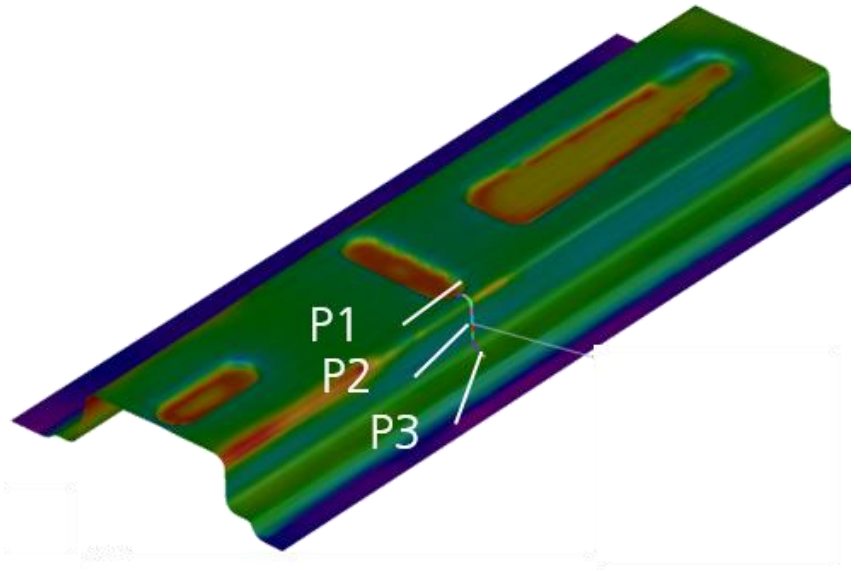


Figure 7-10: Hardness measuring points for blanks formed with conventional tool (Pierschel *et al.*, 2015)

Accordingly; measurements on the blanks formed with the conformal cooling tool were done on the same cross section. To obtain the measurements at similar points to those in the previous experiments, the formed blanks were firstly cut using a Discotom-100 machine as shown in Figure 7-12. The

Discotom machine was used for cutting the cross-section so that the microstructure of the samples was not altered. All the samples were cut to a maximum depth of 40 mm for easier measurement on the Micro-Vickers hardness tester. This was followed by polishing and application of alcohol to clean the surfaces. After the cutting process, measurements were done on eight points shown in Figure 7-11. All the eight points were measured along the indicated section on the samples in order to examine the hardness uniformity across the samples.

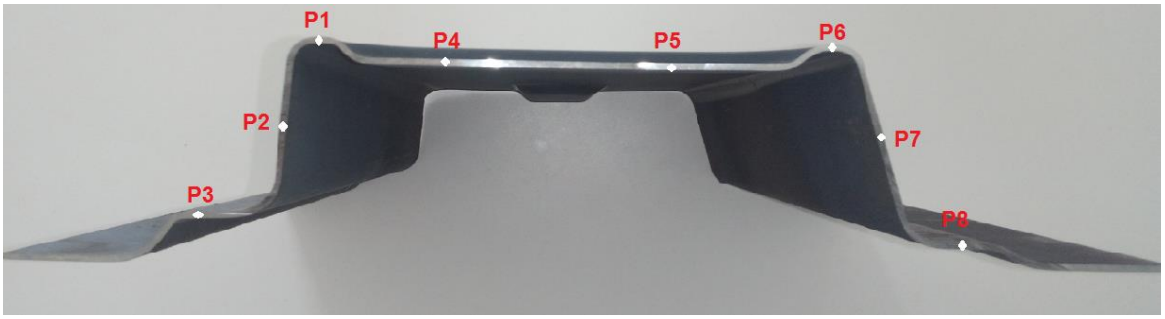


Figure 7-11. Hardness points on cut blanks

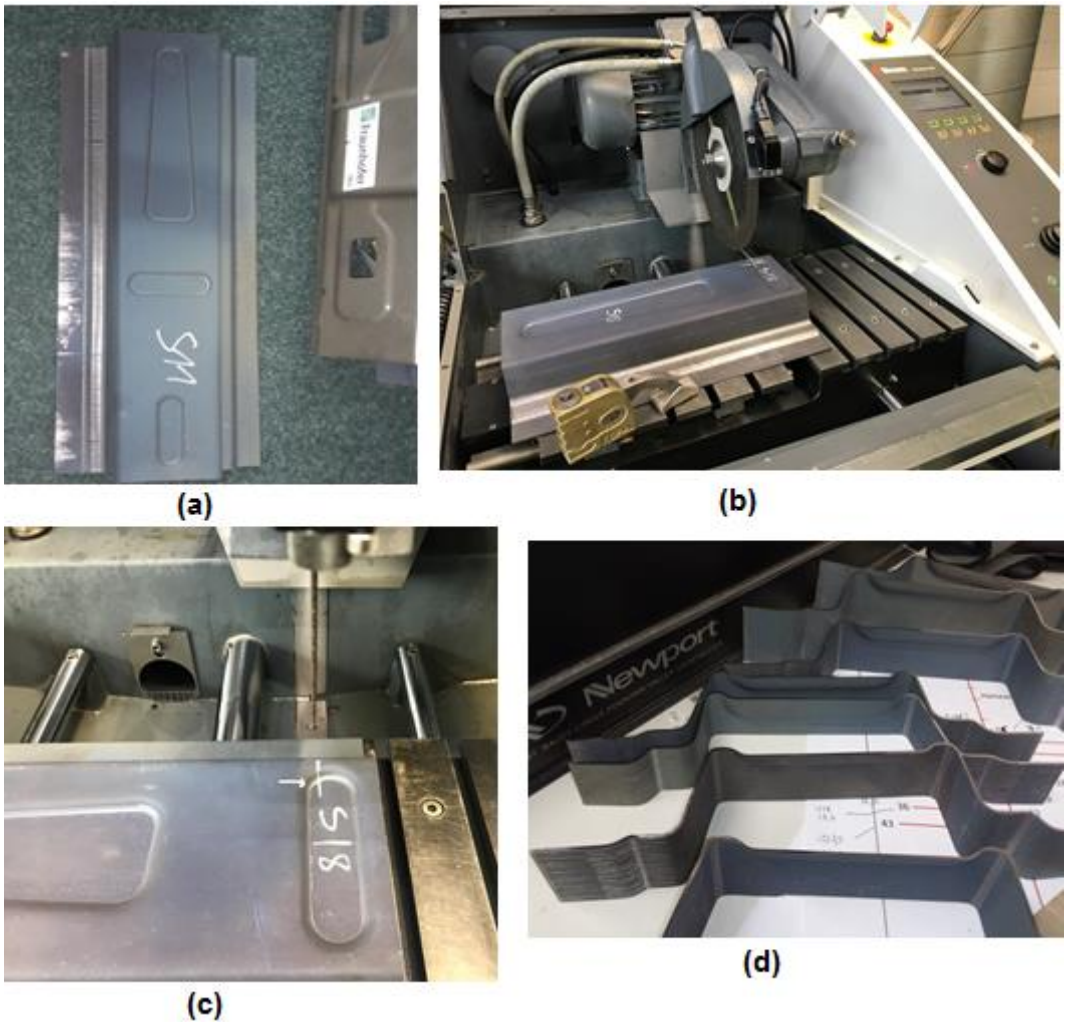


Figure 7-12: Preparation of blank samples

After preparation of the samples, the hardness was measured using a Micro-Vickers hardness test as shown in Figure 7-13. Three measurements were made on every point in Figure 7-11 per sample. Hence, 24 mesurements were taken per blank sample.

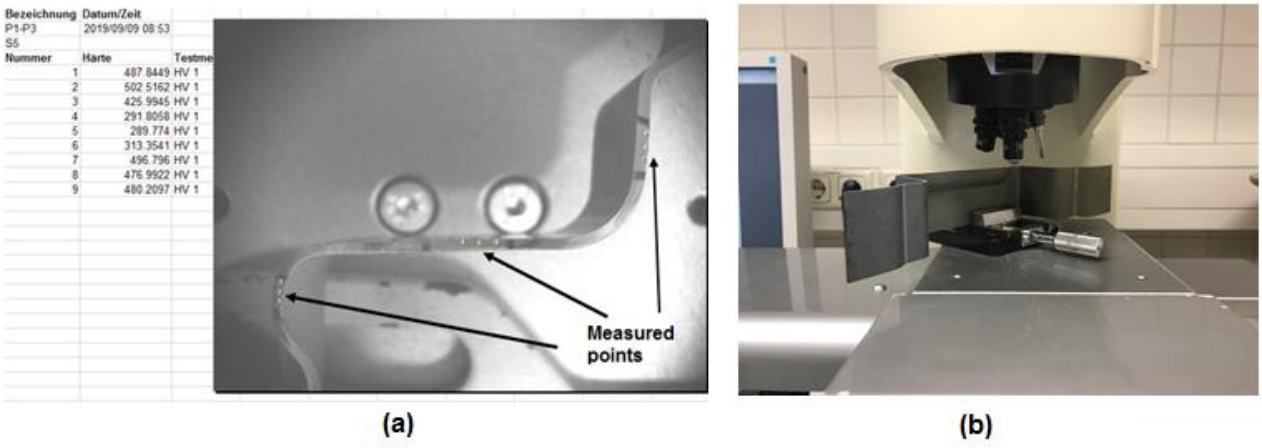


Figure 7-13: Hardness measurements

### 7.4.1. Maximum hardness

Figure 7-14 shows the graphs for maximum hardness for both cooling system layouts at points P1-P3 at different cooling times.

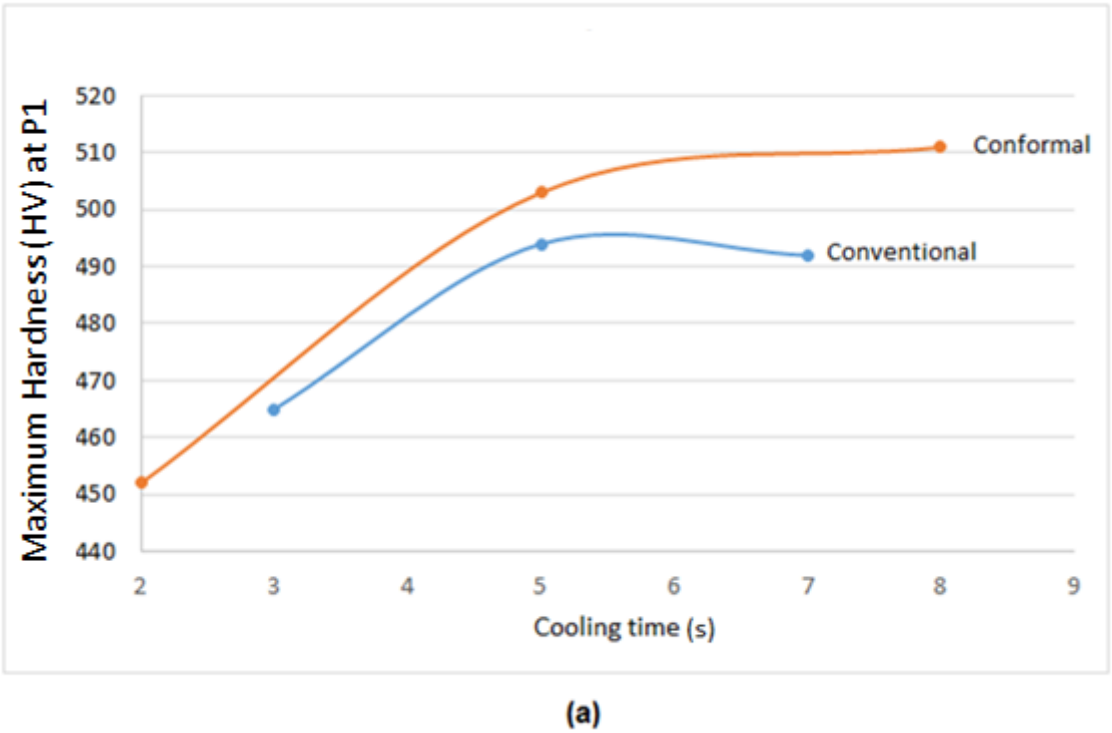

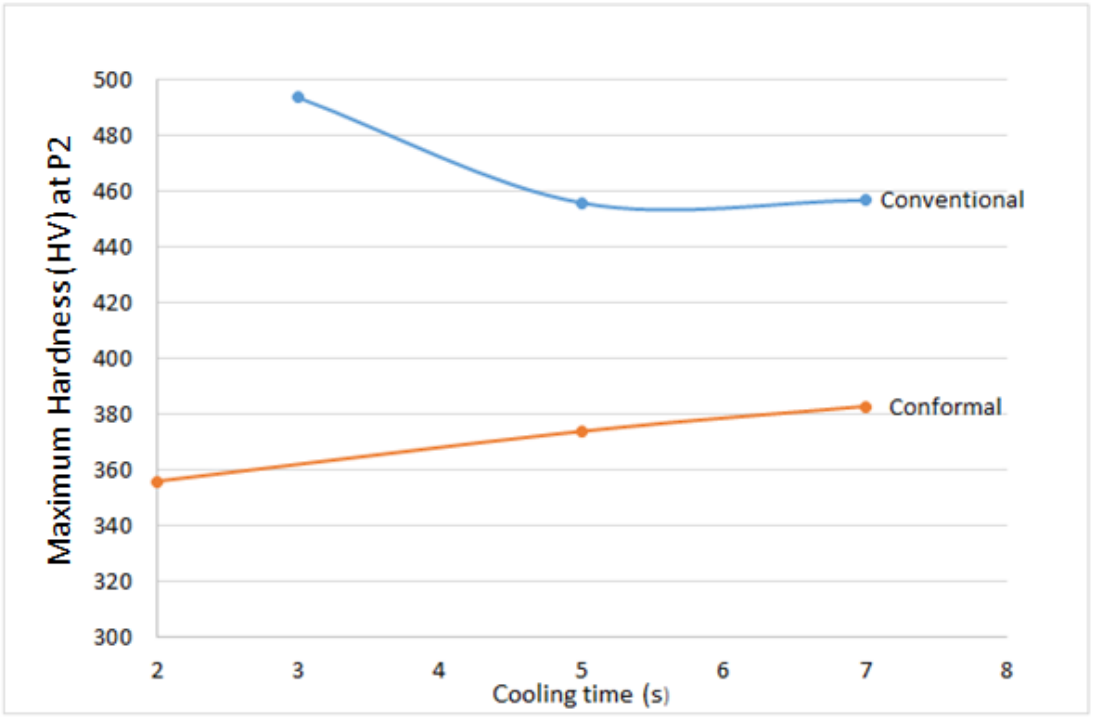


(b)

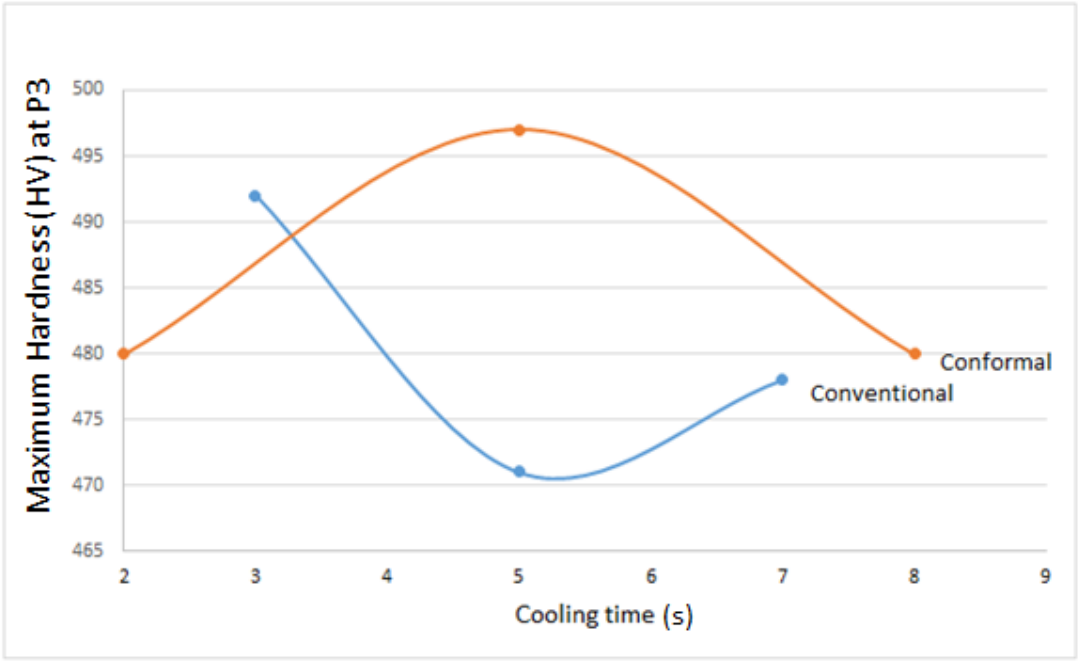


(c)

Figure 7-14: Maximum hardness for a) P1 b) P2 c) P3

The graph shows that P1 and P3 have relatively higher maximum hardness for the conformal cooling tool as compared to the conventional tool. At a cooling time of 5 s and above, the conformal tool causes very high maximum hardness values ranging from 480-511 HV while the conventional tool ranged from 465 to 480 HV. This shows confirms the higher cooling rate (9.6 °C/s) of the conformal cooling tool in those points. However, P2 had very low hardness values for the conformal tool when

compared to the conventional tool. Further investigations on the tool shows that there was inadequate contact between the blank and punch at P2 and P5 which was due to geometric inaccuracy of the conformal cooling tool. This caused an unwanted offset gab (0.5 mm) between the blank at point P2 and punch as shown in Figure 7-15. As a result there was not enough cooling at those points. However, a high hardness is expected when the tool geometry is optimized causing adequate contact.

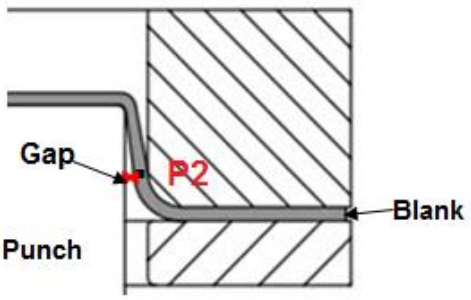


Figure 7-15: Offset at P2

A similar problem was experienced on initial experiments done on the conventional tool before its geometry was further optimized (Pierschel *et al.*, 2015). It was not possible to optimize the geometry of the conformal cooling tool because of resource constraints. Since the geometry of the conventional tool was optimised, P1 and P6 are treated as identical since they are on the same position. The same principle was also applied to P3 and P8. Accordingly, points P1 and P3 on the conventional tool are compared to P6 and P8 on the conformal cooling tool respectively. This is shown in Figure 7-16.

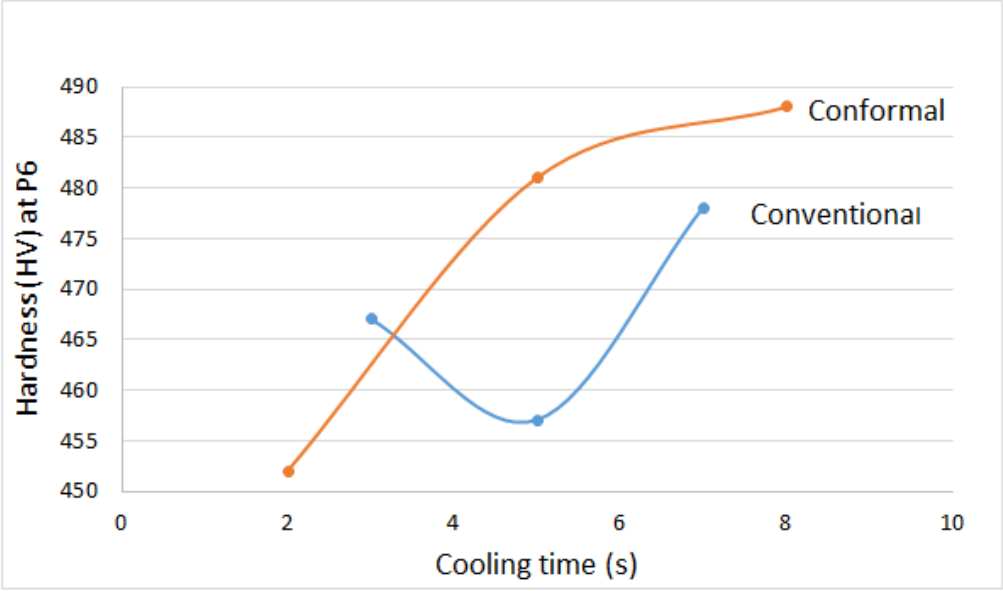


**(a)**

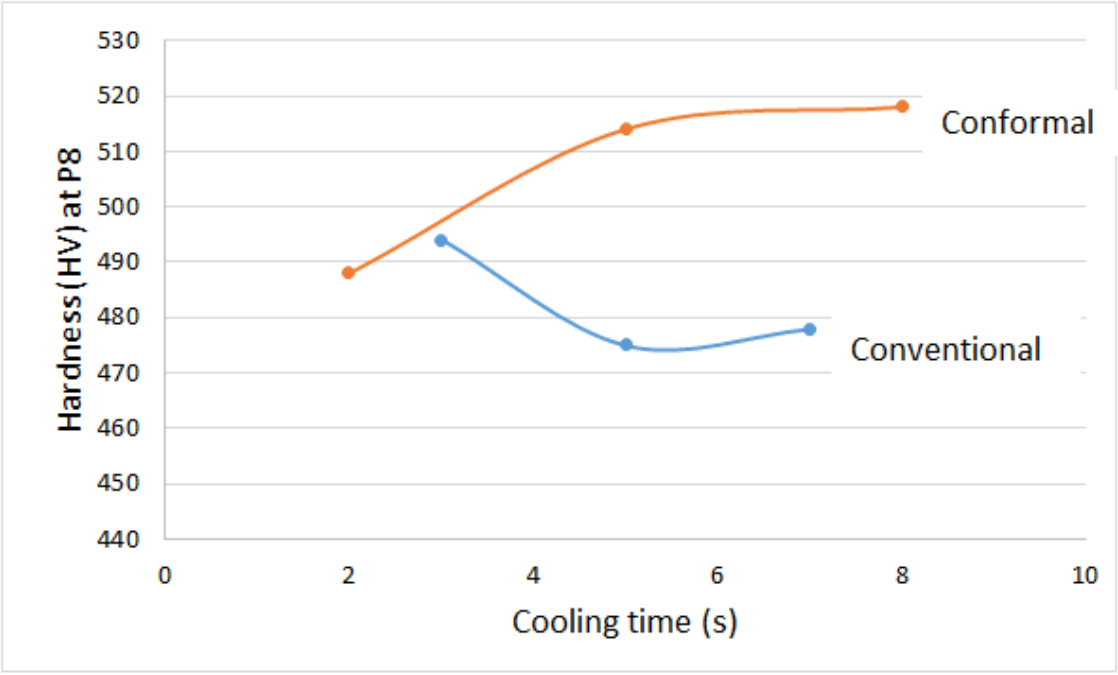


**(b)**

Figure 7-16: Maximum hardness for a) P6 b) P8

The graphs in Figure 7-16 shows that the conformal cooling tool results in higher maximum hardness values when compared to the conventional tool. In all cases the hardness values for the conventional tool did not reach 500 HV. As for the conformal cooling tool the hardness values exceeded 500HV after a cooling time of 5 s at points P1 and P8. The high hardness values indicate a higher cooling rate of the conformal cooling tool as compared to the conventional tool. As seen in Figure 7-14 and Figure 7-16, in the case of conformal cooling tool, there is an increase in hardness with respect to cooling time for points P3, P6 and P8 especially in the period from 2s to 5s.

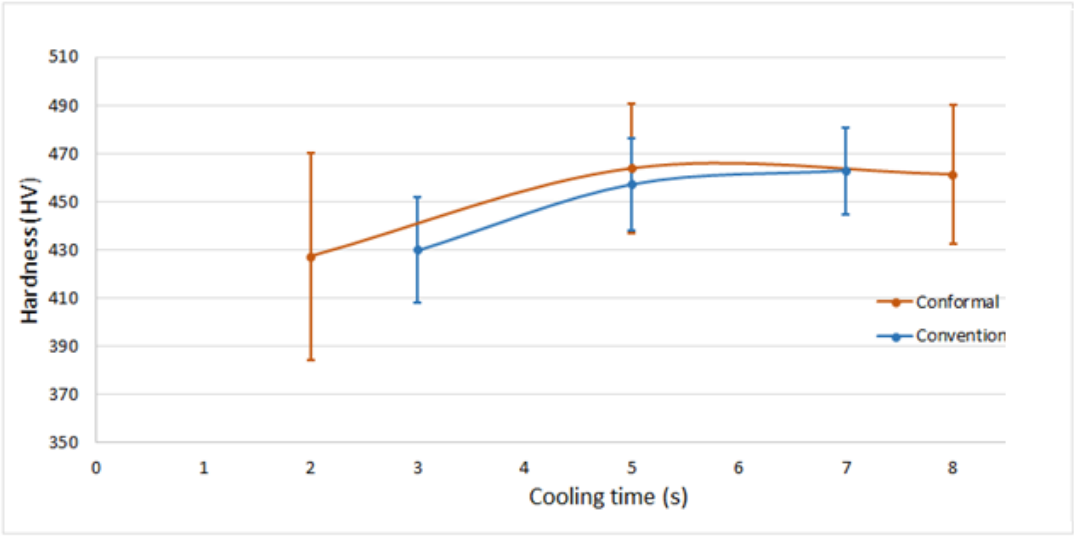


Figure 7-17: Average hardness at all contact points

This is different from the conventional tool which does not show effect on the cooling time at those points. Figure 7-17 shows the variation of the overall average hardness with time. As shown in Figure 7-17, the hardness caused by the conformal cooling tool is higher when compared to the conventional tool. This further confirms the higher cooling rate of the conformal cooling tool.

### 7.4.2. Hardness deviation

Figure 7-18 to Figure 7-20 shows the hardness graphs at points P1 to P8 when the blank was held in the closed tool at different cooling times (2-10 s) and coolant flow rates (11, 15 and 19 *l*/min) for the conformal cooling tool. At a cooling time of 2 s, the hardness at most of the points (P1, P3, P6 and P8) are generally around 400 HV and above at a forming speed of 200 mm/s. The hardness at P2 was generally low (257-394 HV) in all cases. As mentioned earlier, this was attributed to the geometric inaccuracy of the tool causing inadequate contact at this point. The same challenge was experienced at P5. However, further increase in the cooling time tends to override this challenge.

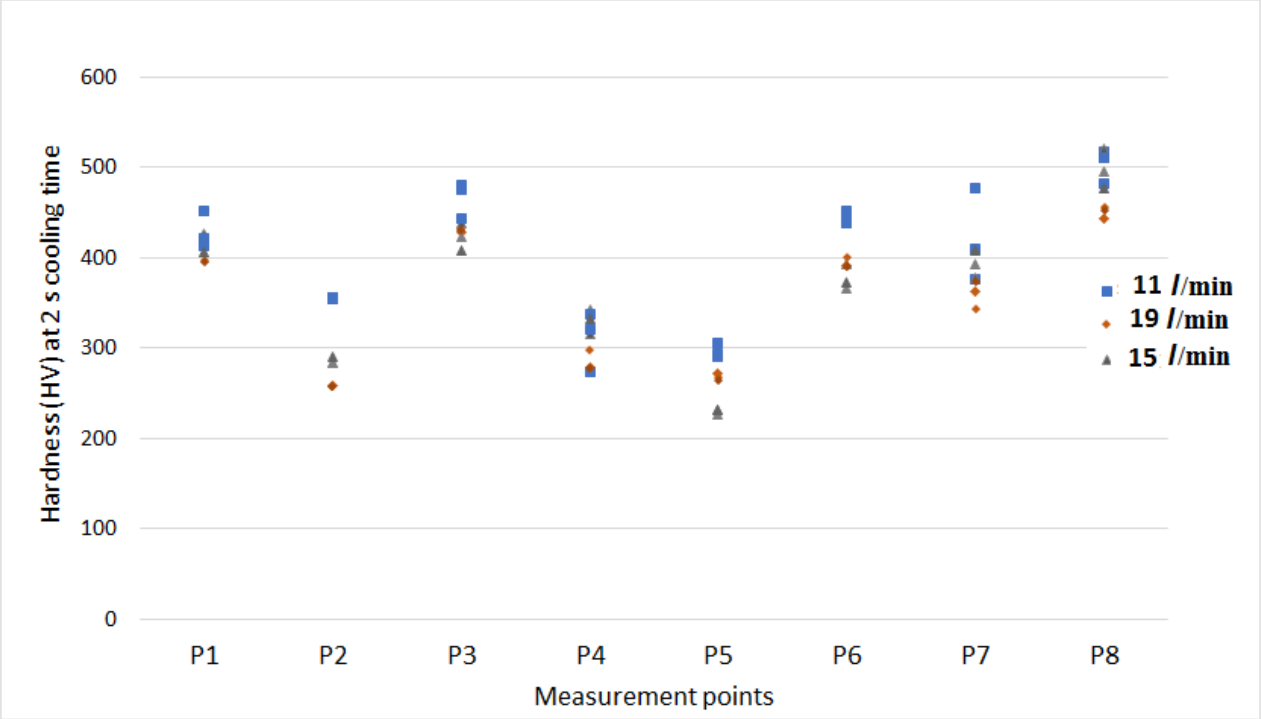


Figure 7-18: Hardness values for conformal cooling tool at 2 s cooling time of the blanks

Generally, as the cooling time of the blank increased from 2 to 5 s, there was a reduction in the difference in average hardness at different points as shown in Figure 7-18 and Figure 7-19. However, there was not much difference when the cooling time was increased from 5 to 8 seconds as shown in Figure 7-19 and Figure 7-20.

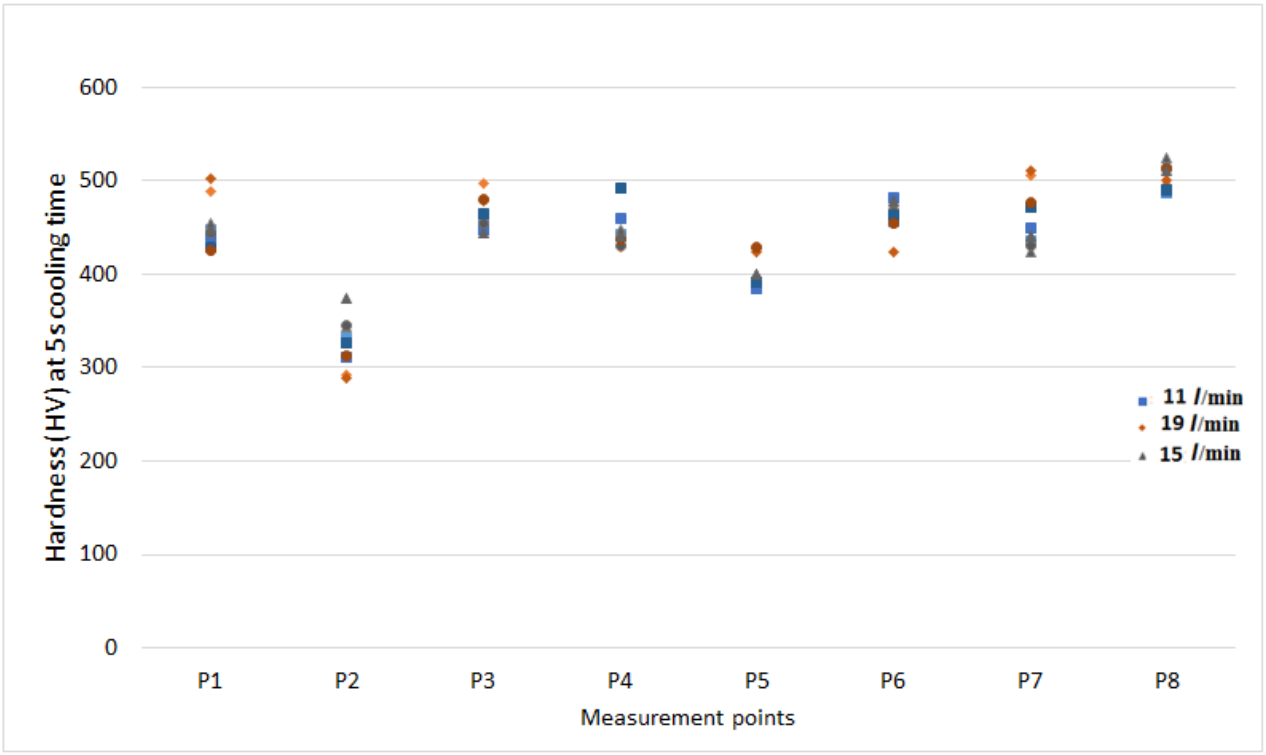


Figure 7-19: Hardness values for conformal cooling tool at 5 s cooling time

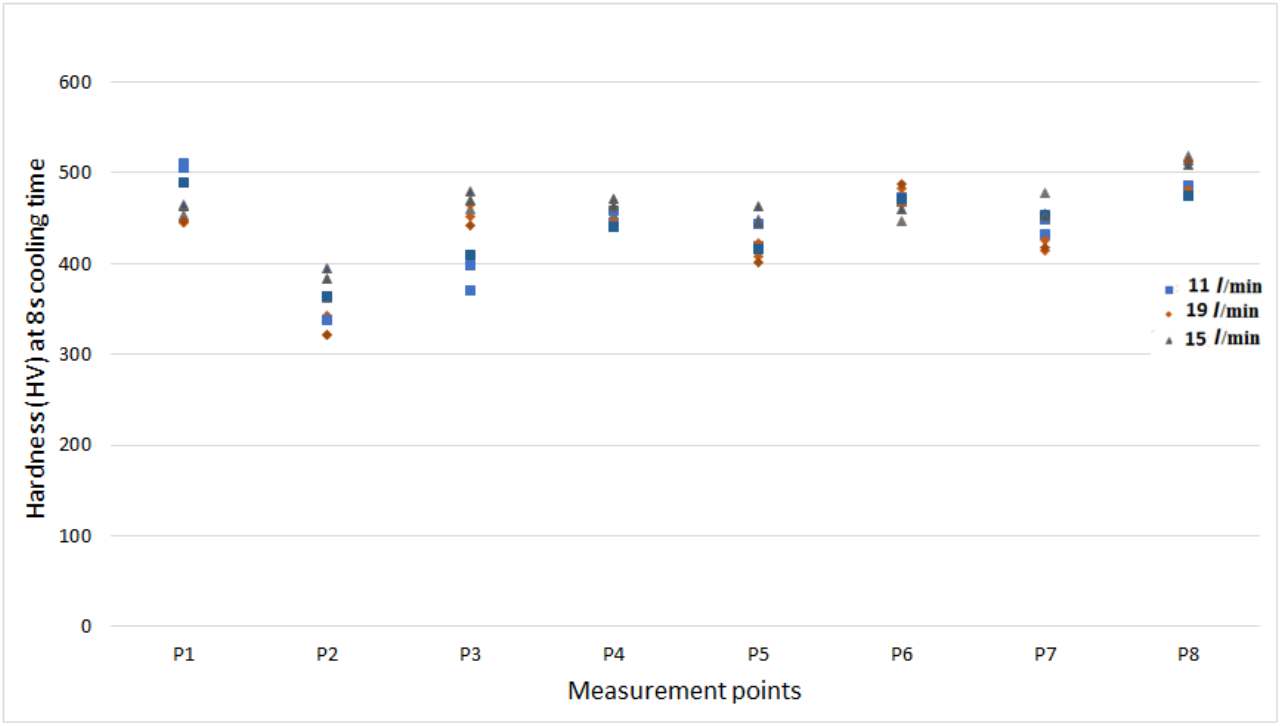


Figure 7-20: Hardness values for conformal cooling tool at 8 s cooling time

### 7.4.3. Effect of coolant flow rate on hardness for conformal cooling tool

Table 7.1 shows the summarry for the satistical results of the conformal cooling tool.

Table 7.1: Statistical summary for conformal cooling tool results

| Effect | Repeated Measures Analysis of Variance (Result analysis2) Sigma-restricted parameterization Effective hypothesis decomposition | | | | |
|---|---|---|---|---|---|
| | SS | Degr. of Freedom | MS | F | p |
| Intercept | 30909964 | 1 | 30909964 | 10682.46 | 0.000000 |
| Cooling time (s) | 40847 | 2 | 20424 | 7.06 | 0.002277 |
| Coolant flow rate (m/s) | 3138 | 2 | 1569 | 0.54 | 0.585451 |
| Cooling time (s)*Coolant flow rate (m/s) | 18363 | 4 | 4591 | 1.59 | 0.195629 |
| Error | 121528 | 42 | 2894 | | |

As seen in the results, the p-value for the coolant velocity is higher than 0.05. Accordingly, it follows that the null hypothesis that coolant flow rate does not have an effect on hardness is not rejected. Normally, it is expected that higher coolant flow rate causes increased heat transfer resulting in higher hardness. However in this case the coolant flow rate does not have significant effect on the resultant hardness of the part. This could be as a result of the geometric inaccuracy of the tool which caused inadequate contact during the cooling process. Thus, the tool was not effectively cooling the blanks as expected. Further results on the effect of coolant flow rate are shown in Figure 7-21.

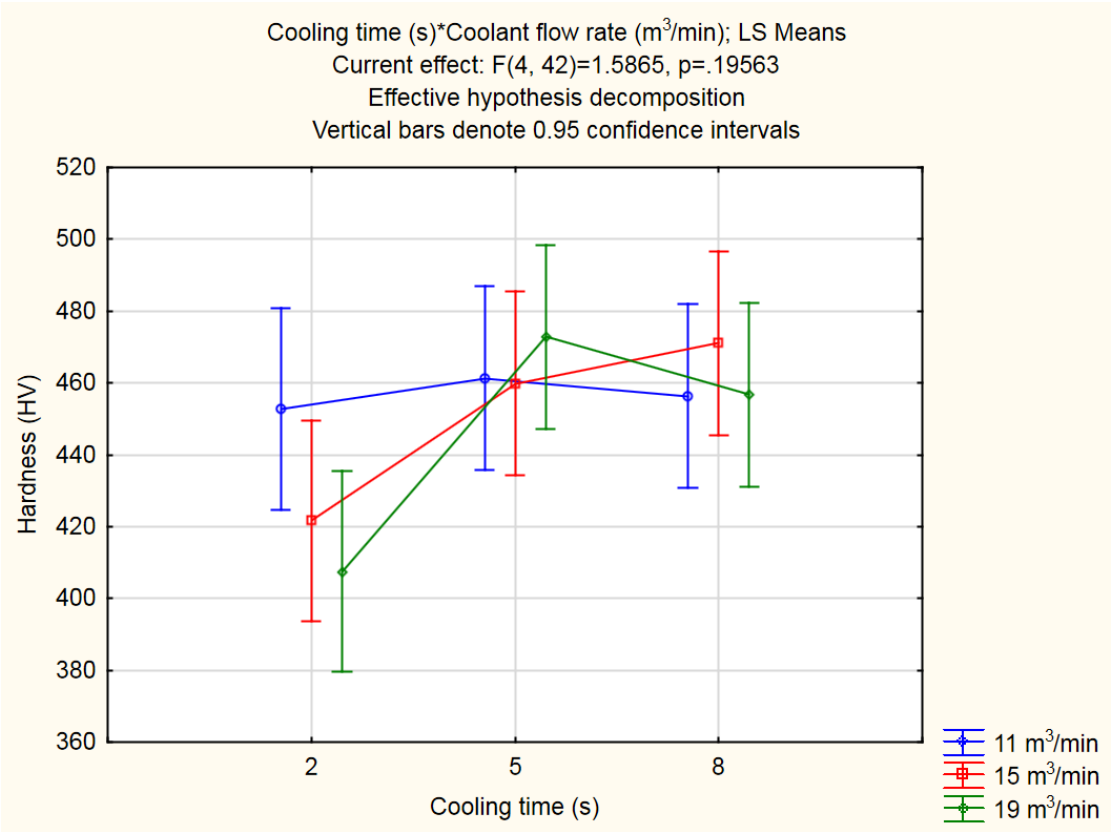


Figure 7-21: Effect of flow rate on hardness

Figure 7-21 confirms that the hardness increases with cooling time, however, it does not have significant impact on the flow coolant flow rate.

### 7.4.4. Preliminary conclusion on the effect of blank hardness on cooling system

The following preliminary conclusions can be drawn on the effect of cooling system layout on hardness.

- The conformal cooling tool caused higher maximum hardness values as compared to the conventional tool. This is explained by the average hardness for the conformable tool at cooling times of 5 and 8 s which were all above 450 HV at contact points (P1, P3, P6, P7 and P8). Also, some of the hardness values at P1 and P8 were above 500 HV. This indicates that the conformal cooling has a higher cooling rate as compared to the conventional tool.
- The hardness consistency of the conformal cooling increased with cooling time from 2 to 5 s. However, there was little impact when the cooling time increased to 8 seconds. Thus, it can be concluded that a cooling time of 5 s is enough for the conformable tool. There was a lesser difference on the average hardness caused by the conformable tool at P1, P3, P6 and P7 at 5 seconds and above. However, P8 had much higher hardness values for the conformable tool.

## 7.5 Comparison of Simulation Results and Experimental Results

Figure 7-22 and Figure 7-23 shows the comparison for the simulation and experimental results.

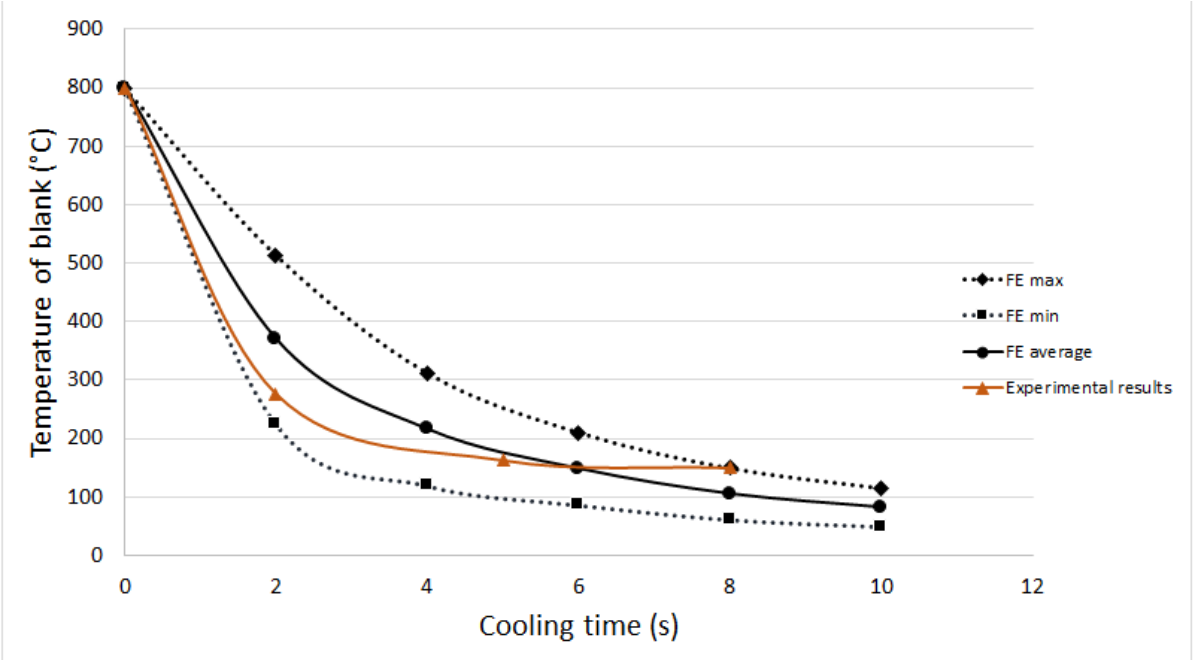


Figure 7-22: Experimental and simulation results for temperature (Conformal)

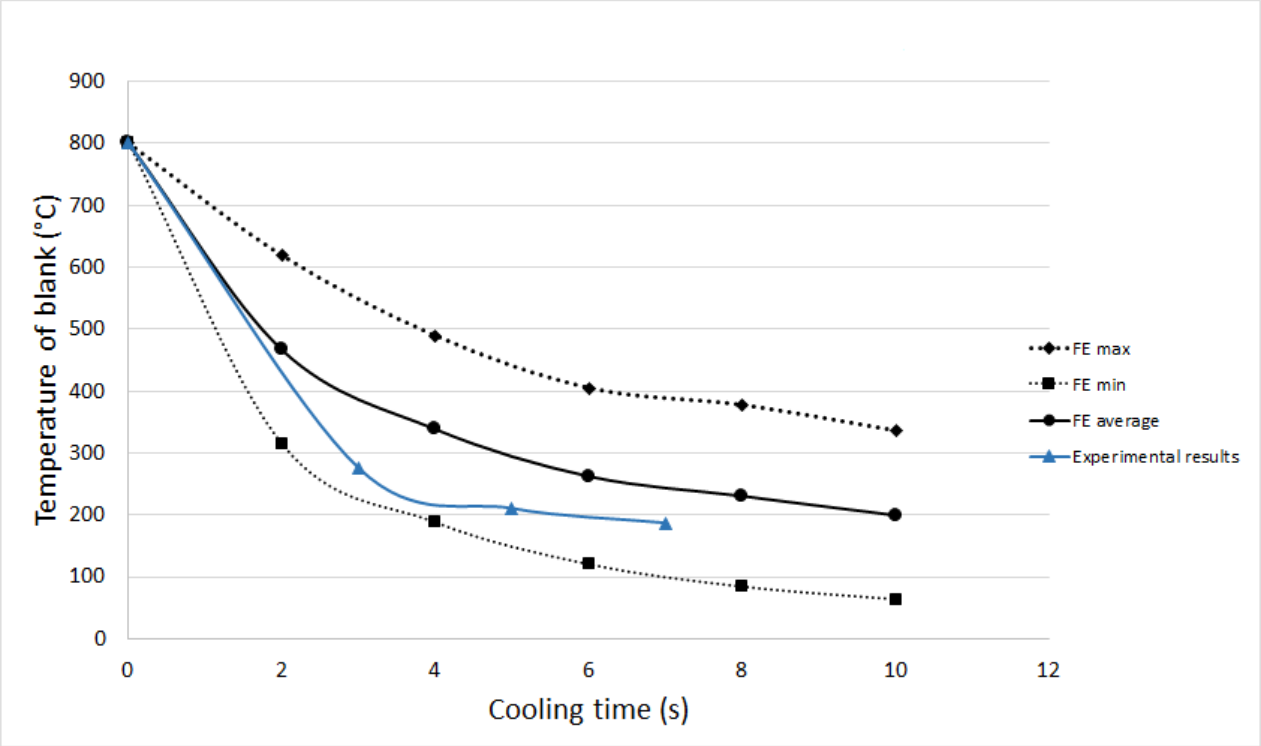


Figure 7-23: Experimental and simulation results for temperature (Conventional)

The graphs show a similar trend in the structure of the cooling curves of the blanks. For the conformal cooling tool, the change in temperature of the blank increases more rapidly with the cooling time than as in the case of the conventional tool.

The difference in the change of cooling rates can be explained by the structure of the cooling system of the conformal cooling tool which affords a large surface area for the extraction of heat from key positions or sections of the blank being formed. Furthermore, the design of the conventional cooling system causes the coolant to gain heat as it moves a greater distance along the cooling channels, making it inefficient in heat extraction form the blank. The cooling curve of the conventional tool is lower than the simulated average temperatures. A possible reason could be that the temperature measurements were done only on a single section of the blank during the experiments and this might not have given a true reflection of the whole temperature profile. Figure 7-24 and Figure 7-25 show the comparison for the simulation and experimental hardness results for the conformal cooling tool and the conventional, respectively.

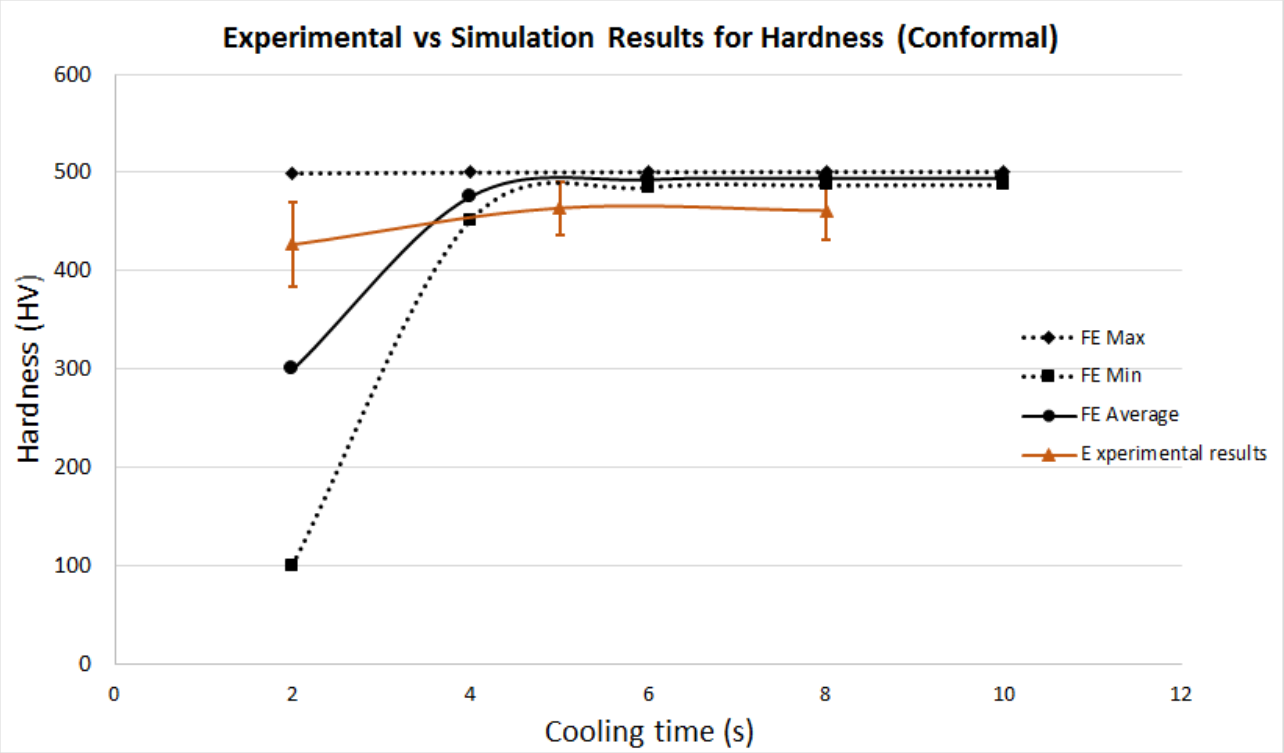


Figure 7-24: Experimental and simulation results for hardness (Conformal)

The graph in Figure 7-24 confirms that the hardness of the conformal cooling tool does not make a significant increase after a cooling time of 5 s. This further confirms that 5 s cooling time is enough for the conformal tool. The experimental hardness values caused by the conformal cooling tool are higher than the values for the average hardness from the simulation at lower cooling time. However, the hardness values fall within the simulation range. Generally, the experimental hardness results are lower than the simulation results. This could have been caused by the insufficient contact of the blank causing other points not to attain lower hardness thus, reducing the overall average hardness.

According to the graph in Figure 7-25, the actual hardness curve of the conventional cooling tool lies within the maximum and minimum range for the simulation values. However, the values are much higher than the simulated average hardness. Nevertheless, the results are considered valid since they were extracted from a hardness map. A reason for this could be the effect of measurement on a single portion during the experimentation. This does not give a true picture of the whole blank.

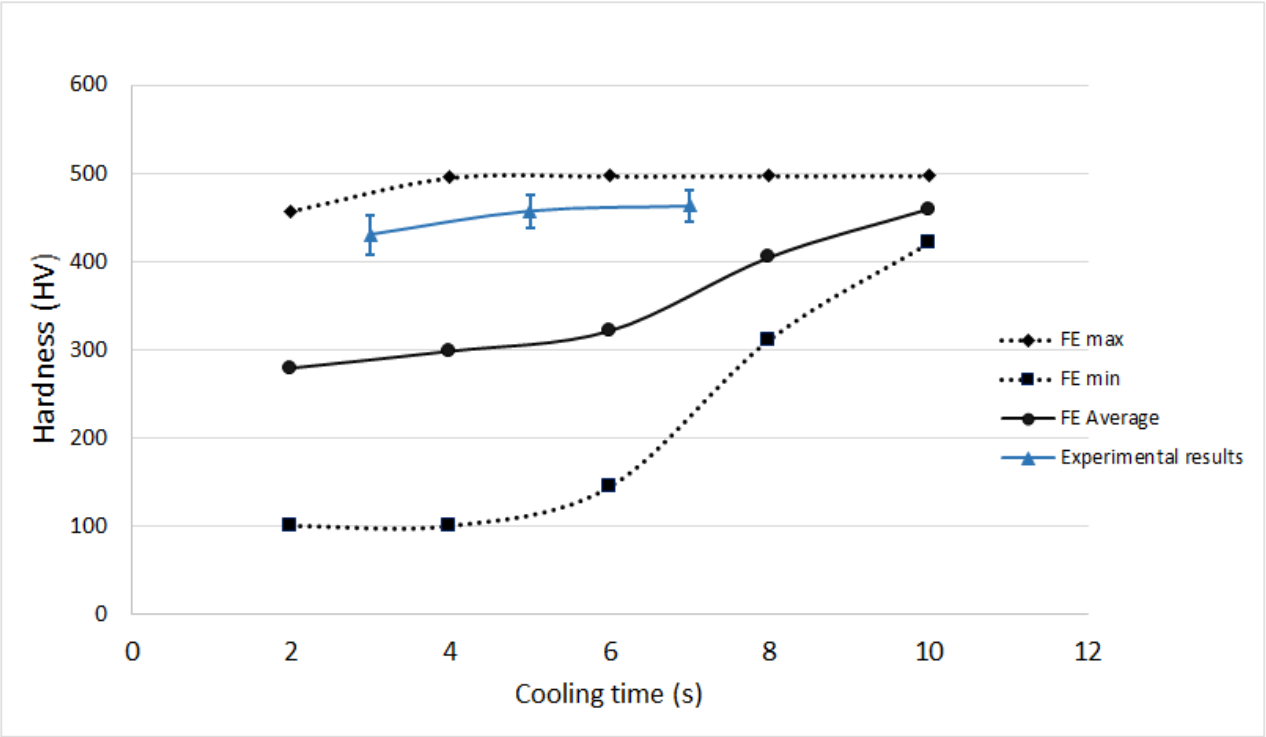


Figure 7-25: Experimental and simulation results for hardness (Conventional)

### 7.5.1. Preliminary results

The following preliminary conclusions can be drawn after comparing the simulation and experimental results.

- The experimental results generally fall within simulated maximum and minimum range of values. Since the simulated values were derived from temperature and hardness maps, the experimental results are considered valid.
- The deviation of the experimental from the simulation hardness values for the conventional tool results could be due to the fewer experimental measurements which might not give an overall presentation of the whole hardness profile. Nevertheless, the results are considered valid since they fall within the simulated range.

## 7.6 Summary

Based on the experiments conducted to evaluate the performance of the manufactured tool. The following conclusions can be made

- The conformal cooling tool has a higher cooling rate as compared to the conventional tool. This is evidenced by the increase in cooling rate by 9.6 °C/s. Also, after stamping 20 blanks, the maximum temperature recorded by the sensors integrated into the conventional and conformal cooling tools were 70 and 45 °C, respectively. Accordingly, there was 36 % reduction in the final temperature of the conformal cooling punch during stamping as compared to the conventional tool. There were no cracks observed on the tool after performing the stamping trials. Hence, the tool could withstand the press force acting on it.
- The conformable tool caused higher maximum hardness values as compared to the conventional tool at contact points. This indicates a higher cooling intensity of the conformal cooling tool.
- A cooling time of 5 s was enough for the conformal cooling tool to attain the required hardness properties. Thus the cooling time can be reduced from 7 to 5 s using the conventional tool. Thus the conformal cooling tool has potential to reduce the cooling time by 29 % as compared to the conventional tool. More consistent and higher hardness values are expected for the conformal tool when the geometry of the punch is optimised to ensure an even contact at all points. This is because the conventional tool caused much lesser hardness before it was optimised (Pierschel *et al.*, 2015). Thus, optimising geometry of the conformable tool would also lead to higher and more uniform hardness properties.

# CHAPTER 8 : CONCLUSION AND RECOMMENDATIONS

## 8.1 Introduction

The goal of this study was to apply AM to improve thermal management of hot stamping tools. To achieve this goal, the first objective was to identify the parameters for effective thermal management of hot stamping tools. The steps taken in arriving at this objective include developing a method for identifying cooling system structural parameters as shown in Chapter 3, section 3.2. Furthermore, a decision matrix for evaluating possible cooling system designs is shown in section 3.5.1. Additionally, a cost effective manufacturing procedure for producing the tool was given in Chapter 5. The second objective was to develop a model for predicting minimum cycle time in hot stamping. The model was developed in section 3.4 using existing knowledge from previous literature, heat transfer and mechanics principles. Equation 3.5.2 gives a mathematical expression of the total cycle time in a typical hot stamping process. The third and fourth objectives were to design and manufacture a typical hot stamping tool with a conformal cooling system. All the stages in the design of the conformal cooling tool are given in the fifth chapter. An account of the manufacturing process chain is explained in the sixth chapter. The final objective was to investigate the impact of the conformal cooling tool on cycle time and quality. In the sixth chapter, a detailed design of experiments for investigating the impact of the tool is given. The research question was focused on parameters viable for the manufacture of hot stamping tools with conformal cooling channels. Accordingly, it can be concluded that the research question was answered because the design and manufacturing parameters were determined in the course of fulfilling the above stated objectives. Table 8-1 gives a summary of the research gaps addressed in the study on the application of conformal cooling channels in hot stamping tools in comparison with the main authors on this subject in literature. In the section below, a concluding summary for each of the steps in the study is given.

## 8.2 Conformal Cooling System Parameters for Hot Stamping Tools

When the developed method was applied in the design and manufacture of the benchmark conformal cooling tool, it caused an increase in the cooling rate of the blank by 9.6 °C/s. The tests done showed that the targeted final blank temperature (≤ 200 °C) was reached after a cooling time of 5 s with the conformal cooling tool. This was faster than the conventional tool which reached the targeted blank temperature in 7s (≤ 200 °C). In addition, there was a reduction in the punch temperature by 36 %. This reduction in the punch temperature translates to reduced thermal stresses within the tool which gives a greater possibility of extending tool service life. Furthermore, the conformal cooling tool led

to improved quality through a higher (400-500 HV) and lesser difference in the average hardness at various points.

Table 8-1: Current state of technology

| **Issue** | **Cortina *et al.*(2018)** | **Mueller *et al.* (2014)** | **Gebauer *et al.*(2015)** | **Muvunzi (2019)** |
|---|---|---|---|---|
| Use of method of obtaining structural conformal cooling parameters | No | No | No | Yes |
| Larger size of tool (L,W,H≥ 250 mm ) | No | - | No | Yes |
| Presentation of procedures used in developing the conformal cooling system | Not given | Not given | Not given | Given and explained |
| Execution of both FE analysis and physical hot stamping experiments | Only FE analysis and no physical hot stamping experiments | Both FE analysis and physical hot stamping experiments (Limited information on the simulation) | Both FE analysis and physical hot stamping experiments (Limited information on the simulation) | Both FE analysis and physical hot stamping experiments (Clarity on the simulation models used) |

The available literature shows that the proposed models for cooling system design in hot stamping were mainly developed for straight drilled channels. To date, there is no literature on the design parameters of AM based conformal cooling systems for hot stamping tools.

## 8.3 Designing and Manufacture of the Conformal Cooling Tool

An innovative cooling channel layout for the benchmark part was designed using the developed method. As part of the design process, alternative layouts were evaluated using the decision matrix in 3.5.1. Accordingly, the most suitable design was further improved and evaluated using the decision matrix. Hybrid manufacturing was used to produce the part. This involved machining the base body of the tool inserts before building the top part additively. The few studies in literature on AM based cooling systems were limited to smaller tool inserts (≤ 250 mm). In the study done by Cortina *et al.* (2018), the demonstrator insert had a length and height of 100 and 74 mm respectively. Also, Gebauer *et al.* (2016) worked on a conformal cooling tool of a gear pan component with a diameter and depth of 123 and 30 mm respectively. Conversely, the benchmark tool in the present study had a length, width and height of 745, 174 and 79 mm respectively.

## 8.4 Evaluating the Impact of the Conformal Cooling Tool.

The performance of the manufactured tool was experimentally evaluated under conditions similar to those in industry. According to the results, the quality of the parts formed using the conformal cooling tool was enhanced in terms of higher and more consistent average hardness (450-500 HV). The hardness values (450-500 HV) of the parts formed by the conformal cooling tool at a cooling time of five seconds are similar to the conventional tool at 7 s. Thus a cooling time reduction of 2 s is possible using the conformal cooling tool. Thus the conformal cooling tool has the potential to reduce the cooling time by 28.6 %.

## 8.5 Original Contributions

The original contributions in the study can be explained under the following six categories:

- ***Method for determining conformal cooling system parameters for hot stamping tools***
  A step by step method for determining conformal cooling system parameters for hot stamping tools was developed (refer to Figure 3.6). The method was formulated considering the technical limitations of the SLM process and mechanical loads in the hot stamping processes. The goal was to design a hot stamping tool with an effective cooling system performance which does not compromise the mechanical strength of the tools. The method can be useful in the design and manufacture of other hot forming tools with conformal cooling channels.

- ***Model for predicting minimum cycle time in hot stamping***

  A model for predicting minimum cycle time in a typical hot stamping process was developed in Equation 3.53. The model is a useful benchmark tool which enables designers to predict the minimum cooling time. In this study it was used to justify the need for further reducing cycle time by improving the design of the conventional tool.

- ***A hot sheet metal forming tool (punch)with an innovative conformal cooling system layout***

  An innovative hot stamping tool with a conformal cooling system was designed and manufactured. All the cooling channels were positioned at 5 mm from the tool surface to ensure even cooling. Additionally, the conformal cooling tool had four inlet and four outlet points while the conventional tool had two inlet and two outlet points. This was done to increase the circulation of coolant in the conformal cooling tool. Accordingly, the results showed the potential to reduce cooling time by 28.6 % using the conformal cooling tool.

- ***A large-sized tool (punch) produced using hybrid manufacturing***

  The tool produced is unique, with a length and width of 745 mm and 174 mm, respectively. In literature, this is the first kind of large tool which was additively manufactured for hot stamping tools. The large size was achieved by segmentation of one of the inserts at the centre. Thus four tool segments were built additively to develop the complete conformal cooling tool.

- ***A simulation model for evaluating the performance of a conformal cooling tool.***

  A unique simulation model for evaluating the cooling system performance of a hot stamping tool was developed in section 5.8. The model was used to predict the resultant quality characteristics of the parts formed using the conformal cooling tool. The experimental hardness and temperature results fall within the simulated maps.

- ***A decision matrix for evaluating hot stamping cooling system layouts***

  The matrix developed in section 5.5.1 is a useful decision making tool for identifying the most suitable cooling system layout during the design stage. The goal of using the matrix is to identify the most suitable cooling system design from a quality and manufacturability perspective.

## 8.6 Recommendations

In line with the study, the following recommendations were made:

(a) The geometry of the punch and die should be optimised to ensure uniform contact during hot stamping.

(b) The cooling channels must be cleaned regularly using diluted mineral acids (muriatic, sulphuric or phosphoric acids) to prevent fouling.

(c) Further tests on the durability of the conformal cooling tool should be conducted.

## 8.7 Future Work

Further research should be conducted in the following subject areas:

(a) Further studies on modelling the effect of surface roughness in the conformal cooling channels.
(b) Further studies on designing the tool for fatigue to cater for high production runs.
(c) Application of AM in the manufacture of tool inserts with conformal cooling and heating systems to achieve tailored properties on a single part. This is because the recent focus in hot stamping is on the production of parts with different strength requirements. Thus the freedom of design offered by AM technology could allow designers to devise tool inserts with both heating and cooling systems for a single part.
(d) Use of AM to manufacture tools with integrated sensor systems for intelligent forming tools. The sensor signal could include stamping pressure, friction or temperature. This would allow a self-controlling forming process for improved quality and tool service life.
(e) Studies on the microstructure of the hybrid tools and ways of improving contact between the machined and built section. This would ensure a more durable tool with a longer service life.
(f) Manufacture of hot stamping tools with interchangeable modules and with separate cooling system designs for improved flexibility. This would help to lower down time and facilitate easier changeover in hot stamping.

## 8.8 Research Output

This research study has led to the publication of articles in accredited journals and in recognised conference proceedings. So far, three journal papers have been published, another has been submitted and a further journal paper is still being written. Table 8-2 and Table 8-3 show the journal publications and conference proceedings.

Table 8-2: Table of journal publications

| | **Journal Publications** | **Chapter with contents of paper** |
|---|---|---|
| 1 | Muvunzi, R., Dimitrov, D.M., Matope, S, Harms, T.M Sterzing, A and Nagel M, 2019. Application of Conformal Cooling To Improve Cooling System Performance Of Hot Stamping Tools *Submitted to the South African Journal of Industrial Engineering (SAJIE).* | 5 |
| 2 | Muvunzi, R., Dimitrov, D.M., Matope, S. and Harms, T.M., 2018. Development of a model for predicting cycle time in hot stamping. *Procedia Manufacturing*, *21*, pp.84-91. | 3 |
| 3 | Muvunzi, R., Dimitrov, D.M., Matope, S. and Harms, T.M., 2017. Evaluation of Models for Cooling System Design in Hot Stamping Tools. *Procedia Manufacturing*, *7*, pp.701-707. | 2 |
| 4 | Muvunzi, R., Dimitrov, D.M., Matope, S. and Harms, T.M., 2017. Heat transfer in a hot stamping process: A review. *R&D Journal*, *33*, pp.75-84. | 2 and 3 |

Table 8-3: Table of Conference proceedings

| | **Conference proceedings** | **Chapter with contents of paper** |
|---|---|---|
| 1 | D. Hagedorn-Hansen, R. Muvunzi, S. Matope, X. Madyibi, C.B. Swart & M Nagel, Industry Case Study: Process Chain for Manufacturing of Large Hybrid Tools With Conformal Cooling Channels *Proceedings for the International Rapid Product Development Association (RAPDASA) Conference* 6-8 November 2019, Bloemfontein, South Africa. | 6 |
| 2 | Muvunzi, R., Dimitrov, D., Matope, S. and Mugwagwa, L., 2018, April. Application Of Surface Modification Technologies to Improve Performance of Hot Sheet Metal Forming Tools: A Review. *In Proceedings of the EAI International Conference on Research, Innovation and Development for Africa* (pp. 65-74). | 2 |
| 3 | L. Mugwagwa, D. Dimitrov, S. Matope and R. Muvunz**i** , Residual Stresses and Distortions in Selective Laser Melting – A Review, *Proceedings for the International Rapid Product Development Association (RAPDASA) Conference* 2-4 November 2016, Vaal, South Africa. | 2 |
| 4 | Muvunzi R, Dimitrov D, Matope S, Improved Cooling System of Hot Stamping Tools Through Additive Manufacturing *Proceedings for the International Rapid Product Development Association (RAPDASA) Conference* 2-4 November 2016, Vaal, South Africa | 5 |
| 6 | Muvunzi R, Dimitrov D, Matope S, Kufazvinei C, (2015) Application Of Additive Manufacturing for Performance Improvement of Tooling In Moulding and Sheet Metal Forming Processes: A Review - *Proceedings for the International Rapid Product Development Association (RAPDASA) Conference*, Pretoria 4-6 November 2015. | 2 |

# REFERENCES

Abdulhay, B., Bourouga, B. and Dessain, C., 2011. 'Experimental and theoretical study of thermal aspects of the hot stamping process', *Applied Thermal Engineering. Elsevier Ltd*, 31(5), pp. 674–685. doi: 10.1016/j.applthermaleng.2010.11.010.

Altan, T. and Tekkaya, A.E. eds., 2012. *Sheet Metal Forming: Processes and Applications*. ASM international.

Anderson, D.M., 2014. *Design For Manufacturability: How to Use Concurrent Engineering to Rapidly Develop Low-Cost, High-Quality Products for Lean Production*. Productivity Press.

Antony, J., 2014. *Design of Experiments for Engineers and Scientists*. Elsevier.

Arpaci, S., Selamet, A. and Kao, S., 2000. *Introduction to Heat Transfer*, Prentice Hall. Upper Saddle River.

Au, K.M. and Yu, K.M., 2013. Conformal cooling channel design and CAE simulation for rapid blow mould. *The International Journal of Advanced Manufacturing Technology*, *66*(1-4), pp.311-324.

Autodesk, 2019. POWERMILL, Available at: https://www.autodesk.com/products/powermill/overview (*Accessed: 1 January 2018).*

Autodesk, 2019 'PowerSHAPE modelling software" [Online]. Available https://www.autodesk.com/products/powershape/features *(Accessed: 01-October-2019).*

ANSYS, 2019 "ANSYS Software." [Online]. Available: https://www.ansys.com *(Accessed: 01-June-2019).*

ANSYS, 2019 "FLUENT Software." [Online]. Available: https://www.ansys.com/products/fluids/ansys-fluent *(Accessed: 01-June-2019).*

Bai, Q., Lin, J., Zhan, L., Dean, T.A., Balint, D.S. and Zhang, Z., 2012. An efficient closed-form method for determining interfacial heat transfer coefficient in metal forming. *International Journal of Machine Tools and Manufacture*, 56, pp.102-110.

Bansal, R. K, 2010. *A Textbook of Strength of Materials*. Fourth Edition. Laxmi Publications, New Dehli.

Bariani, P.F., Bruschi, S., Ghiotti, A. and Turetta, A., 2008. Testing formability in the hot stamping of HSS. *CIRP Annals*, *57*(1), pp.265-268.

Beal, V.E., Erasenthiran, P., Ahrens, C.H. and Dickens, P., 2007. Evaluating the use of functionally graded materials inserts produced by selective laser melting on the injection moulding of plastics parts. *Proceedings of the Institution of Mechanical Engineers, Part B: Journal of Engineering Manufacture*, 221(6), pp.945-954.

Becker, T.H. and Dimitrov, D., 2016. The achievable mechanical properties of SLM produced Maraging Steel 300 components. *Rapid Prototyping Journal*.

Bergman, T.L., Incropera, F.P., DeWitt, D.P. and Lavine, A.S., 2011. *Fundamentals of Heat and Mass Transfer*. John Wiley & Sons.

Bhattacharya, S., Dinda, G.P., Dasgupta, A.K. and Mazumder, J., 2011. Microstructural evolution of AISI 4340 steel during direct metal deposition process. *Materials Science and Engineering: A*, 528(6), pp.2309-2318.

Biamino, S., Penna, A., Ackelid, U., Sabbadini, S., Tassa, O., Fino, P., Pavese, M., Gennaro, P. and Badini, C., 2011. Electron beam melting of Ti–48Al–2Cr–2Nb alloy: Microstructure and mechanical properties investigation. *Intermetallics,* 19(6), pp.776-781.

Billur, E., 2013. *Fundamentals and applications of hot stamping technology for producing crash-relevant automotive parts* (Doctoral dissertation, The Ohio State University). Available at: https://etd.ohiolink.edu/ (Accessed: 18 June 2018).

Boher, C., Le Roux, S., Penazzi, L. and Dessain, C., 2012. Experimental investigation of the tribological behavior and wear mechanisms of tool steel grades in hot stamping of a high-strength boron steel. *Wear*, 294, pp.286-295.

Bohler-Uddeholm, 2016. Hot Work - Hot Stamping. [Online] Available at: http://www.bucorp.com/hot-stamping.htm *(Accessed 5 August 2019).*

Borsetto, F., Ghiotti, A. and Bruschi, S. (2009) 'Investigation of the High Strength Steel Al-Si Coating during Hot Stamping Operations', *Key Engineering Materials*, 410–411, pp. 289–296. doi: 10.4028/www.scientific.net/KEM.410-411.289.

Bosetti, P., Bruschi, S., Stoehr, T., Lechler, J. and Merklein, M., 2010. Interlaboratory comparison for heat transfer coefficient identification in hot stamping of high strength steels. *International Journal of Material Forming*, 3(1), pp.817-820.

Brunelli, M, 2015. *Introduction to the Analytic Hierarchy Process, Learning from Failures*. Springer doi: 10.1016/B978-0-12-416727-8.00003-5.

Campanelli, S.L., Contuzzi, N., Angelastro, A. and Ludovico, A.D., 2010. Capabilities and performances of the selective laser melting process. In *New Trends in Technologies: Devices, Computer, Communication and Industrial Systems*. Intech Open.

Caron, E. J. F. R., Daun, K. J. and Wells, M. A, 2014. 'Experimental heat transfer coefficient measurements during hot forming die quenching of boron steel at high temperatures', *International Journal of Heat and Mass Transfer. Elsevier* Ltd, 71, pp. 396–404. doi: 10.1016/j.ijheatmasstransfer.2013.12.039.

Carson, E. and Cobelli, C., 2013. *Modelling Methodology for Physiology And Medicine*. Newnes.

Casalino, G., Campanelli, S.L., Contuzzi, N. and Ludovico, A.D., 2015. Experimental investigation and statistical optimisation of the selective laser melting process of a maraging steel. *Optics & Laser Technology*, 65, pp.151-158.

Cengel, A., Yunus, J. and Ghajar, A., 2015. *Heat and Mass Transfer, Fundamentals & Application,* Fifth Edition in SI Units, McGraw-Hill, 5th Edition. Available at: http://www.osti.gov/energycitations

Černašėjus, O., Škamat, J., Markovič, V., Višniakov, N. and Indrišiūnas, S., 2019. Surface Laser Processing of Additive Manufactured 1.2709 Steel Parts: Preliminary Study.*Advances in Materials Science and Engineering,* 2019.71.

Chang, Y., Tang, X., Zhao, K., Hu, P. and Wu, Y., 2016. Investigation of the factors influencing the interfacial heat transfer coefficient in hot stamping. *Journal of Materials Processing Technology*, 228, pp.25-33.

Cheah, C.M., Chua, C.K., Lee, C.W., Lim, S.T., Eu, K.H. and Lin, L.T., 2002. Rapid sheet metal manufacturing. Part 2: direct rapid tooling. *The International Journal of Advanced Manufacturing Technology*, 19(7), pp.510-515

Chen, J., Gong, P., Liu, Y., Zheng, X. and Ren, F., 2017. Optimization of hot stamping cooling system using segmented model. *The International Journal of Advanced Manufacturing Technology*, 93(1-4), pp.1357-1365.

Chen, L., Chen, W., Xu, F., Zhu, Y. and Zhu, Y., 2019. A pre-design method for drilled cooling pipes in hot stamping tool based on pipe parameter window. *The International Journal of Advanced Manufacturing Technology*, pp.1-10.

Choi, H.S., Kim, B.M., Kim, D.H. and Ko, D.C., 2014. Application of mechanical trimming to hot stamped 22MnB5 parts for energy saving. *International Journal of Precision Engineering and Manufacturing*, 15(6), pp.1087-1093.

Chuang, P.T., 2001. Combining the analytic hierarchy process and quality function deployment for a location decision from a requirement perspective. *The International Journal of Advanced Manufacturing Technology*, 18(11), pp.842-849.

Chun, Y., Jingjing, W. and Dapeng, L, 2015. 'Numerical Analysis of Hot Stamping Mold Cooling System Based on FLUENT', *Applied Mechanics and Materials*, 713–715(4), pp. 259–262. doi: 10.4028/www.scientific.net/amm.713-715.259.

Cortina Burón, M., Arrate, A., Iñaki, J., Calleja Ochoa, A., Ukar Arrien, E. and Alberdi Gurrutxaga, A., 2018. Case Study to Illustrate the Potential of Conformal Cooling Channels for Hot Stamping Dies Manufactured Using Hybrid Process of Laser Metal Deposition (LMD) and Milling. *Metals*, 8(2). doi: 10.3390/met8020102.

Cortina, M., Arrizubieta, J., Calleja, A., Ukar, E. and Alberdi, A., 2018. Case study to illustrate the potential of conformal cooling channels for hot stamping dies manufactured using hybrid process of Laser Metal Deposition (LMD) and milling. *Metals*, 8(2), p.102.

Coutelieris, F. A. and Kanavouras, A. (2018) Experimentation Methodology for Engineers. *London: Springer International Publishing*. doi: 10.1007/978-3-319-72191-0.

Cosmo Tech, 2019 'COSMO Simulation software" [Online]. Available https://cosmotech.com/platform/ *(Accessed: 03-May-2019).*

Croccolo, D., De Agostinis, M., Fini, S., Olmi, G., Robusto, F., Ćirić Kostić, S., Vranić, A. and Bogojević, N., 2018. Fatigue response of as-built DMLS maraging steel and effects of aging, machining, and peening treatments. *Metals*, *8*(7), p.505.

Homar, D. Kopac, S. D, 2012. 'Additive Manufacturing and High Speed Cutting Included In Hybrid Manufacturing', *Journal of Production Engineering*, 16(1), pp. 5–8.

Dadbakhsh, S., Hao, L. and Sewell, N., 2012. Effect of selective laser melting layout on the quality of stainless steel parts. *Rapid Prototyping Journal*, 18(3), pp.241-249.

Davis, J.R.., 2002. *Surface Hardening of Steels: Understanding the Basics*. ASM international.

Dieter, G. E., 2000. *Engineering Design: A Materials and Processing*. McGraw-Hill, Approa. Singapore:

Dimitrov, D. and Bester, A., 2005. 'New approaches in tooling design and manufacture for the packaging industry', in Virtual Modelling and Rapid Manufacturing - *Advanced Research in Virtual and Rapid Prototyping*, pp. 563–567.

Dimitrov, D. and Moammer, A., 2010. Investigation of the impact of conformal cooling on the performance of injection moulds for the packaging industry. *Journal for New Generation Sciences*, 8(1), pp.29-46

Dutta, B., 2009. 'Direct Metal Deposition', *Advanced. Material. Processing*, 167(3), pp. 33–36. Available at: http://mbraun.com/images/201/POM Group.pdf.

Dym, C., 2004. *Principles of Mathematical Modelling*. Elsevier. doi: 10.1016/B978-0-12-226551-8.X5000-5.

Eastman, C.M. ed., 2012. Design for X: concurrent engineering imperatives. *Springer Science & Business Media.*

EOS. 2011. Material data sheet for tool steel 1.2709. Available at: p-saaseoscms.s3.amazonaws.com/ *(Accessed: 1 August 2018).*

EOS, 2019. Materials for metal Additive Manufacturing. Available at: https://www.eos.info/material-m (Accessed: 15 February 2019).

Mayer, S., 2009. 'Optimised mould temperature control procedure using DMLS', EOS Whitepaper, pp. 1–11. Available at: http://www.3dimpuls.com *(Accessed 1 March 2019).*

ESI, "Pam_stamp Simulation Software." [Online]. Available:https://www.esi-group.com/software-solutions/virtual-manufacturing/sheet-metal-forming/pam-stamp-stamping-simulation-solution. *(Accessed: 01-June-2019).*

ESI, "Visual-Mesh Software." [Online]. Available. https://www.esi-group.com/software-solutions *(Accessed: 01-June-2019).*

ESI Group, PAM-STAMP 2015.1 User Guide (2015)

ESI Group, PAM-STAMP 2018.1 User Guide (2018)

ESI Group, [Online]. Available: https://www.esi-group.com/ *(Accessed: 05-December-2019).*

Escher, C. and Wilzer, J. J, 2015. 'Tool steels for hot stamping of high strength automotive body parts', *International Conference on Stone and Concrete Machining*, 3, pp. 219–228.

Fernández, B., González, B., Artola, G., López de Lacalle, N. and Angulo, C., 2019. A quick cycle time sensitivity analysis of boron steel hot stamping. *Metals*, 9(2), p.235.

Foroozmehr, A., Badrossamay, M., Foroozmehr, E. and Golabi, S.I., 2016. Finite element simulation of selective laser melting process considering optical penetration depth of laser in powder bed. *Materials & Design*, 89, pp.255-263.

Gebauer, M., Müller, B., Polster, S., Feld, T., Klinger, M. and Zurbrügg, A., 2016. High performance sheet metal forming tooling by additive manufacturing. In *iCAT 2016: Proceedings of the 6th International Conference on Additive Technologies* (pp. 354-361).

Geiger, M., Merklein, M. and Lechler, J., 2008. Determination of tribological conditions within hot stamping', *Production Engineering*, 2(3), pp. 269–276

Gharbi, M., Peyre, P., Gorny, C., Carin, M., Morville, S., Le Masson, P., Carron, D. and Fabbro, R., 2014. Influence of a pulsed laser regime on surface finish induced by the direct metal deposition process on a Ti64 alloy. *Journal of Materials Processing Technology*, 214(2), pp.485-495.

GmbH, (2018) Laser generation with the material 1. 709 Specifications for heat treatment Material properties , Hardening Chart of standard 1.2709. Available at http://www.laserbearbeitungscenter.de [Accessed 5 September 2019]

Gong, X., Anderson, T. and Chou, K., 2014. 'Review on powder-based electron beam additive manufacturing technology', *Manufacturing Review*, 1, p. 2. doi:10.1051/mfreview/2014001.

Grauer, S.J., Caron, E.J.F.R., Chester, N.L., Wells, M.A. and Daun, K.J., 2015. Investigation of melting in the Al–Si coating of a boron steel sheet by differential scanning calorimetry. *Journal of Materials Processing Technology*, 216, pp.89-94.

Gu, D.D., Meiners, W., Wissenbach, K. and Poprawe, R., 2012. Laser additive manufacturing of metallic components: materials, processes and mechanisms. *International Materials Reviews*, 57(3), pp.133-164.

Gu, Z.W., Lv, M.M., Lu, G.H., Xu, H. and Li, X., 2015. Heat transfer coefficient evolution of boron steel during hot forming die quenching. *Materials Science and Technology*, *32*(2), pp.173-180.

Gulati, V., 2011. Rapid tooling for producing stretch-formed jewellery. I*nternational Journal of Computer Applications*, 975, p.8887.

Guo, N. and Leu, M. C. 2013, 'Additive manufacturing: Technology, applications and research needs', *Frontiers of Mechanical Engineering*, 8(3), pp. 215–243. doi: 10.1007/s11465-013-0248-8.

Guo, L., Xu, H. and Gong, L., 2015. Influence of wall roughness models on fluid flow and heat transfer in microchannels. *Applied Thermal Engineering*, *84*, pp.399-408.

Hagen, K. (1999) Heat Transfer with applications. New Jersey: Prentice Hall.

Van der Heide, E., 2002. *Lubricant failure in sheet metal forming processes*. PhD thesis, University of Twente, Enschede, The Netherlands.

Hall, M. and Krystofik, M., 2015. Conformal Cooling *Center of Excellence in Sustainable Manufacturing*: Rochester Institute of Technology.

Harvey, P., 2007. *Engineering Properties of Steel*. Second Edition. Ohio: American Society for Metals.

He, B., , Li, X. and Ying, L. (2016) 'Optimal design of hot stamping tools with conformal cooling channels', *Engineering and Technology Edition*, 46(6), pp. 1974–1980. doi:10.13229/j.cnki.jdxbgxb201606029.

He, B., Si, Y., Ying, L. and Hu, P., 2016. Research on optimization design of conformal cooling channels in hot stamping tool based on response surface methodology and multi-objective optimization. *In MATEC Web of Conferences* Vol. 80, p. 10001. EDP Sciences.

He, B., Ying, L., Li, X. and Hu, P., 2016. Optimal design of longitudinal conformal cooling channels in hot stamping tools. *Applied thermal engineering*, 106, pp.1176-1189.

Hexagon, 2019. "Computational Fluid Dynamics Software." [Online]. Available: https://www.mscsoftware.com/application/computational-fluid-dynamics *(Accessed: 01-June-2019).*

Hölker, R., Jäger, A., Khalifa, N.B. and Tekkaya, A.E., 2013. Controlling heat balance in hot aluminum extrusion by additive manufactured extrusion dies with conformal cooling channels. *International Journal of Precision Engineering and Manufacturing*, 14(8), pp.1487-1493.

Hölker-Jäger, R. and Tekkaya, A.E., 2017. Additive manufacture of tools and dies for metal forming. In *Laser Additive Manufacturing*, pp. 439-464

Hosford, W.F. and Caddell, R.M., 2011. *Metal forming: Mechanics and metallurgy*. Fourth Edition. London: Cambridge University Press

Hu, P., He, B. and Ying, L. (2016) 'Numerical investigation on cooling performance of hot stamping tool with various channel designs', *Applied Thermal Engineering. Elsevier* Ltd, 96, pp. 338–351. doi: 10.1016/j.applthermaleng.2015.10.154.

Hu, P., Ying, L., Li, Y. and Liao, Z., 2013. Effect of oxide scale on temperature-dependent interfacial heat transfer in hot stamping process. *Journal of Materials Processing Technology*, 213(9), pp.1475-1483.

Hung, T.H., Wang, S.W., ChiuHuang, C.K. and Chen, F.K., 2019. Performance of die cooling system design in hot stamping process. *Journal of the Chinese Institute of Engineers*, pp.1-9.

Huskic, A., Behrens, B.A., Giedenbacher, J. and Huskic, A., 2013. Standzeituntersuchungen generativ hergestellter *Schmiedewerkzeuge. Schmiede J*, 92013, pp.66-70.

Huskic, A., Giedenbacher, J., Pschebezin, U. and Wild, N., 2012, June. Rapid tooling für Umformwerkzeuge. In RT *Journal-Forum für Rapid Technologie* (Vol. 2012, No. 1).

Ikeuchi, K. and Yanagimoto, J., 2011. 'Valuation method for effects of hot stamping process parameters on product properties using hot forming simulator', *Journal of Materials Processing Technology. Elsevier B.V.*, 211(8), pp. 1441–1447. doi: 10.1016/j.jmatprotec.2011.03.017.

Imran, M.K., Masood, S.H., Brandt, M., Bhattacharya, S., Gulizia, S., Jahedi, M. and Mazumder, J., 2012. Thermal fatigue behavior of direct metal deposited H13 tool steel coating on copper alloy substrate. *Surface and Coatings Technology*, 206(8-9), pp.2572-2580.

Ishizaka, A. and Nemery, P., 2013. *Multi-Criteria Decision Analysis: Methods and Software*. John Wiley & Sons.

Jack, H., 2013. *Engineering Design, Planning, and Management*. Academic Press.

Ji, K., El Fakir, O., Gao, H. and Wang, L., 2015. Determination of heat transfer coefficient for hot stamping process. *Materials Today: Proceedings*, 2, pp.S434-S439.

Jiang, C., Shan, Z., Zhuang, B., Zhang, M. and Xu, Y., 2012. Hot stamping die design for vehicle door beams using ultra-high strength steel. *International Journal of Precision Engineering and Manufacturing*, 13(7), pp.1101-1106.

Kaierle, S., Barroi, A., Noelke, C., Hermsdorf, J., Overmeyer, L. and Haferkamp, H., 2012. Review on laser deposition welding: from micro to macro. *Physics Procedia*, 39, pp.336-345.

Kapoor, R. and Nemat-Nasser, S., 1998. Determination of temperature rise during high strain rate deformation. *Mechanics of Materials*, *27*(1), pp.1-12.

Karbasian, H. and Tekkaya, A.E., 2010. A review on hot stamping. *Journal of Materials Processing Technology*, 210(15), pp.2103-2118.

Karlsson, J., Snis, A., Engqvist, H. and Lausmaa, J., 2013. Characterization and comparison of materials produced by Electron Beam Melting (EBM) of two different Ti–6Al–4V powder fractions. *Journal of Materials Processing Technology*, 213(12), pp.2109-2118.

Karunakaran, K.P., Bernard, A., Suryakumar, S., Dembinski, L. and Taillandier, G., 2012. Rapid manufacturing of metallic objects. *Rapid Prototyping Journal*, 18(4), pp.264-280.

Kempen, K., Yasa, E., Thijs, L., Kruth, J.P. and Van Humbeeck, J., 2011. Microstructure and mechanical properties of Selective Laser Melted 18Ni-300 steel. *Physics Procedia*, 12, pp.255-263.

Khan, M., Afaq, S.K., Khan, N.U. and Ahmad, S., 2014. Cycle time reduction in injection molding process by selection of robust cooling channel design. *ISRN Mechanical Engineering*, 2014.

Kim, G.Y., Park, S.H., Kim, S.K. and Park, D.S., 2018. A Study on Design Automation of Cooling Channels in Hot Form Press Die Based on CATIA CAD System. *Journal of the Korea Academia-Industrial cooperation Society*, 19(3), pp.147-154.

Kim, H.-K., Lee, S. and Choi, H. (2015) 'Evaluation of Contact Heat Transfer Coefficient and Phase Transformation during Hot Stamping of a Hat-Type Part', *Materials*, 8(4), pp. 2030–2042. doi: 10.3390/ma8042030.

Koike, M., Martinez, K., Guo, L., Chahine, G., Kovacevic, R. and Okabe, T., 2011. Evaluation of titanium alloy fabricated using electron beam melting system for dental applications. *Journal of Materials Processing Technology*, 211(8), pp.1400-1408.

Kruth, J.P., Badrossamay, M., Yasa, E., Deckers, J., Thijs, L. and Van Humbeeck, J., 2010. Part and material properties in selective laser melting of metals. In *Proceedings of the 16th International Symposium on Electromachining* (pp. 1-12).2.

Lam, Y.C., Zhai, L.Y., Tai, K. and Fok, S.C., 2004. An evolutionary approach for cooling system optimization in plastic injection moulding. *International Journal of Production Research*, 42(10), pp.2047-2061.

Lee, M. S., Baeck, S. C. and Kang, C. G., 2012. 'Investigation of thin boron steel sheet formability in hot deep-drawing processes according to process parameters', Proceedings of the Institution of Mechanical Engineers, Part B: *Journal of Engineering Manufacture*, 226(5), pp. 898–908. doi: 10.1177/0954405411431376.

Lee, S., Park, J., Park, K., Kweon, D., Lee, H., Yang, D., Park, H. and Kim, J., 2018. A study on the cooling performance of newly developed slice die in the hot press forming process. *Metals*, 8(11), p.947.

Lei, C., Cui, J., Xing, Z., Fu, H. and Zhao, H., 2012. Investigation of cooling effect of hot-stamping dies by numerical simulation. *Physics Procedia*, 25, pp.118-124.

Levy, G. N., Schindel, R. and Kruth, J. P., 2003. 'Rapid Manufacturing and Rapid Tooling with Layer Manufacturing (Lm) Technologies, State of the Art and Future Perspectives', *CIRP Annals - Manufacturing Technology*, 52(2), pp. 589–609. doi: 10.1016/S0007-8506(07)60206-6.

Levy, G.N., Schindel, R., Schleiss, P., Micari, F. and Fratini, L., 2003. On the use of SLS tools in sheet metal stamping. *CIRP Annals*, 52(1), pp.249-252.

Li, H., He, L., Zhang, C. and Cui, H., 2015. Research on the effect of boundary pressure on the boundary heat transfer coefficients between hot stamping die and boron steel. *International Journal of Heat and Mass Transfer*, 91, pp.401-415.

Li, Z., Wang, X., Gu, J., Ruan, S., Shen, C., Lyu, Y. and Zhao, Y., 2018. Topology optimization for the design of conformal cooling system in thin-wall injection moulding based on BEM. *The International Journal of Advanced Manufacturing Technology*, 94(1-4), pp.1041-1059.

Lim, W.S., Choi, H.S., Ahn, S.Y. and Kim, B.M., 2014. Cooling channel design of hot stamping tools for uniform high-strength components in hot stamping process. *The International Journal of Advanced Manufacturing Technology*, 70(5-8), pp.1189-1203.

Lin, T., Song, H.W., Zhang, S.H., Cheng, M. and Liu, W.J., 2014. Cooling systems design in hot stamping tools by a thermal-fluid-mechanical coupled approach. *Advances in Mechanical Engineering*, 6, p.545727.

Lin, Z.C. and Chou, M.H., 2002. Design of the cooling channels in nonrectangular plastic flat injection mould. *Journal of Manufacturing Systems*, 21(3), pp.167-186.

Liu, H., Lei, C. and Xing, Z., 2013. 'Cooling system of hot stamping of quenchable steel BR1500HS: Optimization and manufacturing methods', *International Journal of Advanced Manufacturing Technology*, 69(1–4), pp. 211–223. doi: 10.1007/s00170-013-4996-8.

Lv, M., Gu, Z., Li, X. and Xu, H., 2016. Optimal design for cooling system of hot stamping dies. *ISIJ International*, pp.ISIJINT-2016.

Materialise, 2018. MAGICS Software, Materialise magics. Available at: https://www.materialise.com/en/software/magics *(Accessed: 1 January 2018).*

Mazur, M., Brincat, P., Leary, M. and Brandt, M., 2017. Numerical and experimental evaluation of a conformally cooled H13 steel injection mould manufactured with selective laser melting. *The International Journal of Advanced Manufacturing Technology*, 93(1-4), pp.881-900.

Mazur, M., Leary, M., McMillan, M., Elambasseril, J. and Brandt, M., 2016. SLM additive manufacture of H13 tool steel with conformal cooling and structural lattices. *Rapid Prototyping Journal*, 22(3), pp.504-518.

Mercelis, P. and Kruth, J.-P. 2006, 'Residual stresses in selective laser sintering and selective laser melting', *Rapid Prototyping Journal*, 12(5), pp. 254–265. doi: 10.1108/13552540610707013.

Merklein, M. and Lechler, J., 2006. Investigation of the thermo-mechanical properties of hot stamping steels. *Journal of Materials Processing Technology*, 177(1-3), pp.452-455.

Merklein, M., Lechler, J. and Stoehr, T., 2009. Investigations on the thermal behavior of ultra high strength boron manganese steels within hot stamping', *International Journal of Material Forming*, 2(SUPPL. 1), pp. 259–262.

Mistubishi Materials, 2019. General Catalogue for Drilling. Available at: http://www.mitsubishicarbide.com *(Accessed: 21 May 2019).*

Moammer, A., 2011, 'Thermal management of moulds and dies: a contribution to improved design and manufacture of tooling for injection moulding', (Doctoral dissertation, Stellenbosch: University of Stellenbosch). Available at: http://scholar.sun.ac.za/handle/10019.1/6652 *(Accessed on 1 August 2019)*

Mohamed, O.A., Masood, S.H. and Saifullah, A., 2013. A simulation study of conformal cooling channels in plastic injection molding. *International Journal of Engineering Research*, 2(5), pp.344-348.

Montgomery, D.C., 2017. *Design and Analysis of Experiments*. John wiley & sons.

Mori, K. ichiro. 2015. 'Thermal Conductivity of Tool Steels', in *60 Excellent Inventions in Metal Forming*, pp. 403–408. doi: 10.1007/978-3-662-46312-3_62.

Mori, K.I., 2015. Smart hot stamping for ultra-high strength steel parts. In *60 Excellent Inventions in Metal Forming* pp. 403-408. Springer Vieweg, Berlin, Heidelberg.

Mueller, B., Gebauer, M., Polster, S., Neugebauer, R., Malek, R., Kotzian, M. and Hund, R., 2013. Ressource-efficient hot sheet metal forming by innovative die cooling with laser beam melted tooling components. *In High Value Manufacturing: Advanced Research in Virtual and Rapid Prototyping: Proceedings of the 6th International Conference on Advanced Research in Virtual and Rapid Prototyping*, Leiria, Portugal, pp. 321. CRC Press.

Mueller, B., Hund, R., Malek, R., Gebauer, M., Polster, S., Kotzian, M., Neugebauer, R. and Volkswagen, A.G., 2013, August. Added value in tooling for sheet metal forming through Additive Manufacturing. *In International Conference on Competitive Manufacturing* (pp. 1-7).

Murr, L.E., Gaytan, S.M., Ramirez, D.A., Martinez, E., Hernandez, J., Amato, K.N., Shindo, P.W., Medina, F.R. and Wicker, R.B., 2012. Metal fabrication by additive manufacturing using laser and electron beam melting technologies. *Journal of Materials Science & Technology*, 28(1), pp.1-14.

Muvunzi, R, Dimitrov, DM, H. T. and Matope, S., 2017. 'Heat Transfer in a Hot Stamping Process: A Review', *R & D Journal of the South African Institution of Mechanical* Engineering 2, 33(September 2016), pp. 75–84.

Muvunzi, R., Dimitrov, D.M., Matope, S. and Harms, T.M., 2018. Development of a model for predicting cycle time in hot stamping. *Procedia Manufacturing*, 21, pp.84-91.

Nakagawa, Y., Maeno, T. and Mori, K.I., 2015. Forming and quenching behaviours in hot stamping of thin quenchable sheets. *In MATEC Web of Conferences* (Vol. 21, p. 05002). EDP Sciences.

Naderi, M. and Bleck, W., 2008. *Hot Stamping Of Ultra High Strength Steels* (No. RWTH-CONV-112497). Lehrstuhl und Institut für Eisenhüttenkunde.

Negi, S., Dhiman, S. and Sharma, R.K., 2013. Basics, applications and future of additive manufacturing technologies: A review. *Journal of Manufacturing Technology Research*, 5(1/2), p.75.

Nikravesh, M., Naderi, M., Akbari, G.H. and Bleck, W., 2015. Phase transformations in a simulated hot stamping process of the boron bearing steel. *Materials & Design*, 84, pp.18-24.

Ocylok, S., Alexeev, E., Mann, S., Weisheit, A., Wissenbach, K. and Kelbassa, I., 2014. Correlations of melt pool geometry and process parameters during laser metal deposition by coaxial process monitoring. *Physics Procedia*, 56, pp.228-238.

Oyesola, M., Mathe, N., Mpofu, K. and Fatoba, S., 2018. Sustainability of Additive Manufacturing for the South African aerospace industry: A business model for laser technology production, commercialization and market prospects. *Procedia* CIRP, 72, pp.1530-1535.

Pahl, G. and Beitz, W., 2013. Engineering design: a systematic approach. *Springer Science & Business Media*.

Park, H. S. and Pham, N. H. (2009) 'Design Of Conformal Cooling Channels for an Automotive Part', *International Journal of Automotive Technology*, 10(1), pp. 87–93. Available at: doi 10.1007/s12239−009−0011−7.

Park, H.S., Dang, X.P., Nguyen, D.S. and Kumar, S., 2019. Design of Advanced Injection Mold to Increase Cooling Efficiency. *International Journal of Precision Engineering and Manufacturing*-Green Technology, pp.1-10.

Pierschel, N. Polster, S, Priber, U, Barthel, H, Pierer, A, Schönherr, J. Berndt, B, 2015. *Fraunhofer Institute IGF project*. Chemnitz, Germany

Pinkerton, A.J., 2015. Advances in the modeling of laser direct metal deposition.*Journal of. Laser Applications*, 27(S1).

Qian, Y.P., Wang, Y., Huang, J.H. and Zhou, X.Z., 2012. Study on the Optimization of Conformal Cooling Channels for Plastic Injection Mold. *In Advanced Materials Research* (Vol. 591, pp. 502-506). Trans Tech Publications.

Quan, G.Z., Zhang, Z.H., Wang, X., Mao, A. and Xia, Y.F., 2017. Parameter optimization of cooling system in U-shape hot stamping mold for high strength steel sheet based on MOPSO. *The International Journal of Advanced Manufacturing Technology*, 90(1-4), pp.887-906.

Quan, G.Z., Zhang, Z.H., Wang, X., Mao, A. and Xia, Y.F., 2017. Parameter optimization of cooling system in U-shape hot stamping mold for high strength steel sheet based on MOPSO. *The International Journal of Advanced Manufacturing Technology*, 90(1-4), pp.887-906.

Rännar, L.E., Glad, A. and Gustafson, C.G., 2007. Efficient cooling with tool inserts manufactured by electron beam melting. *Rapid Prototyping Journal*, 13(3), pp.128-135.

Rao, N. S. and Schumacher, G., 2004. Design Formulas for Plastics Engineers. *Carl Hanser Verlag GmbH*. Available at: https://doi.org/10.3139/9783446413009 *(Accessed on 5 September 2019).*

Renzi, C., Leali, F. and Di Angelo, L., 2017. A review on decision-making methods in engineering design for the automotive industry. *Journal of Engineering Design*, 28(2), pp.118-143.

Riza, S.H., Masood, S.H., Wen, C., Ruan, D. and Xu, S., 2014. Dynamic behaviour of high strength steel parts developed through laser assisted direct metal deposition. *Materials & Design*, 64, pp.650-659.

Rodrigues, M.I. and Iemma, A.F., 2014. Experimental design and process optimization. CRC Press.

Rodriguez, E., Medina, F., Espalin, D., Terrazas, C., Muse, D., Henry, C., MacDonald, E. and Wicker, R.B., 2012, August. Integration of a thermal imaging feedback control system in electron beam melting. In *Proceedings of the Solid Freeform Fabrication Symposium*

Shellabear, M. and Weilhammer, J., 2007. Tooling applications with EOSINT M. EOS Whitepaper, Krailling. Available at: http://www.3dimpuls.com *(Accessed on 8 September 2019)*

Saifullah, A. and Masood, S.H., 2007. Optimum cooling channels design and Thermal analysis of an Injection moulded plastic part mould. *In Materials Science Forum* (Vol. 561, pp. 1999-2002). Trans Tech Publications.

Samarskii, A.A. and Mikhailov, A.P., 2014. *Principles of Mathematical Modelling: Ideas, Methods, Examples*. CRC Press.

Schieck, F., Hochmuth, C., Polster, S. and Mosel, A., 2011. Modern tool design for component grading incorporating simulation models, efficient tool cooling concepts and tool coating systems. *CIRP Journal of Manufacturing Science and Technology*, 4(2), pp.189-199.

Schmidt, M., Merklein, M., Bourell, D., Dimitrov, D., Hausotte, T., Wegener, K., Overmeyer, L., Vollertsen, F. and Levy, G.N., 2017. Laser based additive manufacturing in industry and academia. *CIRP Annals*, 66(2), pp.561-583.

Shapiro, A.B., 2009, May. Using LS-Dyna for hot stamping. In *Proceedings of the 7th European LS-DYNA Users Conference*, Salzburg, Austria.

Sheng, Z., Wang, Y., Chang, T., Miller, R. and Liasi, E., 2013. Deep Drawing by Indirect Hot Stamping. *SAE Technical Paper*, (No. 2013-01-1172)..

Shi, D., Ying, L., Hu, P., Liu, W. and Shen, G., 2013, December. Numerical simulation of temperature field, microstructure evolution and mechanical properties of HSS during hot stamping. In *AIP Conference Proceedings* (Vol. 1567, No. 1, pp. 962-965). AIP.

Sing, S.L., An, J., Yeong, W.Y. and Wiria, F.E., 2016. Laser and electron-beam powder-bed additive manufacturing of metallic implants: A review on processes, materials and designs. *Journal of Orthopaedic Research*, 34(3), pp.369-385.

SIMULEON, 2019 "ABAQUS Software." [Online]. Available: https://www.simuleon.com/simulia-abaqus/ *(Accessed: 05-August-2019).*

Song, B., Dong, S., Liu, Q., Liao, H. and Coddet, C., 2014. Vacuum heat treatment of iron parts produced by selective laser melting: microstructure, residual stress and tensile behaviour. *Materials & Design* (1980-2015), 54, pp.727-733.

Steinbeiss, H., So, H., Michelitsch, T. and Hoffmann, H., 2007. Method for optimizing the cooling design of hot stamping tools. *Production Engineering*, 1(2), pp.149-155.

Stephens, R.C., 2013. Strength of materials: theory and examples. *Elsevie*r.

Stoll, P., Spierings, A., Gebauer, M., Müller, B., Polster, S., Feld, T., Klinger, M. and Zurbrügg, A., 2016. High performance sheet metal forming tooling by additive manufacturing. In iCAT 2016: *Proceedings of the 6th International Conference on Additive Technologies* (pp. 354-361). Interesana-zavod.

Stoll, P., Spierings, A., Gebauer, M., Müller, B., Polster, S., Feld, T., Klinger, M. and Zurbrügg, A., 2016. High performance sheet metal forming tooling by additive manufacturing. In iCAT 2016: *Proceedings of the 6th International Conference on Additive Technologies* (pp. 354-361).

Sun, Y. and Hao, M., 2012. Statistical analysis and optimization of process parameters in Ti6Al4V laser cladding using Nd: YAG laser. *Optics and Lasers in Engineering*, 50(7), pp.985-995.

Thijs, L., Verhaeghe, F., Craeghs, T., Van Humbeeck, J. and Kruth, J.P., 2010. A study of the microstructural evolution during selective laser melting of Ti–6Al–4V. *Acta Materialia*, 58(9), pp.3303-3312.

Thomas, D., 2009. *The Development of Design Rules for Selective Laser Melting* (Doctoral dissertation, University of Wales).

Vaidya, O.S. and Kumar, S., 2006. Analytic hierarchy process: An overview of applications. *European Journal of Operational Research*, 169(1), pp.1-29.

Valiantzas, J.D., 2008. Explicit power formula for the Darcy–Weisbach pipe flow equation: application in optimal pipeline design. *Journal of Irrigation and Drainage Engineering*, 134(4), pp.454-461.

Van Belle, L., Vansteenkiste, G. and Boyer, J.C., 2013. Investigation of residual stresses induced during the selective laser melting process. *In Key Engineering Materials* (Vol. 554, pp. 1828-1834). Trans Tech Publications.

Velasquez, M. and Hester, P.T., 2013. An Analysis of Multi-Criteria Decision Making Methods *International Journal of Operations Research* Vol. 10.

Ventola, L., Robotti, F., Dialameh, M., Calignano, F., Manfredi, D., Chiavazzo, E. and Asinari, P., 2014. Rough surfaces with enhanced heat transfer for electronics cooling by direct metal laser sintering. *International Journal of Heat and Mass Transfer*, *75*, pp.58-74.

Vora, P., Mumtaz, K., Todd, I. and Hopkinson, N., 2015. AlSi12 in-situ alloy formation and residual stress reduction using anchorless selective laser melting. *Additive Manufacturing*, 7, pp.12-19.

Vorus, W.S., 2017. Engineering Design. In Hydrodynamics of Planing Monohull *Watercraft* (pp. 71-84). Springer, Cham.

Wang, D., Li, H., Yang, H., Ma, J. and Li, G., 2014. Tribological evaluation of surface modified H13 tool steel in warm forming of Ti–6Al–4V titanium alloy sheet. *Chinese Journal of Aeronautics*, 27(4), pp.1002-1009.

Wang, Y., Yu, K.M., Wang, C.C. and Zhang, Y., 2011. Automatic design of conformal cooling circuits for rapid tooling. *Computer-Aided Design*, 43(8), pp.1001-1010.

Wong, K. V. and Hernandez, A., 2012. A Review of Additive Manufacturing', ISRN *Mechanical Engineering*, 2012, pp. 1–10. doi: 10.5402/2012/208760.

WorldAutoSteel, 2016. ULSAB Programme Report. Available at: http://www.worldautosteel.org/projects/ulsab/ultralight-steel-auto-body-ulsab-programme/ *(Accessed on 1 December 2018)*

Wu, T., Jahan, S.A., Zhang, Y., Zhang, J., Elmounayri, H. and Tovar, A., 2017. Design optimization of plastic injection tooling for additive manufacturing. *Procedia Manufacturing*, 10, pp.923-934.

Wu, X., Liang, J., Mei, J., Mitchell, C., Goodwin, P.S. and Voice, W., 2004. Microstructures of laser-deposited Ti–6Al–4V. *Materials & design*, 25(2), pp.137-144.

Xian, X. D. and Wang, Y. L., 2014. 'The Parametric Design of Cooling System of Hot Stamping Die', *Advanced Materials Research*, 1063, pp. 276–279. doi: 10.4028/www.scientific.net/amr.1063.276.

Xie, H., Cheng, W., Wang, H., Fu, S., Li, W. and Xiong, W., 2018. Multi-objective reliability-based optimization for cooling channel of a UHSS hot-stamping die. *The International Journal of Advanced Manufacturing Technology*, 97(9-12), pp.3237-3249.

Xu, X., 1999. *Conformal cooling and rapid thermal cycling in injection molding with 3D printed tools* (Doctoral dissertation, Massachusetts Institute of Technology).

Xu, X., Sachs, E. and Allen, S., 2001. 'The design of conformal cooling channels in injection molding tooling', *Polymer Engineering and Science*, 41(7), pp. 1265–1279. doi: 10.1002/pen.10827.

Cengel, Y.A. and Ghajar, A.J., 2011, *Heat and Mass Transfer, Fundamentals and Applications* (p. 489). McGraw-Hill New York.

Yadroitsev, I., Bertrand, P. and Smurov, I., 2012. Factor analysis of selective laser melting process parameters and geometrical characteristics of synthesized single tracks. *Rapid Prototyping Journal*, 18(3), pp.201-208.

Yan, C., Hao, L., Hussein, A., Young, P. and Raymont, D., 2014. Advanced lightweight 316L stainless steel cellular lattice structures fabricated via selective laser melting. *Materials & Design*, 55, pp.533-541.

Ye, Y.S., Zhang, M.L. and Wang, B.Y., 2013. Hot-stamping die-cooling system for vehicle door beams. *International Journal of Precision Engineering and Manufacturing*, 14(7), pp.1251-1255.

Yeşildal, R., 2018. The Effect of Heat Treatments on the Fatigue Strength of H13 Hot Work Tool Steel. *Atatürk University Engineering Faculty*

Ying, X. and Zhong-de, S., 2014. Design parameter investigation of cooling systems for UHSS hot stamping dies. *The International Journal of Advanced Manufacturing Technology*, 70(1-4), pp.257-262.7.

Zamri, M.F. and Yusoff, A.R., 2015. Heuristic optimisation of cooling channel design in the hot stamping die for hot stamping process. *Advances in Materials and Processing* Technologies, 1(1-2), pp.27-35.

Zamri, M.F. and Yusoff, A.R., 2018. Heuristic design of U-shaped die cooling channel for producing ultra-high strength steel using hot press forming. *The International Journal of Advanced Manufacturing Technology*, 97(9-12), pp.4101-4114.

Zamri, M.F. and Yusoff, A.R., 2018. Heuristic design of U-shaped die cooling channel for producing ultra-high strength steel using hot press forming. *The International Journal of Advanced Manufacturing Technology*, 97(9-12), pp.4101-4114.-4.

Zhang, K., Wang, S., Liu, W. and Shang, X., 2014. Characterization of stainless steel parts by laser metal deposition shaping. *Materials & Design*, 55, pp.104-119.

Zhao, K., Wang, B., Chang, Y., Tang, X. and Yan, J., 2015. Comparison of the methods for calculating the interfacial heat transfer coefficient in hot stamping. *Applied Thermal Engineering*, 79, pp.17-26.

Zhong-de, S., Mi-lan, Z., Chao, J., Ying, X. and Wen-juan, R., 2010. Basic study on die cooling system of hot stamping process. *International Conference on Advanced Technology of Design and Manufacture*, 67(0 2), pp. 5–8. doi: 10.1049/cp.2010.1248.

Zhu, G., Li, D., Zhang, A., Pi, G. and Tang, Y., 2012. The influence of laser and powder defocusing characteristics on the surface quality in laser direct metal deposition. *Optics & Laser Technology*, 44(2), pp.349-356.

# ADDENDUM A: SIMULATION DATA

## A1: PAM-STAMP Simulation analysis for different layouts

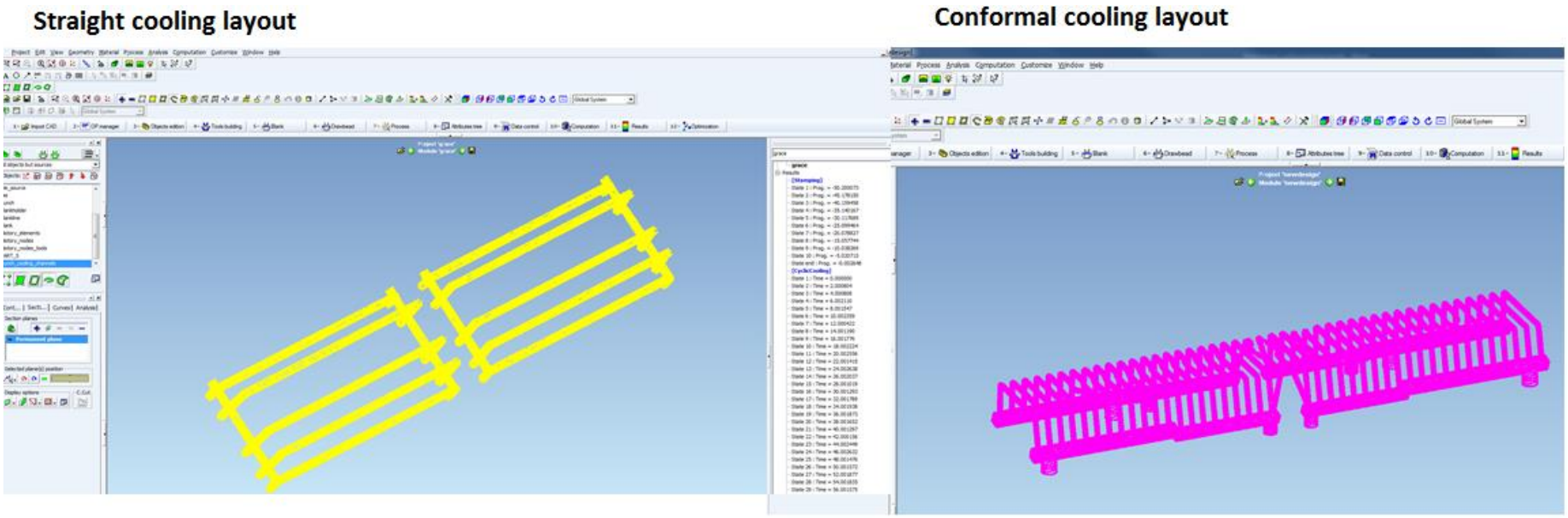


Figure A1.1: PAM-STAMP simulation analysis for conventional (left) and conformal layout (right)

## A2: Temperature map simulation results for blank

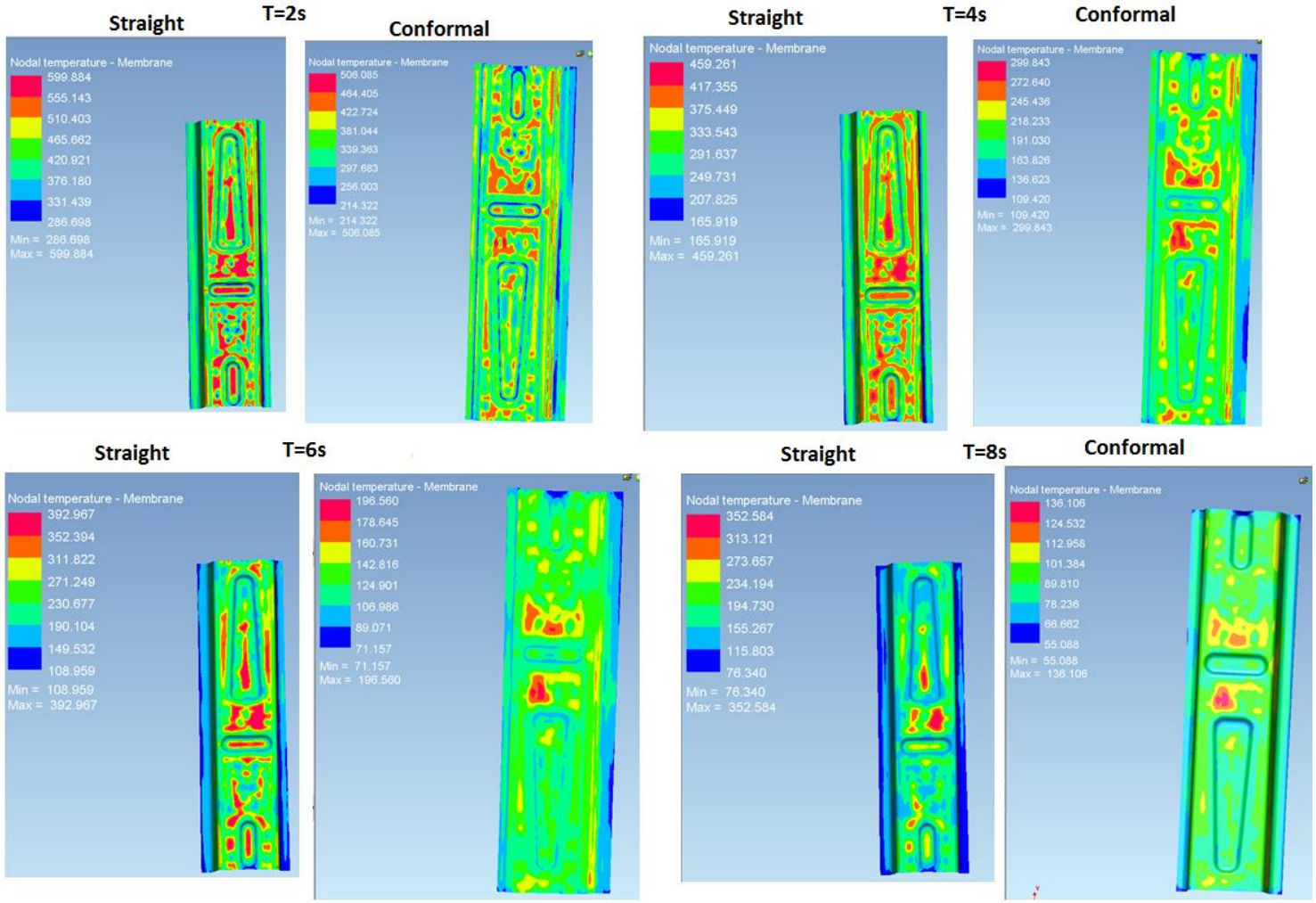


Figure A2.1: Temperature maps for cycle 1

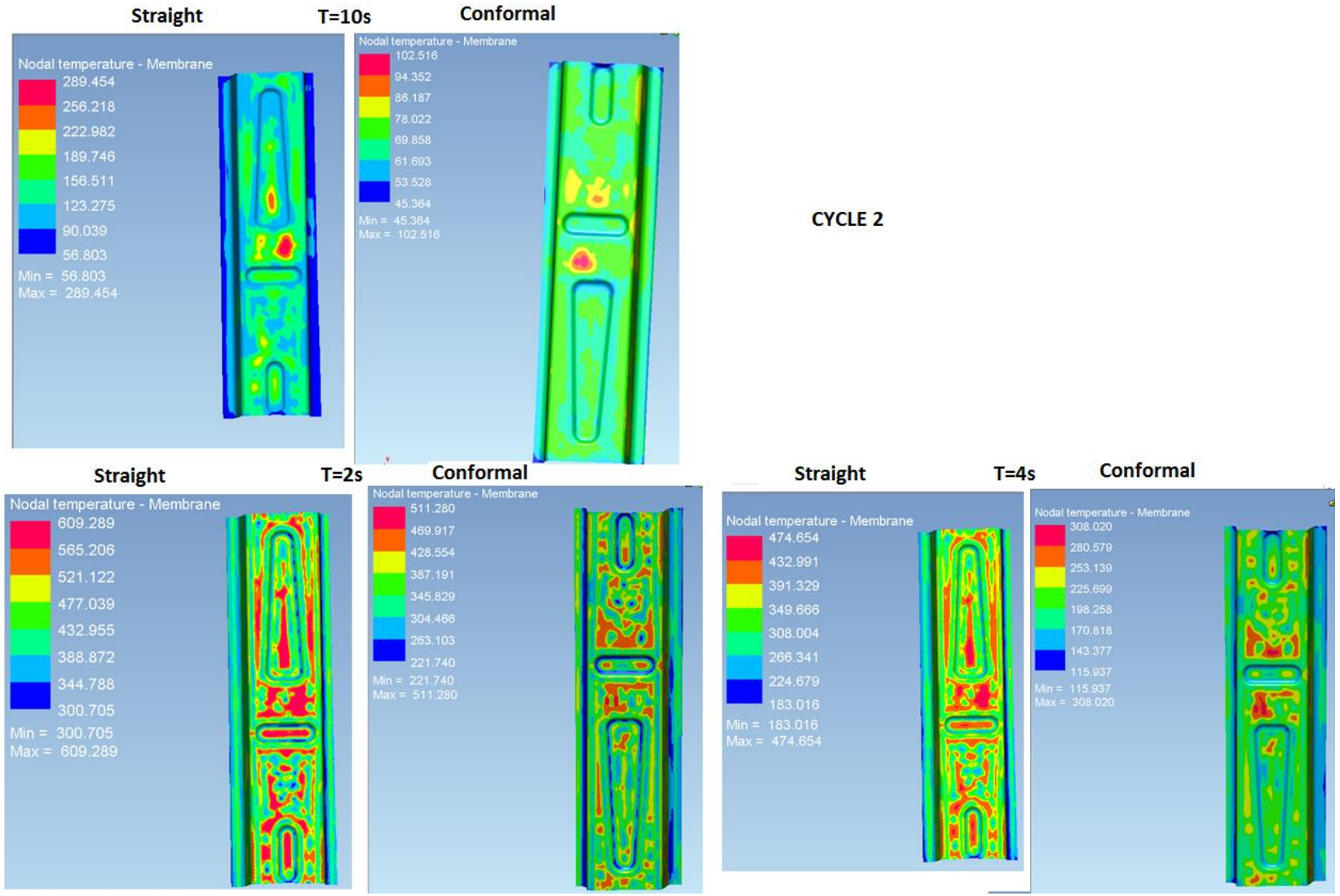


Figure A2.2: Temperature map for 10 s in cycle 1 (top), 2 and 4 s in cycle 2

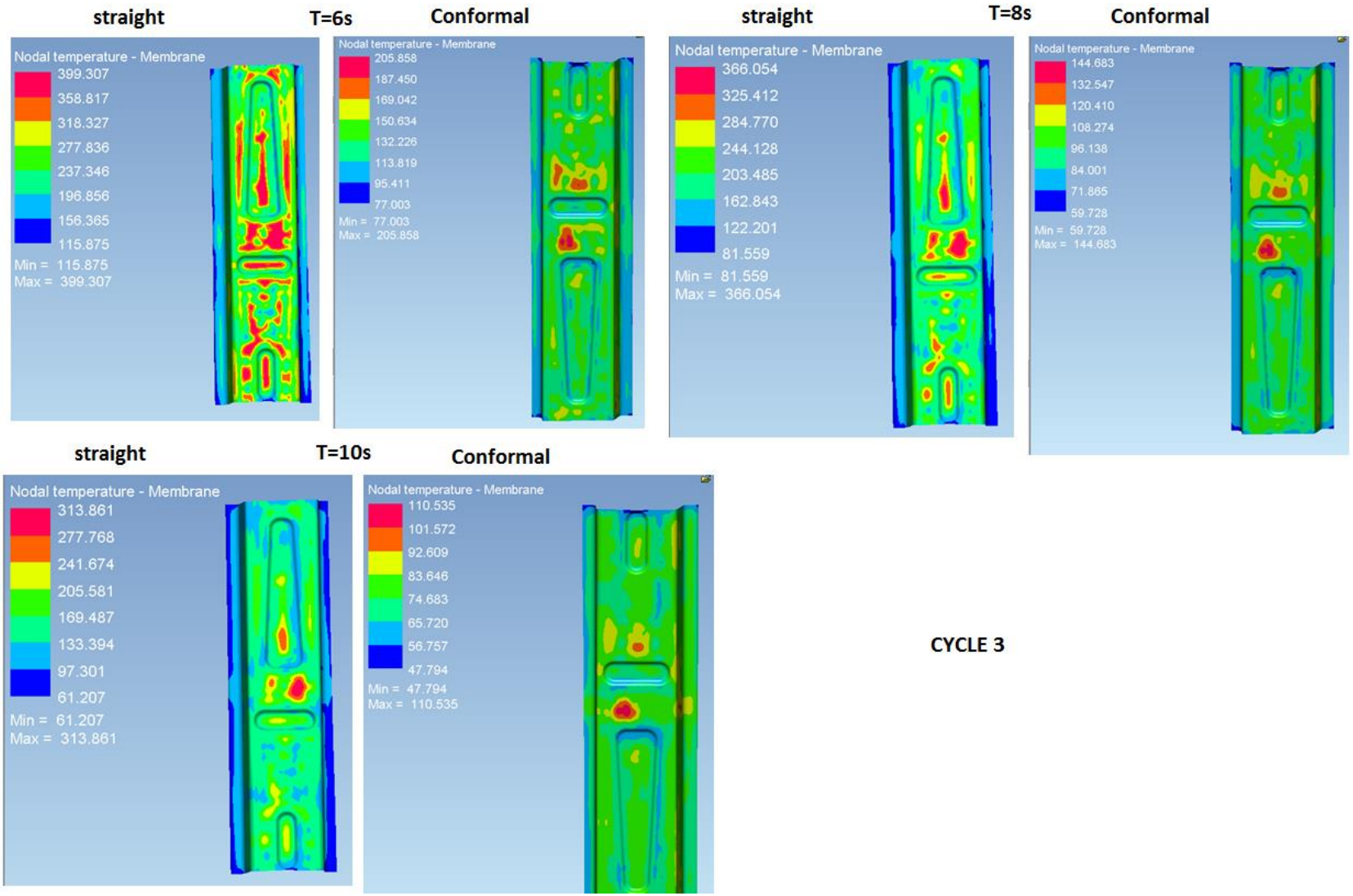


Figure A2.3: Temperature map for 6-8 s in cycle 2

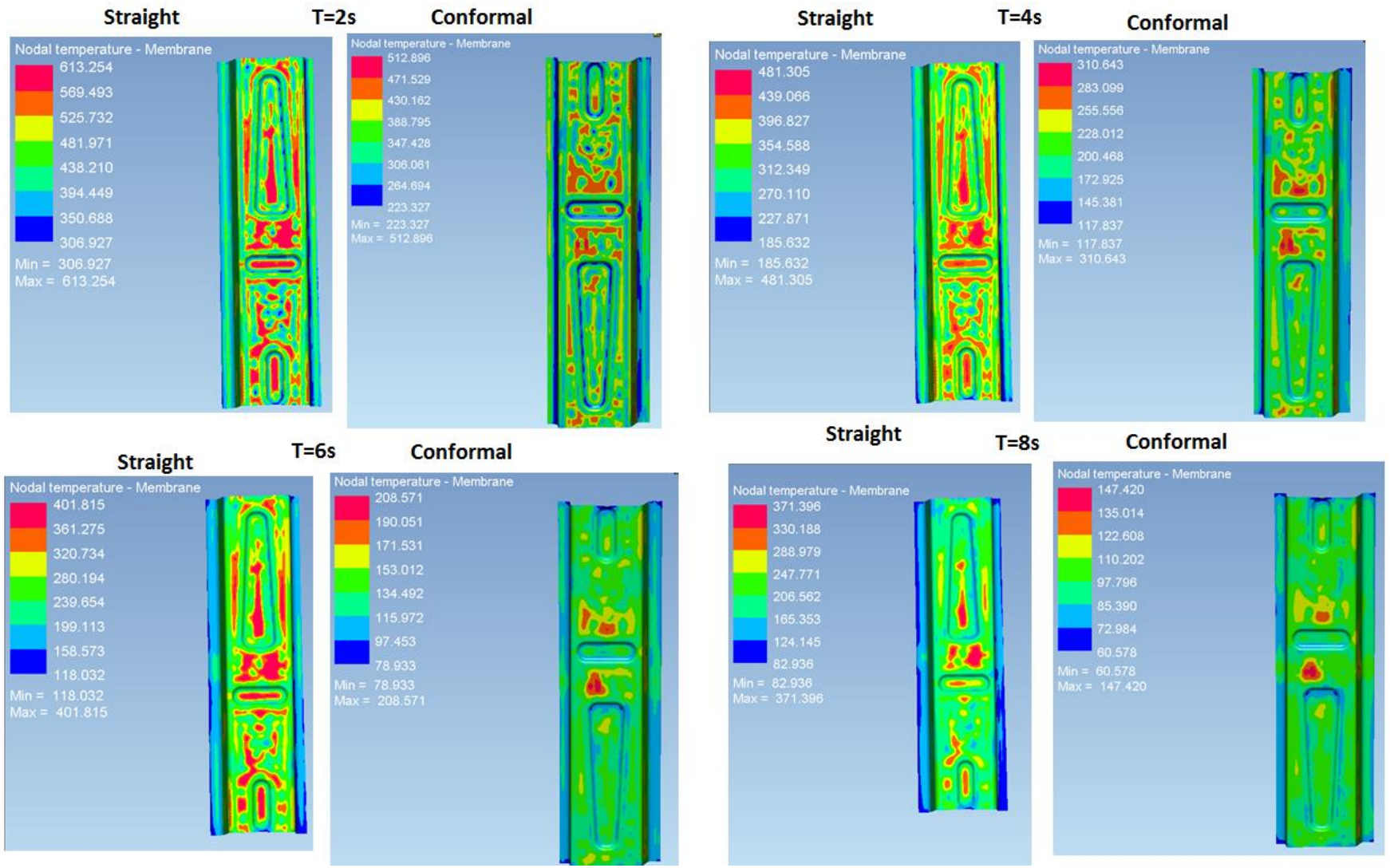


Figure A2.4: Temperature map for 2-8 s in cycle 3

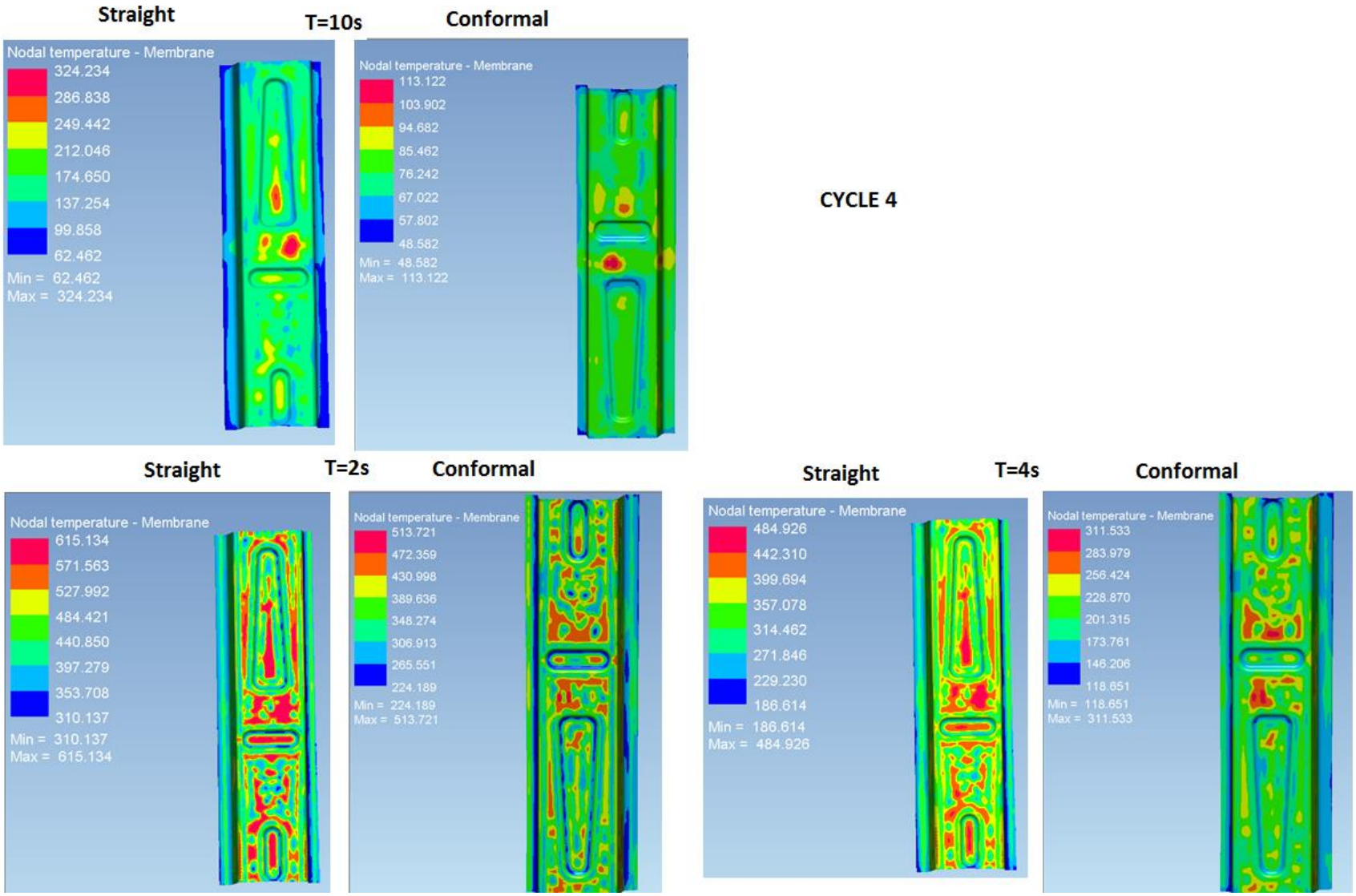


Figure A2.5: Temperature map for 10 s in cycle 3 (top), 2 and 4 s in cycle 4

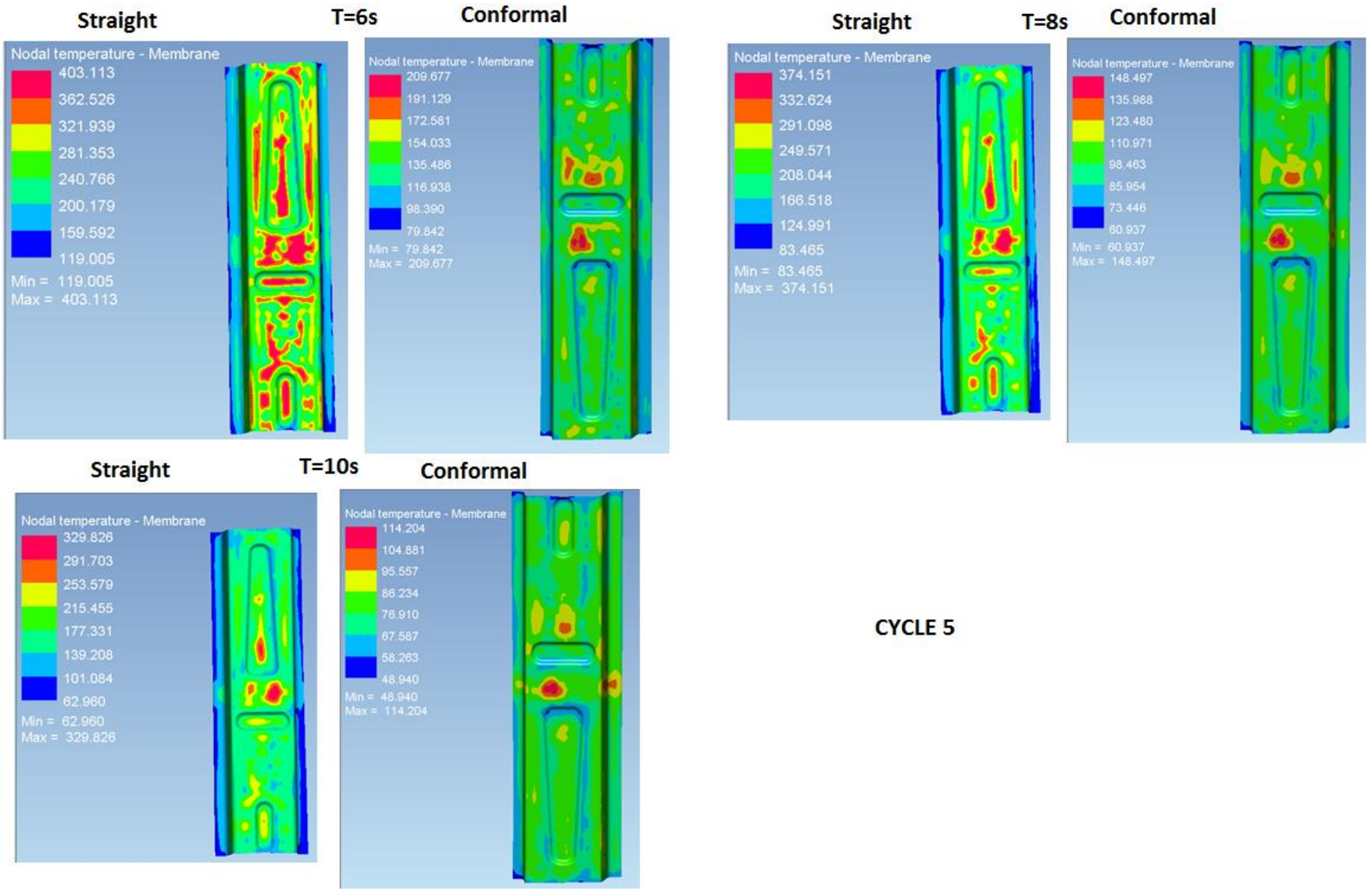


Figure A2.5: Temperature map for 6-10 s in cycle 4

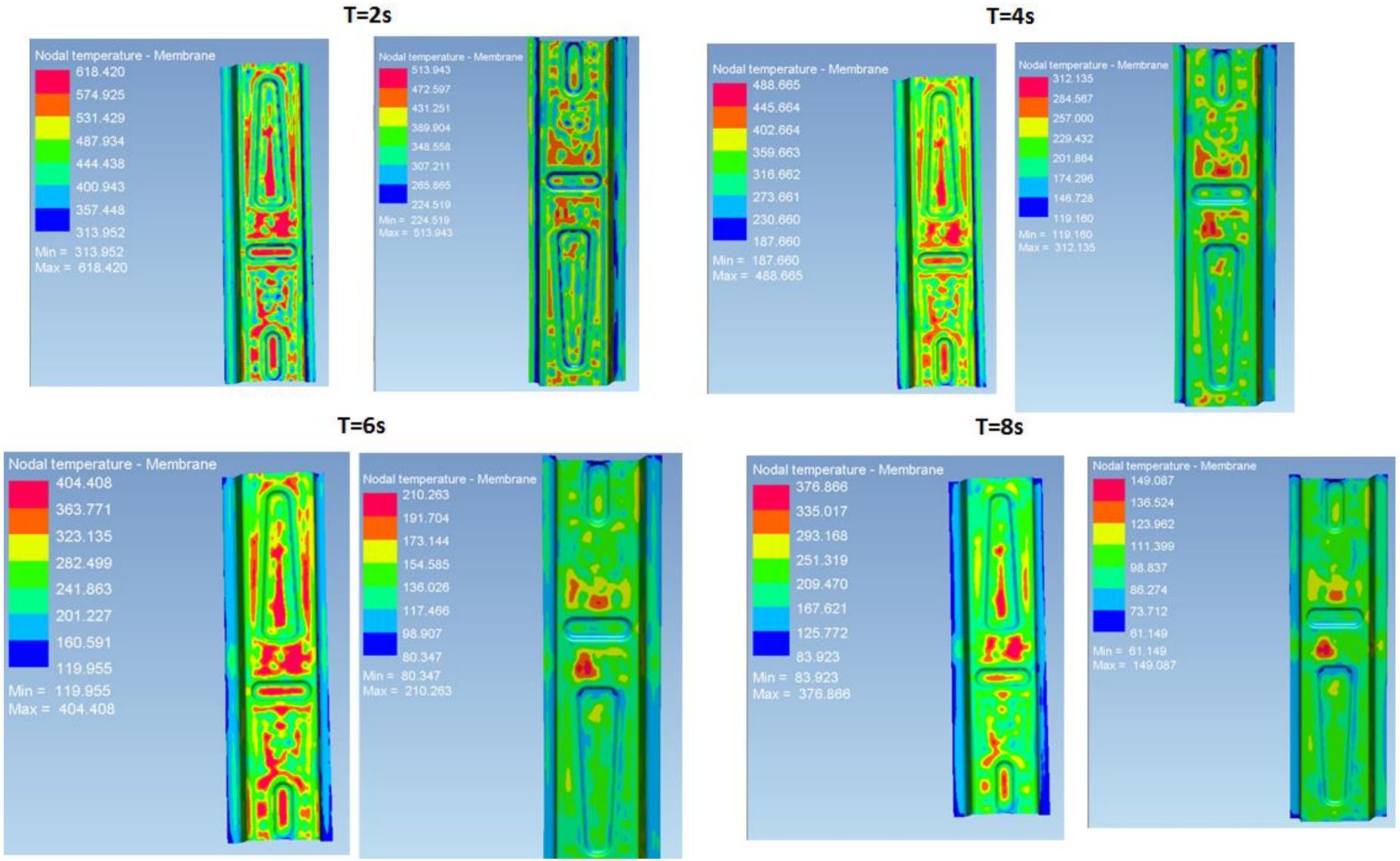


Figure A2.5: Temperature map for 2-8 s in cycle 5

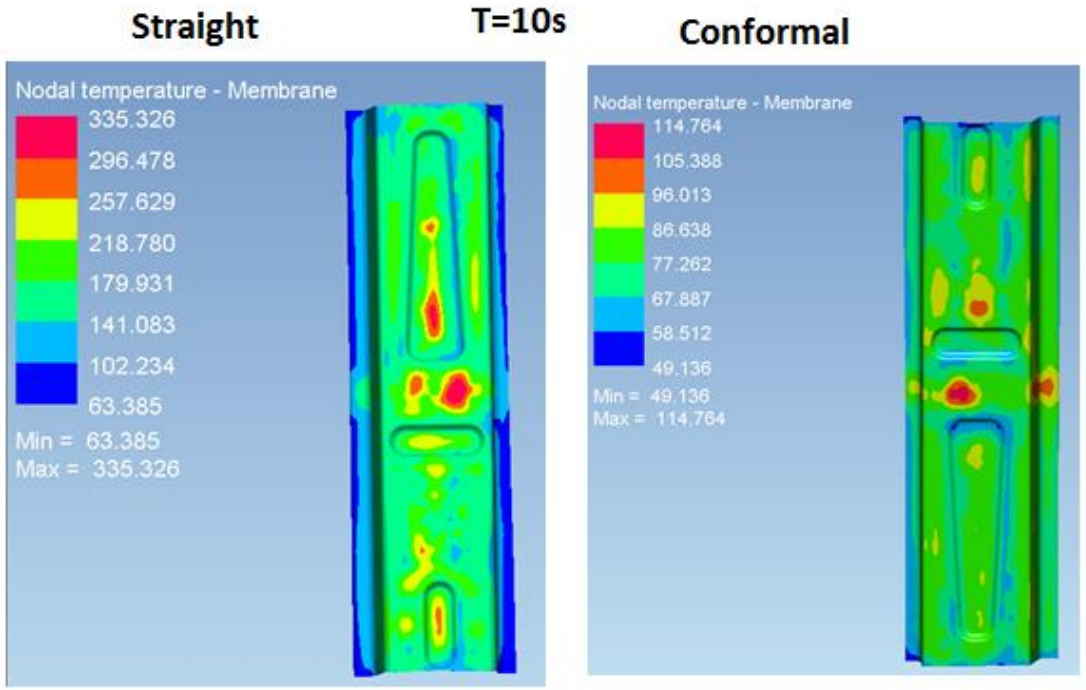


Figure A2.6: Temperature map for 10 s in cycle 5

## A3: Temperature map simulation results for punch

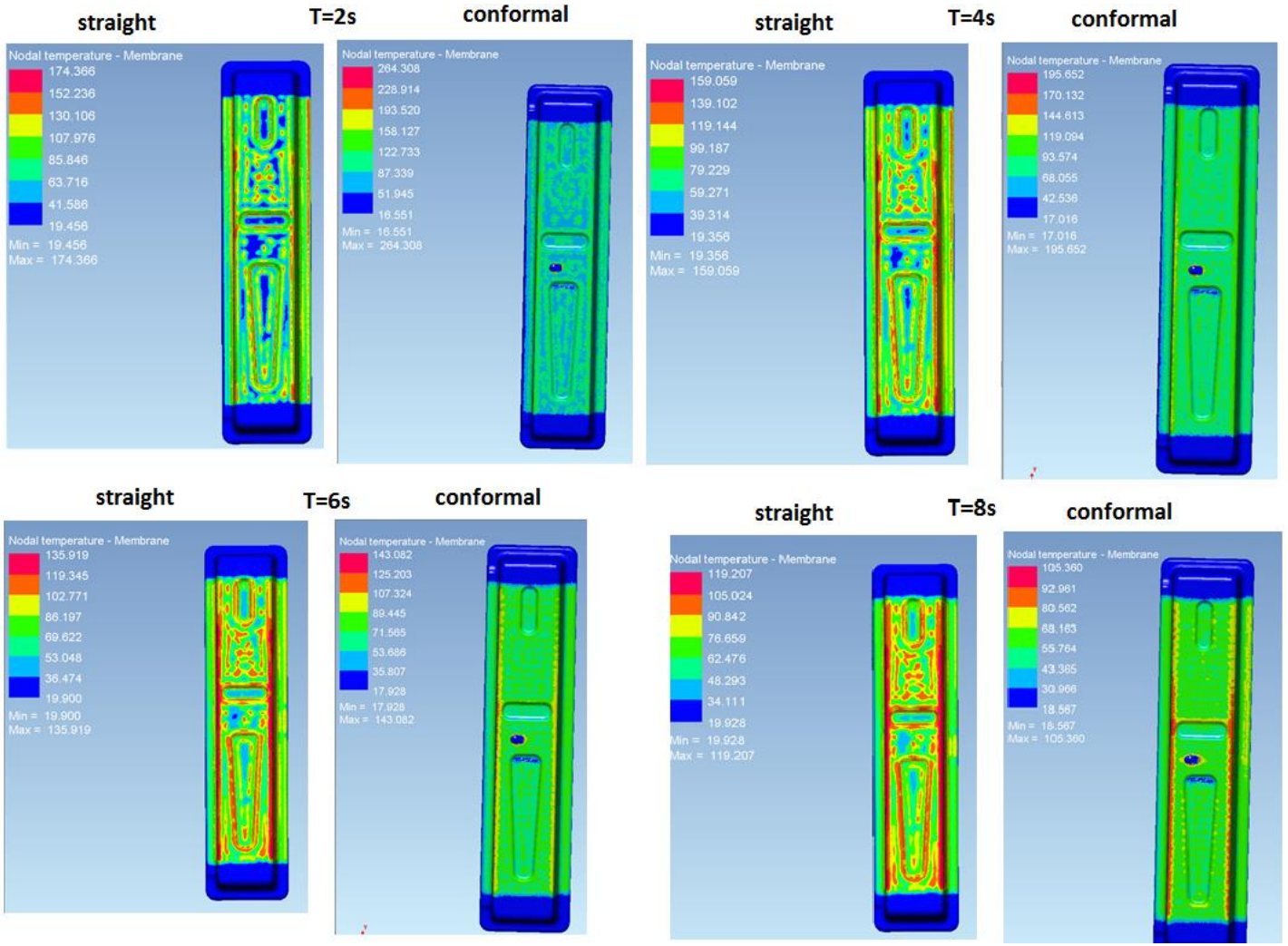


Figure A3.1: Temperature map for 2-8 s in cycle 1

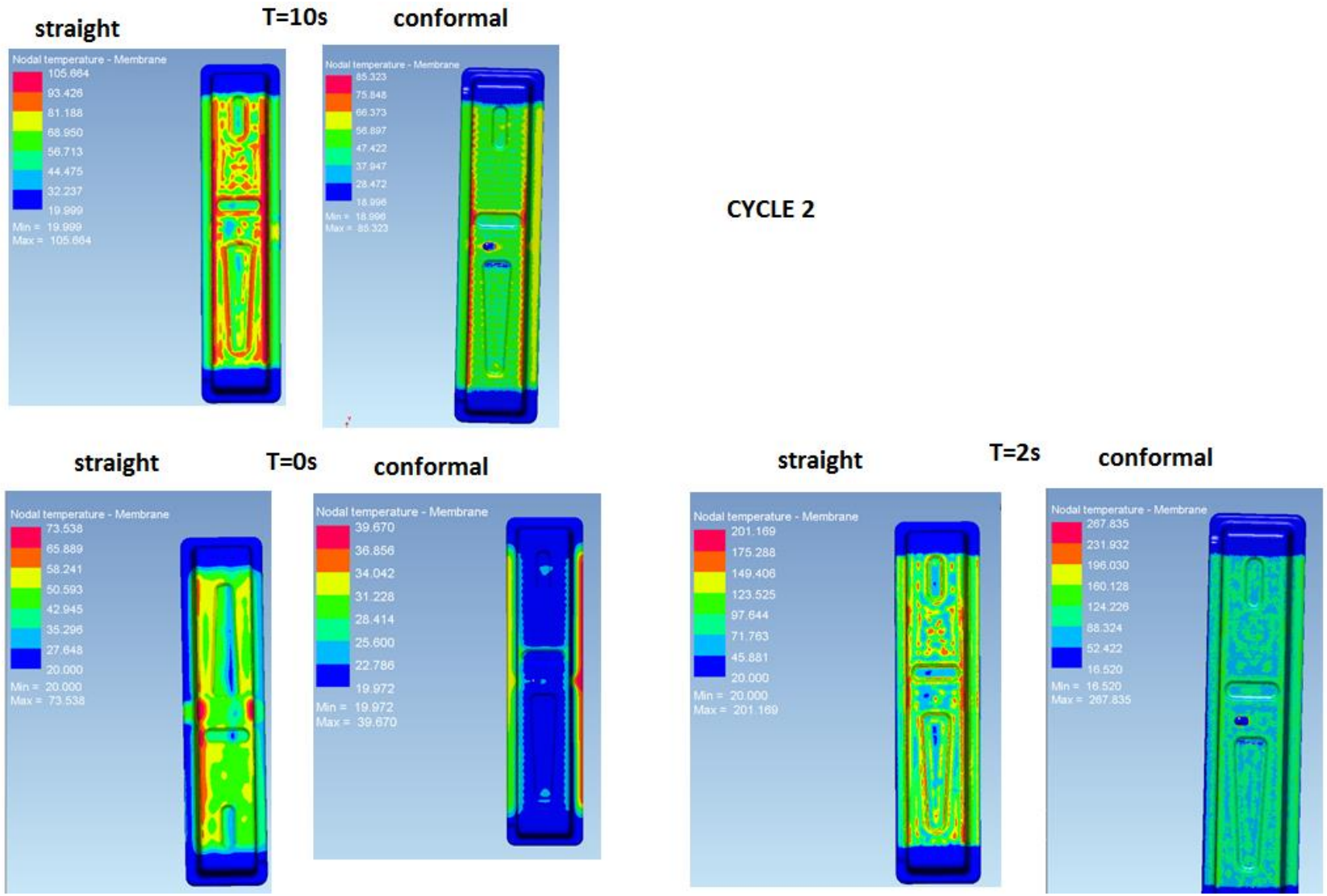


Figure A3.2: Temperature map for 10 s in cycle 1 (top), 0 and 2s in cycle 2

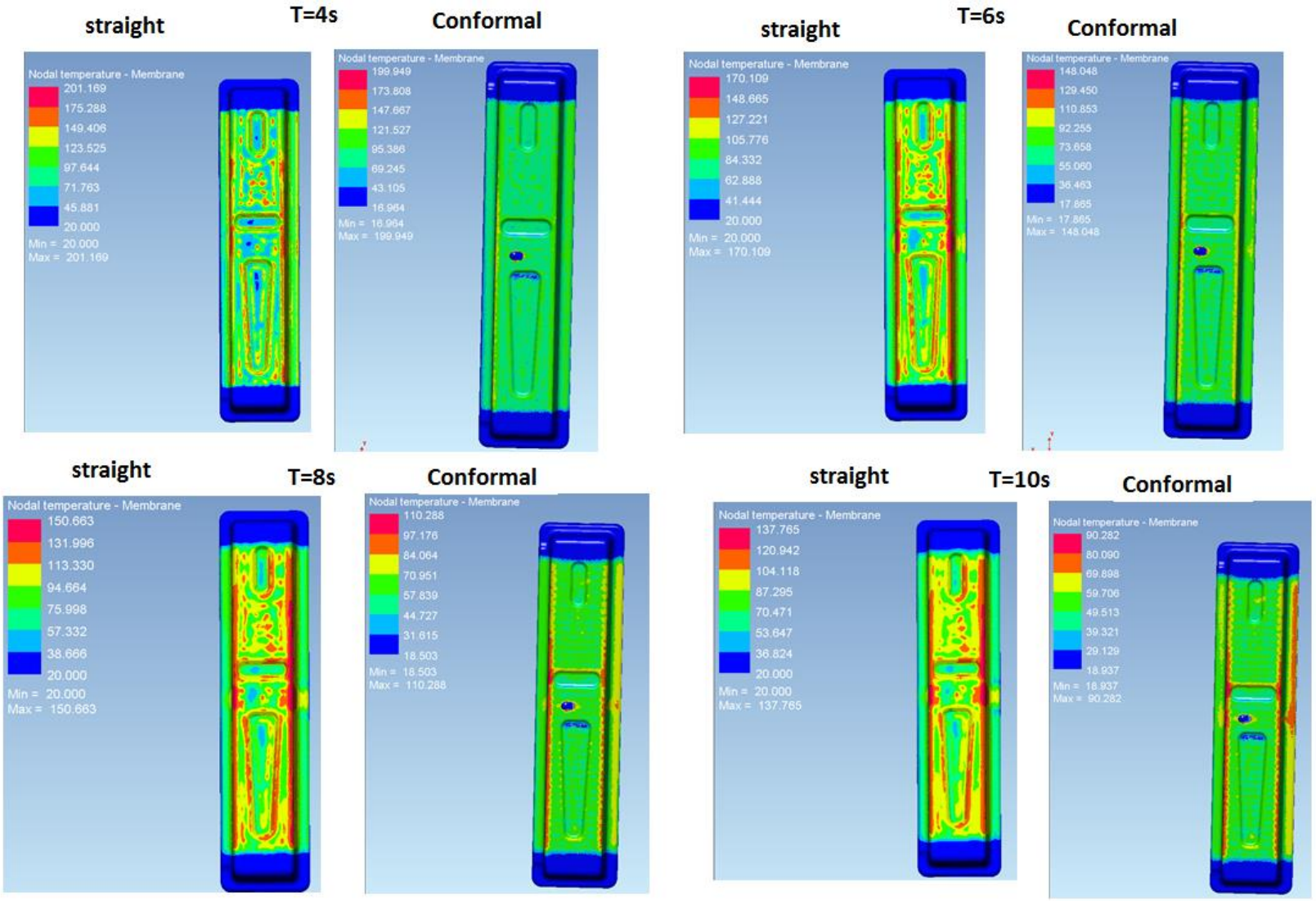


Figure A3.3: Temperature map for 4-10 s in cycle 2

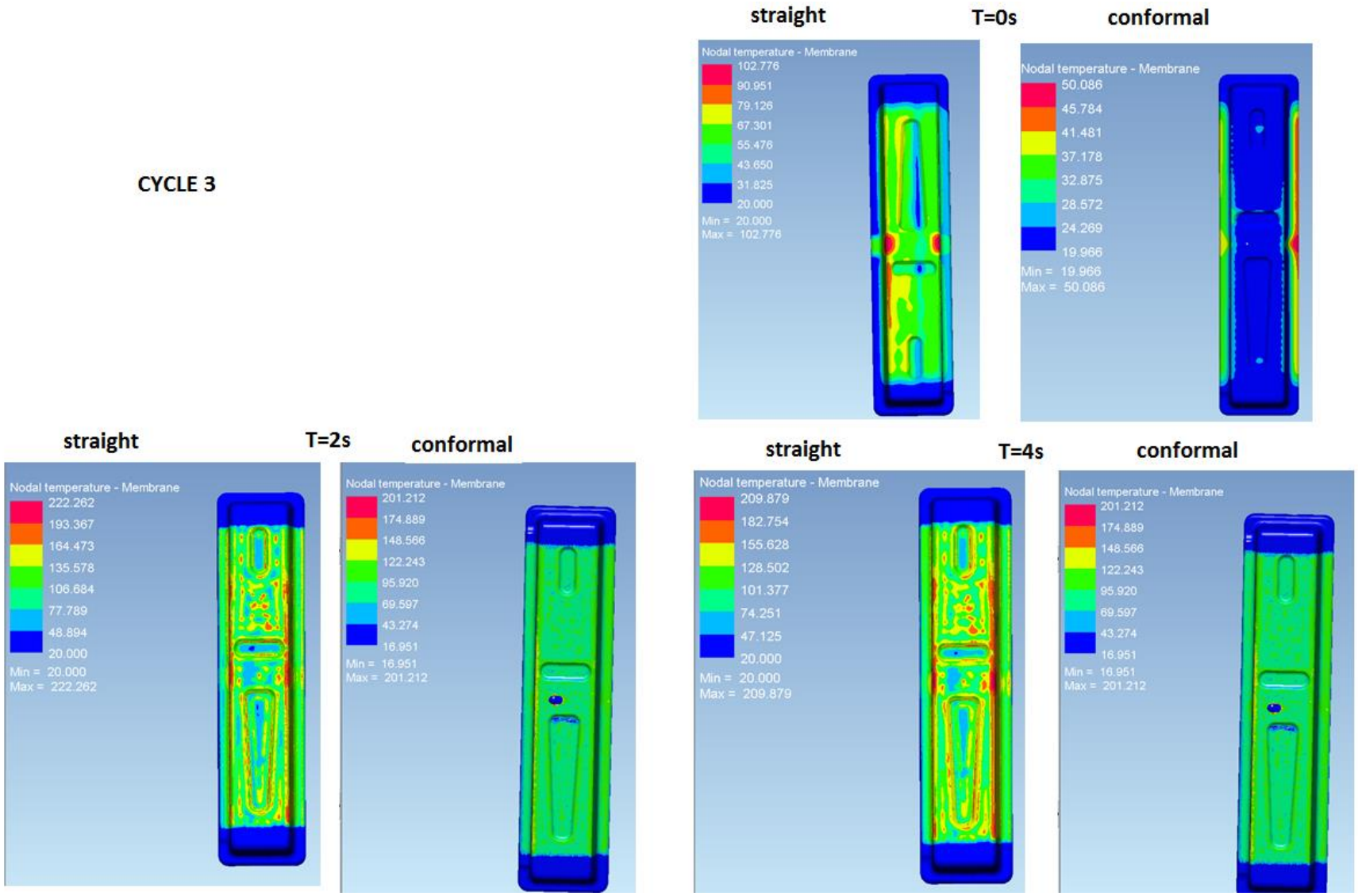


Figure A3.4: Temperature map for 0-4 s in cycle 3

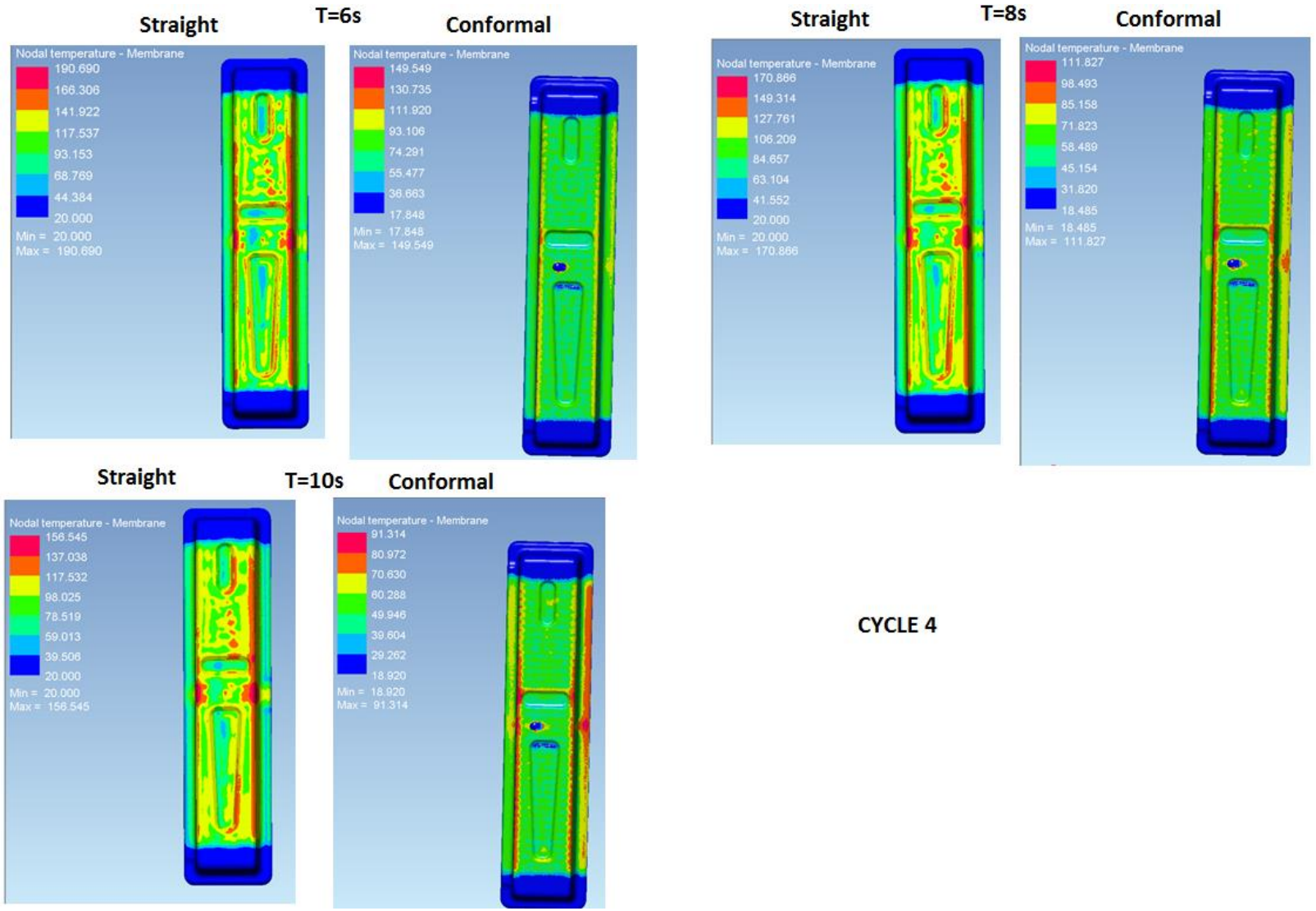


Figure A3.5: Temperature map for 6-10 s in cycle 3

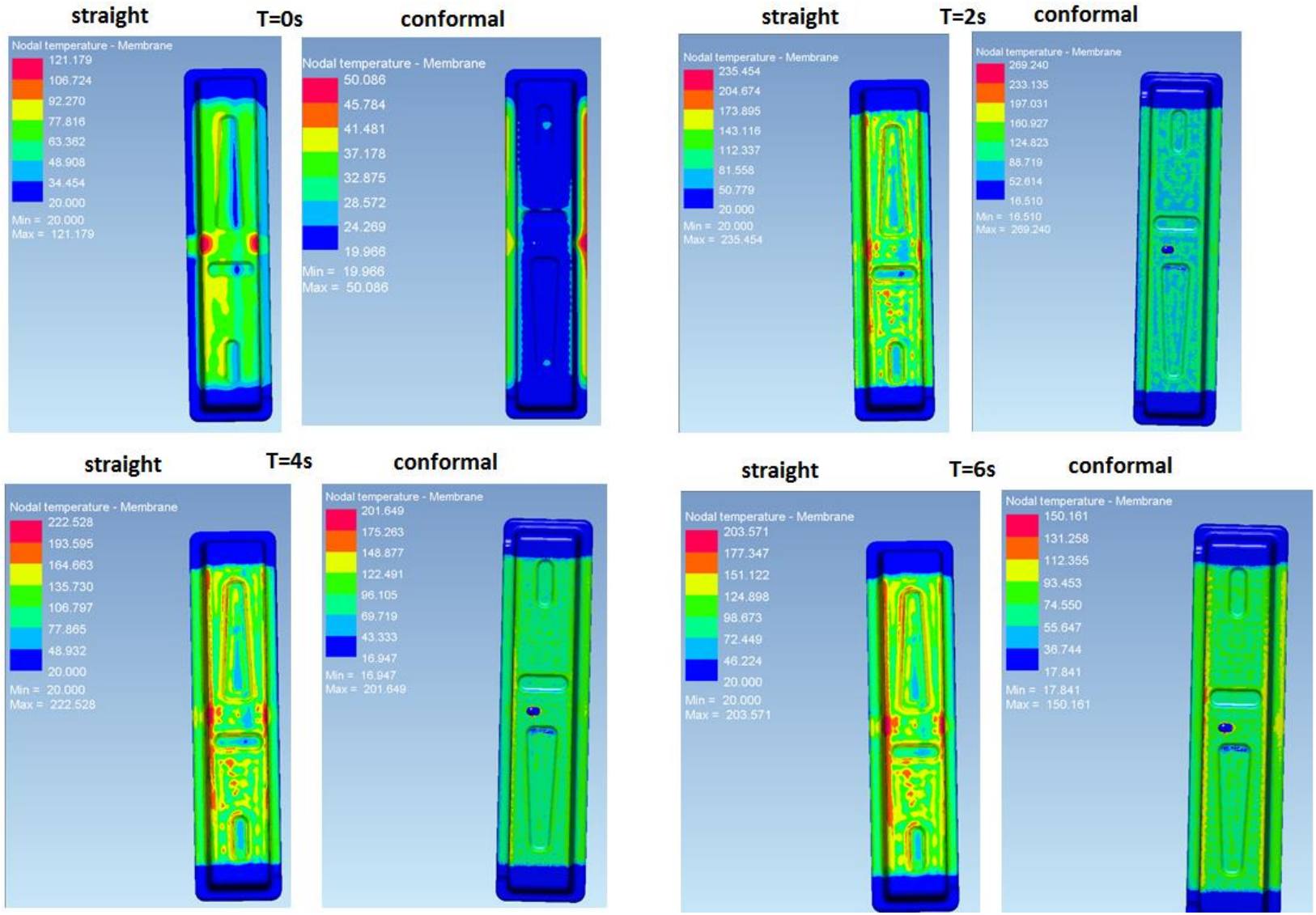


Figure A3.6: Temperature map for 0-6 s in cycle 4

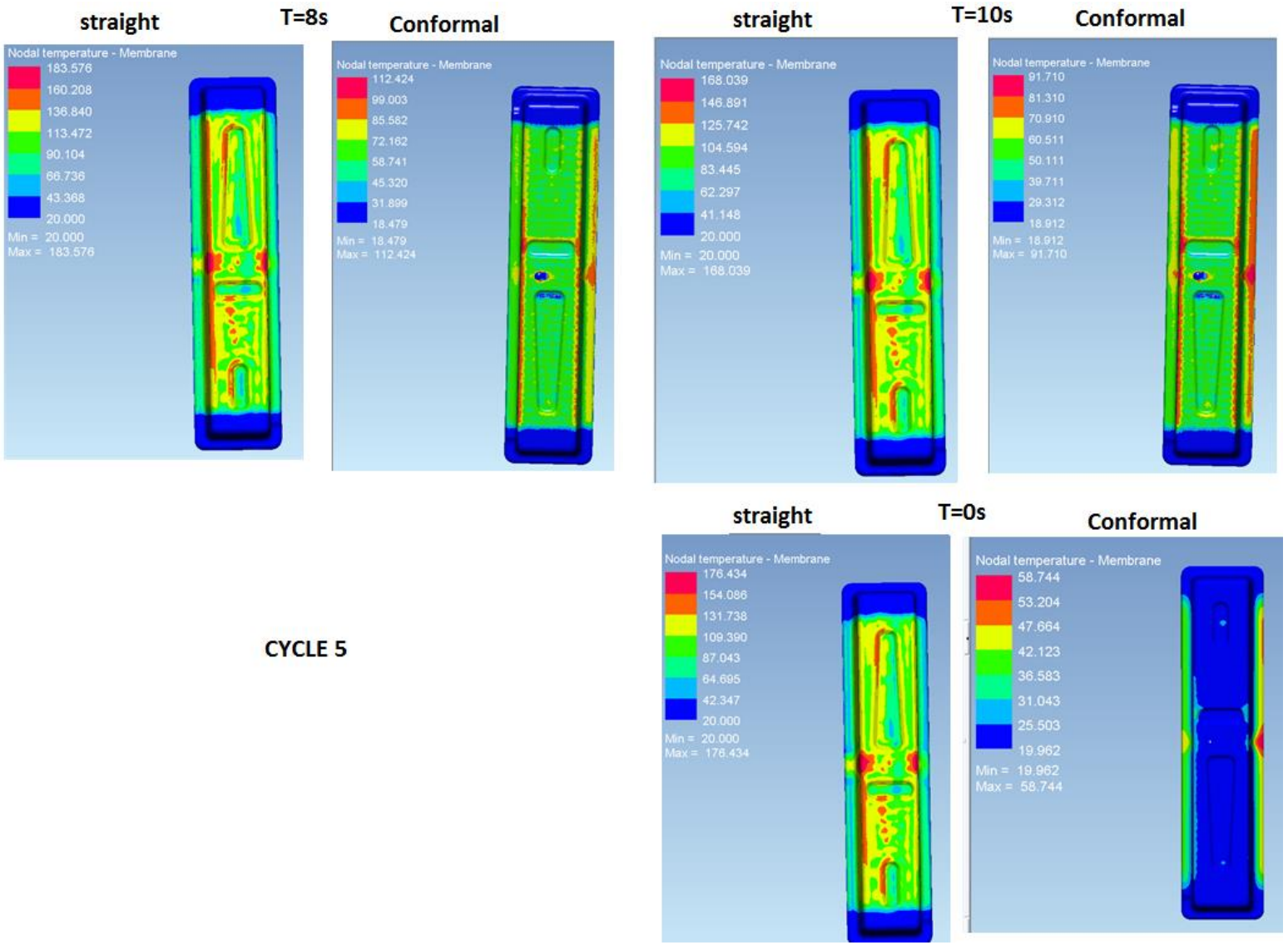


Figure A3.7: Temperature map for 8-10 s in cycle 4 and 0s in cycle 5

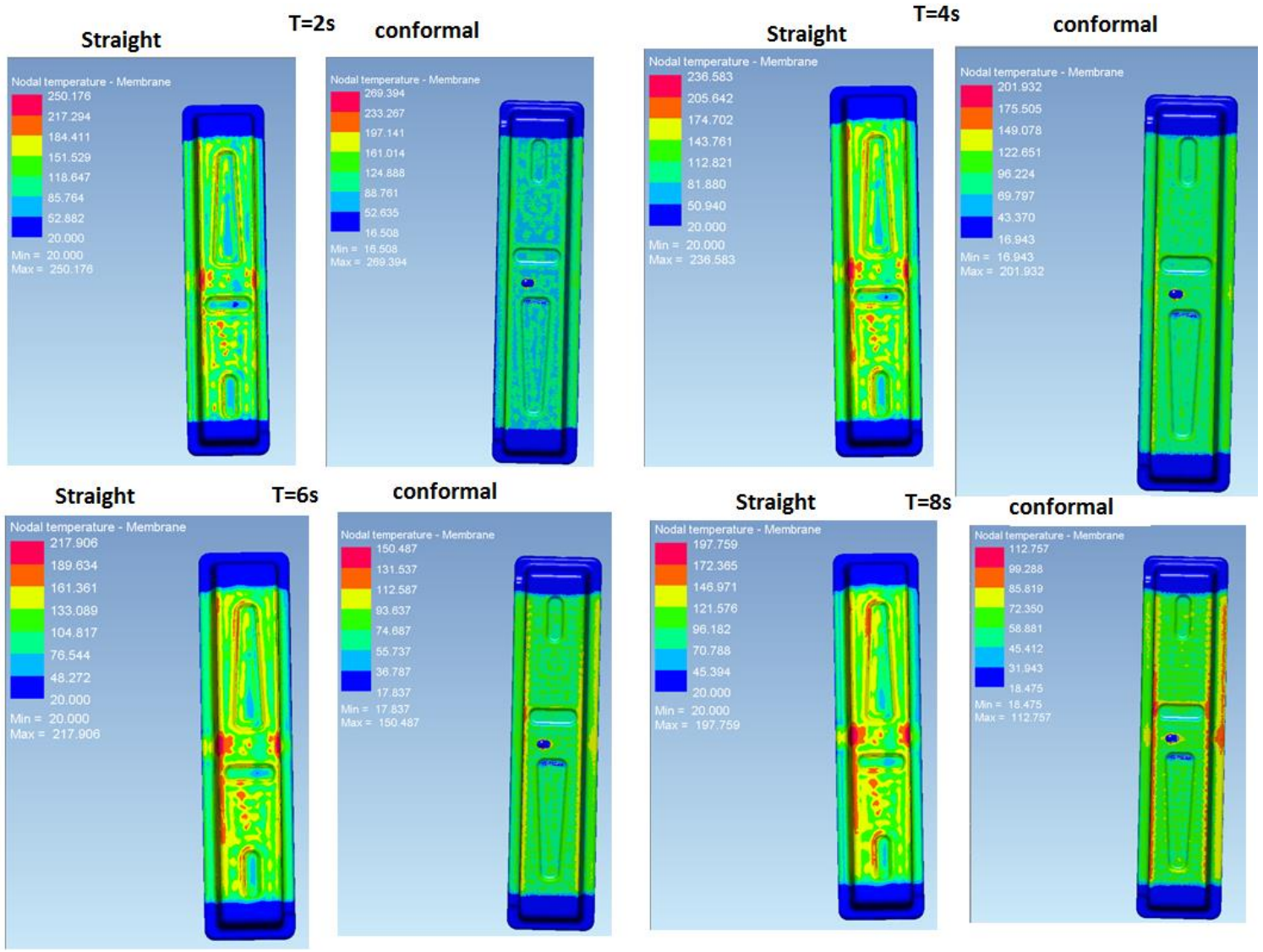


Figure A3.7: Temperature map for 2-8 s in cycle 5

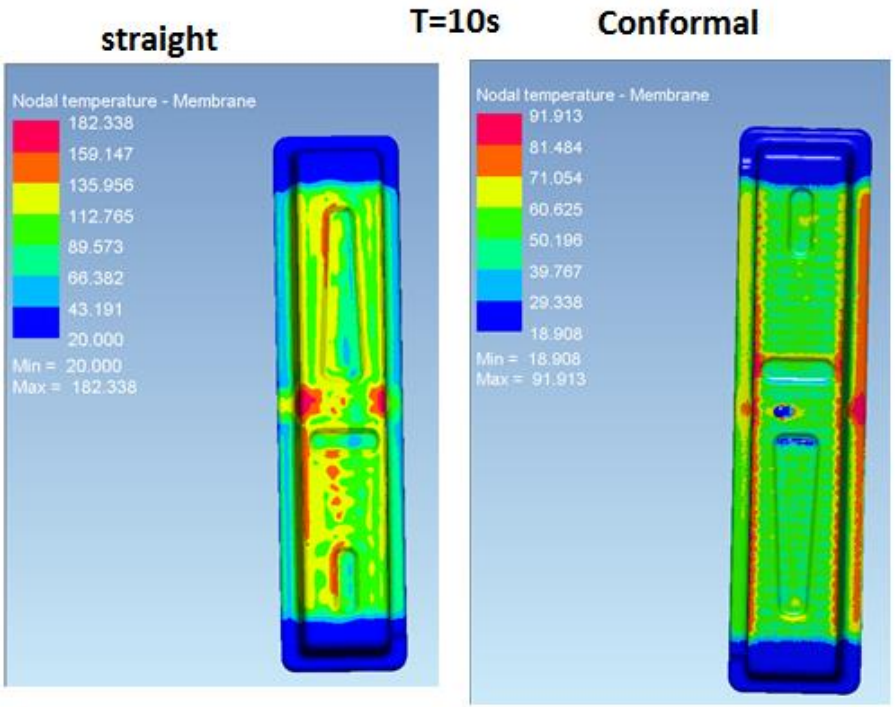


Figure A3.8: Temperature map for 10 s in cycle 5

## A4: Hardness map results for blank

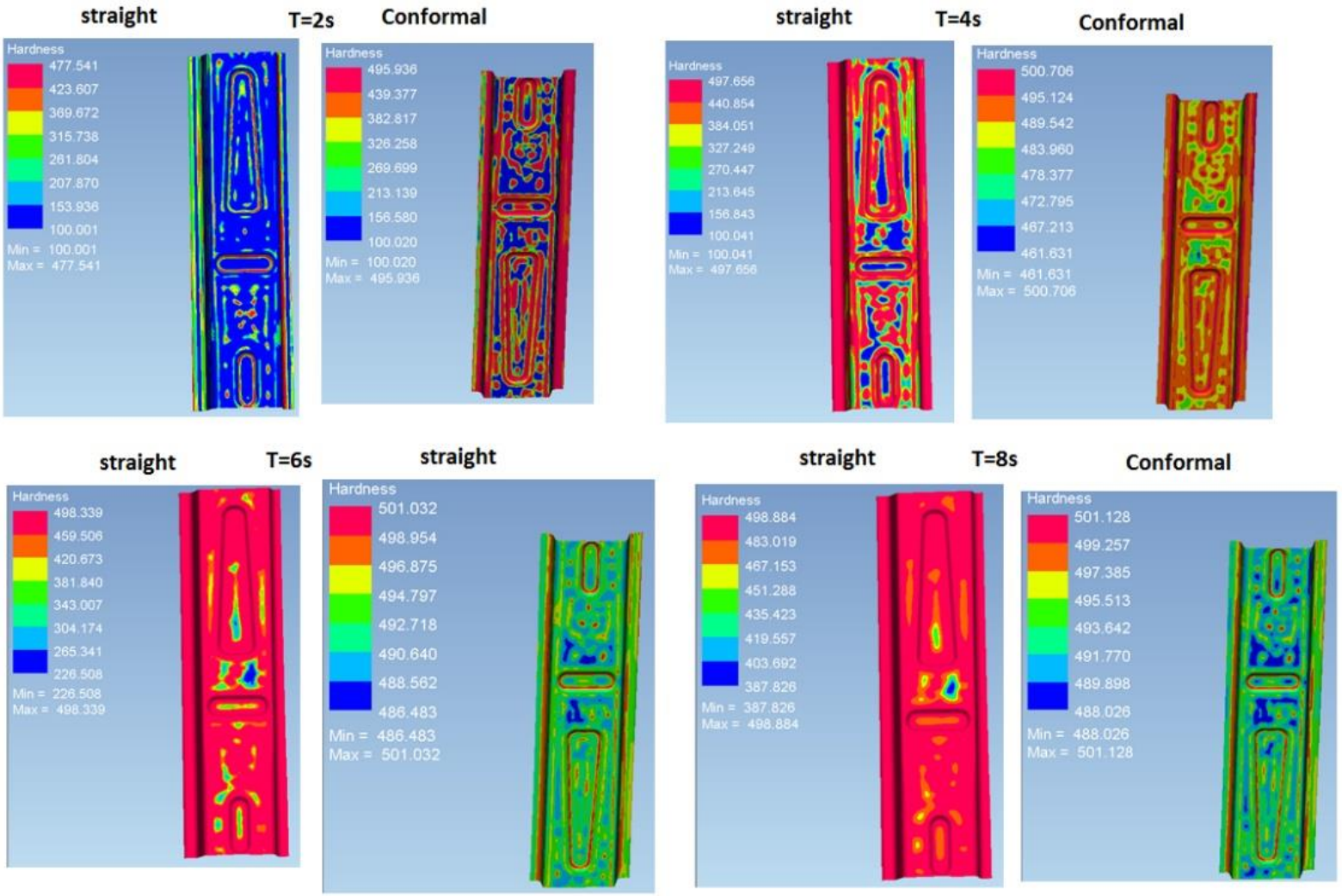


Figure A4.1: Hardness map for 2-8 s in cycle 1

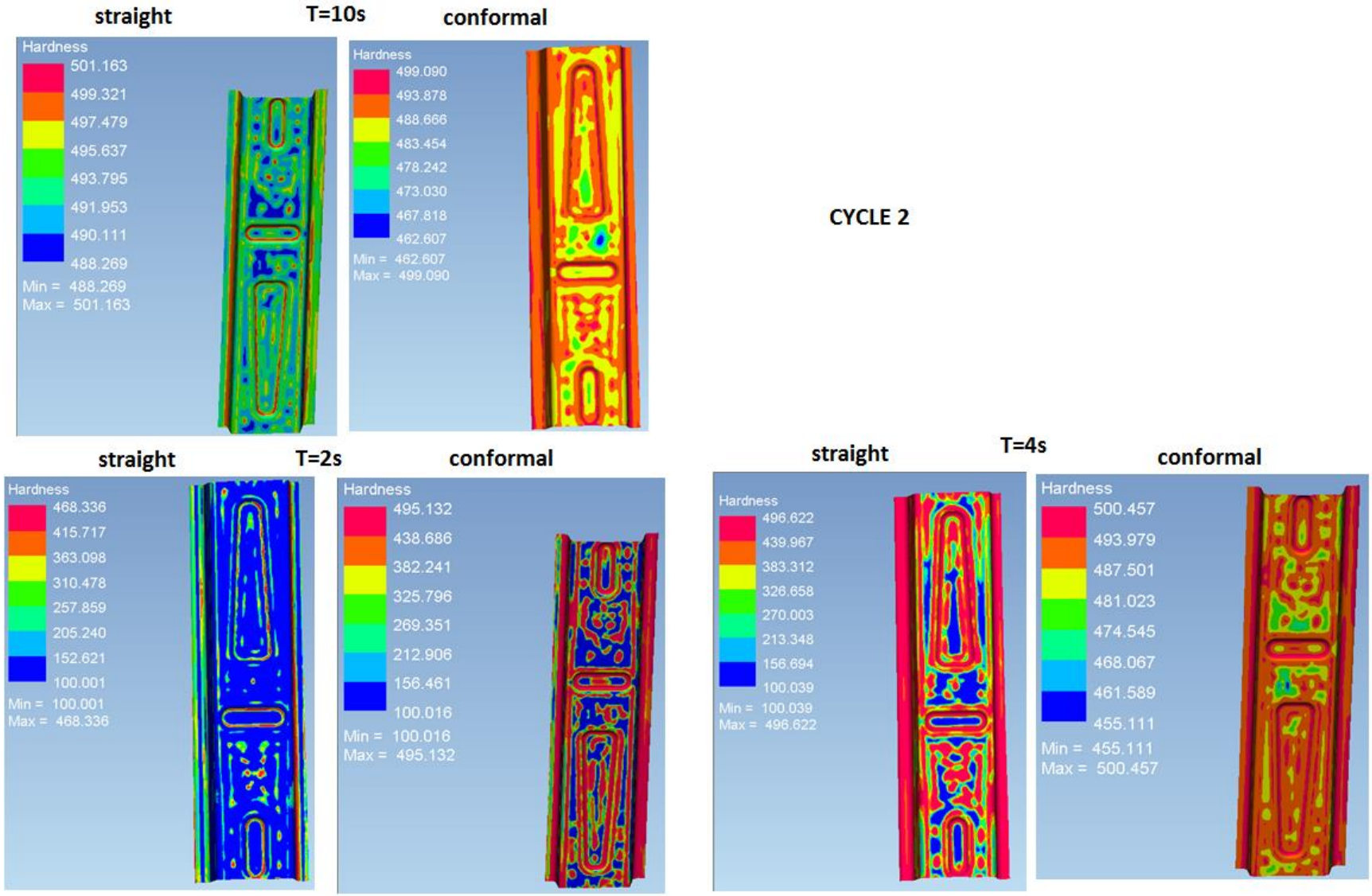


Figure A4.2: Hardness map for 10 s in cycle 1 (top), 2 and 4s in cycle 2 (bottom)

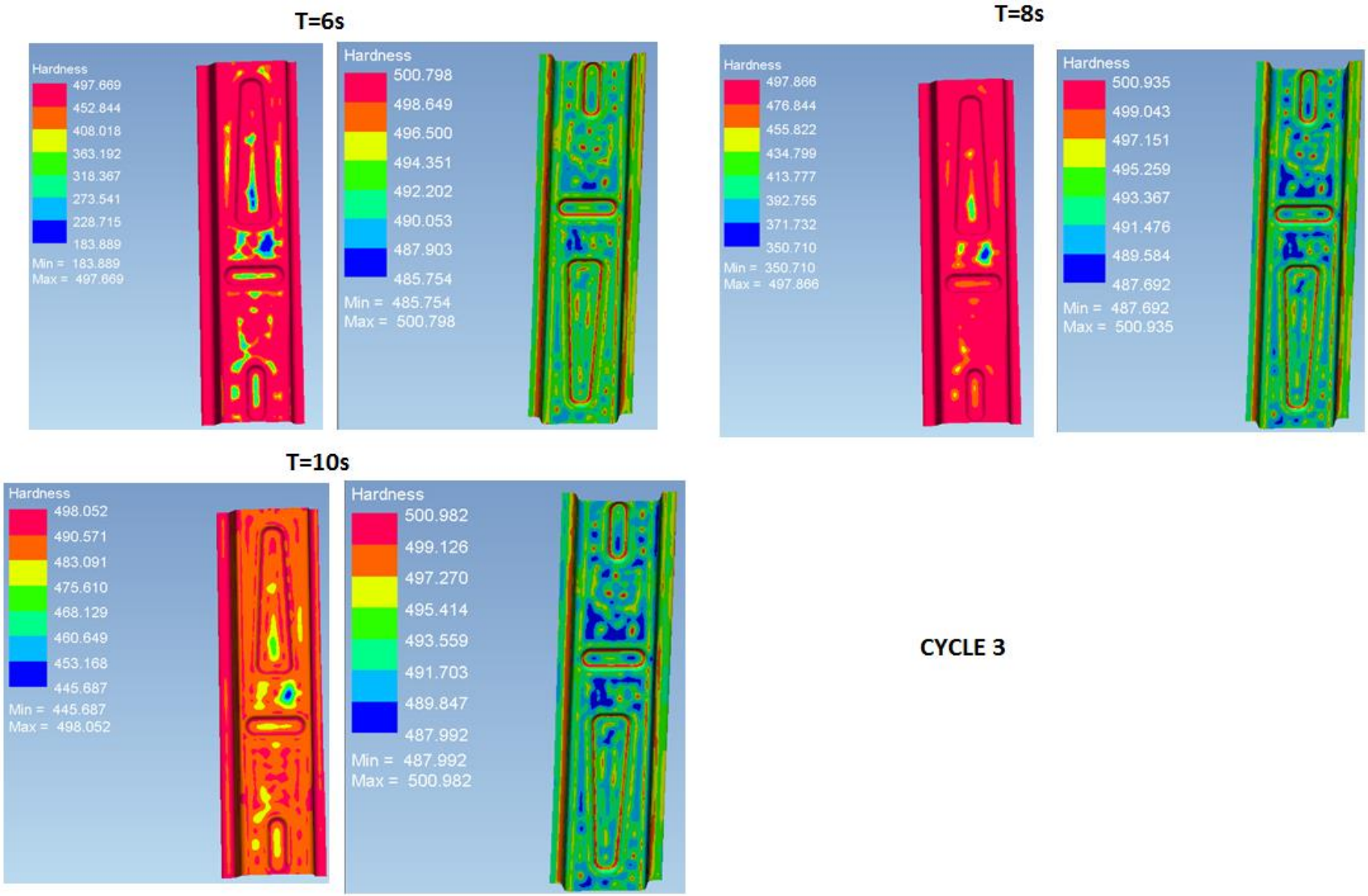


Figure A4.3: Hardness map for 6-10 s in cycle 2

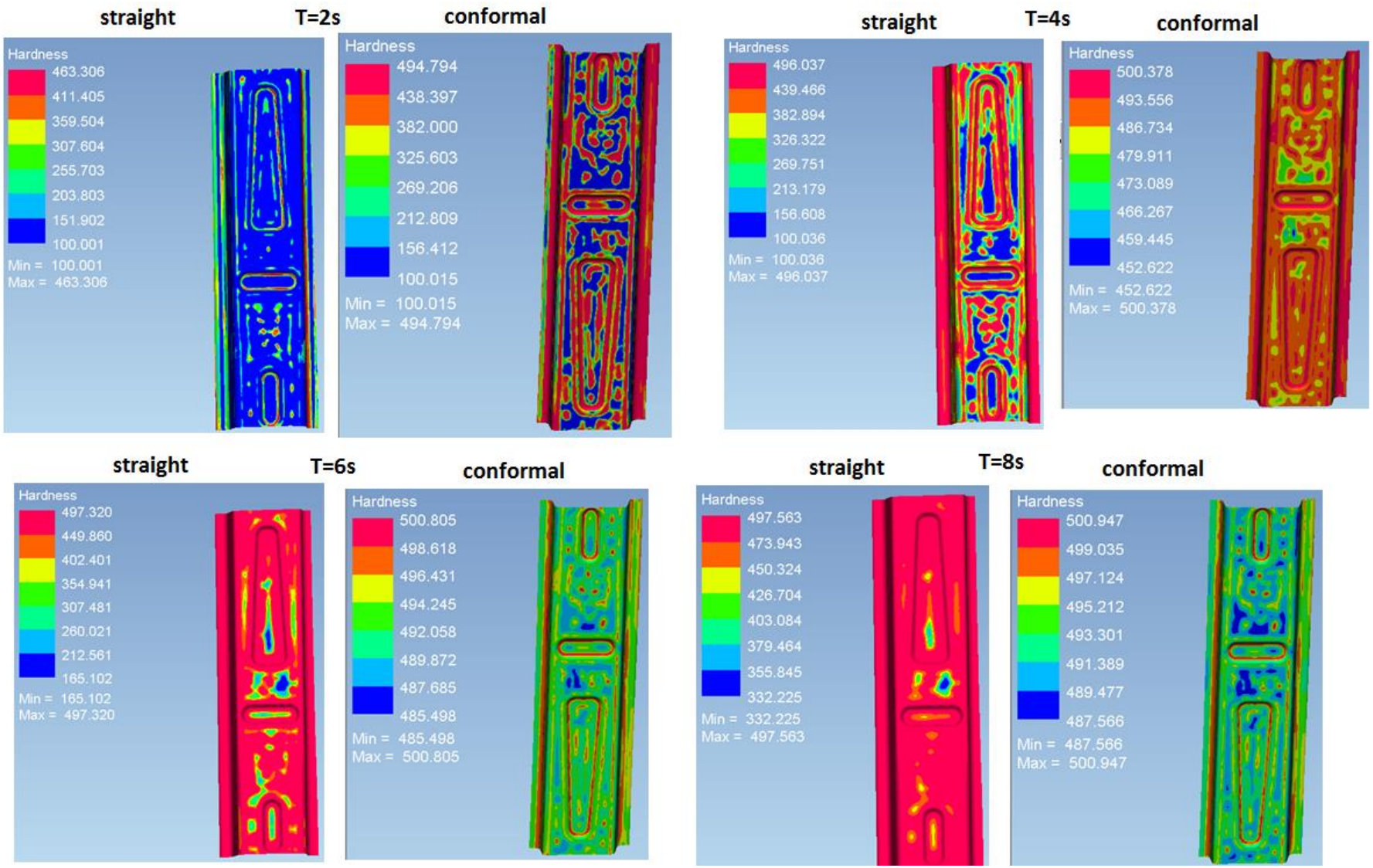


Figure A4.4: Hardness map for 2-8 s in cycle 3

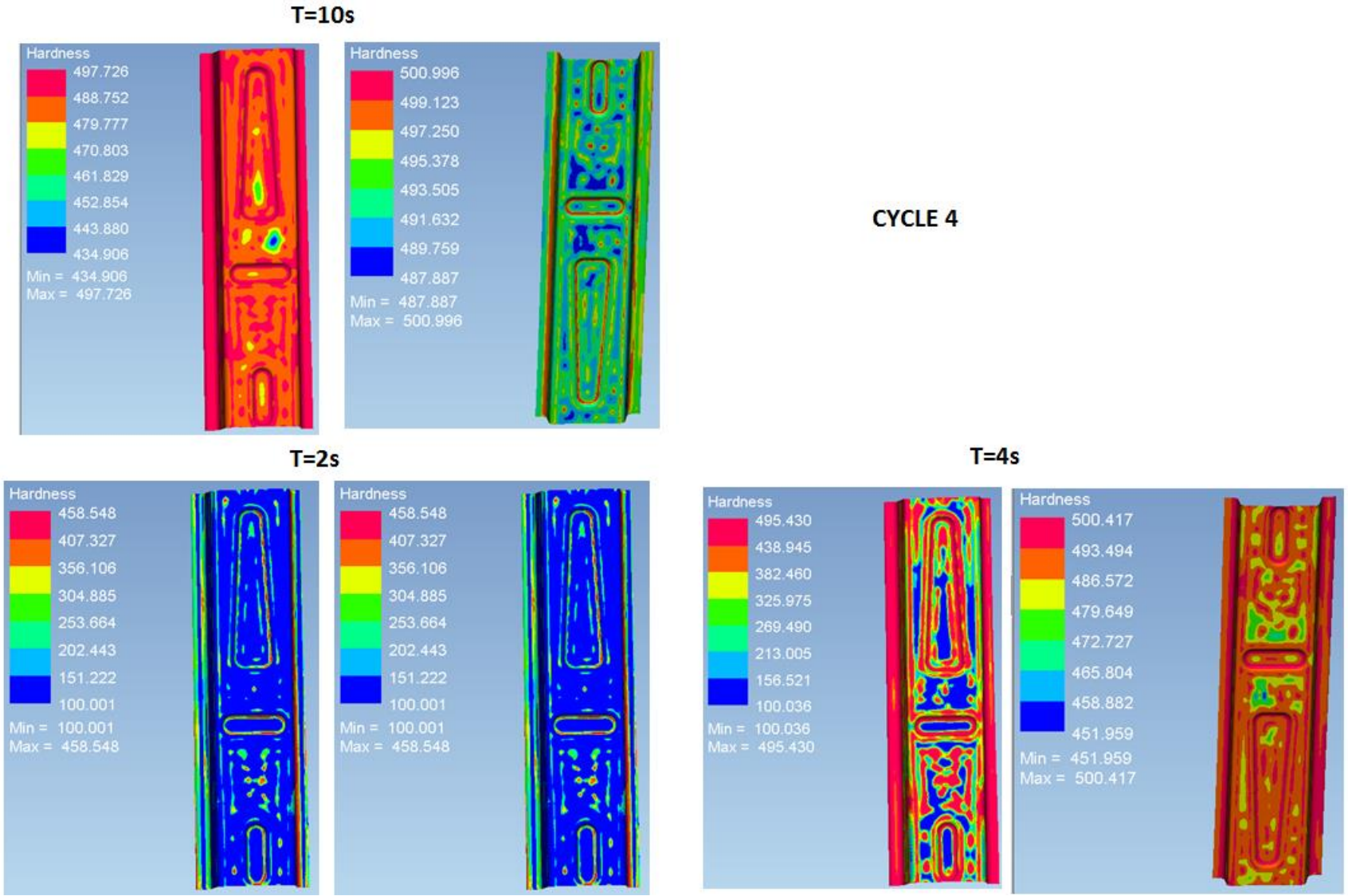


Figure A4.5: Hardness map for 10 s in cycle 3 (top), 2 and 4 s in cycle 4 (bottom)

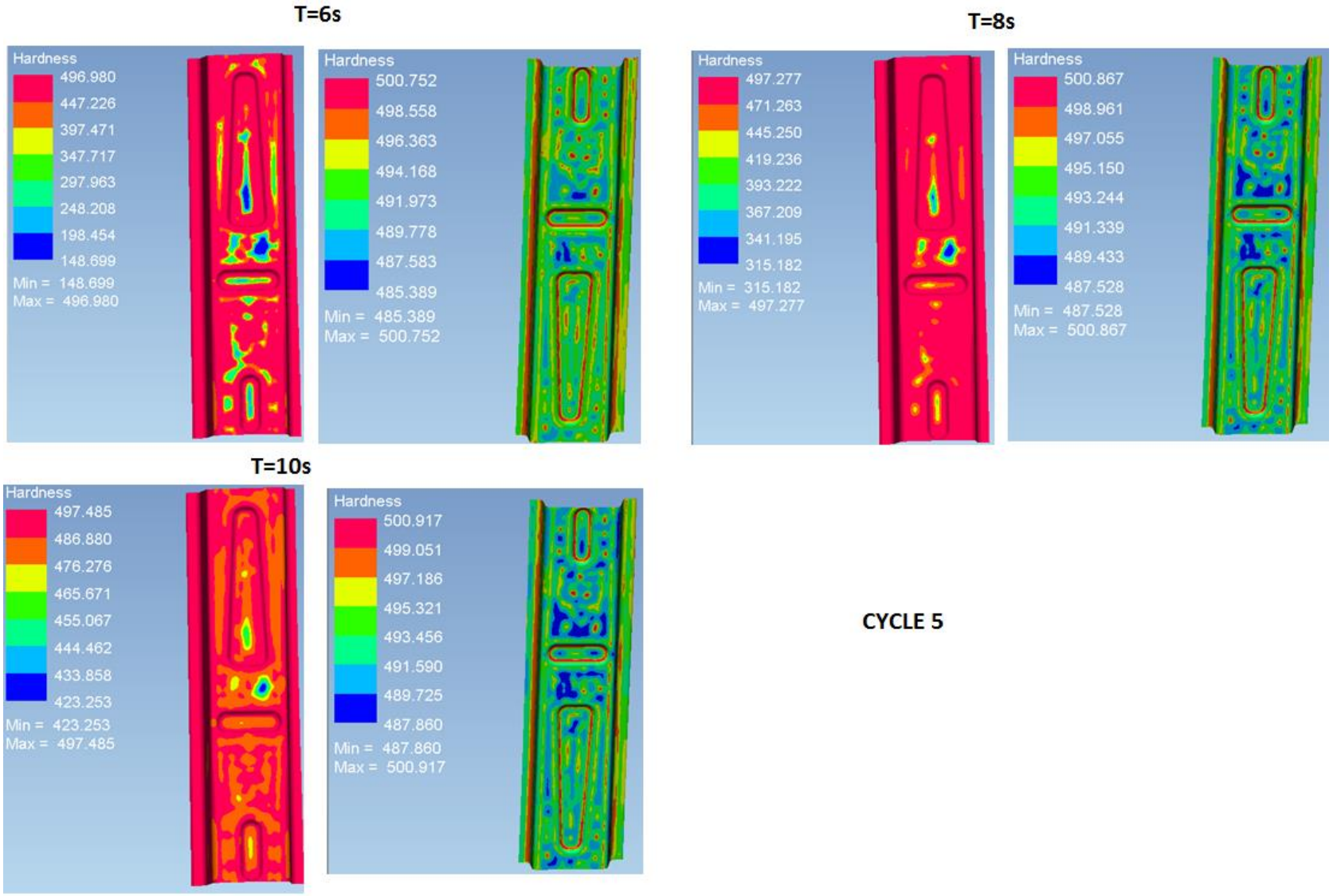


Figure A4.6: Hardness map for 6-10 in cycle 4

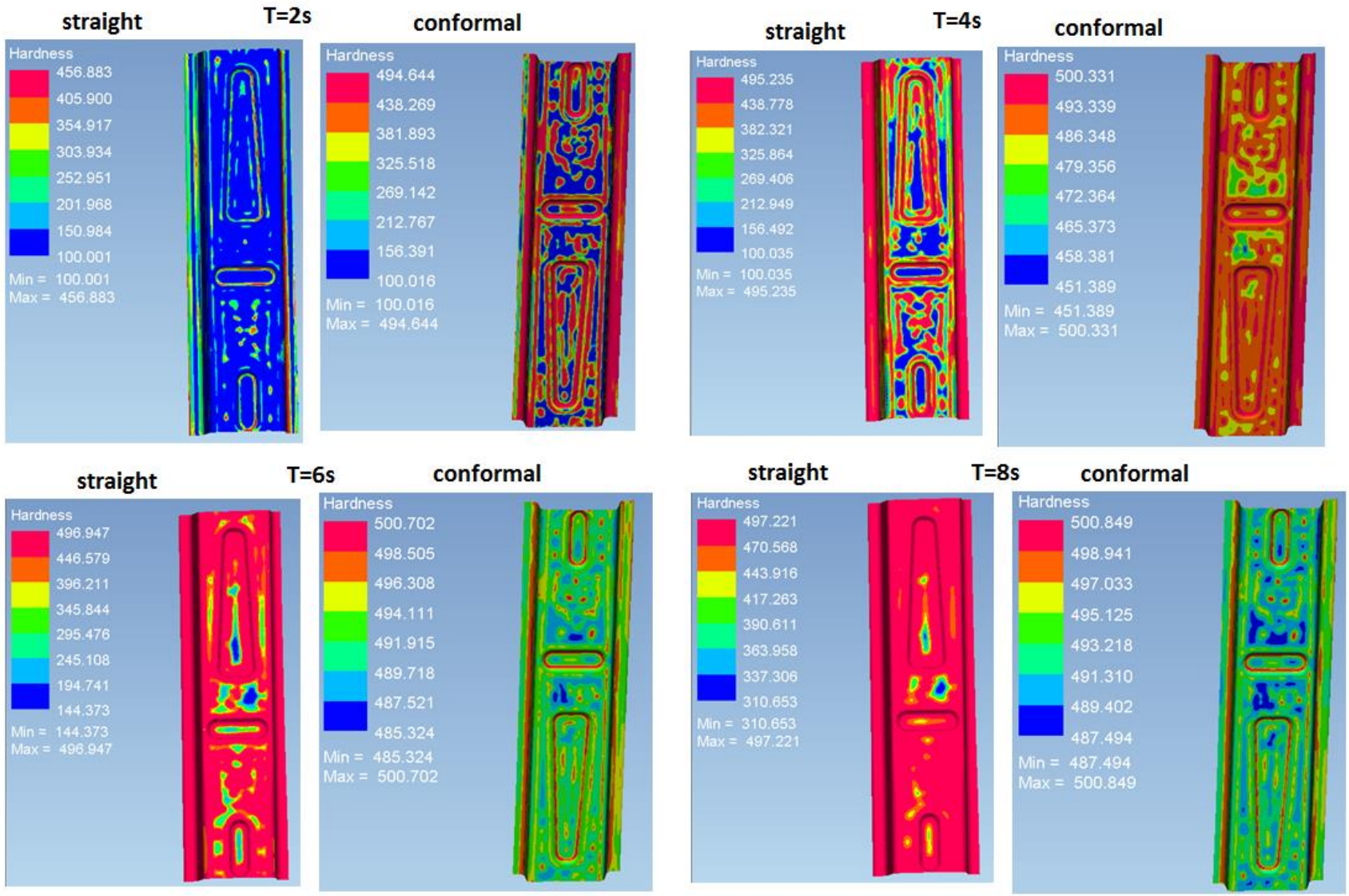


Figure A4.7: Hardness map for 2-8 in cycle 5

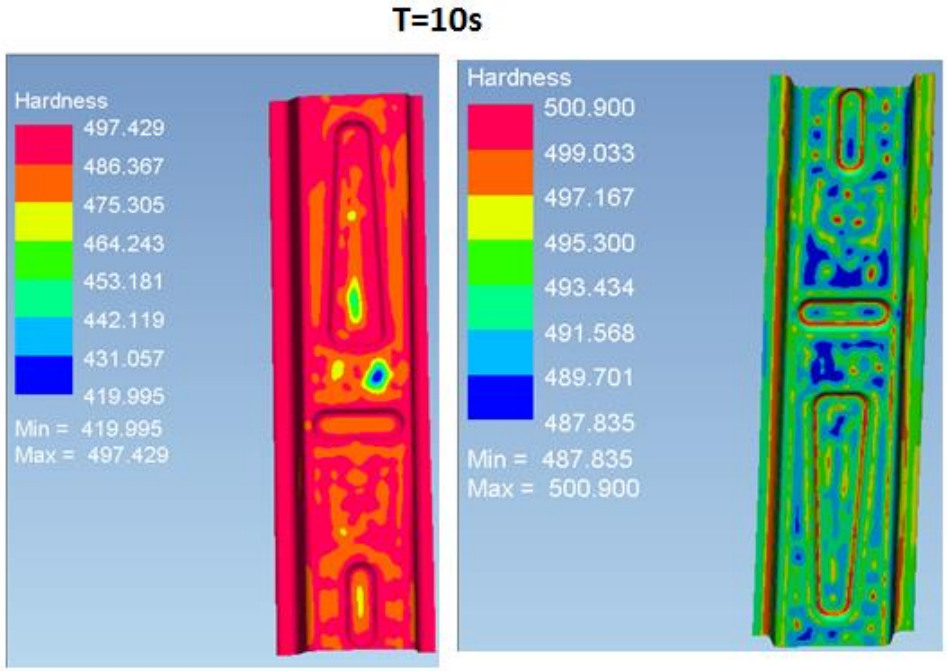


Figure A4.7: Hardness map for 10 s in cycle 5

## A5: Temperature curves

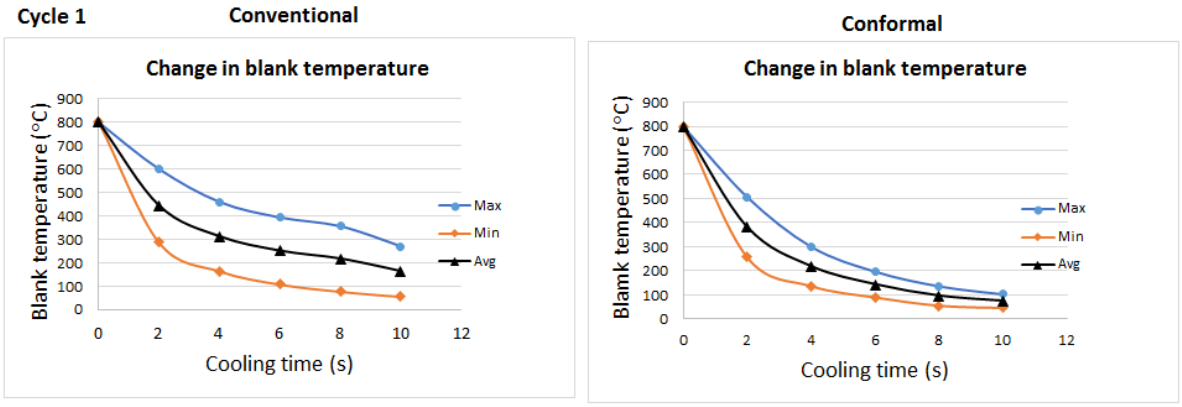


Figure A5:1 Temperature curves for conventional (left) and conformal (right) layout (cycle 1)

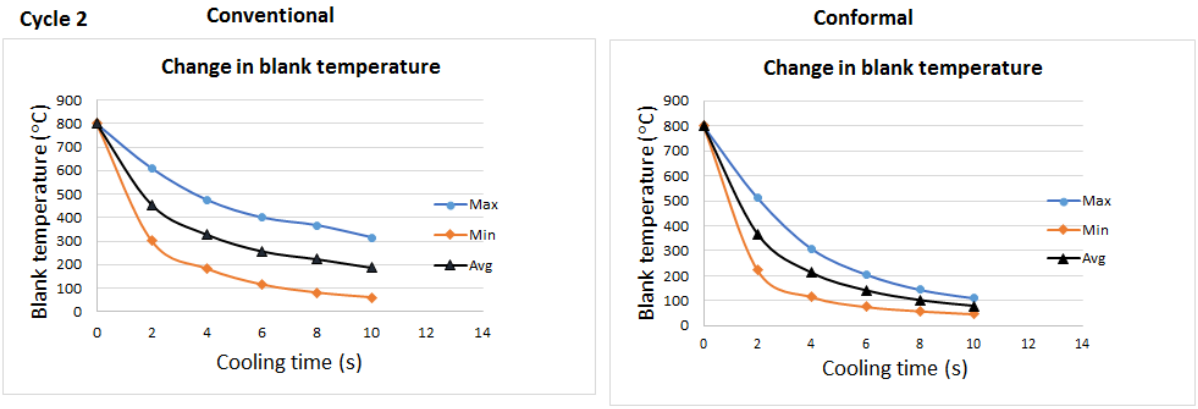


Figure A5.2 Temperature curves for conventional (left) and conformal (right) layout (cycle 2)

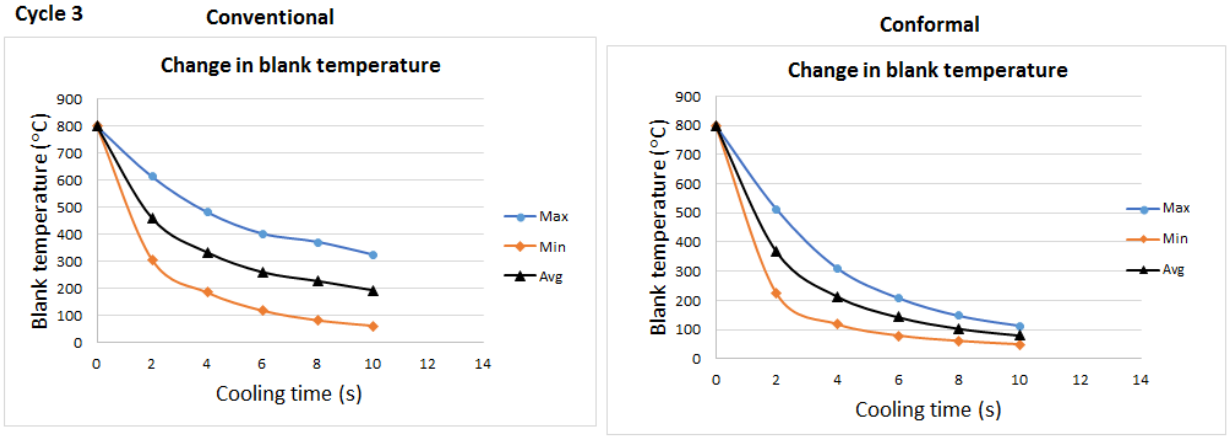


Figure A5.3: Temperature curves for conventional (left) and conformal (right) layout (cycle 3)

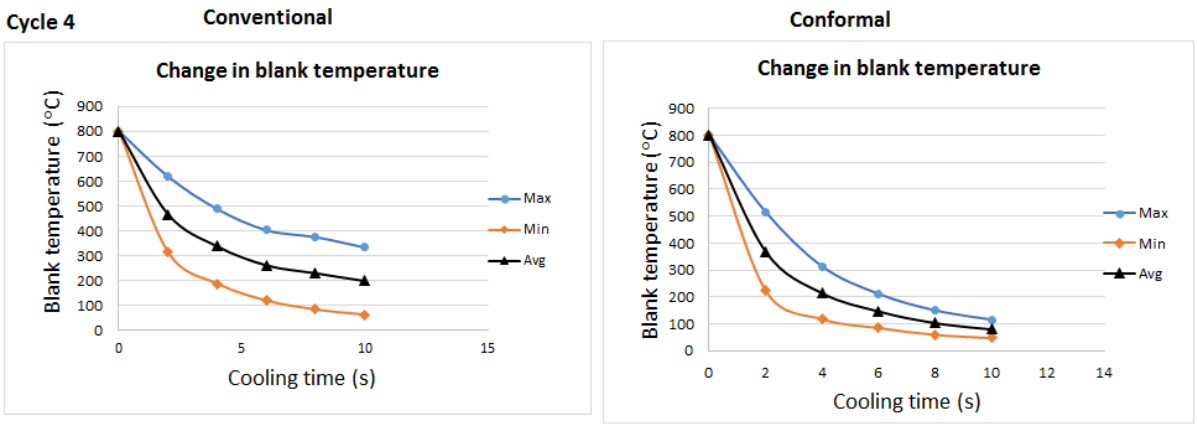


Figure A5.4: Temperature curves for conventional (left) and conformal (right) layout (cycle 4)

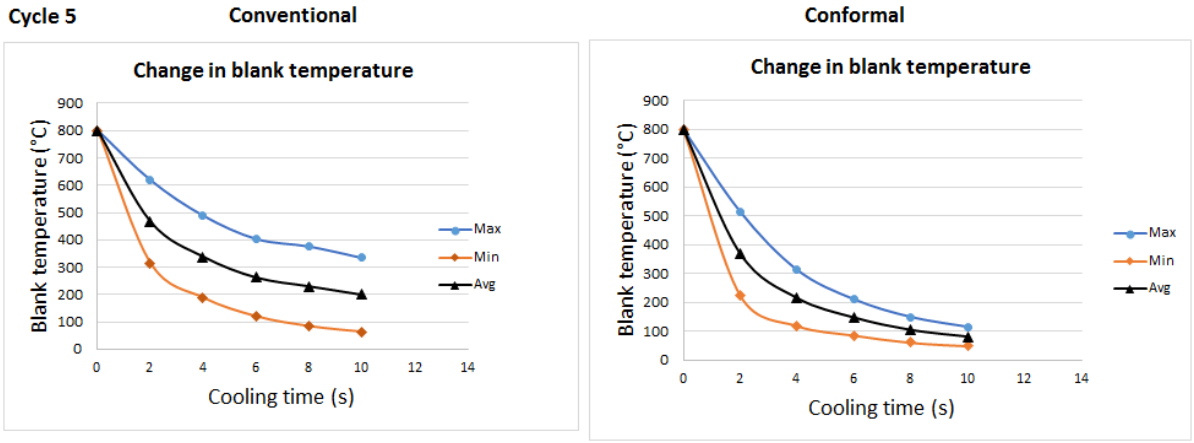


Figure A5.5: Temperature curves for conventional (left) and conformal (right) layout (cycle 5)

## A6: Hardness curves

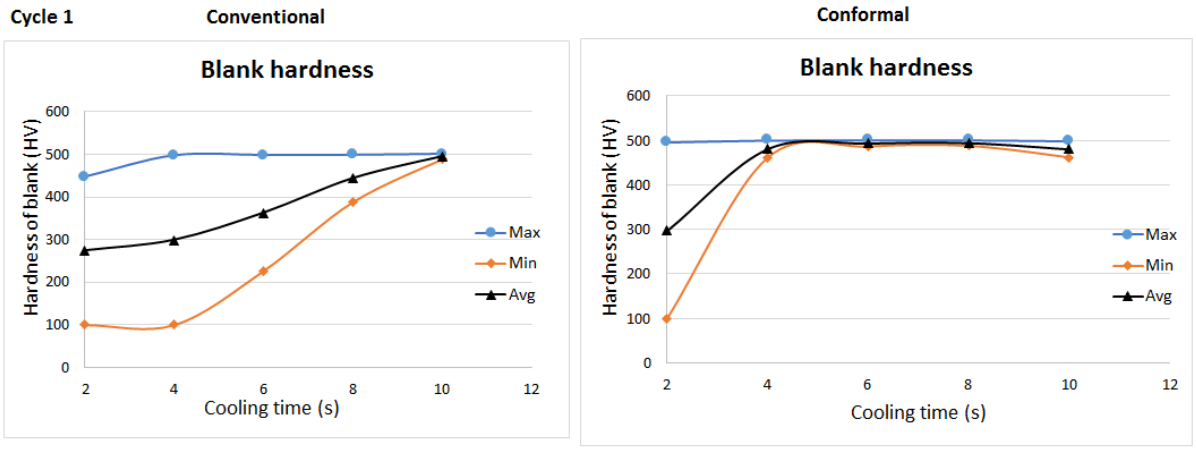


Figure A6.1: Hardness curves for conventional (left) and conformal (right) layout (cycle 1)

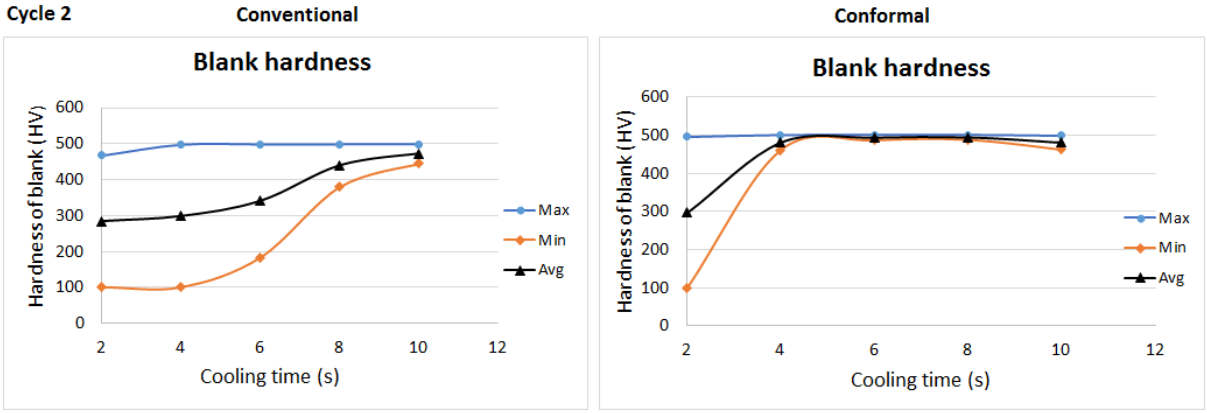


Figure A6.2: Hardness curves for conventional (left) and conformal (right) layout (cycle 2)

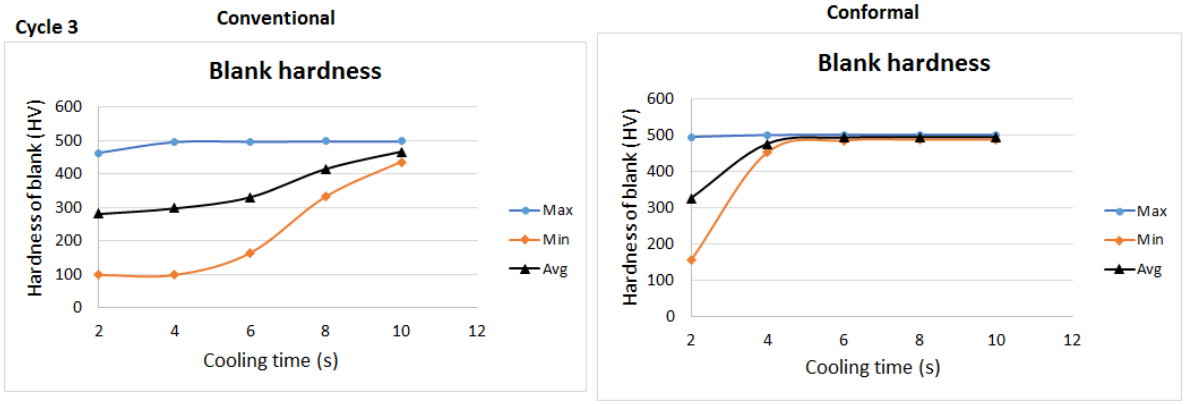


Figure A6.3: Hardness curves for conventional (left) and conformal (right) layout (cycle 3)

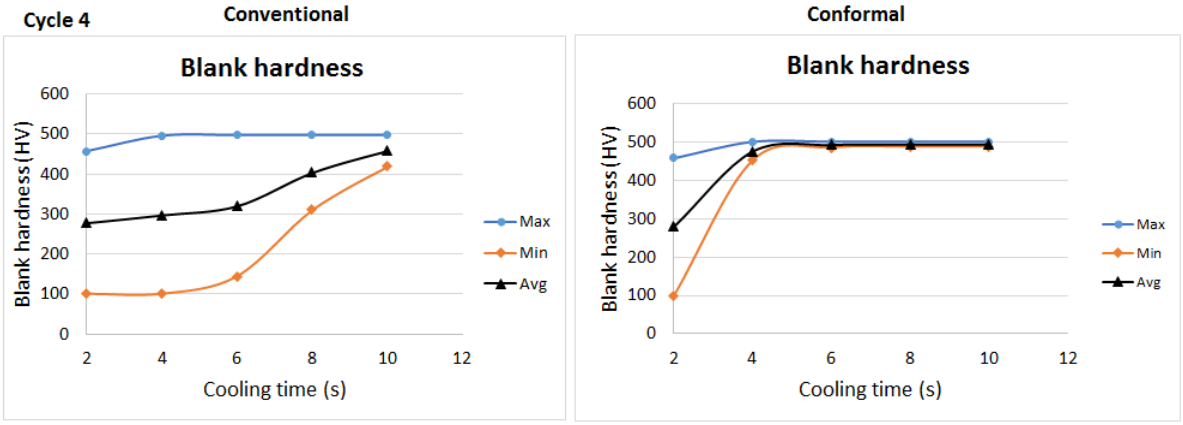


Figure A6.4: Hardness curves for conventional (left) and conformal (right) layout (cycle 4)

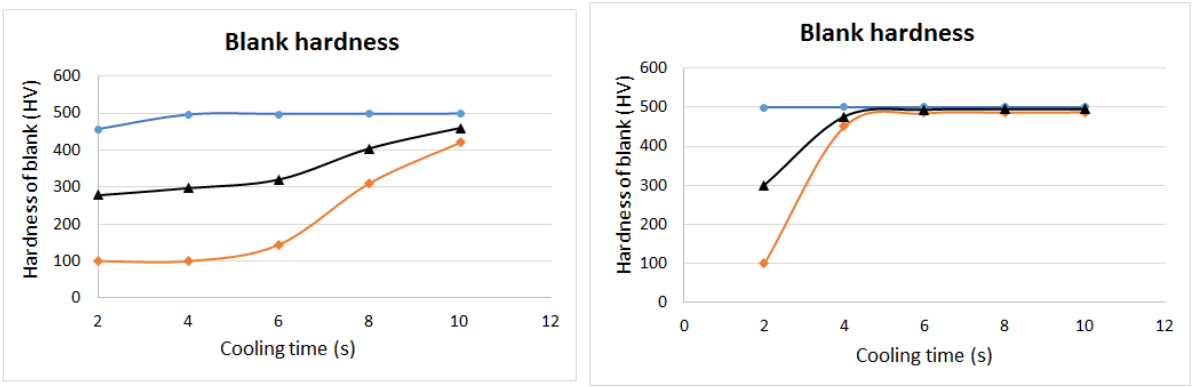


Figure A6.5: Hardness curves for conventional (left) and conformal (right) layout (cycle 5

# ADDENDUM B: MACHINING DATA

Table B1.1: Rough machining of bottom insert

| PROGRAM NAME: Rough_RHS_Insert_Bottom_Half_1.5mm_Stock | |
|---|---|
| | 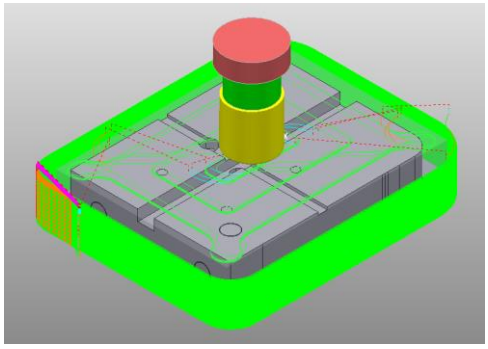 |
| Cutting Tool | AJX DIA50 (5- FLUTE) INSERT CUTTER |
| Tool Path Strategy | Offset Area Clearance- Roughing |
| Speed (Vc) in m/min | 100m/min- Reduced to (Vc) of 94m/min |
| Spindle Speed (N) rpm | 3000 rev/min |
| Feed Rate (F) in mm/min | 650 mm/min |
| ap (Depth of Cut) (mm) | 0.3mm |
| ae (Step Over) (mm) | 30 mm |
| fz (mm) | 0.05mm/tooth |
| Total machining time (min) | 57:14 |

Table B1.2: Rough location of slots and sensor hole

| PROGRAM NAME: ROUGH LOCATION SLOTS & SHALLOW SENSOR HOLE | |
|---|---|
| 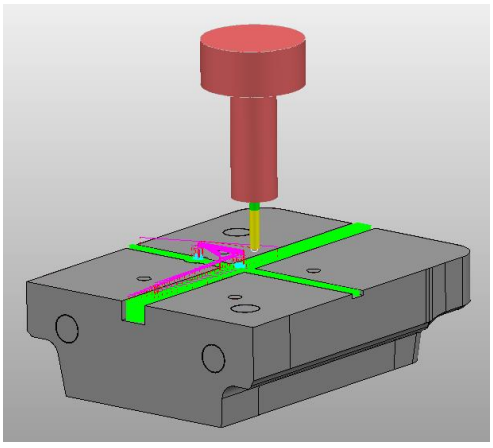 | |
| Cutting Tool | Mitsubishi End Mill Dia6mm- MS4JC |
| Tool Path Strategy | Offset Area Clearance - Roughing |

| | |
|---|---|
| Speed (Vc) in m/min | 131.947 m/min |
| Spindle Speed (N) rpm | 7000 rev/min |
| Feed Rate (F) in mm/min | 1500 mm/min |
| ap (mm) | 2.5 mm |
| ae (mm) | 0.2 mm |
| fz (mm) | 0.05 mm/tooth |
| Total machining time (min) | 1:05:47 |

Table B1.3: Rough machining of base insert

| PROGRAM NAME: Rough_RHS_Insert_Top_Half_Profile_Area_1.5mm_Stock | |
|---|---|
| 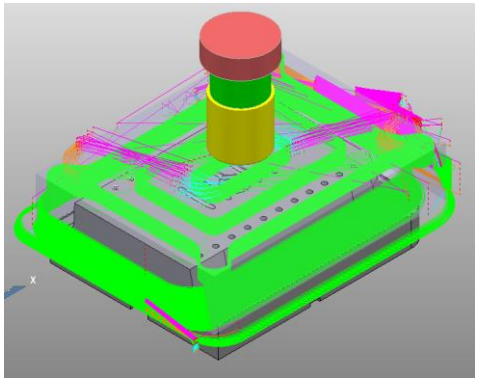 **Top Side Profile Roughing:** | 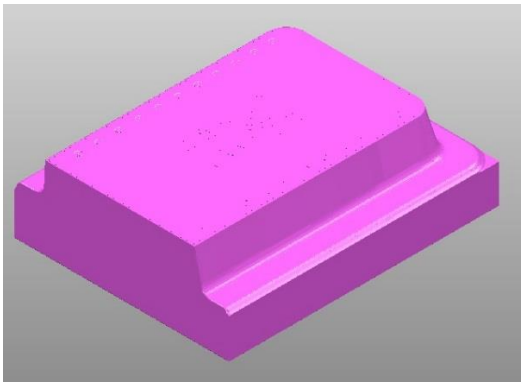 **Stock Model after Roughing:** |
| Cutting Too | AJX DIA50 (5- FLUTE) INSERT CUTTER |
| Tool Path Strategy | Offset Area Clearance- Roughing |
| Speed (Vc) in m/min | 100m/min- Reduced to (Vc) of 94m/min |
| Spindle Speed (N) rpm | 3000 rev/min |
| Feed Rate (F) in mm/min | Feed Rate (F) in mm/min 650 mm/min |
| ap (mm) | 0.3mm |
| ae (mm) | 30 mm |
| fz (mm) | 0.05mm/tooth |
| Total machining time (min) | 1:33:10 |

Table B1.4: Rough machining of conformal cooling channels

| PROGRAM NAME: ROUGH CONFORMAL COOLING CHANNELS | |
|---|---|
| 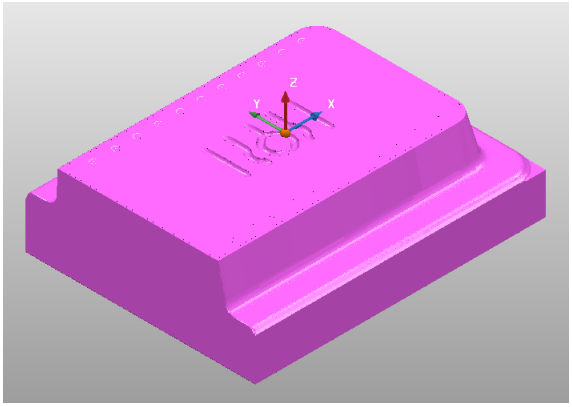 | |
| Cutting Tool | Corner Radius End Mill 4 Flute- D2R0.5 VC-HFRB |
| Tool Path Strategy | Offset Area Clearance- High Feed Machining |
| Speed (Vc) in m/min | 100m/min |
| Spindle Speed (N) rpm | 16000 rev/min |
| Feed Rate (F) in mm/min | 4790 mm/min |
| ap (mm) | 0.05mm |
| ae (mm) | 0.8mm |
| fz (mm) | 0.08mm/tooth |
| Total machining time (min) | 0:45:33 |

# ADDENDUM C: EXPERIMENTS DATA OF CONFORMAL COOLING TOOL

## C1: Experiments sequence for conformable tool

Table C1.1: Experiments sequence

| Exp No | Cooling time | Flow rate (L/min) |
|---|---|---|
| S1 | 2 | 11 |
| S2 | 2 | 15 |
| S3 | 2 | 19 |
| S4 | 5 | 11 |
| S5 | 5 | 15 |
| S6 | 5 | 19 |
| S7 | 8 | 11 |
| S8 | 8 | 15 |
| S9 | 8 | 19 |
| S10 | 2 | 11 |
| S11 | 2 | 15 |
| S12 | 2 | 19 |
| S13 | 5 | 11 |
| S14 | 5 | 15 |
| S15 | 5 | 19 |
| S16 | 8 | 11 |
| S17 | 8 | 15 |
| S18 | 8 | 19 |
| S19 | 6 | 15 |
| S20 | 6 | 19 |

## C2: Temperature results

Table C2.1: Temperature results

| Fowl rate (L/min) | cooling time | Sample number | T1 | T2 |
|---|---|---|---|---|
| 11 | 2 | S1 | 265 | 278 |
| 19 | 2 | S2 | 272 | 269 |
| 15 | 2 | S3 | 281 | 274 |
| 11 | 5 | S4 | 167 | 171 |
| 19 | 5 | S5 | 160 | 159 |
| 15 | 5 | S6 | 163 | 162 |
| 11 | 8 | S7 | 143 | 150 |
| 19 | 8 | S8 | 165 | 171 |
| 15 | 8 | S9 | 152 | 147 |
| 11 | 2 | S10 | 268 | 277 |
| 19 | 2 | S11 | 277 | 269 |
| 15 | 2 | S12 | 281 | 277 |
| 11 | 5 | S13 | 168 | 163 |
| 19 | 5 | S14 | 158 | 157 |
| 15 | 5 | S15 | 170 | 161 |
| 11 | 8 | S16 | 170 | 149 |
| 19 | 8 | S17 | 156 | 160 |
| 15 | 8 | S18 | 157 | 151 |

## C3: Hardness results

Table C3.1: Hardness results for three measurements

| | P1 | P3 | P4 | P5 | P6 | P7 | P8 |
|---|---|---|---|---|---|---|---|
| S1 | 452 | 480 | 274 | 293 | 438 | 377 | 517 |
| S2 | 397 | 433 | 298 | 267 | 400 | 344 | 456 |
| S3 | 427 | 438 | 315 | 232 | 393 | 378 | 521 |
| S4 | 447 | 457 | 443 | 392 | 456 | 436 | 487 |
| S5 | 488 | 497 | 428 | 427 | 460 | 506 | 495 |
| S6 | 454 | 448 | 447 | 400 | 475 | 424 | 525 |
| S7 | 511 | 455 | 445 | 420 | 468 | 448 | 479 |
| S8 | 445 | 451 | 450 | 422 | 464 | 415 | 481 |
| S9 | 454 | 460 | 454 | 448 | 447 | 478 | 518 |
| | | | | | | | |

| | P1 | P3 | P4 | P5 | P6 | P7 | P8 |
|---|---|---|---|---|---|---|---|
| S1 | 421 | 476 | 321 | 290 | 452 | 410 | 510 |
| S2 | 414 | 429 | 279 | 272 | 391 | 362 | 443 |
| S3 | 415 | 423 | 342 | 226 | 366 | 393 | 496 |
| S4 | 441 | 447 | 459 | 384 | 481 | 450 | 489 |
| S5 | 503 | 478 | 437 | 423 | 423 | 511 | 500 |
| S6 | 445 | 454 | 431 | 395 | 467 | 431 | 514 |
| S7 | 506 | 450 | 459 | 443 | 473 | 433 | 486 |
| S8 | 445 | 464 | 445 | 408 | 483 | 425 | 481 |
| S9 | 463 | 469 | 471 | 445 | 471 | 455 | 514 |
| | | | | | | | |
| | P1 | P3 | P4 | P5 | P6 | P7 | P8 |
| S1 | 414 | 444 | 337 | 306 | 442 | 477 | 482 |
| S2 | 395 | 431 | 278 | 265 | 391 | 374 | 453 |
| S3 | 407 | 408 | 332 | 231 | 373 | 409 | 477 |
| S4 | 429 | 465 | 492 | 391 | 463 | 471 | 490 |
| S5 | 425 | 480 | 437 | 428 | 454 | 477 | 512 |
| S6 | 448 | 445 | 440 | 400 | 478 | 441 | 511 |
| S7 | 490 | 445 | 440 | 416 | 472 | 453 | 474 |
| S8 | 447 | 442 | 461 | 402 | 488 | 418 | 512 |
| S9 | 464 | 480 | 463 | 463 | 460 | 452 | 508 |

# ADDENDUM D: EXPERIMENTS DATA OF CONVENTIONAL TOOL

## D1: Temperature results

Table D1.1: Temperature time results for conventional tool

| Cooling time | Temperature |
|---|---|
| 3 | 283 |
| 3 | 283 |
| 3 | 279 |
| 3 | 274 |
| 3 | 273 |
| 3 | 272 |
| 7 | 192 |
| 7 | 181 |
| 7 | 181 |
| 5 | 209 |
| 5 | 209 |
| 5 | 207 |
| 3 | 270 |
| 3 | 270 |
| 3 | 271 |
| 7 | 193 |
| 7 | 190 |
| 7 | 190 |
| 7 | 190 |
| 3 | 274 |
| 3 | 276 |
| 3 | 275 |

| Cooling time | Temperature |
|---|---|
| 5 | 209 |
| 5 | 210 |
| 5 | 205 |
| 7 | 182 |
| 7 | 180 |
| 7 | 183 |
| 3 | 276 |
| 3 | 280 |
| 3 | 278 |
| 3 | 274 |
| 7 | 188 |
| 7 | 185 |
| 7 | 189 |
| 3 | 279 |
| 3 | 275 |
| 3 | 278 |
| 5 | 209 |
| 5 | 221 |
| 5 | 216 |
| 7 | 190 |
| 7 | 190 |
| 7 | 189 |

(Adopted from Fraunhofer, IGF Project, 2015)

## D1: Hardness results

Table D1.2: Hardness results for conventional tool

| Cooling time | P1 | P2 | P3 |
|---|---|---|---|
| 3 | 461 | 424 | 457 |
| 3 | 454 | 417 | 442 |
| 3 | 467 | 416 | 452 |
| 3 | 454 | 400 | 440 |
| 3 | 462 | 402 | 442 |
| 3 | 465 | 415 | 440 |
| 5 | 477 | 434 | 456 |
| 5 | 484 | 439 | 460 |
| 5 | 487 | 434 | 471 |
| 5 | 483 | 449 | 455 |
| 5 | 480 | 456 | 475 |
| 5 | 488 | 455 | 460 |
| 5 | 484 | 434 | 458 |
| 5 | 489 | 447 | 451 |
| 5 | 494 | 451 | 457 |
| 7 | 478 | 425 | 454 |
| 7 | 490 | 444 | 478 |
| 7 | 483 | 449 | 474 |
| 7 | 477 | 428 | 453 |
| 7 | 483 | 451 | 460 |
| 7 | 473 | 440 | 454 |
| 7 | 483 | 457 | 459 |
| 7 | 478 | 438 | 452 |
| 7 | 473 | 438 | 460 |
| 7 | 485 | 443 | 460 |
| 7 | 485 | 441 | 463 |
| 7 | 490 | 438 | 463 |
| 7 | 493 | 450 | 463 |
| 7 | 487 | 444 | 453 |
| 7 | 484 | 458 | 467 |
| 7 | 492 | 457 | 466 |

| Cooling time | P1 | P2 | P3 |
|---|---|---|---|
| 3 | 461 | 424 | 443 |
| 3 | 454 | 417 | 442 |
| 7 | 478 | 425 | 454 |
| 7 | 490 | 444 | 478 |
| 7 | 483 | 449 | 474 |
| 5 | 477 | 434 | 456 |
| 5 | 484 | 439 | 460 |
| 5 | 487 | 434 | 471 |
| 3 | 467 | 416 | 446 |
| 3 | 454 | 400 | 442 |
| 3 | 462 | 402 | 448 |
| 7 | 477 | 428 | 453 |
| 7 | 483 | 451 | 460 |
| 7 | 473 | 440 | 454 |
| 7 | 483 | 457 | 459 |
| 3 | 465 | 415 | 440 |
| 5 | 483 | 449 | 455 |
| 5 | 480 | 456 | 475 |
| 5 | 488 | 455 | 460 |
| 7 | 478 | 438 | 452 |
| 7 | 473 | 438 | 460 |
| 7 | 485 | 443 | 460 |
| 7 | 485 | 441 | 463 |
| 7 | 490 | 438 | 463 |
| 7 | 493 | 450 | 463 |
| 5 | 484 | 434 | 458 |
| 5 | 489 | 447 | 451 |
| 5 | 494 | 451 | 457 |
| 7 | 487 | 444 | 453 |
| 7 | 484 | 458 | 467 |
| 7 | 492 | 457 | 466 |

(Adopted from Fraunhofer, IGF Project, 2015)

# ADDENDUM E: DATA FOR TEMPERATURE SENSORS

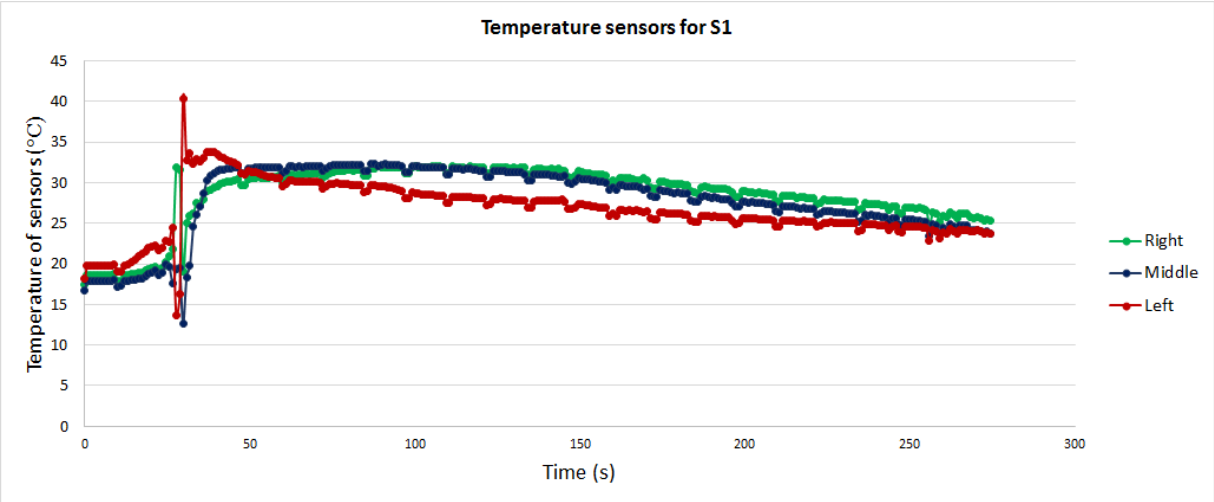


Figure E1.1: Temperature sensor curves for S1

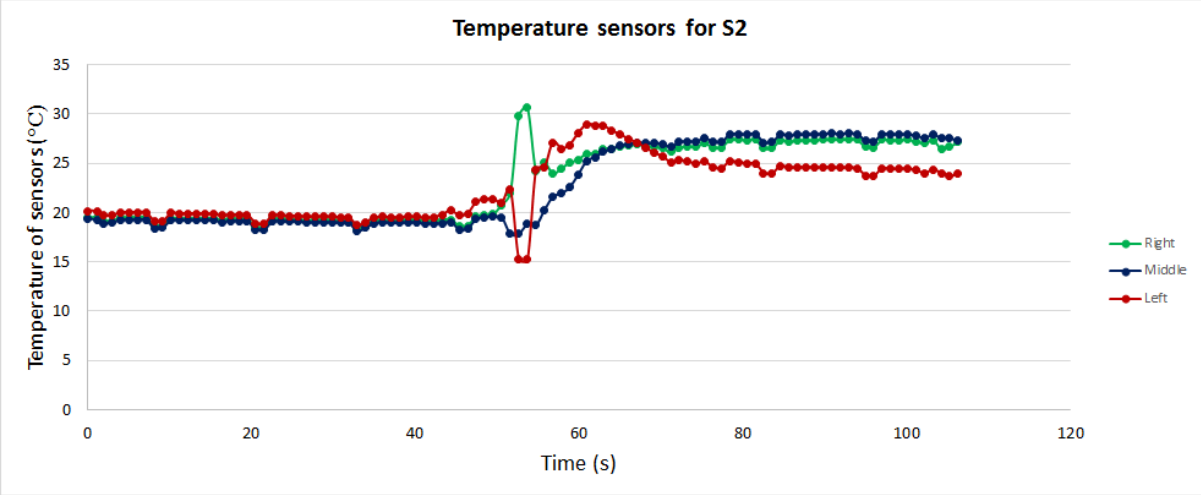


Figure E1.2: Temperature sensor curves for S2

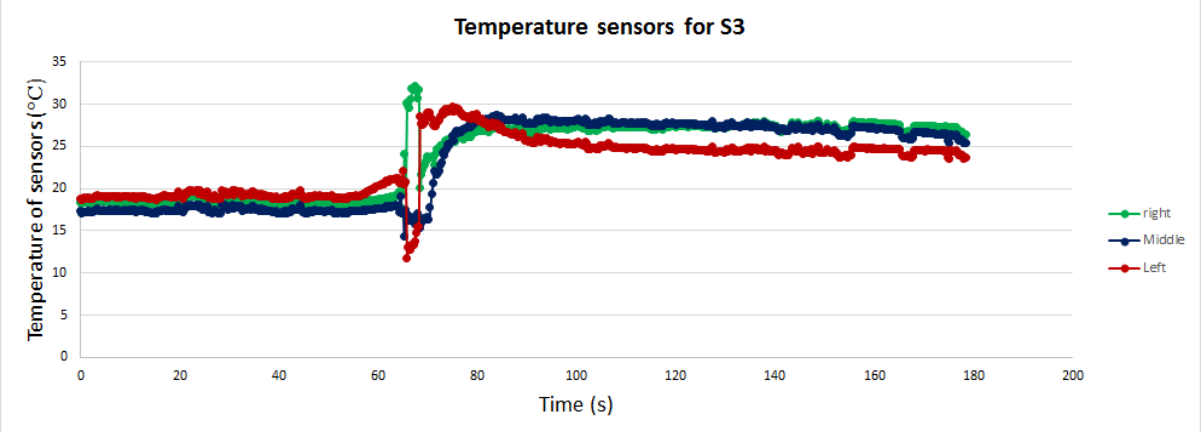


Figure E1.3: Temperature sensor curves for S3

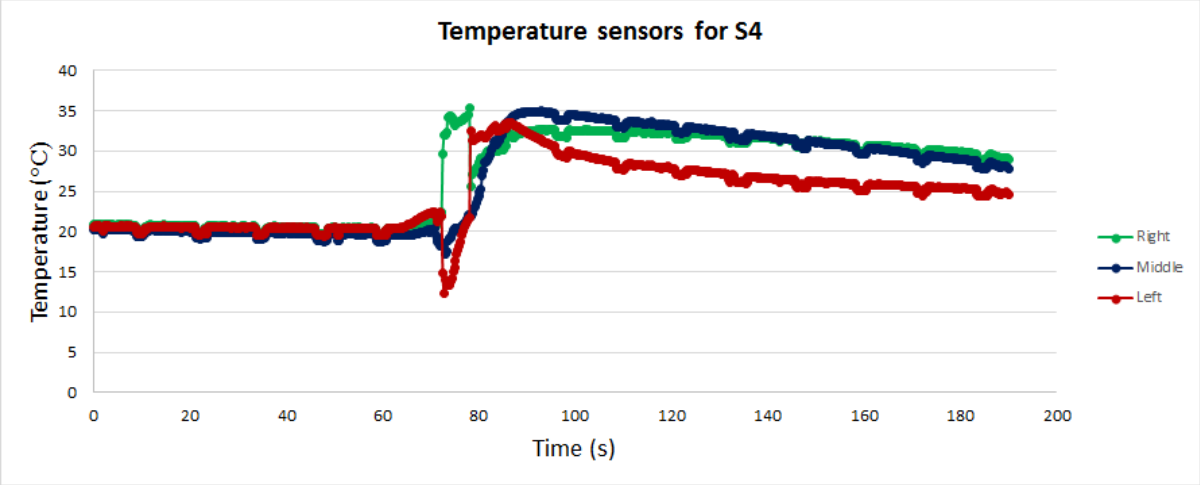


Figure E1.4: Temperature sensor curves for S4

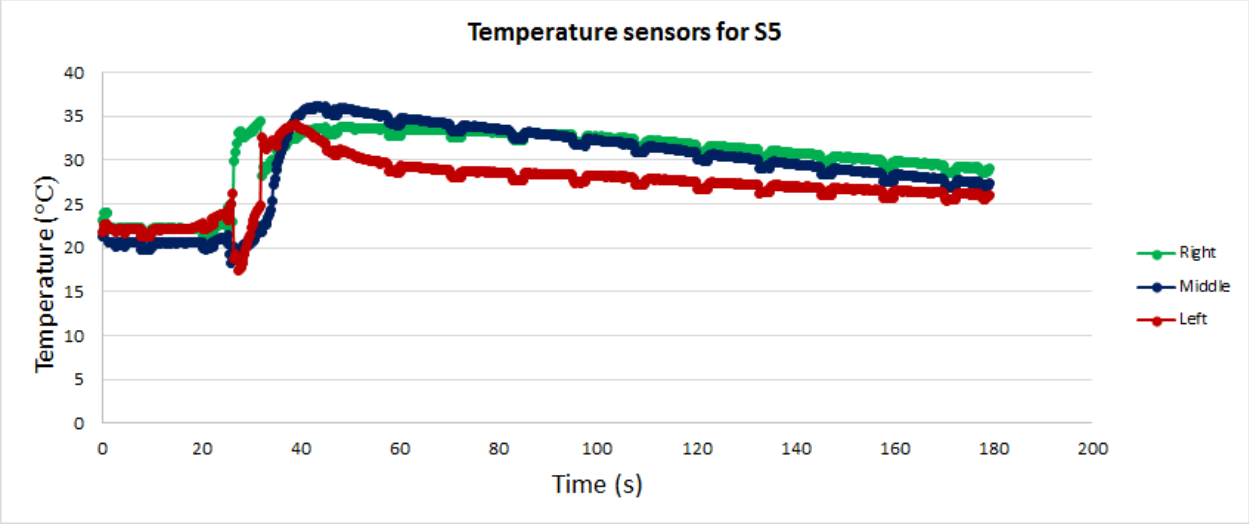


Figure E1.5: Temperature sensor curves for S5

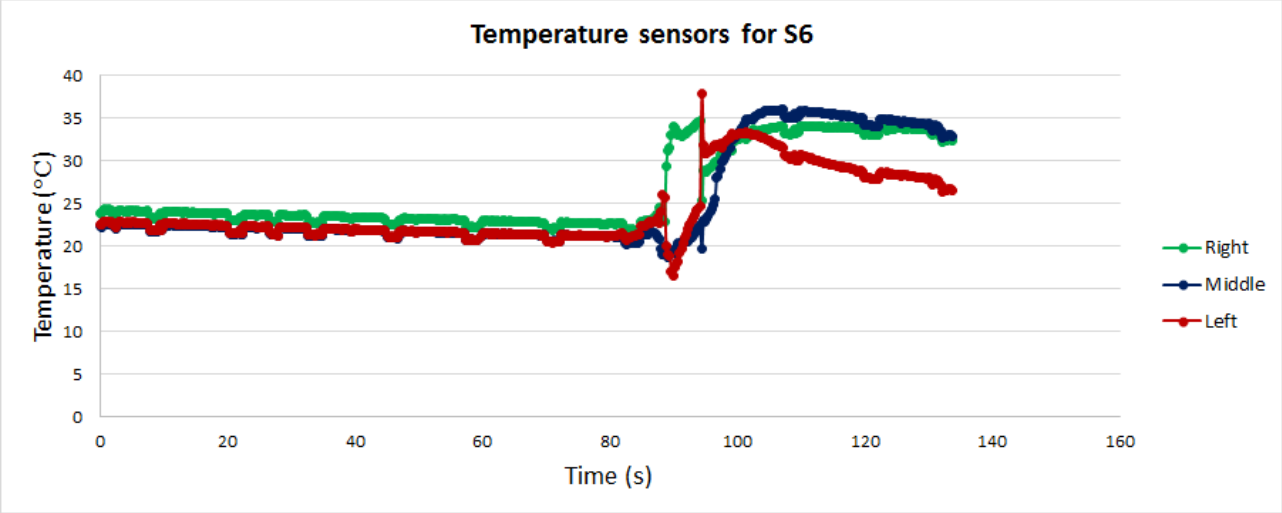


Figure E1.6: Temperature sensor curves for S6

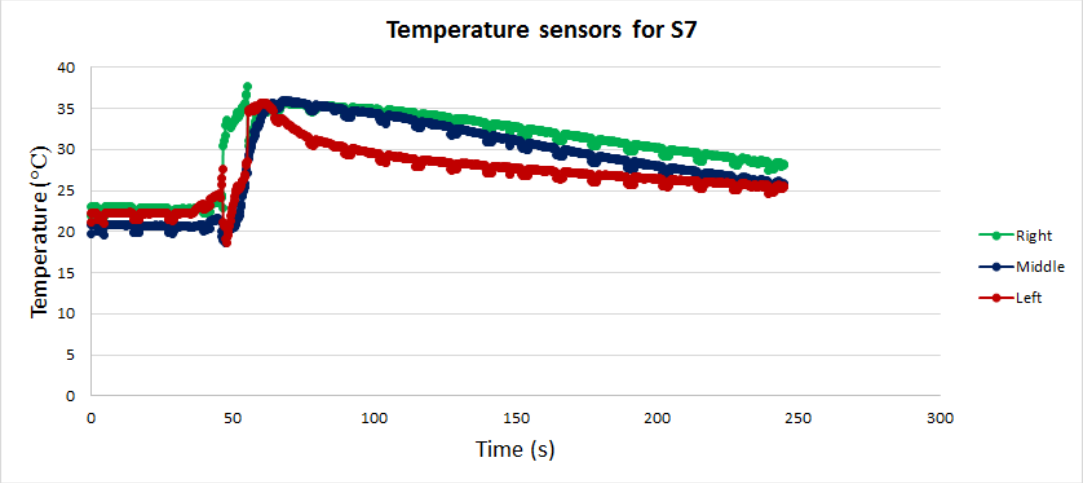


Figure E1.7: Temperature sensor curves for S7

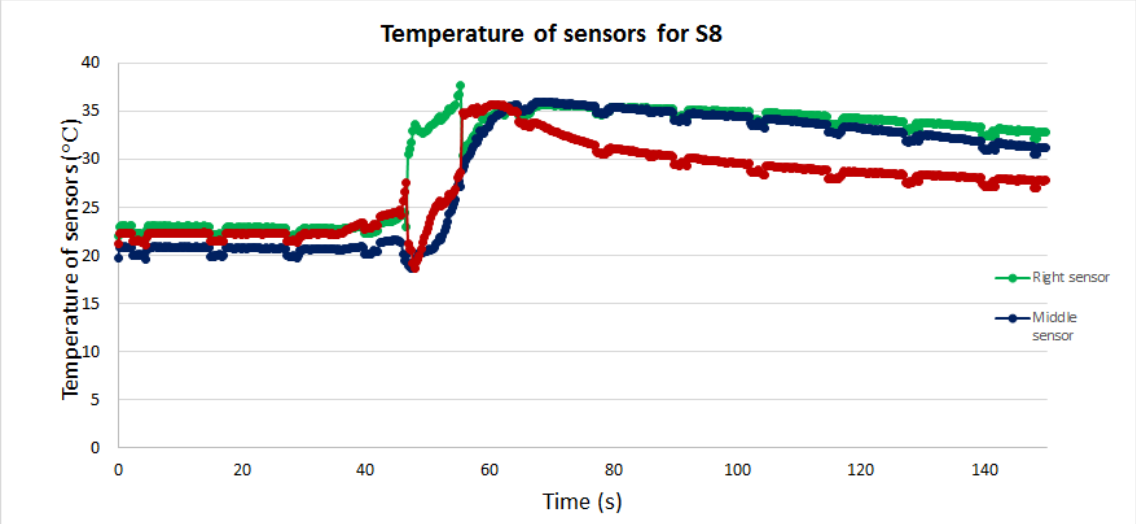


Figure E1.8: Temperature sensor curves for S8

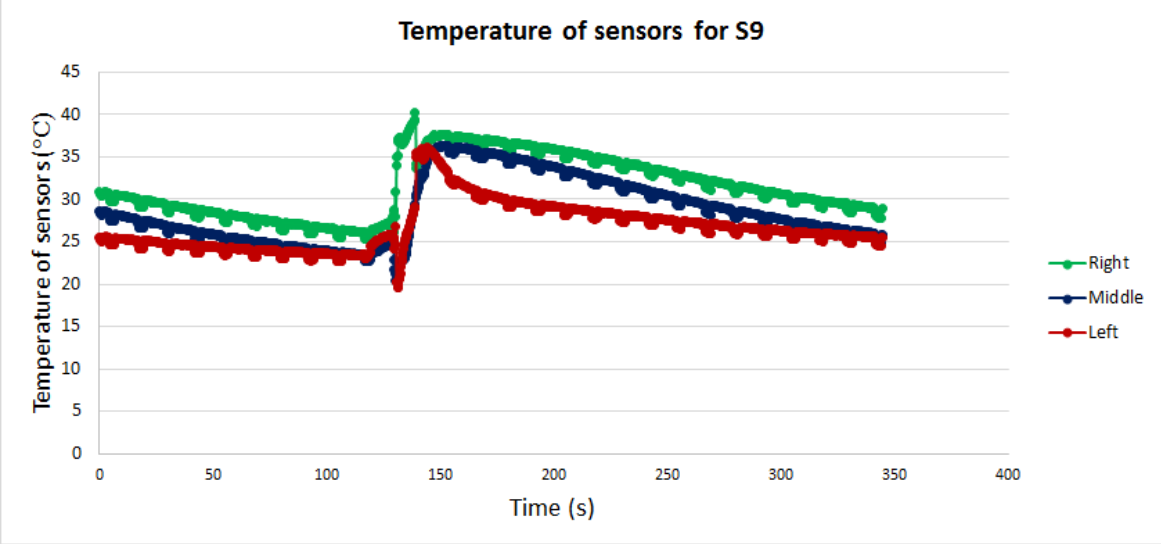


Figure E1.9: Temperature sensor curves for S9

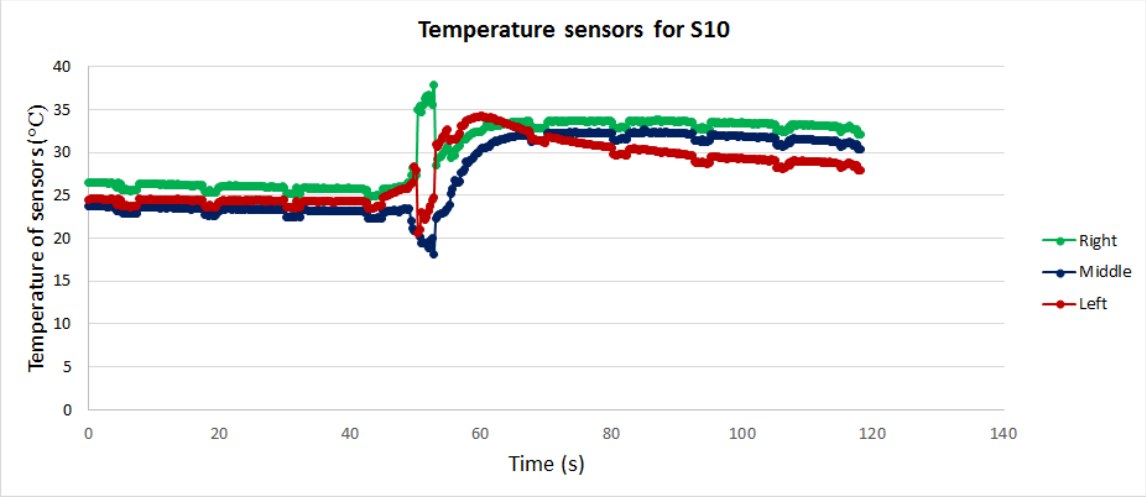


Figure E1.10: Temperature sensor curves for S10

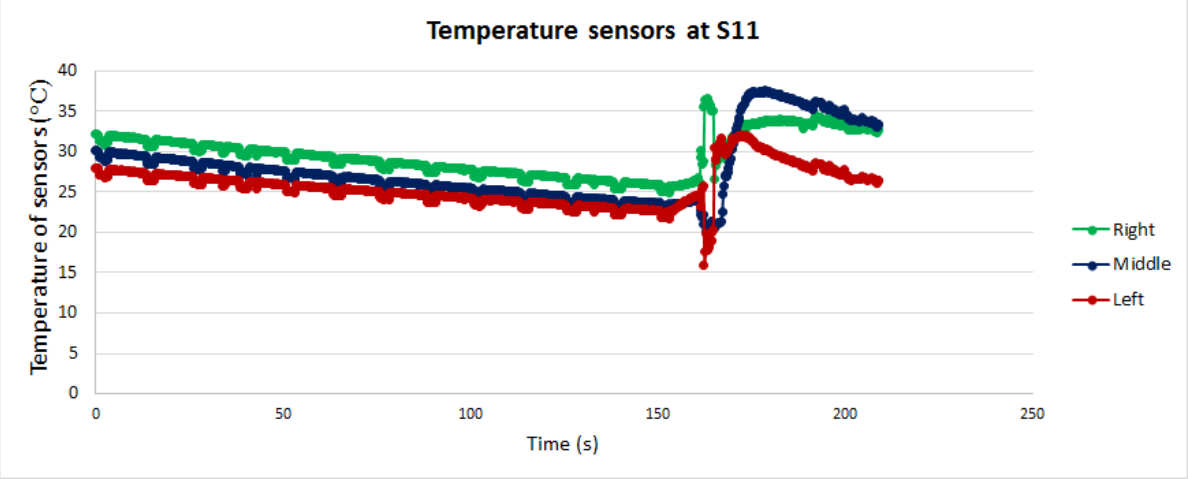


Figure E1.11: Temperature sensor curves for S11

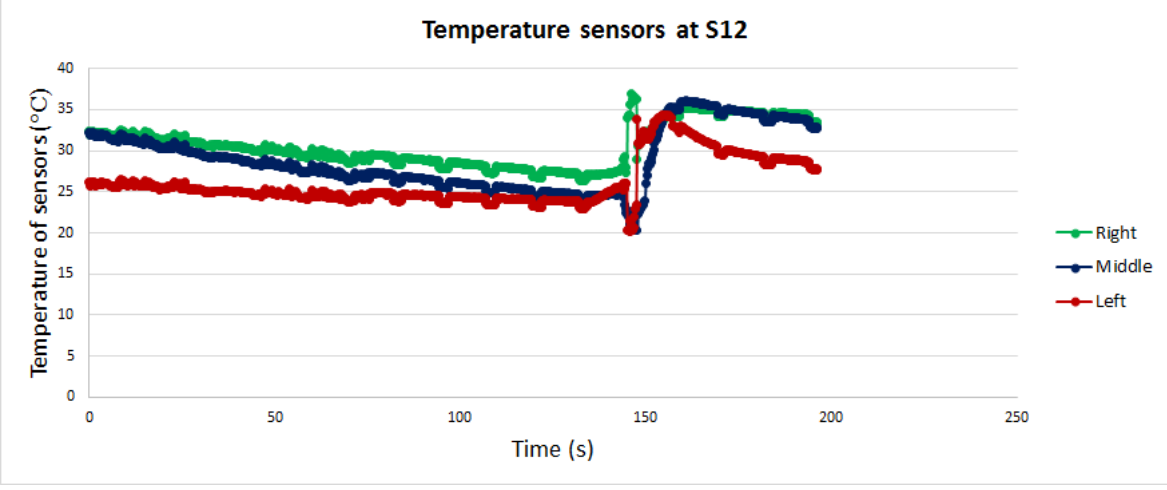


Figure E1.12: Temperature sensor curves for S12

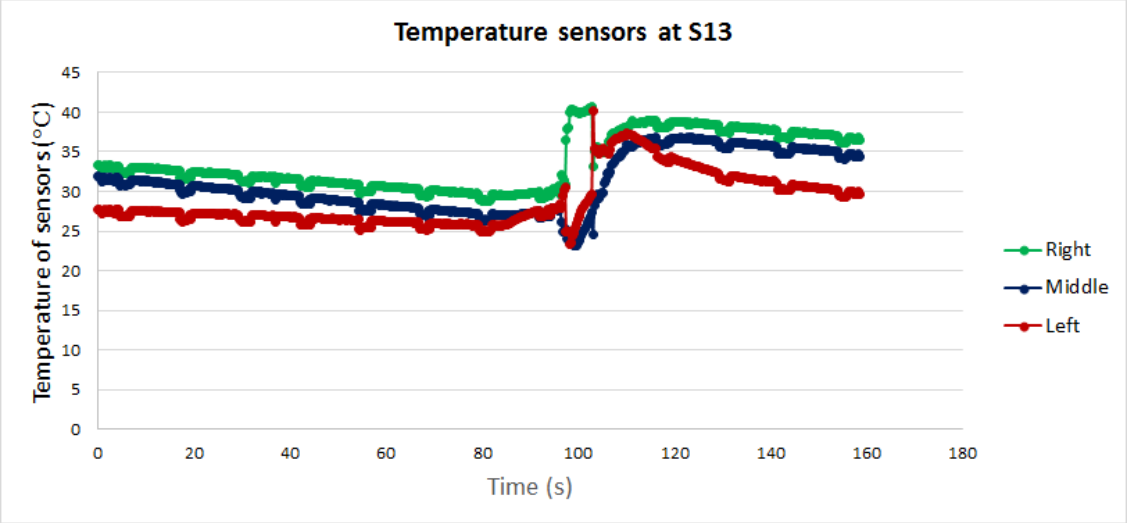


Figure E1.13: Temperature sensor curves for S13

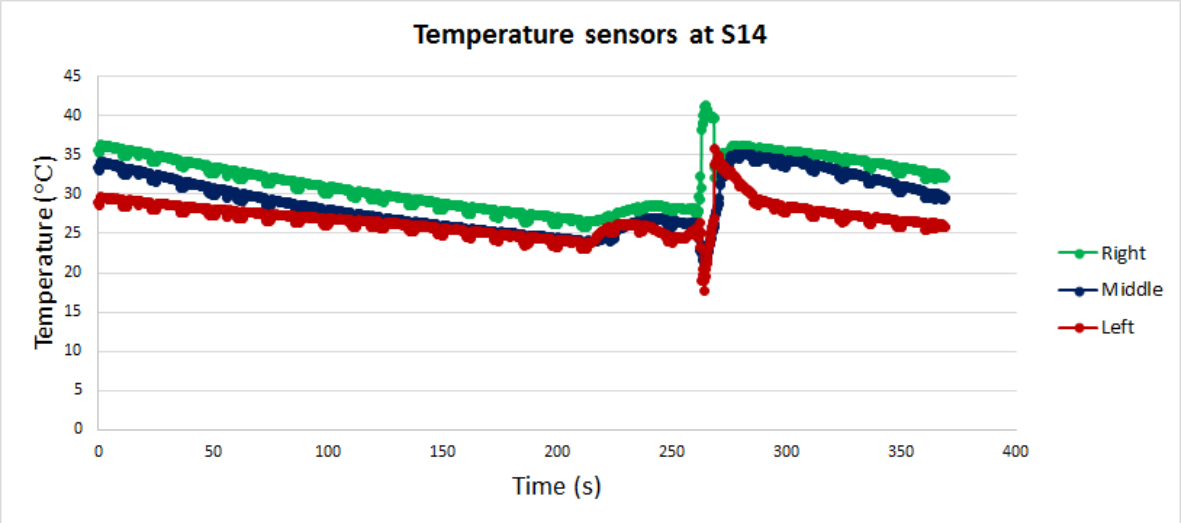


Figure E1.14: Temperature sensor curves for S14

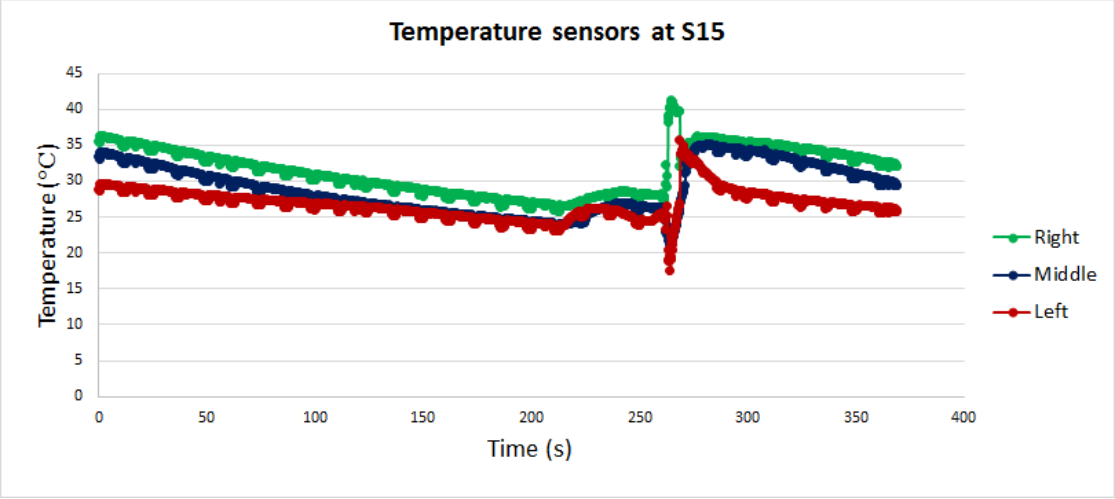


Figure E1.15: Temperature sensor curves for S15

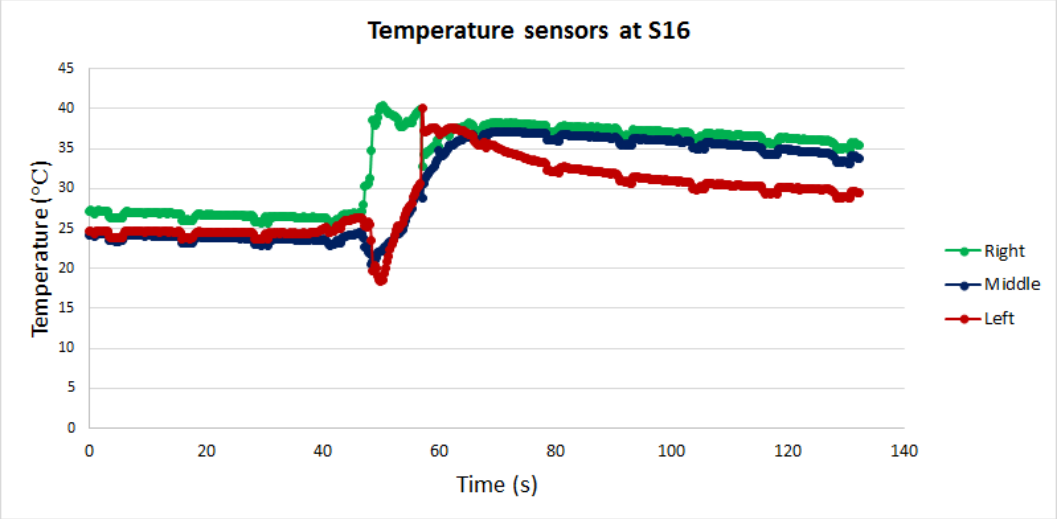


Figure E1.16: Temperature sensor curves for S16

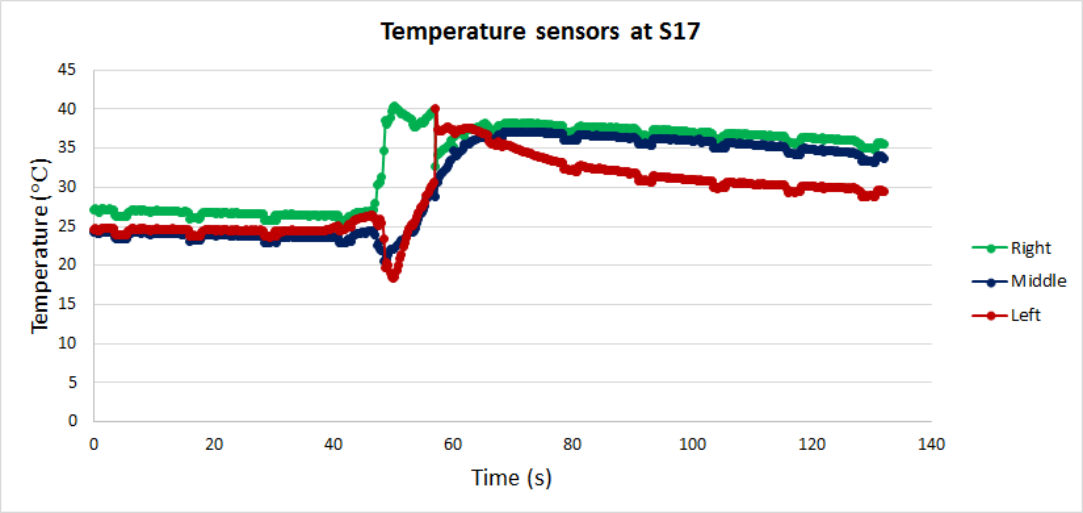


Figure E1.17: Temperature sensor curves for S17

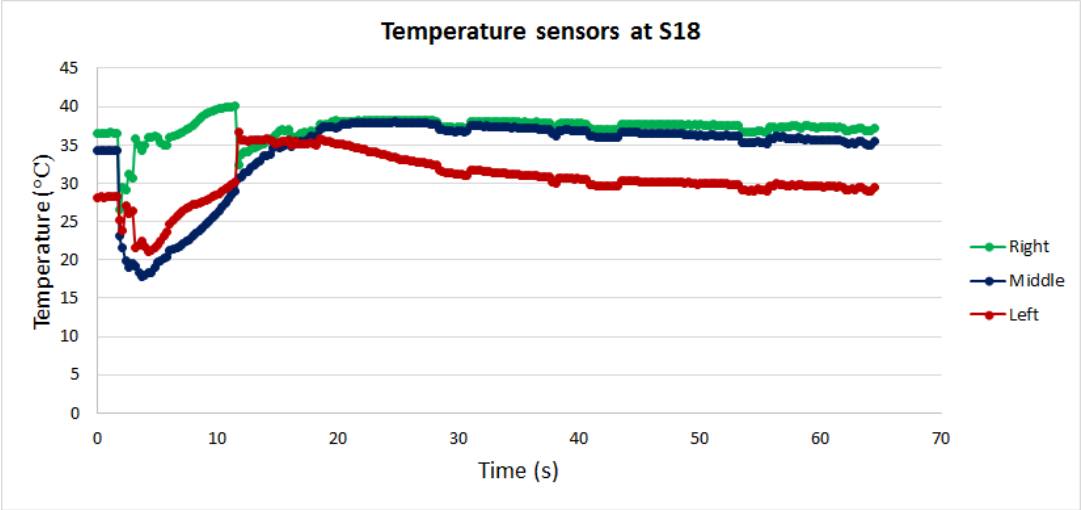


Figure E1.18: Temperature sensor curves for S18

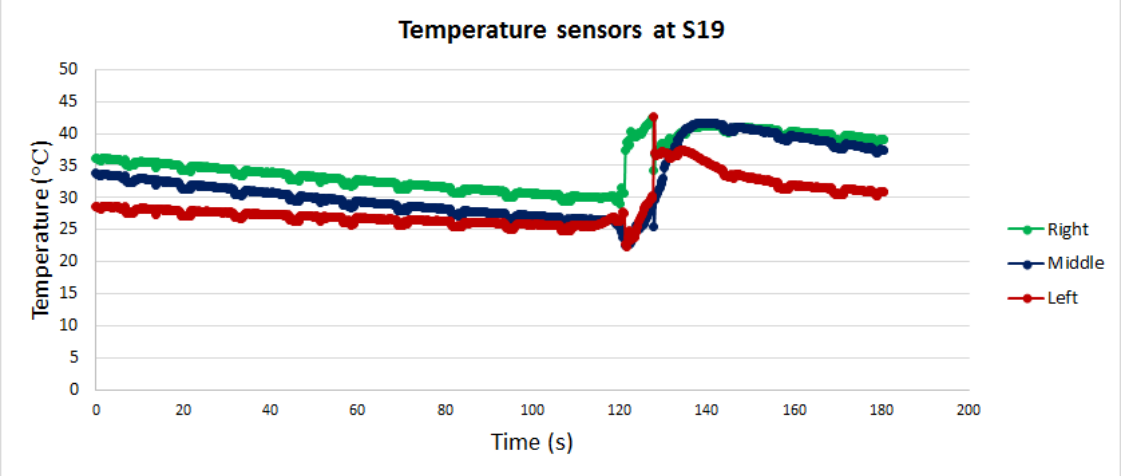


Figure E1.19: Temperature sensor curves for S19

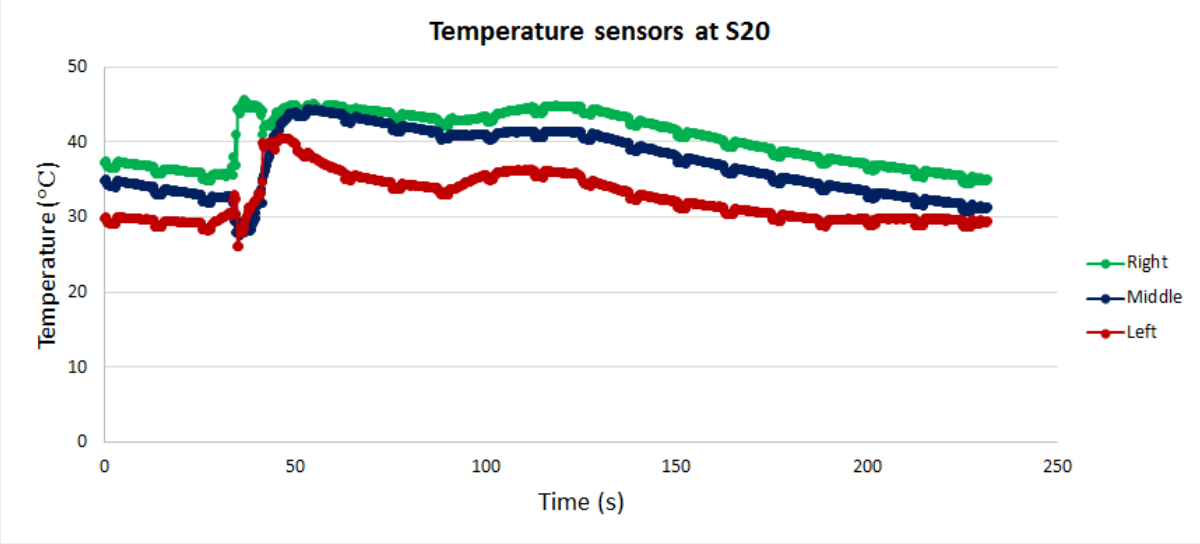


Figure E1.19: Temperature sensor curves for S19

# ADDENDUM F: FLOW STRESS OF 22MNB5 AT DIFFERENT STRAIN RATES (E0S, 2015)